BioMed Research International

Modern Approaches to Quality Assurance of Drug Formulations

Guest Editors: Josef Jampilek, Patrick J. Crowley, Mark Olsen, and Kin Tam

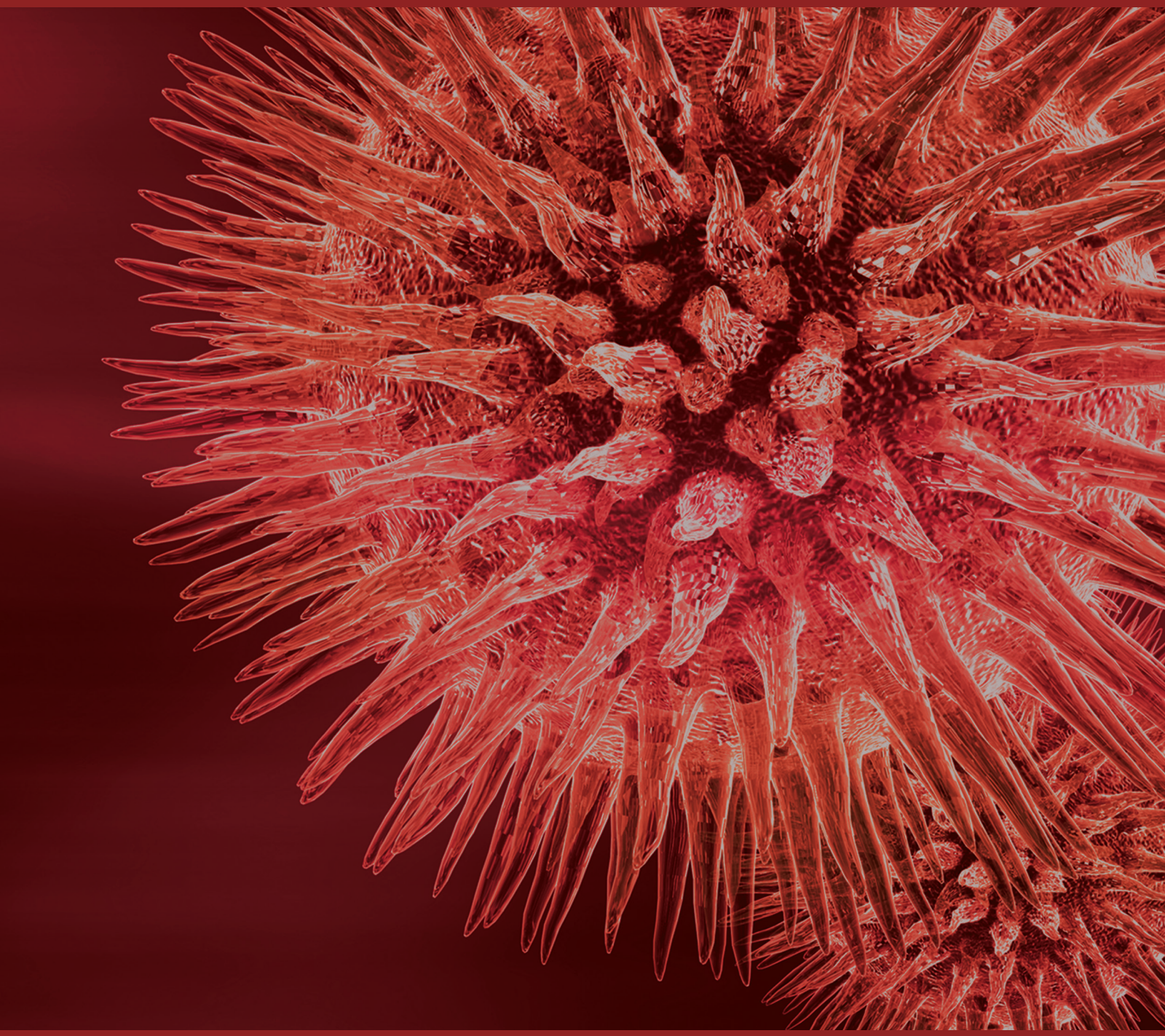

Modern Approaches to Quality Assurance of Drug Formulations

BioMed Research International

Modern Approaches to Quality Assurance of Drug Formulations

Guest Editors: Josef Jampilek, Patrick J. Crowley, Mark Olsen, and Kin Tam

Contents

Hindawi Publishing Corporation
BioMed Research International
Volume 2015, Article ID 126478, 1 page
http://dx.doi.org/10.1155/2015/126478

Editorial

Modern Approaches to Quality Assurance of Drug Formulations

Josef Jampilek,[1] Patrick J. Crowley,[2] Mark Olsen,[3] and Kin Tam[4]

[1]*Department of Chemical Drugs, Faculty of Pharmacy, University of Veterinary and Pharmaceutical Sciences Brno, Palackeho 1/3, 612 42 Brno, Czech Republic*
[2]*Callum Consultancy LLC, 571 Berwyn Baptist Road, Devon, PA 19333, USA*
[3]*Department of Pharmaceutical Sciences, College of Pharmacy, Midwestern University, Glendale Hall 236-18, 19555 N. 59th Avenue, Glendale, AZ 85308, USA*
[4]*Faculty of Health Sciences, University of Macau, Avenida da Universidade, Taipa, Macau*

Correspondence should be addressed to Josef Jampilek; josef.jampilek@gmail.com

Received 1 March 2015; Accepted 1 March 2015

Developments in pharmaceutical sciences have provided sophisticated oral dosage forms to modify drug action by delaying its onset or by slowing or otherwise changing the rate of delivery to reduce side effects or sustain drug action by maintaining constant plasma levels. Delivery of active pharmaceutical ingredients with suboptimal physicochemical properties to the targeted sites could be achieved using recently developed new formulation technologies. More novel modes of delivery have also gained prominence. These may provide (e.g.) transdermal delivery or time-based (chronotherapeutic) release or may target specific organs, tissues, or cellular structures. Numbers of biopharmaceutical products have also increased and will probably continue to do so. These too may benefit from formulating for controlled or site-specific delivery.

Such novel systems, therapeutic agents, and evolving paradigms place increasing demands for assuring and controlling product quality. At the same time they provide opportunities for developing and putting into practice new ideas and technologies to assure quality and performance. Well-designed dosage forms and processes, along with process analytical technologies, can provide insights and online monitoring systems that could largely replace end product testing. Manufacture, testing, and batch approval times could be greatly reduced.

The same principles apply to manufacture and quality assurance of drug-device systems, providing assurance of performance related to amount, rate, and possibly time of drug delivery.

In this special issue readers can find examples of preparation and characterization of modern sophisticated drug delivery systems such as oral mucoadhesive films, wound dressing films, solid dispersions, or liquisolid systems for enhancing dissolution rate and improving *in vivo* bioavailability of poorly soluble drugs. Unique site-specific or controlled release antimicrobial systems based on carmellose cross-linked by copper ions are also described. A paper also focuses on the preparation and characterization of silica-based nanocarrier loaded nootropics, which are designed to enhance the permeation of the drugs from the circulatory system through the blood-brain barrier. Other papers deal with the assurance of medical device quality with quality management systems, quality by design, innovative analytical techniques, and their applications in process monitoring, analysis and control, determination of critical quality attributes, and *in vitro in vivo* correlations based on multicompartmental dissolution data.

Josef Jampilek
Patrick J. Crowley
Mark Olsen
Kin Tam

Hindawi Publishing Corporation
BioMed Research International
Volume 2015, Article ID 790720, 9 pages
http://dx.doi.org/10.1155/2015/790720

Research Article

Antimicrobial Properties of Microparticles Based on Carmellose Cross-Linked by Cu^{2+} Ions

Martina Kejdušová,[1] Jakub Vysloužil,[1] Kateřina Kubová,[1] Vladimír Celer,[2] Magdaléna Krásna,[2] Alena Pechová,[3] Věra Vyskočilová,[3] and Vratislav Košťál[4]

[1]*Department of Pharmaceutics, Faculty of Pharmacy, University of Veterinary and Pharmaceutical Sciences Brno, Palackého Třída 1/3, 612 42 Brno, Czech Republic*
[2]*Department of Infectious Diseases and Microbiology, Faculty of Veterinary Medicine, University of Veterinary and Pharmaceutical Sciences Brno, Palackého 1/3, 612 42 Brno, Czech Republic*
[3]*Department of Biochemistry and Biophysics, Faculty of Veterinary Hygiene and Ecology, University of Veterinary and Pharmaceutical Sciences Brno, Palackého 1/3, 612 42 Brno, Czech Republic*
[4]*Tescan, Libušina Třída 863/21, 623 00 Brno-Kohoutovice, Czech Republic*

Correspondence should be addressed to Kateřina Kubová; kubovak@vfu.cz

Received 16 September 2014; Accepted 14 November 2014

Academic Editor: Kin Tam

Carmellose (CMC) is frequently used due to its high biocompatibility, biodegradability, and low immunogenicity for development of site-specific or controlled release drug delivery systems. In this experimental work, CMC dispersions in two different concentrations (1% and 2%) cross-linked by copper (II) ions (0.5, 1, 1.5, or 2.0 M $CuCl_2$) were used to prepare microspheres with antimicrobial activity against *Escherichia coli* and *Candida albicans*, both frequently occurring pathogens which cause vaginal infections. The microparticles were prepared by an ionotropic gelation technique which offers the unique possibility to entrap divalent copper ions in a CMC structure and thus ensure their antibacterial activity. Prepared CMC microspheres exhibited sufficient sphericity. Both equivalent diameter and copper content were influenced by CMC concentration, and the molarity of copper (II) solution affected only the copper content results. Selected samples exhibited stable but pH-responsive behaviour in environments which corresponded with natural (pH 4.5) and inflamed (pH 6.0) vaginal conditions. All the tested samples exhibited proven substantial antimicrobial activity against both Gram-negative bacteria *Escherichia coli* and yeast *Candida albicans*. Unexpectedly, a crucial parameter for microsphere antimicrobial activity was not found in the copper content but in the swelling capacity of the microparticles and in the degree of CMC surface shrinking.

1. Introduction

Carmellose (CMC) is a water-soluble anionic polysaccharide and semisynthetic derivative of cellulose [1] which has no harmful effects on human health. Its chains are linear $\beta(1 \rightarrow 4)$-linked glucopyranose units. In addition, it contains a hydrophobic polysaccharide backbone and many hydrophilic carboxyl groups and, as a result, exhibits amphiphilic characteristics. CMC is used in a number of applications throughout the food, cosmetic, textile, paper, and ceramic industries as a viscosity modifier, thickener, emulsion stabilizer, and water retention and adhesive agent [2]. It also has tremendous potential for use in pharmaceutical products including site-specific or controlled release drug delivery carrier matrices thanks to its high biocompatibility, biodegradability [3], and low immunogenicity [4]. In spite of the numerous positive properties of CMC, it does not have any antimicrobial properties as it lacks antimicrobial functional groups [5]. To bestow CMC with antimicrobial properties, different possibilities have been proposed, such as (i) adding different antimicrobial agents, for example, potassium sorbate [6] or silver nitrate [7], (ii) grafting CMC with different antimicrobial substances, for example, guanidine hydrochloride [8], (iii) combining CMC with other polymers that exhibit antimicrobial properties,

for example, carboxymethyl chitosan [9, 10], or (iv) preparing nanoparticles of certain metals, for example, with silver [7] or copper [11], and incorporating them into the CMC structure.

Copper is one of the most abundant trace elements found in the human body. It is an essential nutrient involved in catalyzing biochemical reactions. However, excessive copper levels can be toxic, mainly because they cause oxidative damage to the body. Copper can change its redox status by accepting and donating electrons, shifting between cuprous (Cu^{+}) and cupric (Cu^{2+}) forms, and therefore participate in reactions that generate superoxide radicals and hydrogen peroxide, which are major reactive oxygen species in the body. That is why a systemic usage of copper is limited in the human body with exception of rheumatoid arthritis treatment [12–14]. New options for copper utilization can be found in its local effect via vaginal application of dosage forms based on copper ions for their strong antibacterial and spermicidal and/or spermiostatic effect. The vagina produces fluid at a rate of 3-4 g/4 h [15] which can reduce the potent local toxic effect of the copper compounds. Mucus efficiently traps foreign particles and particulates by both steric and adhesive mechanisms, facilitating rapid clearance [16]. Daunter used copper ethylenediaminetetraacetic acid/L-ascorbic acid as a fertilization-preventing agent that can be delivered via nonbiodegradable, polyurethane, or polyvinyl acetate vaginal discs [17].

An aqueous CMC solution can undergo a sol-gel transformation in the presence of cross-linking cations and thus allow for the creation of solid gel microparticles. This method is known as an ionotropic gelation technique and is based on the impact of physical (electrostatic) forces and polyelectrolyte complexation with the presence of polyvalent ions [18]. In general, divalent cations (e.g., Ba^{2+}, Sr^{2+}, Cd^{2+}, Co^{2+}, Ca^{2+}, Mn^{2+}, Ni^{2+}, Pb^{2+}, and Zn^{2+}) are suitable cross-linking agents for this method [19]. Thus, ionotropic gelation offers a unique possibility to incorporate divalent copper ions into the CMC structure and form microspheres with potential antimicrobial properties.

The aim of the presented research was to prepare Cu^{2+} cross-linked CMC microspheres using external ionic gelation and assess their antimicrobial activity against Gram-negative *Escherichia coli* and *Candida albicans* yeast, both frequently occurring pathogens responsible for vaginal infections.

2. Materials and Methods

2.1. Materials. Blanose-carmellose (CMC) with a medium viscosity grade (1500–3100 mPa·s for 2% in water) and a DS of 1.2 was used as the polymer carrier (Ashland, Covington, USA), copper (II) chloride was used as a cross-linking agent (Sigma Aldrich, St. Louis, USA), and HNO_3 (65% v/v) and H_2O_2 (30% v/v) used for the determination of copper content were purchased from Analytika (Prague, Czech Republic). Calibration solutions were prepared using a dilution of 1000 mg/L stock copper reference solvent (Analytika, Prague, Czech Republic). Deionised water with a resistivity of 18 MΩ was used for all necessary dilution.

Table 1: Variables during preparation of microparticles samples.

Sample	CMC concentration (%)	Molarity of $CuCl_2$ (mol/dm^3)
MP-1_0.5	1	0.5
MP-1_1.0	1	1.0
MP-1_1.5	1	1.5
MP-1_2.0	1	2.0
MP-2_0.5	2	0.5
MP-2_1.0	2	1.0
MP-2_1.5	2	1.5
MP-2_2.0	2	2.0

2.2. Methods

2.2.1. Microparticles Preparation. Copper cross-linked CMC microparticles were prepared by a method of external ionic gelation. CMC dispersions (1% and 2%) were prepared by dispersing 1 g and 2 g of CMC in purified water, respectively. The dispersions were heated to 80°C to increase the rate of swelling. They were then homogenized using an Ultra-Turrax (T25 basic, IKA-Werke, Staufen, Germany) at 13,000 rpm for 5 min. The volume of each dispersion was ultimately adjusted to 100 mL with purified water. The resulting dispersions were then extruded through a needle with an internal diameter of 0.4 mm at a dropping rate of 2.0 mL/min into 50 mL of 0.5, 1.0, 1.5, or 2.0 M $CuCl_2$ aqueous solution, respectively. The distance between the edge of the needle and the surface of the solution was adjusted to 5.0 cm. Microparticle formation was instantaneous and the particles were left in the cross-linking solution for 1 hour to harden while being gently mixed. The resulting beads were subsequently washed three times with purified water and dried at 25°C in a cabinet drier (HORO – 048B, Dr. Hofmann GmbH, Ostfildern, Germany) for 24 hrs before testing. Prepared samples were named in accordance with the type and values of the altered variables (CMC concentration and molarity of the cross-linking medium). Samples characteristics are shown in Table 1.

2.2.2. Viscosity Measurement. To investigate the influence of the viscosity on the characteristics of the prepared microparticles, rheological measurements of CMC dispersions were performed. Dispersions (1.0 and 2.0 wt%) were prepared and then homogenized with Ultra-Turrax (T25 BASIC, IKA-Werke GmbH & Co. KG, Staufen, Germany) at 16,000 rpm. Dynamic viscosity was measured by a Brookfield DV-II+Pro rotary viscometer (Brookfield Engineering, Middleboro, USA) and Rheocalc software (Brookfield Engineering, Middleboro, USA) at 37°C and 200 rpm. A small sample adapter was employed for this step. Each sample was measured three times and the results were expressed as mean values with standard deviations (SD).

2.2.3. Scanning Electron Microscopy. In order to observe microparticle morphology and surface topography, scanning electron microscopy (SEM) was employed. The samples were

mounted directly onto the SEM sample holder using double-sided sticking tape and then coated with a 10 nm thick layer of Au. Images were taken using the MIRA3 scanning electron microscope (Tescan, Brno, Czech Republic) at an accelerating voltage of 5.0 kV.

2.2.4. Optical Microscope Analysis. Particle size of the copper microparticles was measured using a NIKON SMZ 1500 stereoscopic microscope (Nikon, Tokyo, Japan) equipped with a 72AUC02 USB camera (The Imaging Source, Bremen, Germany). Microparticles were visualized under ×15 magnification. The obtained images of 200 randomly chosen microparticles were stored and subsequently processed using the NIS-Elements AR 4.0 computer software (Nikon, Tokyo, Japan).

Equivalent diameter (ED) and sphericity factor (SF) were calculated from the measured values and expressed as arithmetic mean ± standard deviation.

2.2.5. Copper Content in Microparticles. The copper content in the prepared microparticles was determined by atomic absorption. To digest the microparticles, 6 mL of concentrated nitric acid (65% v/v) and 2 mL of hydrogen peroxide (30% v/v) were added to 10 mg of every sample and placed in a TFM digestion vessel. The vessels were closed and placed into the segment and the content was mineralized using an Ethos SEL Microwave Labstation (Milestone, Italy) at 220°C for 35 min, applying a maximal power of 1000 W. The microwave programme was started by steadily increasing the temperature over 15 min, followed by holding the temperature for an additional 20 min. After cooling, each resulting solution was transferred to 50 mL glass flasks and filled to the mark with deionized water. Samples were diluted to 1 : 19 with deionized water prior to further analysis. Copper content was measured using air-acetylene flame atomization in a contrAA 700 atomic absorption spectrometer (Analytik Jena, Germany). All samples were measured in triplicate and the obtained values were processed by Aspect CS software, version 2.1.

2.2.6. Swelling Capacity. To determine swelling capacity, a previously reported method was improved [20]. The test was performed in a medium that properly simulates vaginal conditions. 100 mg of each sample was put into fine mesh baskets and immersed in a pH 4.5 medium (natural vaginal environment—6.80 g of potassium dihydrogen phosphate R in 1000.0 mL of water R) and a pH 6.0 medium (infected vaginal environment—6.8 g of sodium dihydrogen phosphate R in 1000.0 mL of water R, pH adjustment with strong sodium hydroxide solution R). The baskets were pulled out at time intervals of 5, 10, 15, 30, and 45 min and 1, 2, 3, 4, 5, and 6 hours after the first immersion, properly dried, and weighed. Swelling capacity was calculated using the following equation [21]:

$$S_{SW} = \left(\frac{W_t - W_0}{W_0} \right) \times 100\,(\%)\,. \quad (1)$$

S_{SW} is swelling capacity expressed as a percentage of weight addition, W_t is the weight of a sample at the relevant time interval, and W_0 represents the initial weight of the sample. For each batch, the measurement was performed three times and results were expressed as mean values with standard deviations.

2.2.7. Antimicrobial Activity: Bacterial Strains and MIC Determination. *E. coli* (CCM 4517) was maintained in a blood agar. To determine minimal inhibition concentration (MIC), an overnight culture of *E. coli* cells was suspended in a fresh LB (Luria broth) medium and grown to OD_{600} 0.5 at 37°C at a shaking speed of 250 rpm.

Candida albicans (CCM 8186) was maintained in an YNB (Yeast Nitrogen Base with ammonium sulfate) medium at 37°C. For MIC determination, an overnight culture was suspended in a fresh YNB medium and grown to OD_{600} 0.5 at 37°C at a shaking speed of 250 rpm.

A suitable amount of CMC microparticles was suspended in the growth media (LB medium for *E. coli*, YNB for *C. albicans*) to prepare a 10% suspension and incubated for 60 min at room temperature to release the copper into solution. Undissolved particles were then separated by centrifugation and discarded and atomic absorption was used to determine copper concentration. Twofold dilutions of copper suspension were prepared in appropriate mediums in a microtiter plate (100 μL/well in triplicate). Then, 10e6 cells (*E. coli* or *C. albicans*) were added to each well of the microtiter plate and incubated at 37°C. To monitor cell growth, optical density was measured spectrophotometrically (OD_{600}) after 20 hrs of incubation. The mean of the three wells was calculated to evaluate antimicrobial activity. Wells containing the *E. coli* or *C. albicans* without copper inhibition were included in triplicate in all tested plates as controls. The MIC value was expressed as the concentration of copper in a well showing at least a fourfold reduction of OD_{600} absorbance compared to each subsequent well.

3. Results and Discussion

The copper cross-linked carmellose microparticles were evaluated for particle size, sphericity factor, and copper content (Table 2). The equivalent diameter of the prepared particles ranged from 738.1 ± 30.3 to 1078 ± 12.4 μm. It seems that particle size did not depend on the concentration of the Cu^{2+} hardening solution. However, it was observed that it did increase with increasing CMC concentration which can be attributed to the increased viscosity [22, 23]. Viscosity of the 1% CMC dispersion was found to be 162 ± 0.21 mPa·s and that of the 2% CMC dispersion 766.67 ± 0.47 mPa·s. A polymer dispersion with higher viscosity is more difficult to form into smaller droplets [24]; thus these dispersions yielded larger particles. Another influence on the particle size of microspheres could be seen in the degree of CMC chain shrinkage. Generally, particle size decreases inversely with the degree of shrinkage. It has been well documented that the degree of shrinkage is typically higher for beads prepared from a dispersion with lower polymer concentration [25, 26].

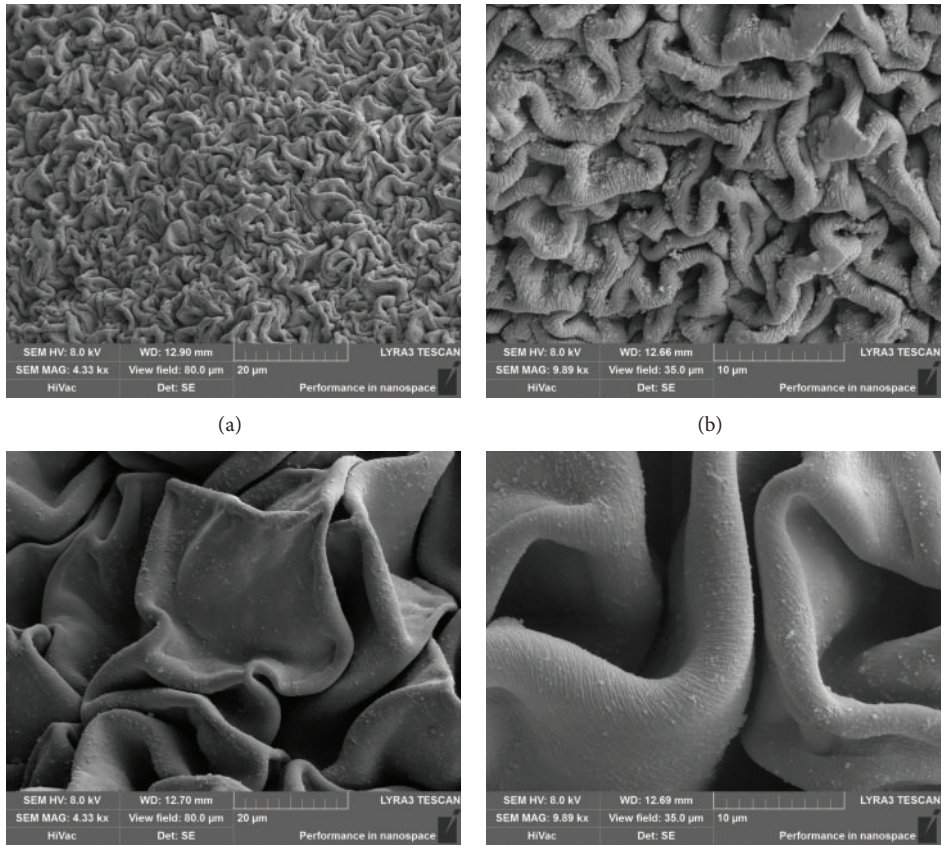

Figure 1: SEM photographs of surface topography of CMC microparticles: (a) MP-1_0.5 (magnification 4330x), (b) surface detail of MP-1_0.5 (magnification 9890x), (c) MP-2_0.5 (magnification 4330x), and (d) surface detail of MP-2_0.5 (magnification 9890x).

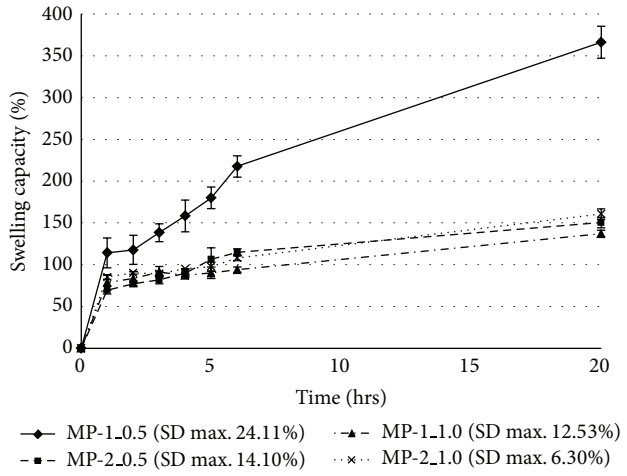

Figure 2: Degree of swelling in Cu^{2+} cross-linked microparticles at pH 4.5.

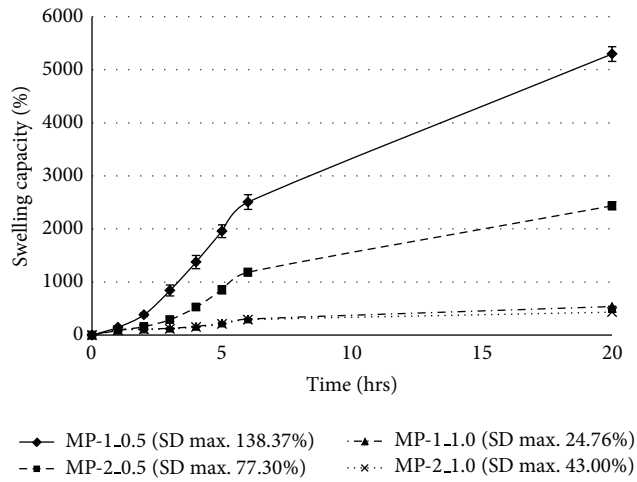

Figure 3: Degree of swelling in Cu^{2+} cross-linked microparticles at pH 6.0.

A comparison of the microparticle surfaces (MP-1_0.5; ED = 775.7 μm versus MP-2_0.5; ED = 1016.9) in Figure 1 confirms these findings. From these SEM photographs, it is evident that the degree of CMC shrinkage was significantly higher for the smaller 1% CMC microspheres.

Prepared CMC microspheres exhibited sufficient sphericity, ranging from 0.850 ± 0.067 to 0.934 ± 0.038. Previous studies indicate that particles with this parameter value above 0.8 are considered to have good sphericity [27]. It can be observed from the results that the sphericity was not clearly

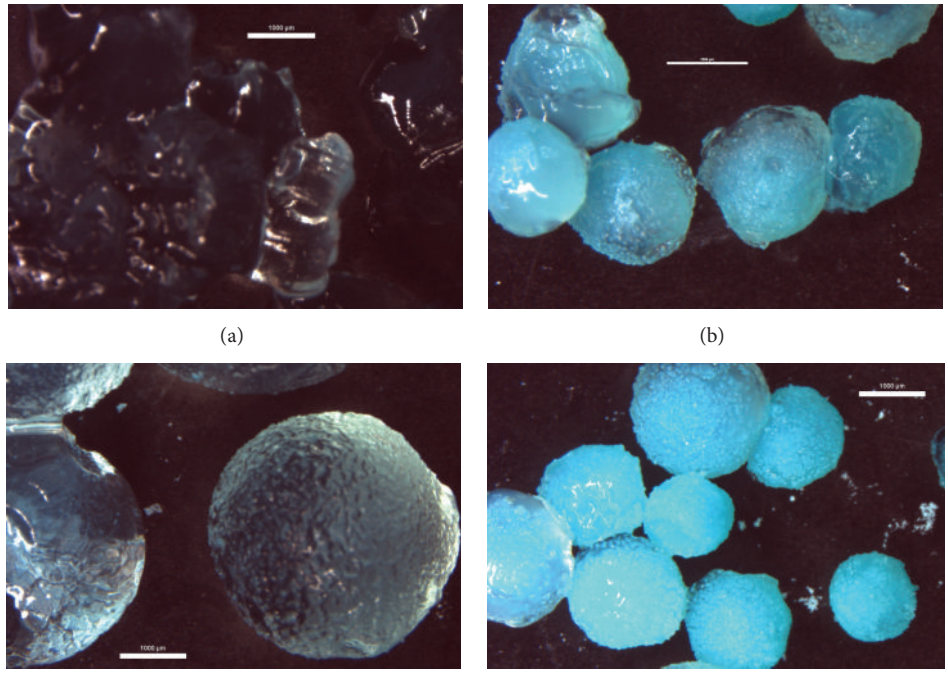

(a) (b) (c) (d)

Figure 4: Optical microscope images of CMC particles after 20-hour swelling capacity test in pH 6.0 buffer; bars correspond to 1000 μm: (a) MP-1_0.5, (b) MP-1_1.0, (c) MP-2_0.5, and (d) MP-2_1.0.

Table 2: Microparticle characteristics: equivalent diameter, sphericity factor, and copper content.

Sample	ED (μm)	SD (μm)	SF	SD	Copper content (g/kg)	SD (g/kg)
MP-1_0.5	775.7	30.2	0.906	0.044	101.3	0.65
MP-1_1.0	888.5	58.4	0.934	0.038	143.6	2.31
MP-1_1.5	738.1	30.3	0.887	0.056	152.3	0.19
MP-1_2.0	798.6	87.9	0.855	0.059	173.0	2.15
MP-2_0.5	1016.9	22.8	0.891	0.040	143.6	0.26
MP-2_1.0	1078.0	12.4	0.886	0.071	164.7	0.40
MP-2_1.5	922.1	57.6	0.850	0.067	187.6	1.32
MP-2_2.0	933.6	38.6	0.874	0.057	200.3	1.03

influenced by increasing the concentration of the hardening solution, but it was noticed that hardening solutions with lower molarity of $CuCl_2$ (0.5 and 1.0%) yielded microspheres with higher sphericity values. On the other hand, particle sphericity was lower in samples prepared with a higher polymer concentration, with the exception of samples MP-1_2.0 and MP-2_2.0, which were prepared with 2 M of $CuCl_2$ hardening solution. Previously reported results confirmed that increasing the concentration of CMC solutions linearly increases the solution viscosity [28] and sphericity of particles. Our results generally coincide with findings that overly viscous polymer solutions (2% in our case) form less spherical, tail-shaped particles [29] and particles with a rough surface [30].

Table 2 also shows the results of atomic absorption analysis for copper content. Copper content in the prepared microparticles ranged from 101.3 ± 0.65 to 200.3 ± 1.03 g/kg. It was observed that the content significantly increased with increases in hardening solution concentration as well as polymer concentration.

The samples of microspheres with the highest sphericity (MP-1_0.5, MP-1_1.0, MP-2_0.5, and MP-2_1.0), which is one the most important criteria for the preparation of particle systems, were then investigated for swelling capacity in phosphate buffers with pH 4.5 [31] and pH 6.0 [32], respectively, to simulate natural and inflamed vaginal conditions and to predict their behaviour on vaginal mucosa for a 20-hour time interval (20-hour interval represents an estimated time of therapy). The obtained results can be seen in Figure 2 for pH 4.5 and in Figure 3 for pH 6.0. Figure 4 shows images of microparticles after a 20-hour swelling capacity test in a pH 6.0 buffer. Generally, it was observed that the swelling capacity of all samples gradually increased during the test. Selected samples exhibited pH-responsive behaviour which differed based on the tested environments; swelling was substantially higher at pH 6.0 [33]. It is obvious from

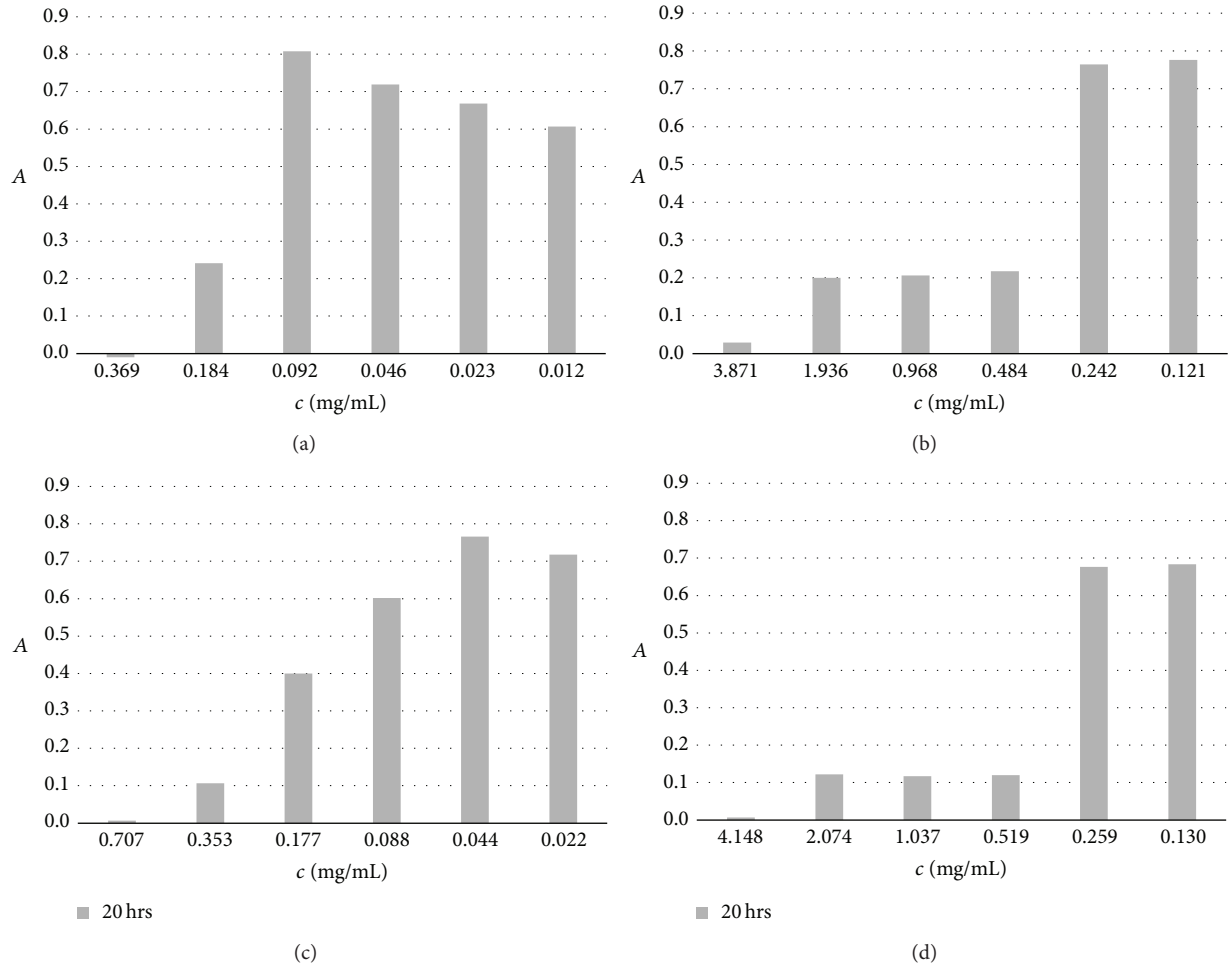

Figure 5: MIC results of CMC microparticles against *Escherichia coli*; (a) MP-1_0.5, (b) MP-1_1.0, (c) MP-2_0.5, and (d) MP-2_1.0.

Figures 2 and 3 that sample MP-1_0.5, prepared with a less-concentrated hardening solution (0.5 M) and a lower CMC concentration (1%), had the highest swelling capacity at both pH values (366.2% at pH 4.5 after 20 hrs, 5296.3% at pH 6.0 after 20 hrs). These values of formulation variables led to the creation of favourable conditions for water uptake into the microsphere matrix, resulting in the creation of an amorphous gel structure at pH 6.0 (see Figure 4(a)). Also, the enormous loss of the blue colour in comparison with sample MP-2_1.0 (Figure 4(d)) can be noticed, probably related to high water uptake and higher release of the copper ions which are responsible for the blue colour. This is uniquely in accordance with previously published data saying that increased polymer or hardening solution concentrations can significantly reduce water uptake due to the increased density of the polymer network [34]. At pH 6.0, sample MP-2_0.5 followed with swelling capacity of 2436.0% in 20 hrs. At pH 4.5, however, its swelling was comparable with samples cross-linked with 1 M $CuCl_2$, which exhibited a lower swelling capacity ranging from 137.2% to 160.7% after 20 hrs at pH 4.5 and 433.0%–539.1% at pH 6.0 (results for pH 6.0 are clearly evident in Figures 4(b) and 4(d)). No influence on swelling capacity as a result of particle size was observed.

The mechanism for the antibacterial activity of Cu^{+} ions is based on their energetically easier movement across a lipid bilayer and uptake by the cell, generating reactive oxygen species, leading to lipid peroxidation and protein oxidation [35]. The excess of copper causes a decrease in the membrane integrity of a microorganism, which causes the particular cell to leak nutritional elements, like potassium and glutamate, which lead to desiccation and, ultimately, cell death [36]. The antimicrobial activity of selected CMC microparticles cross-linked by Cu^{2+} was evaluated by MIC test using Gram-negative *Escherichia coli* and *Candida albicans* yeast (see Figures 5 and 6). The test expresses the minimum concentration of antimicrobial agent that inhibits the visible growth of microorganisms [37]. The test was triplicated. For *E. coli,* MIC values after 20 hrs of incubation were 0.184, 0.484, 0.353, and 0.519 mg/mL for samples MP-1_0.5, MP-1_1.0, MP-2_0.5, and MP-2_1.0, respectively. MIC values for *C. albicans* were higher for the same samples: 0.740, 1.639, 0.598, and 1.087 mg/mL, respectively. Higher MIC values for *C. albicans* in comparison with the values for *E. coli* can be explained by the higher resistance of the yeast to the copper's antibacterial effect. Weissman et al. confirm this, reporting on the isolation of two genes involved

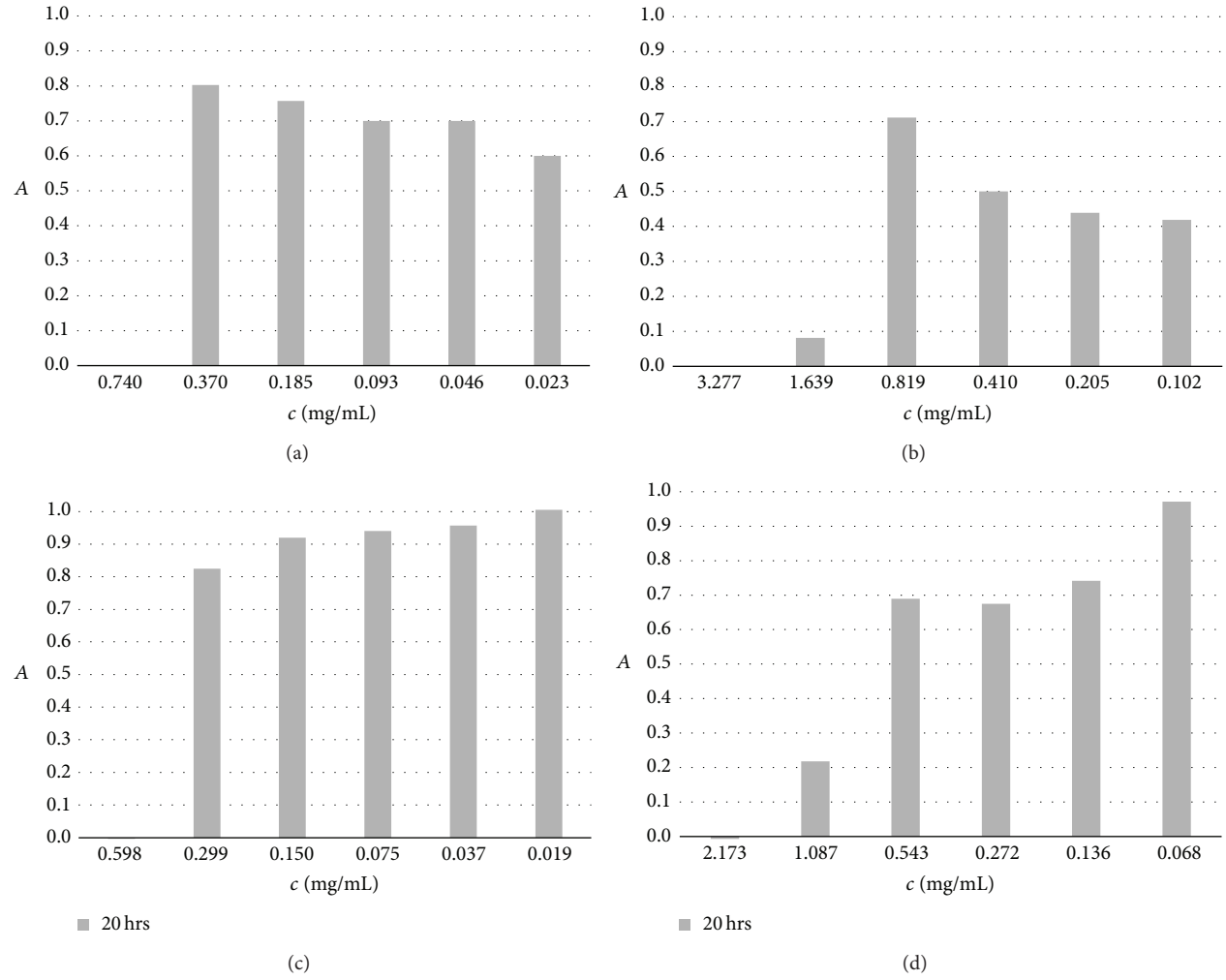

Figure 6: MIC results of CMC microparticles against *Candida albicans*; (a) MP-1_0.5, (b) MP-1_1.0, (c) MP-2_0.5, and (d) MP-2_1.0.

in copper detoxification in *C. albicans*: metallothionein, CaCUP1, and a copper-transporting P-type ATPase, CaCRP1 [38]. These two genes account for *C. albicans*'s resistance to copper and consequently the vast differences in our results.

The obtained MIC values prove substantial antimicrobial activity against both microorganisms tested in this study and are in good agreement with copper MIC values against strains of *E. coli* and *C. albicans* described by different authors in other studies. Martínez Medina et al. reported MIC values for Cu(II) complexes of 0.375 mg/mL and >1.5 mg/mL for *E. coli* and *C. albicans*, respectively [39]. Copper nanoparticles prepared by Zain et al. (200 nm) showed MIC values of 0.433 mg/L for *E. coli* [40], and those prepared by Ruparelia et al. (9 nm) showed MIC values of 0.280 mg/mL for *E. coli* [41].

Despite the lower content of copper in microspheres, the samples prepared using the less-concentrated $CuCl_2$ (0.5 M) solution—MP-1_0.5 and MP-2_0.5—exhibited lower MIC values and so better antibacterial activity against both tested pathogens in comparison with samples cross-linked in the more potent 1 M $CuCl_2$ solution. These results confirmed the great influence of the microparticle swellability on MIC values. Both samples exhibited high swelling capacity at pH 6.0 (see Figure 3) and thus good conditions for the release of copper ions from particles (pH of LB and YNB medium was also close to 6.0). Against *E. coli*, sample MP-1_0.5 was found to be the most effective, as it probably exhibited faster copper release. This could be a result of the higher cumulation of copper ions on more rougher surface (see Figures 1(a) and 1(b)) and also smaller particle size (see Table 2) and thus larger surface area [42]. These characteristics could promote faster swelling, leading to the creation of an amorphous structure during the 20-hour interval (Figure 4(a)). Against the more resistant *C. albicans*, however, the most effective sample was MP-2_0.5, exhibiting probably more uniform copper release due to the higher CMC concentraction (2%), more uniform copper distribution in the microspheres, and larger particle size (see Table 2). This theory is also supported by the fact that the MP-2_0.5 microparticles maintained their shape-specific structure after 20 hrs of swelling (Figure 4(c)).

4. Conclusion

In this experimental work, CMC dispersions of two different concentrations (1% and 2%) were cross-linked by copper (II) ions (0.5, 1, 1.5, or 2.0 M $CuCl_2$) to prepare microspheres with antimicrobial activity against frequently occurring vaginal pathogens *Escherichia coli* and *Candida albicans*. All tested samples exhibited stable but pH responsive behaviour in environments corresponding with natural and inflamed vaginal conditions and proved substantial antimicrobial activity against both pathogens. The most effective samples were those hardened in a less-concentrated $CuCl_2$ (0.5 M) solution. Unexpectedly, a crucial parameter for microsphere antimicrobial activity was not found in the copper content but in the swelling capacity of the microparticles and in the degree of CMC surface shrinking. The sample prepared using a 1% CMC dispersion cross-linked by 0.5 M $CuCl_2$ seemed to be the most suitable for potential vaginal use not only due to its antibacterial activity but also due to its gradual change to a nonspecific-shaped gel which is preferable when considering vaginal dosage forms.

Conflict of Interests

The authors declare that there is no conflict of interests regarding the publication of this paper.

References

[1] L. Fan, M. Peng, Z. Zhou et al., "Modification of carboxymethyl cellulose Grafted with collagen peptide and its antioxidant aktivity," *Carbohydrate Polymers*, vol. 112, pp. 32–38, 2014.

[2] N. Haleem, M. Arsah, M. Shahid, and A. M. Tahir, "Synthesis of carboxymethyl cellulose from waste of cotton ginning industry," *Carbohydrate Polymers*, vol. 113, pp. 249–255, 2014.

[3] J.-F. Su, Z. Huang, X.-Y. Yuan, X.-Y. Wang, and M. Li, "Structure and properties of carboxymethyl cellulose/soy protein isolate blend edible films crosslinked by Maillard reactions," *Carbohydrate Polymers*, vol. 79, no. 1, pp. 145–153, 2010.

[4] H. Kono, "Characterization and properties of carboxymethyl cellulose hydrogels crosslinked by polyethylene glycol," *Carbohydrate Polymers*, vol. 106, no. 1, pp. 84–93, 2014.

[5] E. A. Hassn, M. L. Hassan, N. C. Moorefield, and G. R. Newkome, "New supramolecular metallo-terpyridine carboxymethyl cellulose derivatives with antimicrobial properties," *Carbohydrate Polymers*, vol. 116, pp. 2–8, 2014.

[6] S. Sayanjali, B. Ghanbarzadeh, and S. Ghiassifar, "Evaluation of antimicrobial and physical properties of edible film based on carboxymethyl cellulose containing potassium sorbate on some mycotoxigenic *Aspergillus* species in fresh pistachios," *LWT—Food Science and Technology*, vol. 44, no. 4, pp. 1133–1138, 2011.

[7] A. A. Hebeish, M. H. El-Rafie, F. A. Abdel-Mohdy, E. S. Abdel-Halim, and H. E. Emam, "Carboxymethyl cellulose for green synthesis and stabilization of silver nanoparticles," *Carbohydrate Polymers*, vol. 82, no. 3, pp. 933–941, 2010.

[8] K. Liu, Y. Xu, X. Lin et al., "Synergistic effects of guanidine-grafted CMC on enhancing antimicrobial activity and dry strength of paper," *Carbohydrate Polymers*, vol. 110, pp. 382–387, 2014.

[9] L. Upadhyaya, J. Singh, V. Agarwal, and R. P. Tewari, "Biomedical applications of carboxymethyl chitosans," *Carbohydrate Polymers*, vol. 91, no. 1, pp. 452–466, 2013.

[10] A.-H. Yu, H.-Y. Hsieh, J.-C. Pang et al., "Active films from water-soluble chitosan/cellulose composites incorporating releasable caffeic acid for inhibition of lipid oxidation in fish oil emulsions," *Food Hydrocolloids*, vol. 32, no. 1, pp. 9–19, 2013.

[11] T. Zhong, G. S. Oporto, J. Jaczynski, A. T. Tesfai, and J. Armstrong, "Antimicrobial properties of the hybrid copper nanoparticles-carboxymethyl cellulose," *Wood and Fiber Science*, vol. 45, no. 2, pp. 215–222, 2013.

[12] G. E. Jackson, P. M. May, and D. R. Williams, "Metal-ligand complexes involved in rheumatoid arthritis-I: justifications for copper administration," *Journal of Inorganic and Nuclear Chemistry*, vol. 40, no. 6, pp. 1189–1194, 1978.

[13] O. A. El-Gammal, E. A. Elmorsy, and Y. E. Sherif, "Evaluation of the anti-inflammatory and analgesic effects of Cu(II) and Zn(II) complexes derived from 2-(naphthalen-1-yloxy)-N'-(1-(pyridin-2-1) ethylidene) acetohydrazide," *Spectrochimica Acta Part A: Molecular and Biomolecular Spectroscopy*, vol. 120, pp. 332–339, 2014.

[14] S. Odisitse and G. E. Jackson, "In vitro and in vivo studies of N,N′-bis[2(2-pyridyl)-methyl]pyridine-2,6-dicarboxamide-copper(II) and rheumatoid arthritis," *Polyhedron*, vol. 27, no. 1, pp. 453–464, 2008.

[15] A. Hussain and F. Ahsan, "The vagina as a route for systemic drug delivery," *Journal of Controlled Release*, vol. 103, no. 2, pp. 301–313, 2005.

[16] L. M. Ensign, T. E. Hoen, K. Maisel, R. A. Cone, and J. S. Hanes, "Enhanced vaginal drug delivery through the use of hypotonic formulations that induce fluid uptake," *Biomaterials*, vol. 34, no. 28, pp. 6922–6929, 2013.

[17] B. B. Saxena, M. Singh, R. M. Gospin, C. C. Chu, and W. J. Ledger, "Efficacy of nonhormonal vaginal contraceptives from a hydrogel delivery system," *Contraception*, vol. 70, no. 3, pp. 213–219, 2004.

[18] M. L. González-Rodríguez, M. A. Holgado, C. Sánchez-Lafuente, A. M. Rabasco, and A. Fini, "Alginate/chitosan particulate systems for sodium diclofenac release," *International Journal of Pharmaceutics*, vol. 232, no. 1-2, pp. 225–234, 2002.

[19] C. H. Goh, P. W. S. Heng, and L. W. Chan, "Alginates as a useful natural polymer for microencapsulation and therapeutic applications," *Carbohydrate Polymers*, vol. 88, no. 1, pp. 1–12, 2012.

[20] W.-C. Lin, D.-G. Yu, and M.-C. Yang, "pH-sensitive polyelectrolyte complex gel microspheres composed of chitosan/sodium tripolyphosphate/dextran sulfate: swelling kinetics and drug delivery properties," *Colloids and Surfaces B: Biointerfaces*, vol. 44, no. 2-3, pp. 143–151, 2005.

[21] K. G. H. Desai and H. J. Park, "Preparation and characterization of drug-loaded chitosan-tripolyphosphate microspheres by spray drying," *Drug Development Research*, vol. 64, no. 2, pp. 114–128, 2005.

[22] K. M. Rao, B. Mallikarjuna, K. K. Rao, M. N. Prabhakar, K. C. Rao, and M. C. Subha, "Preparation and characterization of pH sensitive poly(vinyl alcohol)/sodium carboxymethyl cellulose IPN microspheres for in vitro release studies of an anti-cancer drug," *Polymer Bulletin*, vol. 68, no. 7, pp. 1905–1919, 2012.

[23] M. A. Saleem, Y. D. Murali, M. D. Naheed, P. Jaydeep, and M. Dhaval, "Prepapation and evaluation of valsartan loaded hydrogel beads," *International Research Journal of Pharmacy*, vol. 3, no. 6, pp. 80–85, 2012.

[24] Y. Y. Yang, J. P. Wan, T. S. Chung, P. K. Pallathadka, S. Ng, and J. Heller, "POE-PEG-POE triblock copolymeric microspheres containing protein. I. Preparation and characterization," *Journal of Controlled Release*, vol. 75, no. 1-2, pp. 115–128, 2001.

[25] H. Brandenberger and F. Widmer, "A new multinozzle encapsulation/immobilisation system to produce uniform beads of alginate," *Journal of Biotechnology*, vol. 63, no. 1, pp. 73–80, 1998.

[26] E.-S. Chan, B.-B. Lee, P. Ravindra, and D. Poncelet, "Prediction models for shape and size of ca-alginate macrobeads produced through extrusion-dripping method," *Journal of Colloid and Interface Science*, vol. 338, no. 1, pp. 63–72, 2009.

[27] P. B. Deasy and M. F. L. Law, "Use of extrusion-spheronization to develop an improved oral dosage form of indomethacin," *International Journal of Pharmaceutics*, vol. 148, no. 2, pp. 201–209, 1997.

[28] X. H. Yang and W. L. Zhu, "Viscosity properties of sodium carboxymethylcellulose solutions," *Cellulose*, vol. 14, no. 5, pp. 409–417, 2007.

[29] E.-S. Chan, "Preparation of Ca-alginate beads containing high oil content: influence of process variables on encapsulation efficiency and bead properties," *Carbohydrate Polymers*, vol. 84, no. 4, pp. 1267–1275, 2011.

[30] M. S. Kim, S. J. Park, B. K. Gu, and C.-H. Kim, "Ionically crosslinked alginate-carboxymethyl cellulose beads for the delivery of protein therapeutics," *Applied Surface Science*, vol. 262, pp. 28–33, 2012.

[31] C. Valenta, "The use of mucoadhesive polymers in vaginal delivery," *Advanced Drug Delivery Reviews*, vol. 57, no. 11, pp. 1692–1712, 2005.

[32] S. F. Borges, J. G. L. Silva, and P. C. M. Teixeira, "Survival and biofilm formation of Listeria monocytogenes in simulated vaginal fluid: influence of pH and strain origin," *FEMS Immunology and Medical Microbiology*, vol. 62, no. 3, pp. 315–320, 2011.

[33] R. Barbucci, A. Magnani, and M. Consumi, "Swelling behavior of carboxymethylcellulose hydrogels in relation to cross-linking, pH, and charge density," *Macromolecules*, vol. 33, no. 20, pp. 7475–7480, 2000.

[34] J. Berger, M. Reist, J. M. Mayer, O. Felt, N. A. Peppas, and R. Gurny, "Structure and interactions in covalently and ionically crosslinked chitosan hydrogels for biomedical applications," *European Journal of Pharmaceutics and Biopharmaceutics*, vol. 57, no. 1, pp. 19–34, 2004.

[35] U. Bogdanović, V. Lazić, V. Vodnik, M. Budimir, Z. Marković, and S. Dimitrijević, "Copper nanoparticles with high antimicrobial activity," *Materials Letters*, vol. 128, pp. 75–78, 2014.

[36] J. Konieczny and Z. Rdzawski, "Antibacterial properties of copper and its alloys," *Archives of Materials Science and Engineering*, vol. 56, no. 2, pp. 53–60, 2012.

[37] S. M. Magaña, P. Quintana, D. H. Aguilar et al., "Antibacterial activity of montmorillonites modified with silver," *Journal of Molecular Catalysis A: Chemical*, vol. 281, no. 1-2, pp. 192–199, 2008.

[38] Z. Weissman, I. Berdicevsky, B.-Z. Cavari, and D. Kornitzer, "The high copper tolerance of *Candida albicans* is mediated by a P-type ATPase," *Proceedings of the National Academy of Sciences of the United States of America*, vol. 97, no. 7, pp. 3520–3525, 2000.

[39] J. J. Martínez Medina, M. S. Islas, L. L. López Tévez, E. G. Ferrer, N. B. Okulik, and P. A. M. Williams, "Copper(II) complexes with cyanoguanidine and o-phenanthroline: theoretical studies, in vitro antimicrobial activity and alkaline phosphatase inhibitory effect," *Journal of Molecular Structure*, vol. 1058, no. 1, pp. 298–307, 2014.

[40] N. M. Zain, A. G. F. Stapley, and G. Shama, "Green synthesis of silver and copper nanoparticles using ascorbic acid and chitosan for antimicrobial applications," *Carbohydrate Polymers*, vol. 112, pp. 195–202, 2014.

[41] J. P. Ruparelia, A. K. Chatterjee, S. P. Duttagupta, and S. Mukherji, "Strain specificity in antimicrobial activity of silver and copper nanoparticles," *Acta Biomaterialia*, vol. 4, no. 3, pp. 707–716, 2008.

[42] J. Zhao, H. J. Feng, H. Q. Tang, and J. H. Zheng, "Bactericidal and corrosive properties of silver implanted TiN thin films coated on AISI317 stainless steel," *Surface and Coatings Technology*, vol. 201, no. 9–11, pp. 5676–5679, 2007.

Hindawi Publishing Corporation
BioMed Research International
Volume 2015, Article ID 328628, 13 pages
http://dx.doi.org/10.1155/2015/328628

Research Article

Development of *In Vitro-In Vivo* Correlation/Relationship Modeling Approaches for Immediate Release Formulations Using Compartmental Dynamic Dissolution Data from "Golem": A Novel Apparatus

Martin Čulen,[1,2] Paweł K. Tuszyński,[3] Sebastian Polak,[4,5] Renata Jachowicz,[3] Aleksander Mendyk,[3] and Jiří Dohnal[6]

[1] *Department of Chemical Drugs, Faculty of Pharmacy, University of Veterinary and Pharmaceutical Sciences Brno, Palackého 1-3, 612 42 Brno, Czech Republic*
[2] *Department of Internal Medicine, Hematology and Oncology, Faculty of Medicine, Masaryk University, Kamenice 5, 625 00 Brno, Czech Republic*
[3] *Department of Pharmaceutical Technology and Biopharmaceutics, Faculty of Pharmacy, Jagiellonian University Medical College, Medyczna 9 Street, 30-688 Kraków, Poland*
[4] *Department of Pharmacoepidemiology and Pharmacoeconomics and Department of Social Pharmacy, Faculty of Pharmacy, Jagiellonian University Medical College, Medyczna 9 Street, 30-688 Kraków, Poland*
[5] *Simcyp (a Certara Company) Limited, Blades Enterprise Centre, John Street, Sheffield S2 4SU, UK*
[6] *Department of Applied Pharmacy, Faculty of Pharmacy, University of Veterinary and Pharmaceutical Sciences Brno, Palackého 1-3, 612 42 Brno, Czech Republic*

Correspondence should be addressed to Martin Čulen; mculen@gmail.com

Received 30 June 2014; Accepted 18 August 2014

Academic Editor: Kin Tam

Different batches of atorvastatin, represented by two immediate release formulation designs, were studied using a novel dynamic dissolution apparatus, simulating stomach and small intestine. A universal dissolution method was employed which simulated the physiology of human gastrointestinal tract, including the precise chyme transit behavior and biorelevant conditions. The multicompartmental dissolution data allowed direct observation and qualitative discrimination of the differences resulting from highly pH dependent dissolution behavior of the tested batches. Further evaluation of results was performed using IVIVC/IVIVR development. While satisfactory correlation could not be achieved using a conventional deconvolution based-model, promising results were obtained through the use of a nonconventional approach exploiting the complex compartmental dissolution data.

1. Introduction

An orally administered drug has to be released from its dosage form, dissolved in the surrounding fluid and absorbed by the gut wall, in order to enter the blood stream. Dissolution testing in pharmacy studies the first two processes and is not only a vital tool for assessment of quality of a pharmaceutical, but also a tool for elucidation and simulation of these effects *in vitro*. The research in drug development facilitates dissolution to uncover and predict many crucial aspects influencing the fate of an administered active pharmaceutical ingredient (API) in the gastrointestinal tract (GIT), while employing a wide variety of innovative and special apparatuses, either based on the conventional pharmacopeial tools or having a completely original design [1]. Such instruments usually involve only one or two compartments, and they functionally often address only a specific focus of a study, that is, drug precipitation, mechanical qualities of a dosage form, and so forth [2]. However, a more complex simulation of the GIT is often needed, and currently only TIM-1 apparatus fully

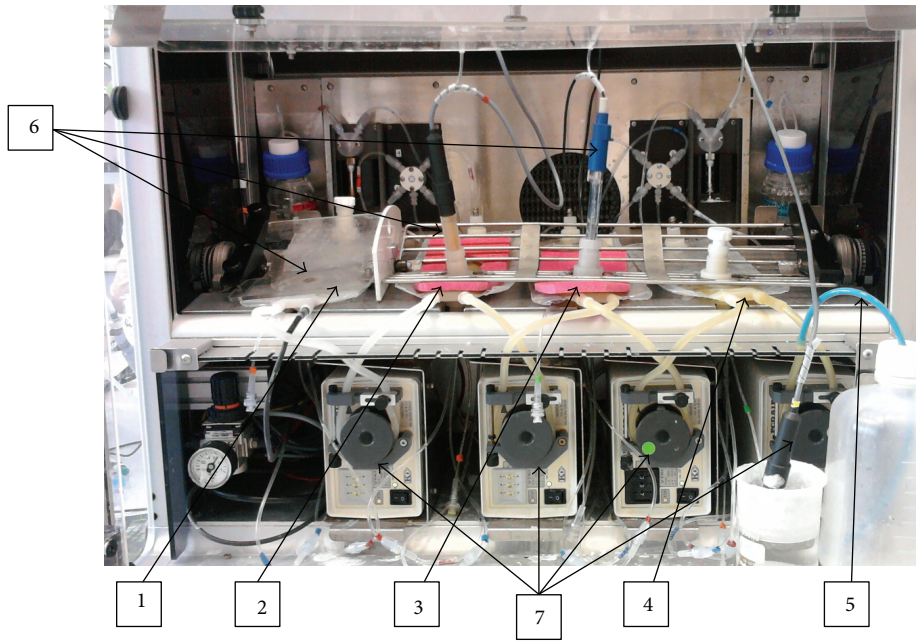

Figure 1: Front view with description of main components: (1) stomach, (2) duodenum, (3) jejunum, (4) ileum, (5) collection canister tubing, (6) pH probes, and (7) peristaltic pumps.

enables *in vitro* testing in completely biorelevant conditions ranging from stomach to ileum [3].

In order to provide other means of highly biorelevant and dynamic dissolution testing, our team has developed a novel four-compartmental dissolution apparatus, named "Golem," which simulates the dissolution processes in stomach and small intestine (SI). This paper discusses the application and evaluation of this apparatus, performed with several generic and reference batches of immediate release tablets containing atorvastatin (ATV). This drug was chosen due to the availability of *in vivo* data from subsequent bioequivalence (BE) studies for the tested formulations.

ATV is characterized by low solubility in water and high permeability and is hence classified as a Class II drug in the Biopharmaceutical Classification System (BCS) [4]. Dissolution is the rate-limiting step in absorption of ATV, and IVIVC could be expected according to the BCS theory. But being a drug of limited bioavailability, due to high variability in first-pass metabolism, makes it difficult to correlate the conventional *in vitro* tests results with blood concentration in time (or other pharmacokinetic parameters). Therefore an attempt to establish an *in vitro-in vivo* correlation/relationship model for this drug was made, based on the dissolution data obtained from this novel unconventional dissolution instrument.

2. Materials and Methods

2.1. Golem Apparatus. The instrument is a computer controlled artificial digestive tract, designed for dynamic dissolution testing of oral dosage forms and consisting of four compartments: stomach, duodenum, jejunum, and ileum (see Figure 1). Physiological conditions are maintained in the system with the possibility of adjusting all method parameters, for example, pH, volumes, transit times, temperature, and so forth. The dissolution in fed state can be tested with liquid meal (e.g., Nutridrink, Ensure Plus, or very finely homogenized solid meal to prevent clogging of the pump tubes). The transport of chyme in Golem is driven by peristaltic pumps placed between each two subsequent compartments, where the fourth pump leads the chyme from the ileum into the collection canister (waste). The pH in the compartments is checked automatically by pH probes and is manually adjusted by injection of either 1 M NaOH + 0.24 M $NaHCO_3$ or 1 M HCl solution.

The compartments are made from modified common intravenous bags (the plastic was tested for interaction with various APIs). The bags involve three ports: one holds plastic tubes for injection of pH altering solutions, enzymes, and sample collection; second port serves as a mouthpiece for the pH probe, and the third port is used for tablet insertion into the compartments. Temperature is kept at physiological 37°C and continuously checked separately for: (a) the heater platform; (b) the stomach compartment; (c) the air inside the apparatus box. Peristaltic movement is simulated by a V-shaped grate, pressed down on the bags, which rocks from side to side, driven by compressed air.

The operation of the apparatus requires one person for manual collection of samples and injection of enzymes, using common syringes.

From perspective of biorelevancy, the Golem apparatus is one of the three most complex dissolution apparatuses described to date (other two being TIM-1 and Dynamic Gastric Model) [3]. Its main advantage is that the complex

Table 1: Dissolution method description.

	Stomach	Duodenum	Jejunum	Ileum
Starting volume (mL)	30 (gastric juice) + 200 (deionized water)	33	33	33
Residence/transit time (min)	30; linear emptying	10	60	90
pH	2.4 (at 37°C)	6.5	6.6	7.4
Pepsin (mg/mL)	1.3	—	—	—
Lipase activity (U/mL)	—	70	70	70
Bile salts (mM)	—	3	3	3

functions are based on simple technical solutions which make the apparatus user friendly and easy to modify, and at the same time significantly less expensive than the alternatives.

The instrument was designed by Řezáčová, Dohnal, Jampílek and Čulen, and constructed by Development Workshops of the Institute of Organic Chemistry and Biochemistry of the Czech Academy of Sciences [5].

2.2. Dissolution Method. A method simulating fasted state and developed according to previous work was used in the study [6].

Prior to the dissolution experiments, the contents of the compartments were heated to 37°C. The experiments were started directly after insertion of a dosage form into the first stomach compartment. The gastric medium containing both the dissolved and undissolved contents of the dosage form was gradually moved by the peristaltic pump from stomach into the duodenal compartment and then into the following two compartments (an approximate scheme of chyme transfer in Golem is depicted in Figure 2). The medium thus underwent a dynamic change as it merged with the contents (starting volumes) of the next compartments. The starting dissolution medium was based on a physiological solution with pH modified by hydrochloric acid or bicarbonate buffer; pepsin was added only to the gastric compartment. The pH values, concentration of bile salts (bile extract porcine, Sigma-Aldrich), and lipase (pancreatin, Zentiva) in the SI compartments were maintained at steady levels throughout the experiment. The pH in stomach compartment was left to change, being influenced by the studied formulation. The detailed information on the method design is given in Table 1.

All experiments were performed in duplicates.

2.3. Sample Analysis. The samples were collected manualy using common syringe; 1 mL of sample was filtered through a 0.25 μm syringe filter, and the rest was returned into the apparatus. The withdrawal of the medium and dissolved API was considered in the calculations. The filtered sample was analyzed with HPLC (Waters) at $\lambda = 246$ nm.

2.4. Formulations Tested. In total, five generic (Zentiva) and three reference originator immediate release tablet batches were tested with Golem, all containing 80 mg of atorvastatin, present as a calcium salt. From the generic batches, four contained amorphous form of the drug (batches 85, 82, 01, and 02), which had higher intrinsic dissolution rate compared with the crystal form contained in the generic batch80 and

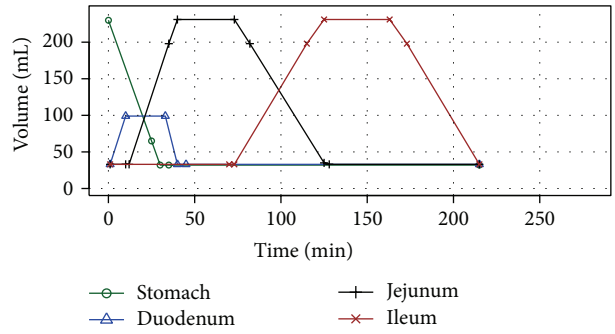

Figure 2: An approximated visual scheme of chyme transit in the Golem apparatus. A residual volume equal to the starting volume remained in each compartment, therefore the "total" amount moved through the apparatus was 200 mL.

all the reference batches (Lipitor, Sortis06, Sortis10) [10]. All formulations with the crystal ATV also contained $CaCO_3$ as a buffering agent used to raise the gastric pH and thus facilitate very early dissolution of ATV, which is a weak acid almost insoluble in pH below 4. The amorphous generic batches, on the other hand, contained no buffer, which was to slow down the faster dissolution of the amorphous form of the drug.

2.5. Pharmacokinetic (PK) Studies. The BE studies of the five generic formulations were evaluated in four crossover PK studies, performed by other contract workplaces: (a) Batch85 versus Sortis03, 24 subjects; (b) batches 01 and 02 versus Sortis03, 24 subjects; (c) batch82 versus Sortis10, 102 subjects; (d) batch80 versus Lipitor, 81 subjects.

2.6. Modeling. In order to establish a relationship between dissolution test results and actual results from *in vivo* studies, different modeling approaches were applied.

2.6.1. Classical Approach. A conventional method was based on a numeric deconvolution, where whole *in vitro* profiles of cumulative fraction dissolved were taken into account, with or without exclusion of the measurements from selected compartments. The *R* statistical computing software was used for modeling. An `Rivivc` package [11] and self-written *R* scripts were used to preprocess data and perform numerical deconvolution. In order to calculate fraction of drug absorbed in time, simulated *in vivo* profile (*i.v.* administration) was used as an equivalent to the unit impulse response (UIR).

Table 2: Intravenous administration simulation parameters.

Parameter group	Parameter	Value			Source
Physicochemical and binding	Mol. weight (g/mol)	**558.6**			[http://www.drugbank.ca/]
	log *P*	**5.7**			[http://www.drugbank.ca/]
	Compound type	Monoprotic Acid			[http://www.drugbank.ca/]
	pK_a 1	4.330			[http://www.drugbank.ca/]
	B/P	0.610			[7]
	Fu	0.107			[8]
ADME	Enzymatic clearance				
	Pathway	p-Hydroxy	o-Hydroxy	p-Hydroxy	
	Enzyme	CYP3A4	CYP3A4	CYP2C8	
	V_{max}	**29.800**	**29.300**	**0.290**	[9]
	K_m	**25.600**	**29.700**	**35.900**	
	fu mic	**0.662**	**0.662**	**0.662**	
	Total plasma clearance-CL (Hep)	**26.93 L/h**			[Fitted to the clinical data]

log *P*—logarithm of the octanol-water partition coefficient; pK_a—dissociation constant; B/P—blood-to-plasma partition coefficient; fu—fraction unbound in plasma; V_{max}—maximum reaction rate achieved by the system; K_m—substrate concentration at which the reaction rate is half of V_{max}.

Simulation of *in vivo* profile after *i.v.* administration was carried out on Simcyp Population-based Simulator V13R1 and was based on the results for ten virtual healthy patients [12]. Minimal PBPK model with single adjusting compartment (SAC) was utilized. Volume of distribution was calculated with use of the model based upon a modified version of the Poulin and Theil method [13]. Input information covered system data specific for the chosen population (as provided by simulator), trial design information (single 30 seconds long *i.v.* bolus, 80 mg), and compound specific data. Physicochemical, binding, and ADME (absorption, distribution, metabolism, and excretion) data are presented in Table 2. Renal clearance of ATV was assumed to be negligible [14].

2.6.2. Compartmental Approach. A second approach was based on direct scaling of the outcome of tests carried on Golem apparatus, where particular compartments were correlated with *in vivo* profiles.

2.7. Model's Predictability Evaluation. A proper IVIVC model should be established using formulations with different release rates. At minimum three (slow, medium, and fast dissolving) dosage forms should be designed, where the extreme ones are used to build a model able to predict *in vivo* bioperformance of the "middle" formulation. Such an approach is common when sustained-release dosage forms are tested but becomes problematic with immediate-release formulations (IR). All batches of the model drug, atorvastatin, were of immediate release and in the case of either the buffered or the nonbuffered formulations were behaving similarly. Therefore, external predictability and validation were evaluated when one formulation was characterized by medium rate release kinetics, used as testing formulation, and two other formulations were used for model building. In case of internal validation, testing formulation was included in model building phase. Whole or partial area under the curve (pAUC) prediction error (PE) (1) and C_{max} prediction error (2) was calculated [15]:

$$\text{pAUC\_PE}\,[\%] = \left[\frac{\left|\text{pAUC}_{\text{observed}} - \text{pAUC}_{\text{predicted}}\right|}{\text{pAUC}_{\text{observed}}}\right] * 100, \quad (1)$$

$$C_{\text{max}}\text{\_PE}\,[\%] = \left[\frac{\left|C_{\text{max,observed}} - C_{\text{max,predicted}}\right|}{C_{\text{max,observed}}}\right] * 100. \quad (2)$$

3. Results and Discussion

3.1. PK Studies. Bioavailability of the five generic batches was compared with three batches of the reference product (atorvastatin 80 mg manufactured by Pfizer, under the brand names Lipitor and Sortis, sold on different markets), in total of four consecutive PK studies. The PK data served as a qualitative "ladder" for the dissolution experiments and as basis for IVIV correlations.

The particular BE study results were as follows: (a) generic batch85 compared with Sortis03 showed C_{max} below the approved range for bioavailability (90% confidence interval (CI) ratio of 75%); (b) both batches 01 and 02 later showed much higher C_{max} than the reference Sortis03 (90% CI ratio 160 and 140%, resp.); (c) the batch82 was bioequivalent to Sortis10; (d) the much later developed batch80 (first generic batch with crystal API) has shown slightly higher but unacceptable bioavailability, with upper 90% CI of 127%. The average plasma concentration-time profiles are plotted together in Figure 3.

In general, the drug's pharmacokinetics showed a considerable interindividual variability, which is well reflected in the average PK profiles (see Figure 2). The most important origin of the variability seems to be the gut and liver metabolism of the drug [16]. An important observation from the average

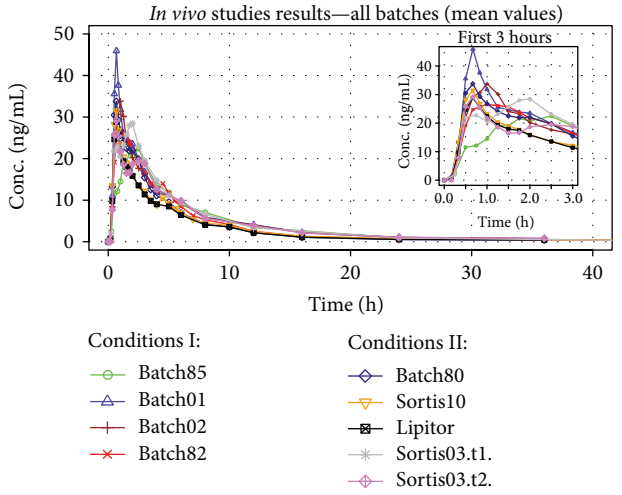

Figure 3: Bioequivalence studies results. Sortis03 was tested twice, in two PK studies.

PK curves is the very short T_{max} values (0.67–1.00 h), which suggested a very rapid dissolution and absorption in GIT.

3.2. Dissolution Results. The Golem dissolution experiments were started with batch80 and its reference product Lipitor, since both products contained the same crystal form of ATV, and both were buffered by $CaCO_3$, as excipient. The two formulations were run with the full-length fasted state dissolution method, lasting 215 min. Figure 4 shows the dissolution results as concentration or fraction of drug dissolved for all four Golem's compartments separately and also in a cumulative profile. Both formulations showed almost parallel dissolution profiles, but with higher dissolved amount in case of batch80, which qualitatively corresponded with the *in vivo* results. Generally, the tablets were observed to disintegrate in the first 3 min; the API quickly dissolved and the slight increase in the cumulative dissolved amount of API after 100 min could be mainly accounted for the higher pH in ileum. The fact that the fraction dissolved did not surpass 45% was most probably caused by the salting out effect of the Ca^{2+} counter-ion coming from the buffering excipient.

Since the maximum plasma concentrations *in vivo* were reached between 40 and 60 min and the dissolution profiles of the IR tablets provided little information at later time points, all further dissolution tests with the remaining batches were decided to be run with the same fasted state method but terminated directly after the sampling point at 43 min.

The further tested buffered formulations included two reference batches from the BE studies (Lipitor and Sortis10), plus one other batch of the reference product, Sortis06. All three reference batches showed almost identical dissolution behavior (see Figure 5), which confirmed that they were interchangeable in the dissolution experiments.

The dissolution testing of nonbuffered generic formulations revealed that no API dissolved in the stomach compartment, although the tablets disintegrated completely in less than 3 min. In contrast, all buffered formulations, generic and reference alike, raised the gastric pH to 7-8, which enabled rapid dissolution of ATV. The results came as a surprise in comparison with traditional USP II tests, which were performed with 900 mL of simple buffered media, where the pH was raised by the buffered formulations only to values around 4, thus prohibiting discrimination between the two formulation designs (unpublished results). This observed difference between the buffered and nonbuffered formulation in Golem provided a useful hint on the manner of *in vivo* dissolution behavior.

As for the nonbuffered batches, these generally provided higher fraction dissolved as they did not contain the $CaCO_3$ buffering agent. Other than that, the batch85 with low bioavailability *in vivo* had the lowest dissolution performance, followed by the bioequivalent batch82, and then the two batches with highest bioavailability—batch01 and batch02. However, the dissolution profiles for batches 01 and 02 were identical, and, according to similarity and difference factor, they also did not differ from the profile of batch82. Moreover, API powder which served as a control also showed identical dissolution performance to batches 01 and 02, indicating that the dissolution method lacked discriminatory power for these highly dissolving batches. This was caused by low medium volume (although physiological) in combination with lack of an absorption step (sink-condition). Nevertheless, the dissolution method was developed as a universal, most physiologically relevant simulation of fasted state, and as such it provided results beyond expectation. The obvious and simple option for improvement of dissolution testing of drugs with low solubility (such as atorvastatin) would be modification of the method by employing higher (unphysiological) medium volumes in the individual compartments, which would prevent early saturation of medium with the tested API. Of course, certain very lipophilic drugs would require unachievably high medium volumes to enable full dissolution of the administered dose. It is however questionable whether this is necessary when considering the fact that such drugs would neither be expected to fully dissolve *in vivo*. However, study of these effects was beyond the scope of the present study.

3.3. IVIVC-Classical Approach. The results depicted below follow a general agenda of *in vitro-in vivo* correlation level A, where fraction absorbed *in vivo* is directly correlated to the fraction dissolved *in vitro*. A linear function is preferred for this correlation, although other reasonable mathematical relationships are allowed when properly justified. The key procedure here was a deconvolution of a PK profile into the cumulative curve describing fraction absorbed *in vivo*. Since atorvastatin PK p.o. profile does not follow 1-compartment nor even 2-compartment model, classical Wagner-Nelson or Loo-Riegelman deconvolution methods could not be applied here. Instead, more sophisticated numerical deconvolution was employed. Numerical deconvolution relies on the availability of a PK profile of drug administered intravenously (*i.v.*), thus representing pure distribution/elimination phase, without absorption. Since in the presented case, bioassay protocol did not include such atorvastatin administration, an approximation of *i.v.* profile by computer simulations, carried out with Simcyp software, was used.

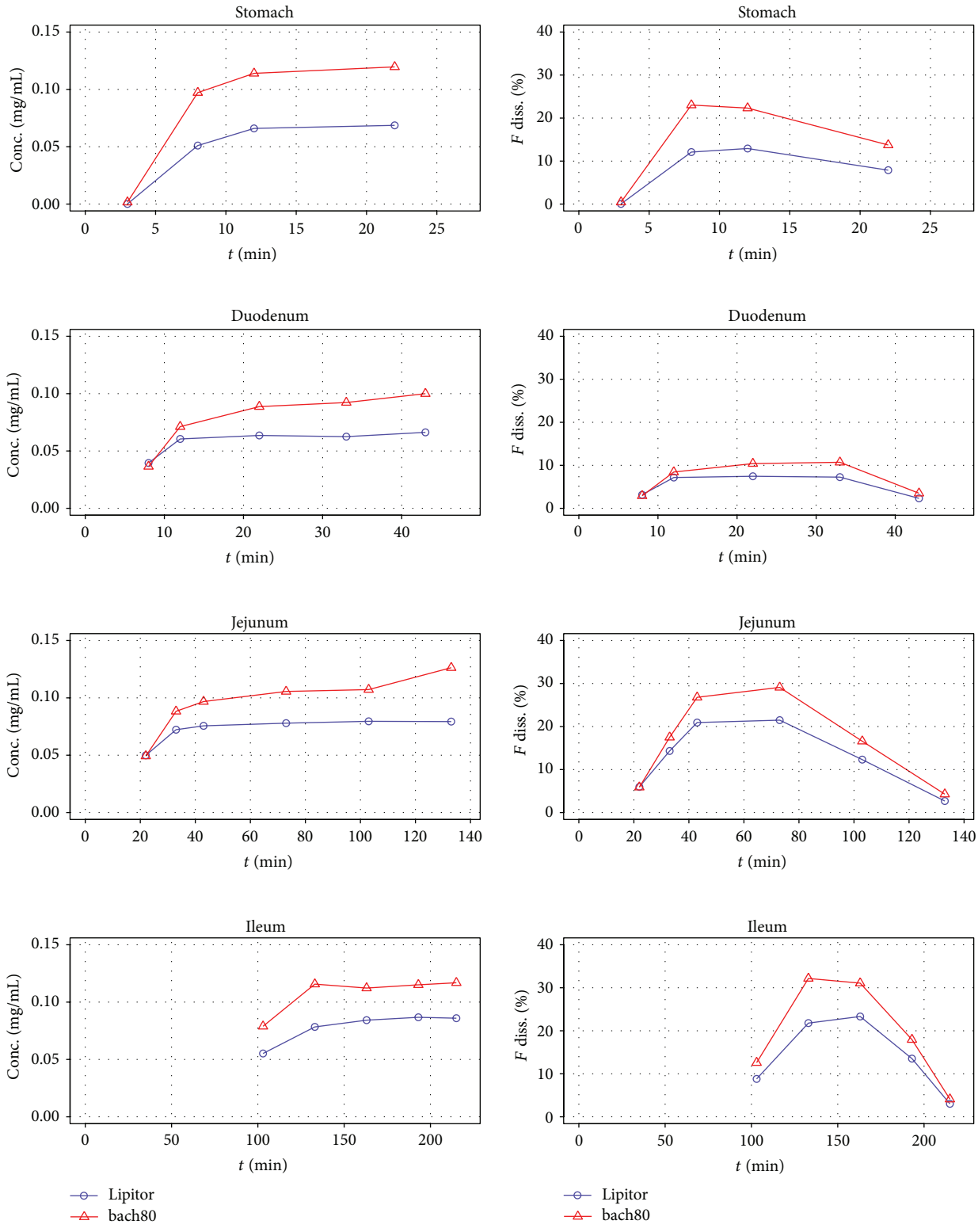

FIGURE 4: Golem dissolution results for nonbuffered generic batch80 and its reference product Lipitor. The plots show dissolution behavior measured in separate compartments, as well as cumulative profile showing the amount of drug dissolved in the whole apparatus including the amount gradually transferred from ileum into the collection canister. The terminal decrease of dissolved amount in individual compartments was caused by transfer of portions of the medium into the following compartment, or into the collection canister in case of ileum.

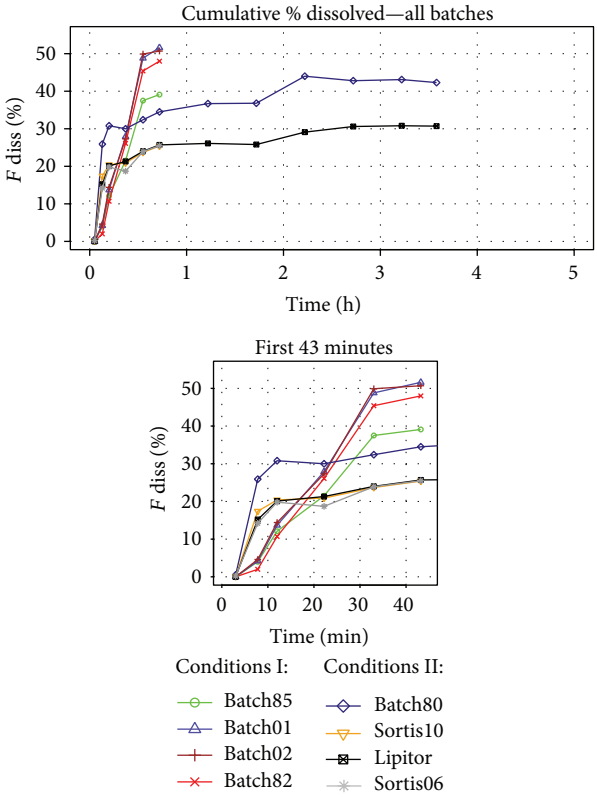

Figure 5: Cumulative fraction of ATV dissolved in whole apparatus.

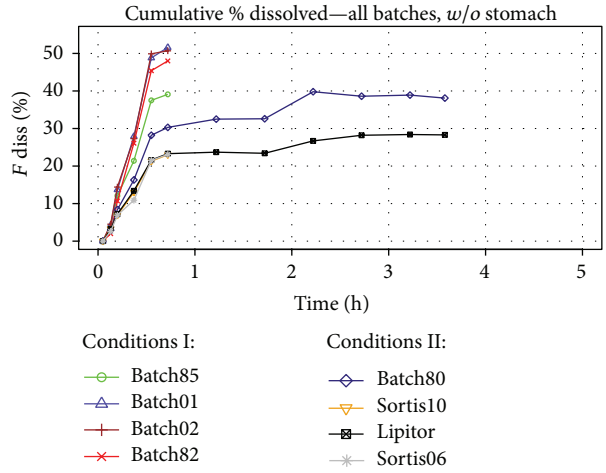

Figure 6: Cumulative fraction of ATV dissolved in duodenum, jejunum, and ileum compartments.

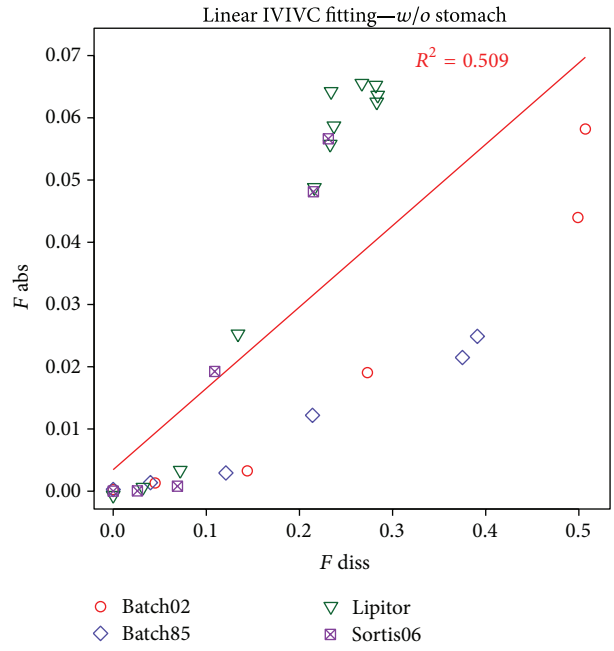

Figure 7: IVIVC plot for batches tested in two different conditions.

In case of the dissolution results available, the presence or absence of the buffering agent affected whether drug did dissolve in the stomach compartment, which produced two distinct cumulative profile patterns and significantly limited the comparison of the two formulation designs. *In vivo* absorption of atorvastatin is believed to start only in small intestine and thus a deconvolution of plasmatic profile would yield a fraction of drug absorbed only from small intestine. According to this, the fraction of drug dissolved in stomach compartment was excluded from the cumulative profiles used for the IVIV correlations. The final profiles used for correlation are depicted in Figure 6.

Despite the previous modification of the profiles, the lower solubility of ATV in the presence of $CaCO_3$ and the resulting overall lower dissolution performance of the buffered batches caused that it was difficult to build a reliable model using combination of buffered and nonbuffered formulations. Therefore, models had to be built for Design I (buffered batches) and Design II (nonbuffered) separately. Figure 7 depicts deconvolution results for two formulations of both designs and the lack satisfactory level of correlation ($R^2 = 0.37$). Deconvolution was performed using simulated *in vivo* response after intravenous administration of 80 mg of ATV (Figure 8).

In vitro-in vivo correlation was described by both linear and nonlinear (polynomial) relationship (3). The`lm()` *R* base function was used:

$$\text{FABS} = B_0 + B_1 * \text{FDISS} + B_2 * \text{FDISS}^2 + E, \quad (3)$$

where FABS is the fraction absorbed, B_0 is the y-intercept, B_1 and B_2 are coefficients, FDISS is the fraction dissolved, and E are residuals.

3.3.1. Design I. In the nonbuffered group a model was built based on batch01 and batch85 and nonlinear (polynomial) correlation was obtained with $R^2 = 0.951$ (Figure 9).

Predictability evaluation was performed by calculating fraction of ATV absorbed versus time with regression equation with *in vitro* profile as an input. With intravenous response profile, numerical convolution was performed, and the prediction of *in vivo* curve was obtained. Figure 10 depicts simulation of *in vivo* profile of batch82.

The model's prediction errors for C_{max} and AUC did not meet the FDA criteria [15] and were to be rejected.

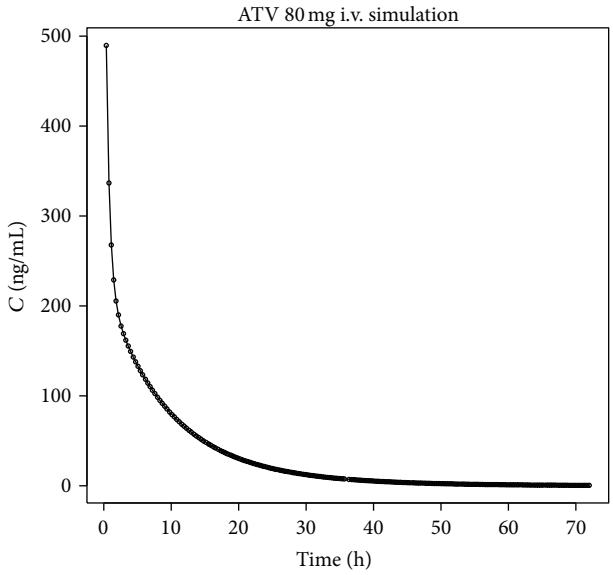

FIGURE 8: Simulated *in vivo* profile after administration of 80 mg of ATV.

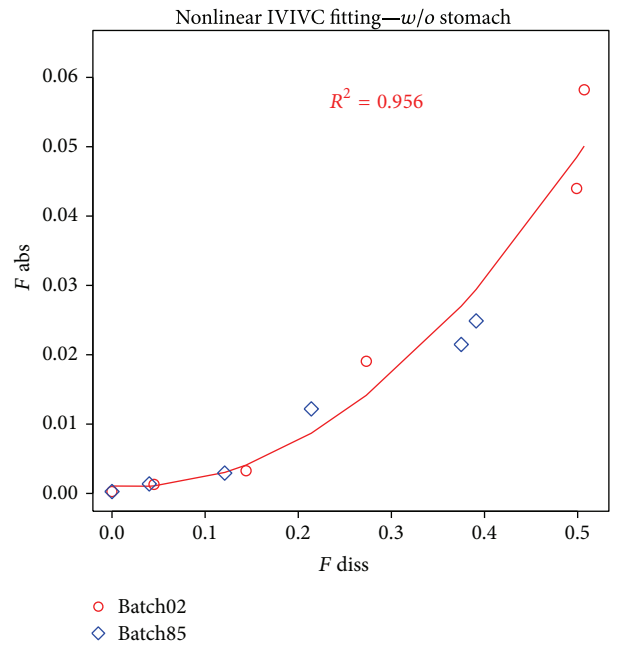

FIGURE 9: Deconvolution results for nonbuffered batch02 and batch85.

3.3.2. Design II. Deconvolution results for buffered batches are presented in Figures 11 and 12. In most cases, nonlinear correlation was observed.

In Figure 13, prediction of Sortis10 plasma concentration is shown. Although AUC PE was low (5.75%), the prediction of C_{max} was not satisfactory.

An example of internal predictability is presented in Figure 14. In general, predictions of C_{max} were good, but the descending curves could not properly reflect the *in vivo* behavior resulting in high AUC PE. This was partially due to the fact that the simulated *i.v.* profile used for deconvolution (and later convolution in the validation phase) was the same for all batches and not fitted to each group of patients participating in clinical trials.

3.4. IVIVC/IVIVR-Compartmental Approach. In order to fully exploit Golem's features, it was attempted to create IVIVR introducing completely nonstandard approaches, where no conventional convolution/deconvolution methods are necessary. This implies no more requirements for *i.v.* administration results, and therefore results obtained in a more cost-saving manner, utilizing the Golem data for IVIVC/IVIVR development.

The Golem apparatus allows measuring the concentration of API in each compartment separately. An example of distribution of dissolved API for Lipitor is depicted in Figure 15.

Various approaches were examined to correlate results for each compartment with corresponding *in vivo* profiles, but successful outcome was reached only with jejunum compartment. As shown in Figure 16, profiles were described by nonlinear function:

$$f(t) = A * e^{(-k1*t)} + B * e^{(-k2*t)} + C * e^{(-k3*t)}, \quad (4)$$

where $f(t)$ is the concentration of an API at given sampling time t; A, B, and C are the equation constants; $k1$, $k2$, and $k3$ are constants.

The model presented above follows a general equation for 2-compartment model with p.o. administration, and despite the previously mentioned claim that ATV PK profile does not follow such model well, it was chosen as a compromise between modeling accuracy and optimization procedure stability.

Formula was optimized with nonlinear Solver (DEPS: differential evolution and particle swarm optimization) available in LibreOffice Calc (ver. 4.1.5.3). Figure 16 represents measurements for jejunum compartment for each batch (Figure 16(a)). A complete measurement was available only for Lipitor and batch80, and the descending part of the *in vitro* curves for the six remaining batches had to be introduced by addition of two time points (Figure 16(b)) in order to perform *in vivo* time scaling and correlation. Correlation of full profiles was performed for Lipitor and batch80 and was used for internal validation of the model. Only the ascending (and *in vitro* measured) parts of profiles were correlated for the remaining batches.

As shown in Figure 17, *in vivo* time scale was scaled nonlinearly, however with a simple reversible mathematical function.

Finally, with (5), predicted plasma concentrations were calculated for all batches. Two constants were introduced for linear scaling of *in vitro* profile and were optimized with nonlinear Solver:

$$f(t) = \text{CONST1} * \left[A * e^{(-k1*t)} + B * e^{(-k2*t)} + C * e^{(-k3*t)}\right] + \text{CONST2}, \quad (5)$$

where $f(t)$ is the predicted plasma concentration at given time t; A, B, C, $k1$, $k2$, and $k3$ are constants calculated

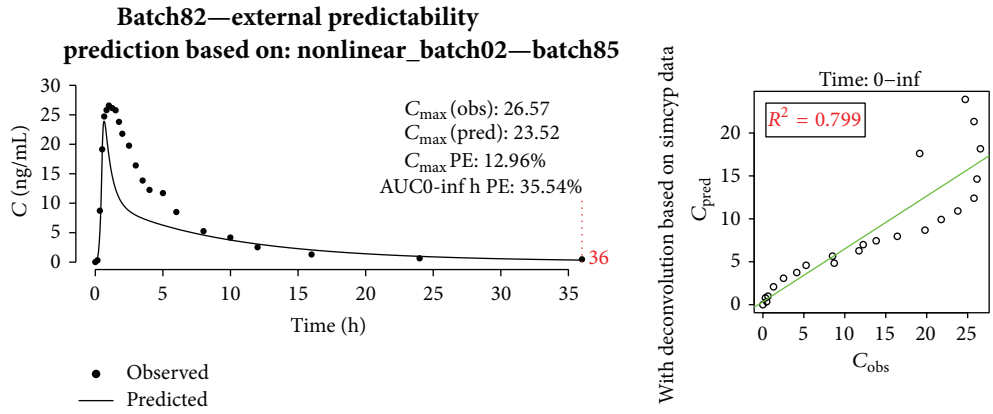

Figure 10: Prediction of *in vivo* profile of batch82 with nonlinear model built on batch02 and batch85.

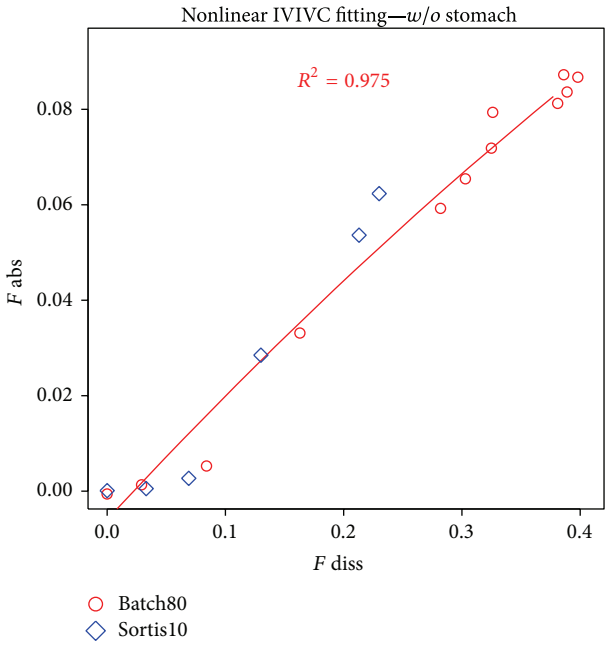

Figure 11: Nonlinear IVIVC example.

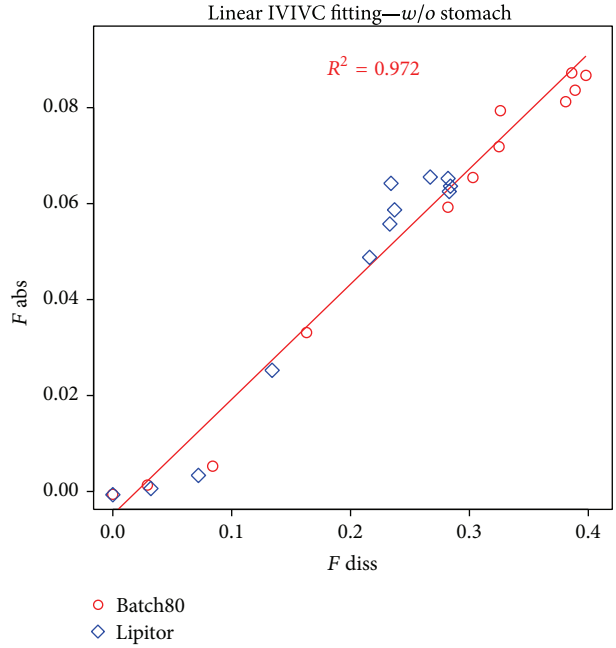

Figure 12: Linear IVIVC example.

for *in vitro* jejunum profile (4); CONST1 and CONST2 are constants for whole *in vitro* model linear scaling.

For CONST1 and CONST2 optimization, only two formulations were used and a middle one (with medium dissolution rate) was predicted.

3.4.1. Designs I and II. Results for external prediction of batch01 (amorphous ATV, nonbuffered) PK profile are presented in Figure 18. Although constants for *in vitro* profile scaling were optimized for batch80 and Lipitor (buffered conditions), pAUC PE and C_{max} PE for batch01 were below 10%.

3.4.2. Design II. Model was optimized for batch80 and Lipitor, since these were the two most extensively studied batches (215 min *in vitro* profiles), and their *in vivo* profiles sufficiently differed between each other (Figure 19).

In Figure 20, the prediction for Sortis06 is shown. Prediction errors were below 20%, which means that according to FDA guidance [15] the model is not to be rejected, but additional data should be provided in order to be fully validated.

In summary, the compartmental approach directly correlated the *in vitro* jejunal dissolution profile with the course of the plasmatic versus time profile. The logical basis for this correlation was the assumption that any dissolved portion of API *in vivo* would be immediately absorbed due to the nonlimiting permeability of ATV, which allows direct correlation of the ascending part of the dissolution and plasmatic profiles. This approach provided the best correlation options even for the combination of both formulation designs. This could be accounted for the fact that each compartment of the SI contained additional 33 mL of starting volume,

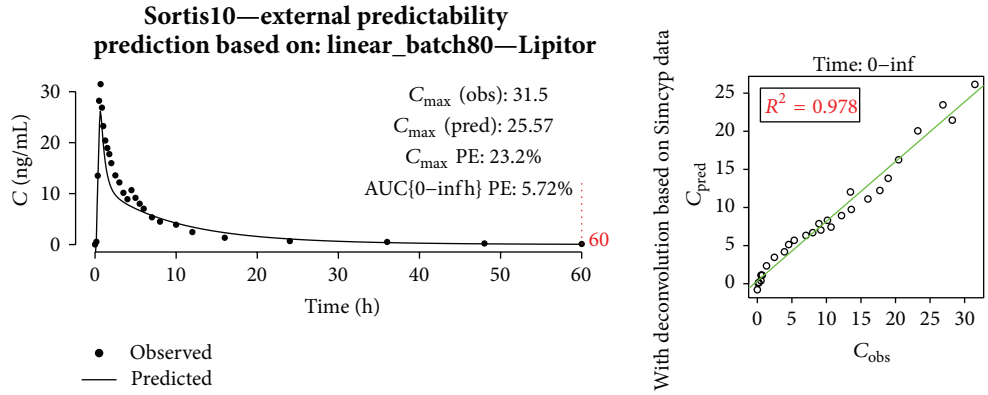

Figure 13: Prediction of Sortis10 profile.

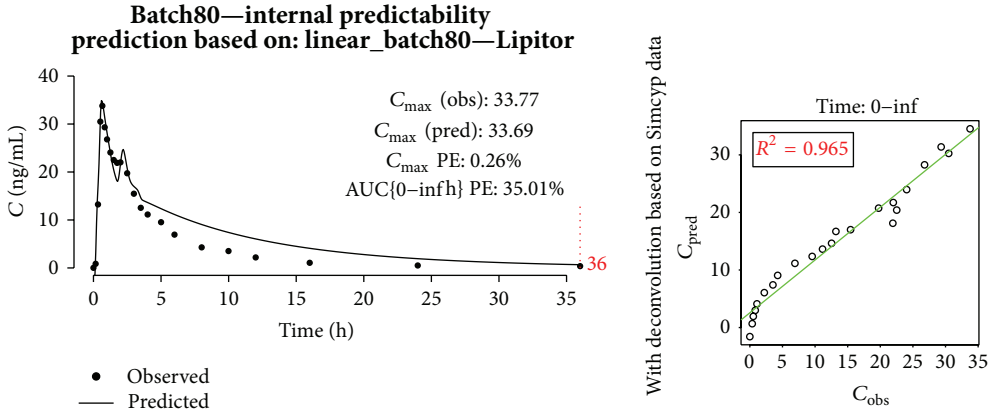

Figure 14: Prediction of generic batch80 profile with linear model built on batch80 and Lipitor.

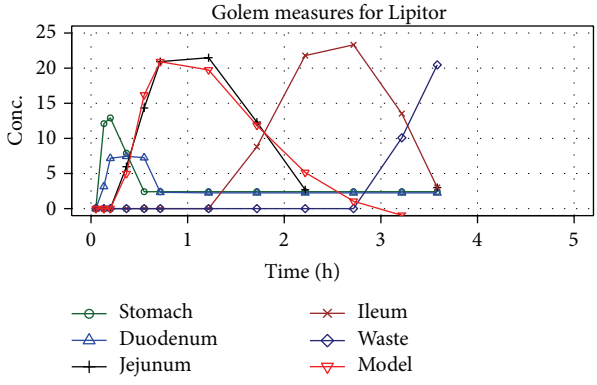

Figure 15: Example of measurements performed with Golem apparatus (for Lipitor).

and this portion of fresh medium in the jejunum provided sufficient sink-condition to allow dissolution of API without saturation of the solution during the early minutes in this compartment. The differences between the batches were thus more pronounced here than elsewhere in the apparatus.

From the correlation-development view, however, the basis for direct correlation was purely empirical. The approach with direct mapping of jejunum profiles with the PK profiles was based on the observation of profound similarity of both types of the results. Regardless of any mechanistic considerations presented above, the most appealing point here was to discard complicated convolution/deconvolution methods in favor of simple linear or nonlinear mapping of *in vitro* to the *in vivo* profiles. Thus, intravenous administration of the API was no longer necessary here, and mathematical limitations of convolution/deconvolution techniques were not anymore applicable. It should be, however, pointed out that in order to achieve such a relatively simple mathematical model, it is necessary to provide physiologically relevant dissolution results. In theory, this can be regarded as an inverse proportion between the sophistication of numerical procedures necessary for IVIVC/IVIVR and the degree of faithful representation of biological processes by the dissolution method. Therefore, the presented models demonstrating very good correlation could serve as an indirect proof of the Golem's biorelevance. Moreover, in the future, the Golem's flexibility could allow defining its critical operational parameters that could be optimized in order to achieve its maximum biorelevance in regard to the individual formulations tested. An apparatus like Golem can utilize dissolution method easily tailored to a particular formulation or API, based on the quantitative and qualitative composition, knowledge on the API's physicochemical and biopharmaceutical characteristics and other factors. An individual formulation-related

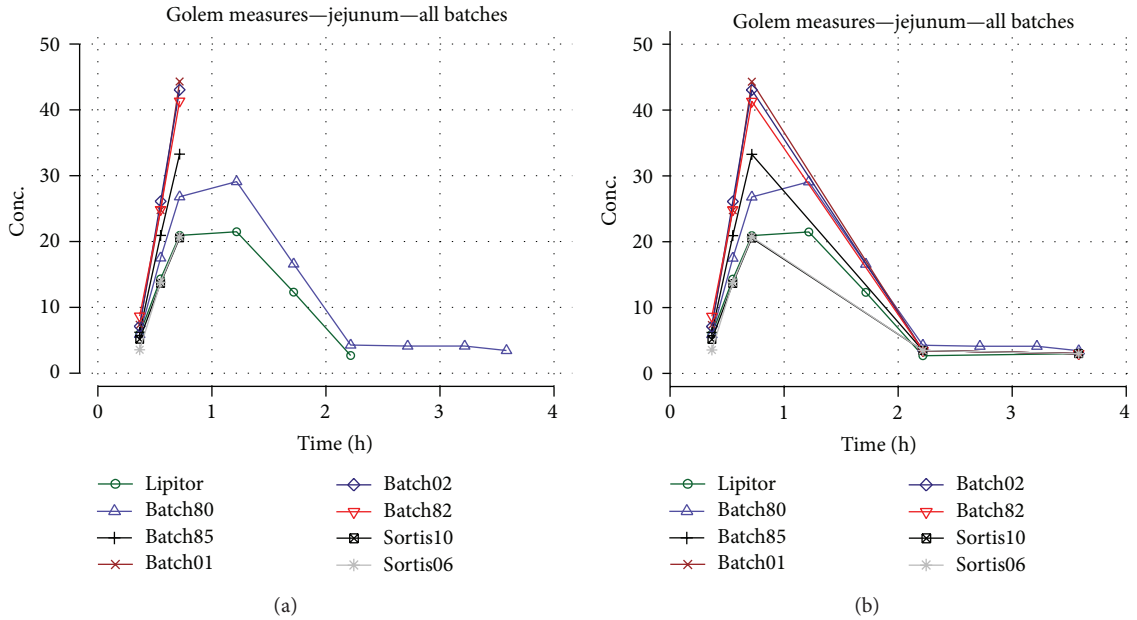

Figure 16: Dissolution in jejunum compartment (a) and addition of two additional time points (b).

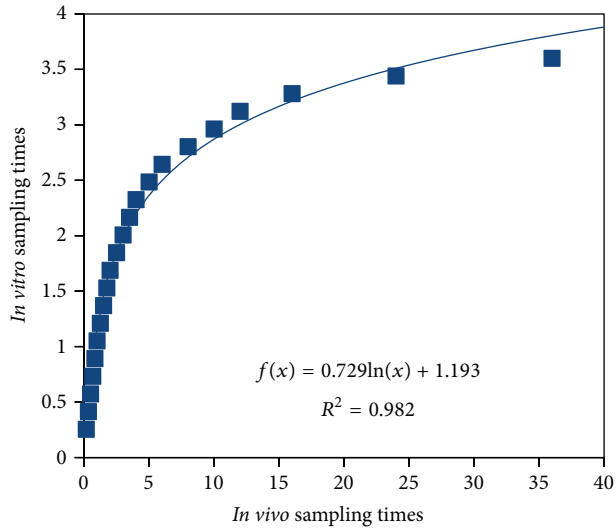

Figure 17: Logarithmic scaling of *in vivo* profile.

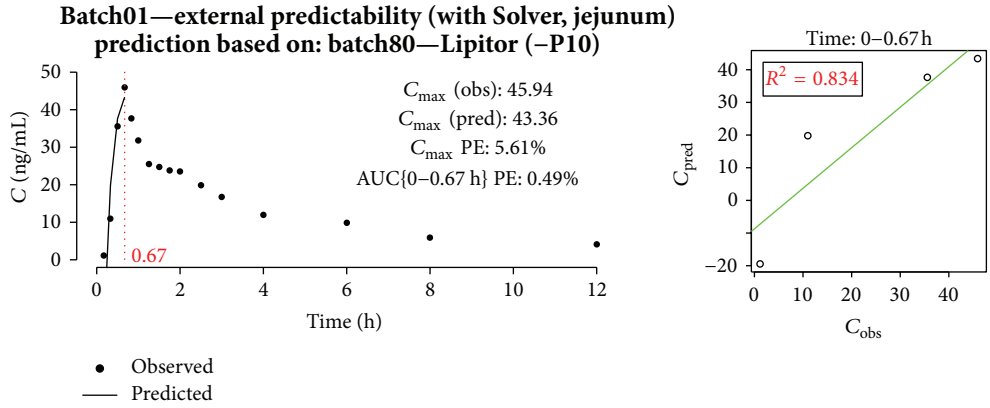

Figure 18: Prediction of batch01 profile with model built on batch80 and Lipitor.

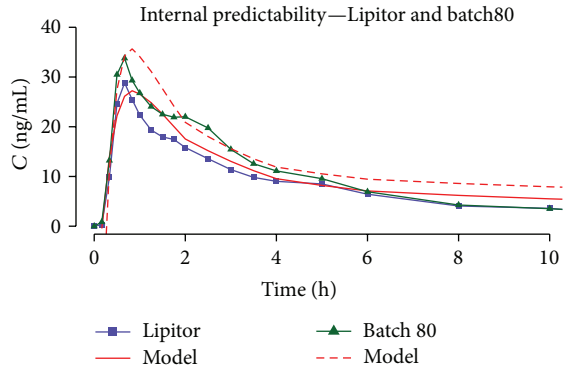

Figure 19: Comparison of Lipitor and batch80 predicted and actual plasma concentration profiles.

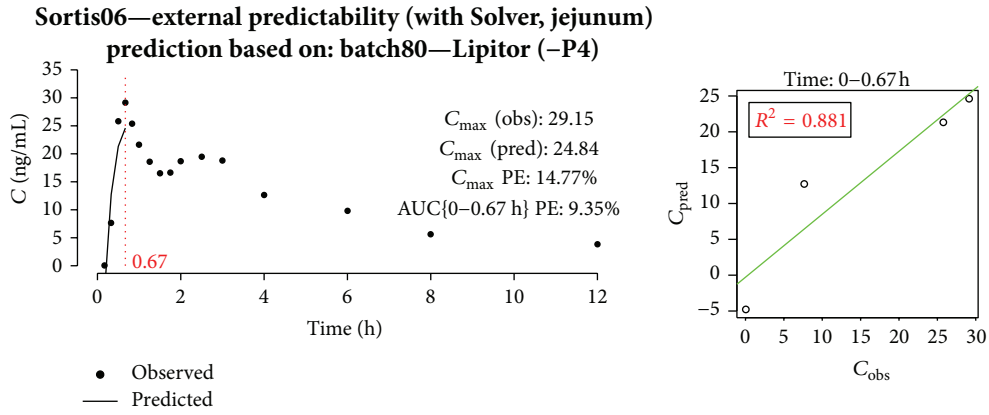

Figure 20: Prediction of Sortis06 profile with model built on batch80 and Lipitor.

dissolution protocol could thus be an answer to the industrial need for discriminative and at the same time biorelevant dissolution methods, whereas standardization could be achieved on the level of algorithmic approach to the adjustment of the dissolution protocol.

4. Conclusions

Dissolution of eight IR batches of ATV was tested using a novel dissolution apparatus allowing dynamic simulation of stomach and small intestine. The biorelevant conditions and observation of succeeding dissolution processes in separate compartments provided comprehensive information on the dissolution behavior expected *in vivo*. Such information and elucidation of the connections between processes happening under different conditions, which are however connected *in vivo*, are often inaccessible with the use of less complex apparatuses. The dissolution testing was performed with a basic universal dissolution method based on a faithful simulation of the GI tract. As such, it defined the main effects influencing dissolution performance of the tested batches, which is an important and often difficult step in research and development (R&D) and is a basic prerequisite for further dissolution method optimization, performed according to the characteristics of the given API and its formulation. Due to the complex nature of the presented apparatus, any modification of the dissolution method can be easily performed. In case of the correlation options, the structure of Golem apparatus allowed treating different compartments separately, adding or subtracting the measurement results for each compartment. As a result, two approaches to *in vitro-in vivo* correlation could be developed. The main advantage of the presented methods was no requirement for additional intravenous drug administration (simulated data for *i.v.* administration was used in first approach) which might be inaccessible in certain cases. Whole analysis with deconvolution was performed in a single *R* script and therefore results are completely reproducible. Compartmental approach can be redone in a spreadsheet and standardized according to the industrial requirements, thus presenting simple and effective tool for quick establishment of IVIVC/IVIVR based on Golem's results.

In order to fully evaluate the Golem's capabilities and the presented correlation techniques, larger dataset with greater differences in dissolution rates should be used.

The future work with the apparatus will be aimed at generating and processing of further larger datasets for further verification of the hypotheses presented in this paper.

Conflict of Interests

The authors declare that there is no conflict of interests regarding the publication of this paper.

Acknowledgments

Authors would like to thank company-Zentiva Group, a.s., Czech Republic, for providing the tested batches and *in vivo* results. This work was supported by the project "Employment of Best Young Scientists for International Cooperation Empowerment" (CZ.1.07/2.3.00/30.0037) cofinanced from European Social Fund and the state budget of the Czech Republic. The work was further supported by the Czech Science Foundation—GACR P304/11/2246.

References

[1] M. McAllister, "Dynamic dissolution: a step closer to predictive dissolution testing?" *Molecular Pharmaceutics*, vol. 7, no. 5, pp. 1374–1387, 2010.

[2] M. Culen and J. Dohnal, "Advances in dissolution instrumentation and their practical applications," *Drug Development and Industrial Pharmacy*, 2013.

[3] S. Souliman, E. Beyssac, J.-M. Cardot, S. Denis, and M. Alric, "Investigation of the biopharmaceutical behavior of theophylline hydrophilic matrix tablets using usp methods and an artificial digestive system," *Drug Development and Industrial Pharmacy*, vol. 33, no. 4, pp. 475–483, 2007.

[4] G. L. Amidon, H. Lennernas, V. P. Shah, and J. R. Crison, "A theoretical basis for a biopharmaceutic drug classification: the correlation of in vitro drug product dissolution and in vivo bioavailability," *Pharmaceutical Research*, vol. 12, no. 3, pp. 413–420, 1995.

[5] J. Bárta, P. Mudra, V. Pešek et al., "Digestive tract simulator," 2011, http://patentscope.wipo.int/search/en/WO2011069472.

[6] M. Culen, A. Rezacova, J. Jampilek, and J. Dohnal, "Designing a dynamic dissolution method: a review of instrumental options and corresponding physiology of stomach and small intestine," *Journal of Pharmaceutical Sciences*, vol. 102, no. 9, pp. 2995–3017, 2013.

[7] T. Watanabe, H. Kusuhara, K. Maeda et al., "Investigation of the rate-determining process in the hepatic elimination of HMG-CoA reductase inhibitors in rats and humans," *Drug Metabolism and Disposition*, vol. 38, no. 2, pp. 215–222, 2010.

[8] M. Ishigami, T. Honda, W. Takasaki et al., "A comparison of the effects of 3-hydroxy-3-methylglutaryl-coenzyme a (HMG-CoA) reductase inhibitors on the CYP3A4-dependent oxidation of mexazolam in vitro," *Drug Metabolism and Disposition*, vol. 29, no. 3, pp. 282–288, 2001.

[9] W. Jacobsen, B. Kuhn, A. Soldner et al., "Lactonization is the critical first step in the disposition of the 3-hydroxy-3-methylglutaryl-CoA reductase inhibitor atorvastatin," *Drug Metabolism and Disposition*, vol. 28, no. 11, pp. 1369–1378, 2000.

[10] J.-S. Kim, M.-S. Kim, H. J. Park, S.-J. Jin, S. Lee, and S.-J. Hwang, "Physicochemical properties and oral bioavailability of amorphous atorvastatin hemi-calcium using spray-drying and SAS process," *International Journal of Pharmaceutics*, vol. 359, no. 1-2, pp. 211–219, 2008.

[11] A. Mendyk, "CRAN—Package Rivivc," http://cran.r-project.org/web/packages/Rivivc/index.html.

[12] M. Jamei, S. Marciniak, D. Edwards et al., "The simcyp population based simulator: architecture, implementation, and quality assurance," *Silico Pharmacology*, vol. 1, no. 1, p. 9, 2013.

[13] P. Poulin and F.-P. Theil, "Prediction of pharmacokinetics prior to in vivo studies. 1. Mechanism-based prediction of volume of distribution," *Journal of Pharmaceutical Sciences*, vol. 91, no. 1, pp. 129–156, 2002.

[14] H. Lennernäs, L. Aarons, P. Augustijns et al., "Oral biopharmaceutics tools—time for a new initiative—an introduction to the IMI project OrBiTo," *European Journal of Pharmaceutical Sciences*, vol. 16, no. 57, pp. 292–299, 2014.

[15] FDA, *Guidance for Industry: Extended Release Oral Dosage Forms: Development, Evaluation, and Application of in Vitro/in Vivo Correlations*, 1997.

[16] H. Lennernäs, "Clinical pharmacokinetics of atorvastatin," *Clinical Pharmacokinetics*, vol. 42, no. 13, pp. 1141–1160, 2003.

Hindawi Publishing Corporation
BioMed Research International
Volume 2015, Article ID 892671, 11 pages
http://dx.doi.org/10.1155/2015/892671

Research Article

Formulation of Novel Layered Sodium Carboxymethylcellulose Film Wound Dressings with Ibuprofen for Alleviating Wound Pain

Lenka Vinklárková,[1] Ruta Masteiková,[1] David Vetchý,[1] Petr Doležel,[1] and Jurga Bernatonienė[2]

[1]*Department of Pharmaceutics, Faculty of Pharmacy, University of Veterinary and Pharmaceutical Sciences Brno, Palackého Třída 1/3, 612 42 Brno, Czech Republic*
[2]*Department of Drug Technology and Social Pharmacy, Faculty of Pharmacy, Lithuanian University of Health Sciences, Eiveniu Street 4, LT-50103 Kaunas, Lithuania*

Correspondence should be addressed to Ruta Masteiková; masteikovar@vfu.cz

Received 15 September 2014; Accepted 2 December 2014

Academic Editor: Oluwatoyin A. Odeku

Effective assessment and management of wound pain can facilitate both improvements in healing rates and overall quality of life. From a pharmacological perspective, topical application of nonsteroidal anti-inflammatory drugs in the form of film wound dressings may be a good choice. Thus, the aim of this work was to develop novel layered film wound dressings containing ibuprofen based on partially substituted fibrous sodium carboxymethylcellulose (nonwoven textile Hcel NaT). To this end, an innovative solvent casting method using a sequential coating technique has been applied. The concentration of ibuprofen which was incorporated as an acetone solution or as a suspension in a sodium carboxymethylcellulose dispersion was 0.5 mg/cm^2 and 1.0 mg/cm^2 of film. Results showed that developed films had adequate mechanical and swelling properties and an advantageous acidic surface pH for wound application. An *in vitro* drug release study implied that layered films retained the drug for a longer period of time and thus could minimize the frequency of changing the dressing. Films with suspended ibuprofen demonstrated higher drug content uniformity and superior *in vitro* drug release characteristics in comparison with ibuprofen incorporation as an acetone solution. Prepared films could be potential wound dressings for the effective treatment of wound pain in low exuding wounds.

1. Introduction

The European Wound Management Association (EWMA) Position Document acknowledges that pain is a major issue for patients with acute and chronic wounds [1]. Pain produces stress, which can affect individuals in both psychological and physiological ways and results in delayed wound healing and detrimental effects on quality of life [2]. Therefore, effective assessment and management of wound pain could facilitate an improvement in healing rates and overall quality of life.

Wound-related pain can be temporary (acute) or persistent (chronic) [3]. Acute wound pain can be exacerbated whenever the wound is handled or manipulated: during dressing removal, wound cleansing, or debridement (removing of necrotic tissues). In contrast, persistent (chronic) wound pain is the background symptom that exists at rest and between wound-related procedures.

Wound pain management includes nonpharmacological and pharmacological measures. Multiple pharmacological agents may be used to combat pain. Guidelines for pharmacological wound pain management based on the recommendations by the World Health Organization recommend the use of nonsteroidal anti-inflammatory drugs (NSAIDs) or acetaminophen for patients with mild to moderate pain [3, 4]. NSAIDs provide good pain relief. Moreover, they can positively influence inflammatory processes in the wound,

since there is a tendency in chronic wounds for the inflammatory response (an important element in the initial wounding response) to become exaggerated. This results in the increased production of proinflammatory cytokines, reactive oxygen species, and proteolytic enzymes. The chronic wound environment therefore shows sustained inflammation with matrix degradation [5]. Unfortunately, oral use of NSAIDs can lead to serious side effects such as gastrointestinal damage, risk of renal failure, and prolonged bleeding time due to impaired coagulation [6, 7]. For this reason, nonpharmacological strategies and topical agents to achieve optimal wound-related pain management are an attractive solution. Topical agents and correctly selected dressings play a critical role in alleviating wound-related pain [3]. Pain during wound dressing changes or debridement (acute pain) can be substantially reduced using local anesthetics such as lidocaine, tetracaine, or prilocaine applied as a solution, gel, or cream [8, 9]. In the case of chronic wound pain, treating the cause, such as infection or inflammation, as well as optimal wound dressing is of the utmost importance [10]. Wound dressings which are nonadherent and maintain a moist wound environment lead to faster healing and less pain. The pain reduction is attributed to the bathing of the exposed nerve ending in fluid which prevents dehydration of the nerve receptors [10]. Nevertheless, pharmacological measures may be necessary when maintenance of moist wound environment itself is not effective enough for pain reduction or in case of inflammation. For this purpose, topical NSAIDs are an effective option [11].

Topical NSAIDs are formulated for direct application to the painful site and for producing a local pain-relieving effect while avoiding body-wide distribution of the drug at physiologically active levels [12]. Once the drug has reached the site of action, it must be present at a sufficiently high concentration to inhibit cyclooxygenase (COX) enzymes and produce pain relief. Tissue levels of NSAIDs applied topically reach levels high enough to inhibit COX-2 activity [12]. Plasma concentrations found after topical administration, however, are only a fraction of the levels found following oral administration. Recently, an evaluation of the effect of ibuprofen in the form of a foam dressing (Biatain Ibu) on persistent and temporary wound pain underwent clinical trials [13–17]. The ibuprofen foam dressing was shown to consistently relieve wound pain in exuding wounds of various etiologies, irrespective of basal pain intensity. Petersen et al. [18] estimated the ibuprofen foam potential to reduce the need for oral pain killers in two controlled ibuprofen foam trials with the conclusion that local wound pain treatment with ibuprofen foam dressing appears to provide pain relief to the same degree as oral NSAIDs or opioids. Thus, local pain relief by an ibuprofen foam dressing is possible in the most common, painful, exuding, chronic, and acute/traumatic wounds and therefore is a safer alternative for systemic pain treatment [16]. The Biatain Ibu foam dressing may be very useful for patients with painful wounds. However, this dressing has one significant drawback. It would seem that wounds need to have at least a moderate exudate to activate the release of ibuprofen from the dressing; so for those patients with wounds that have low exudate it may not be an option [19]. In such cases, a film made from hydrophilic polymer containing ibuprofen may be a good alternative. The film is thin and needs only a small amount of exudate to activate the release of the drug. For dry wounds, the film may be slightly wetted with normal saline. Moreover, the film is transparent, allowing clinicians to observe a wound's progress without needing to remove it, preserving a moist wound environment [20].

Different polymers may be used to prepare the film. Polyurethane is currently the most used material for such purposes [21]. Polyurethanes, however, are synthetic materials and less friendly on body tissues than materials of a natural origin. Moreover, polyurethane films are intended for the protection of nonexuding wounds and, unless additionally modified, are less suitable for use as drug carriers [20]. For this reason, there have been many studies into how to prepare film wound dressings from natural materials [22–25].

For our experiment, carboxymethylcellulose (CMC), more specifically its sodium salt (sodium carboxymethylcellulose: NaCMC), was chosen because it ranks among the materials with excellent film-forming properties [26]. NaCMC is widely used in pharmaceutical formulations primarily for its ability to increase viscosity [27]. It may also be used for stabilizing emulsions or producing gels. Likewise, the bioadhesive properties of NaCMC are well known. CMC is generally regarded as a nontoxic, nonirritant, and biocompatible material which predestines it for use in food, cosmetic, pharmaceutical, and biomedical applications, including materials for wound care [27]. The suitability and benefits of CMC for application on wounds have been proved by a range of experimental studies. Garrett et al. explored its potential to promote corneal epithelial wound healing [28]. Karami et al. observed its positive effects on wound healing in diabetic male rats [29] and Ramli and Wong observed them on the partial thickness wounds of rats [24]. Currently, NaCMC is used as an absorptive dressing to create conditions for moist wound healing in the field of wound care [27, 30]. The NaCMC dressings on the market do not contain an active substance, with the exception of incorporated silver [30]. NaCMC films have not been employed in wound care yet. Ramli and Wong studied the effect of nonmedicated NaCMC scaffolds on wound healing of rats [24]. Vetchý et al. evaluated the mucoadhesive properties of NaCMC-based films used as dressings to separate the lesion from the environment of the oral cavity [31]. Although CMC films with an active substance as wound dressings have not been investigated yet, there is a whole range of scientific works dealing with the preparation and evaluation of medicated CMC films for other applications, mainly for oral/buccal drug delivery [32–38]. And so the suitability of CMC in the preparation of medicated films has been widely proved. Nevertheless, the application properties of film wound dressings differ quite significantly from those intended for buccal applications. Wound dressings are applied on a much larger surface area than buccal preparations. For this reason, good mechanical properties of medicated CMC films are required. Especially after wetting, they must maintain the cohesiveness that enables them to be easily manipulated and removed without residues.

Table 1: Preparation of layered films.

Film	1st step	2nd step	3rd step	4th step
0.5-Ibu-1	NaCMC → Sanatyl → pre-drying	1% Ibu sol. → evaporation	NaCMC	pre-drying and drying
0.5-Ibu-2	NaCMC → Sanatyl → pre-drying	NaCMC with Ibu	—	pre-drying and drying
1.0-Ibu-1	NaCMC → Sanatyl → pre-drying	2% Ibu sol. → evaporation	NaCMC	pre-drying and drying
1.0-Ibu-2	NaCMC → Sanatyl → pre-drying	NaCMC with Ibu	—	pre-drying and drying
1-blank	NaCMC → Sanatyl → pre-drying	acetone → evaporation	NaCMC	pre-drying and drying
2-blank	NaCMC → Sanatyl → pre-drying	NaCMC	—	pre-drying and drying
3-blank	NaCMC → pre-drying	acetone → evaporation	NaCMC	pre-drying and drying
4-blank	NaCMC → pre-drying	NaCMC	—	pre-drying and drying
0.5-Ibu-1 without Sanatyl	NaCMC → pre-drying	1% Ibu sol. → evaporation	NaCMC	pre-drying and drying
0.5-Ibu-2 without Sanatyl	NaCMC → pre-drying	NaCMC with Ibu	—	pre-drying and drying

As for other cellulose-based materials, the mechanical properties of CMC-containing films decrease with increasing moisture content [26]. Degree of substitution (DS) also negatively influences the properties of wetted films, since the hydrophilic nature of the film increases with higher DS [39]. On the other hand, the filler, for example, microcrystalline cellulose, if well dispersed in the polymer matrix, usually improves these mechanical properties [26]. So microfibrous NaCMC with relatively low DS (partially carboxymethylated cotton textile) can have a positive effect on the mechanical properties of the film. Partially carboxymethylated cellulose retains its original fibrous nature [40] thus allowing microfibers to act as the filler, whereas the dissolved NaCMC acts as the film-forming agent. The resulting combination can provide improved handling characteristics of the wetted film.

The aim of the presented research was to prepare novel layered films with microfibrous NaCMC and ibuprofen and evaluate their physicochemical properties as well as the influence of the method of ibuprofen incorporation on *in vitro* drug release by modern methods.

2. Materials and Methods

The partially substituted (DS 0.35) sodium carboxymethylcellulose in the form of nonwoven textile (Hcel NaT) was supplied by Holzbecher, spol. s r. o., Bleaching & Dyeing Plant in Zlíč (Czech Republic), ibuprofen, macrogol 300, and acetone (all Ph. Eur. grade) were purchased from Fagron (Czech Republic), and the Sanatyl 20 medical grade polyester mesh was purchased from Tylex Letovice, a. s. (Czech Republic). All other chemicals and reagents used in the study were of analytical grade.

2.1. Preparation of Films

2.1.1. Preparation of NaCMC Dispersion without and with Ibuprofen. The polymer dispersion was composed of 1% w/w NaCMC and 2% w/w macrogol 300 in purified water. Nonwoven sodium carboxymethylcellulose textile (Hcel NaT) was cut into small pieces and poured over with a solution of macrogol in hot water (80°C). This mixture was then heated to maintain a temperature of 80°C for 3 hours and then left to cool at an ambient temperature for 24 hours. The resulting dispersion was homogenized for 3 min using an ULTRA-TURRAX T 25 dispersing device (IKA Werke Staufen, Germany) at 16,000 rpm. Polymer dispersion with ibuprofen was prepared in the following way. Thoroughly grinded ibuprofen (82.5 mg or 165 mg for one film) was added to the NaCMC dispersion after 24 hours of swelling, and the mixture was homogenized for 8 min using an ULTRA-TURRAX T 25 dispersing device at 16,000 rpm.

2.1.2. Procedure of Preparation. Layered films with or without ibuprofen were prepared with an innovative solvent casting method using a sequential coating technique. This technique involved forming one film and pouring the next layer directly onto the previous one after predrying. The polymer dispersion was casted on an 11 × 15 cm (165 cm^2) stainless steel plate. Four types of layered films, differing in both concentration and incorporation method of ibuprofen, were prepared (Table 1). The concentration of ibuprofen was 0.5 mg/cm^2 or 1.0 mg/cm^2 of film. Ibuprofen was either incorporated between two NaCMC layers or dispersed in the second (upper) layer. The first step was the same for all films. 45 g of NaCMC dispersion were casted on a stainless steel plate, immediately covered with Sanatyl polyester mesh, and then predried in the oven (Heratherm, Germany) at 70°C for 1 hour. The second step was the same for two films (0.5-Ibu-1 and 1.0-Ibu-1): 8.25 g of 1% or 2% ibuprofen solution in acetone were poured on the top of predried film and acetone was evaporated in the hood (approx. 1 hour). Then a layer of 60 g of NaCMC dispersion was poured onto the film and then again predried in the oven at 70°C for 1 hour followed by 24 hours of drying at ambient conditions. For the other two films (0.5-Ibu-2 and 1.0-Ibu-2), 60 g of NaCMC dispersion containing 82.5 mg or 165 mg of ibuprofen were casted, following predrying and drying at the same conditions as previous films. The dried films were peeled from the plates, examined visually for morphological defects (e.g., cracks, shrinking, etc.) which can affect handling, testing, and application as well as aesthetic appearance, and stored in a closed box prior to testing. Films without ibuprofen were made in the same manner for comparison of physical properties (1-blank–4-blank). For the evaluation of morphology of ibuprofen particles, films without Sanatyl polyester mesh were also prepared (0.5-Ibu-1 and 0.5-Ibu-2 without Sanatyl).

2.2. Evaluation of Films

2.2.1. Microscopic Properties and Thickness of Films. Microscopic properties of the prepared films were evaluated using an optical microscope (STM-902 ZOOM, Opting, Czech Republic) and a color digital camera (DFW X700, Sony, Japan). The appearance of the films was observed at a magnification factor of 7.5, 20, and 50. Illustrative digital images were taken at the same time.

At the measurement of film thickness, a rectangular sample of the film was vertically secured in a holder, the microscope was focused on the edge of the film, and sample thickness was measured at 5 different places of the film at the points with and without Sanatyl fiber. This was repeated 3 times with each film sample.

2.2.2. Surface pH. Surface pH of the prepared films was evaluated using a WTW pH 3210 SET 2 pH-meter (WTW, Germany) with a flat glass electrode. A moistened pH meter electrode was enclosed in the surface of the film and the value was recorded after stabilization (approximately 30 s). All measurements were taken in triplicate on both sides of the film.

Alterations of the surface pH in the conditions simulating the wound environment were assessed using an artificial wound model (Petri dish, sponge soaked with a physiological buffer solution of pH 7.2). Four cm^2 (2×2 cm) samples of the film were cut and put on the surface of the wound model. The Petri dish was covered with a lid to prevent water evaporation, and surface pH was measured at determined time intervals in triplicate on both sides of the film.

2.2.3. Swelling Property of Films. Swelling properties of the prepared films were measured in a physiological buffer solution of pH 7.2. For these purposes, an artificial wound model was used (Petri dish, sponge soaked with a test liquid). Four cm^2 (2×2 cm) samples of the film were cut and weighed (W_d). The sample was placed on the surface of the wound model, the Petri dish was covered with a lid to prevent water evaporation, and swollen films were then weighed at determined time intervals (W_s). The degree of swelling Sw in the film was calculated as

$$\mathrm{Sw} = \frac{(W_s - W_d)}{W_d}. \quad (1)$$

2.2.4. Mechanical Properties. A modified method according to Shidhaye et al. was used to evaluate the mechanical properties of the prepared films [41]. A CT3 Texture Analyzer (Brookfield, USA) equipped with a 4.5 kg load cell and TexturePro CT software was used to determine the tensile strength of the prepared films. Film samples (10×40 mm) were held between two clamps of a TA-DGA probe positioned at a distance of 2 cm. The lower clamp was stationary and the strips of the film were stretched by the upper clamp moving at a rate of 0.5 mm/s until the strip broke. The work done during this process and the deformation (elongation) of the film at the moment of tearing were also measured. This process was repeated ten times for each film sample.

2.2.5. Drug Content Uniformity. The drug content uniformity test was performed to ensure the uniform distribution of the drug throughout the films. Standard solutions of 0.005, 0.01, 0.015, 0.02, and 0.025% ibuprofen (w/w) were prepared using a physiological buffer solution of pH 7.2 (PBS, pH 7.2). The absorbance values of the standard solutions at 264 nm were measured using a UV spectrophotometer (Lambda 25, Perkin Elmer Instruments, USA), and calibration curves were constructed. Samples (2×2 cm) were precisely cut from ten random sites in each film ($n = 10$) and dissolved separately in beakers containing 20 mL of PBS (pH 7.2). Then (after 12 hours) the ibuprofen concentration in the films was determined by measuring the absorbance of the film, relative to the blank (PBS) sample. The average concentrations of ibuprofen (mg/cm^2) in each sample and SD were then calculated.

2.2.6. In Vitro Drug Release. *In vitro* drug release studies on film formulations were performed according to a modified version of Pawar et al.'s method [42]. Specifically, a Franz diffusion cell with an effective diffusion area of 4.73 cm^2 was used. The receptor compartment of the cell was filled with 20 mL of PBS pH 7.2 as a dissolution medium, while the donor compartment was empty. The prepared film was placed on a thin polyester net between the donor and receptor chambers of the cells. A net was used in order to ensure correct contact between the film's surface and dissolution medium while avoiding immersion. The receptor phase was kept constantly stirred throughout the experiment using magnetic stir bars. The temperature of the receptor compartment was maintained at 32°C using circulating water jackets. At predetermined intervals, 2 mL samples were withdrawn from the receptor phase and replaced with the same amount of PBS pH 7.2 to maintain a constant volume. Drug release was quantified spectrophotometrically at 264 nm and was expressed as cumulative percent released versus time for the 8-hour duration of the study. The kinetics of ibuprofen release from the films were evaluated by determining the best fit of the dissolution data (percentage release versus time) to the Higuchi, Korsmeyer-Peppas, Baker-Lonsdale, Hixson-Crowell, zero order, and first order equations.

2.3. Statistical Data Analysis. Data were first analyzed with descriptive statistics and statistical tests (QC Expert, v. 3.2, Trilobyte software) and subsequently with multiple linear regression (MLR) using multiway ANOVA (analysis of variance) with the Unscrambler X program (v. 1.3, Camo software). The design was set for a full factorial with two concentrations of ibuprofen (0.5-Ibu, 1.0-Ibu) and two methods of ibuprofen incorporation (Ibu-1, Ibu-2). Experiments were carried out a minimum of three times, depending on the measured properties. The resulting MLR models were used to identify the influence of process-formulation variables or the effects of their interactions on the measured properties. Film thickness was evaluated by Scheffe's test of pair comparisons in R software, R package: agricolae (v. 1.2-1, Felipe de Mendiburu, 2014).

3. Results and Discussion

3.1. Formulation and Preparation of Films Containing Ibuprofen. An ideal film dressing must be supple and possess homogenous and smooth surfaces [25]. Transparency is another important property allowing for the wound's assessment without removing the dressing [20]. Films prepared from NaCMC possess all these characteristics and therefore were chosen for the preparation of film dressings with ibuprofen. Partially substituted microfibrous NaCMC (nonwoven textile Hcel NaT) was used in order to increase the mechanical resilience of the films after wetting. This assumption has been proven in our previous experiments, along with the suitability of macrogol 300 as a plasticizer (data have not been published yet). Regardless of the excellent cohesiveness of the wetted films, it was necessary to reinforce them enough to be resistant to surgical devices such as tweezers or in case of application on large areas. For this reason, Sanatyl medical grade polyester mesh was chosen.

In the case of medicated film, an active substance may be dissolved, suspended, or emulsified. Since ibuprofen is poorly water soluble, it is very difficult to achieve its solubility in the film formulation. Thu et al. [25] used cosolvents (propylene glycol and ethanol) for this purpose. In our case, it was impossible because ethanol precipitated the NaCMC from prepared dispersions. The effort to absorb ibuprofen on the Sanatyl led to a high loss of active substance. Thus, ibuprofen was incorporated into the films in solid state in the form of a suspension of previously grinded particles or after crystallization from an acetone solution.

The ibuprofen concentration in the films was expressed as mg/cm^2 of film. This expression facilitates dosage since wound dressings are applied to a certain surface area. Moreover, it is independent of the weight of the film which may vary considerably, as NaCMC films are hydrophilic with fluctuating moisture content. The same 0.5 mg/cm^2 concentration of ibuprofen was chosen as in the foam dressing Biatain Ibu [43], which was proved in clinical trials to be effective enough to relieve wound pain [13–17]. Films with double the concentration of 1.0 mg/cm^2 were prepared for comparison.

3.2. Evaluation of Prepared Films

3.2.1. Microscopic Evaluation and Thickness of Films. Visual examination did not show differences between prepared films—all of them were homogenous and translucent with smooth surface independently of the method of ibuprofen incorporation. Therefore, microscopic evaluation which is capable of imaging inner structure was necessary. Observation of microscopic appearance of prepared films confirmed that partially substituted CMC maintained fibrous nature—digital images showed well-marked microfibrous structures (Figure 1). The films with ibuprofen were found to contain suspended particles of ibuprofen or crystals that formed during acetone evaporation. The suspended particles of ibuprofen seemed smaller (Figure 2) than the crystallized ones (Figure 3) and were distributed in the film more evenly. The crystallized drug was concentrated mostly in the Sanatyl meshes (Figure 4). These findings were important for understanding and explaining results of following evaluations mainly the drug content uniformity and process of ibuprofen release *in vitro*.

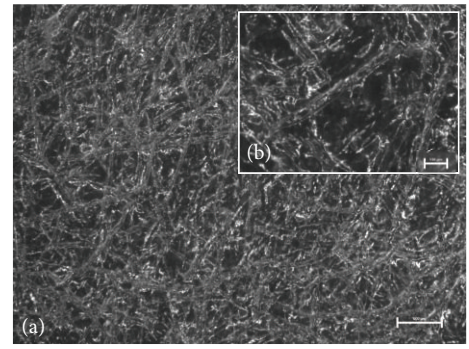

Figure 1: Microscopic appearance of NaCMC film without ibuprofen and Sanatyl: (a) magnification 20x, bar 500 μm; (b) magnification 50x, bar 100 μm.

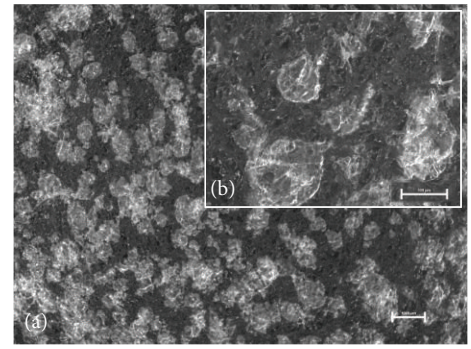

Figure 2: Microscopic appearance of the film with suspended ibuprofen (0.5-Ibu-2 without Sanatyl): (a) magnification 7.5x, bar 1000 μm, (b) magnification 20x, bar 500 μm.

Film thickness is an important parameter from the technological point of view. Uniform thickness means correct method of preparation and good assumption to drug content uniformity as well as to regular process of drug release. The thickness of all films with ibuprofen and Sanatyl did not differ significantly and ranged from 152.3 ± 11.7 μm to 165.4 ± 13.9 μm (in points without Sanatyl fiber, α = 0.05) or from 340.3 ± 15.3 μm to 361.8 ± 10.3 μm (in points with Sanatyl fiber, α = 0.05). The absence of ibuprofen had a negligible effect on the thickness of the film which ranged from 151.6 ± 10.3 μm to 160.9 ± 6.6 μm (in points without Sanatyl fiber) or from 308.5 ± 32.5 μm to 322.1 ± 13.7 μm (in points with Sanatyl fiber). The thickness of films without Sanatyl and without ibuprofen was 186.3 ± 11.6 μm. The results of the film thickness measurement evidenced by low S.D. values showed the sufficient reproducibility of the film preparation method. Higher S.D. values in points with Sanatyl fiber in some samples were owing to material properties of Sanatyl.

Table 2: Surface pH of the films.

Film	pH of the surface intended for contact with wound	pH of the outside
0.5-Ibu-1	5.17 ± 0.17	5.25 ± 0.26
0.5-Ibu-2	5.18 ± 0.27	5.07 ± 0.26
1.0-Ibu-1	5.12 ± 0.1	5.22 ± 0.19
1.0-Ibu-2	5.27 ± 0.23	4.95 ± 0.23
1-blank	5.42 ± 0.02	5.47 ± 0.09
2-blank	5.62 ± 0.06	5.49 ± 0.08
3-blank	5.67 ± 0.11	5.61 ± 0.08
4-blank	5.61 ± 0.09	5.51 ± 0.06

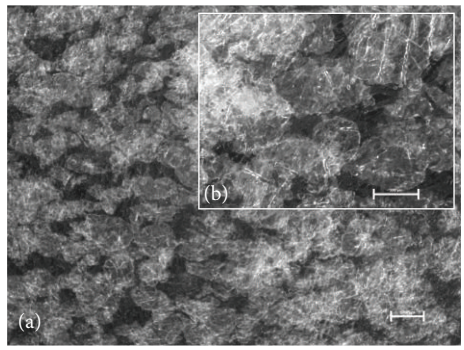

Figure 3: Microscopic appearance of the film with ibuprofen crystallized from acetone solution (0.5-Ibu-1 without Sanatyl): (a) magnification 7.5x, bar 1000 μm, (b) magnification 20x, bar 500 μm.

3.2.2. Surface pH. Values of surface pH of all prepared films were below 6 (Table 2); that is, surface of the films was acidic. Films without ibuprofen were less acidic and did not differ significantly from each other. Films with the suspended drug had lower pH values on the outside (upper layer) which coincides with the acidic nature of ibuprofen incorporated in the upper layer. By contrast, films prepared using the drug solution in acetone showed lower pH values on the surface intended for contact with the wound, most likely due to a diffusion of acetone solution into the bottom NaCMC layer during evaporation. The null hypothesis of equality of the means (t-test) between the sets of films with ibuprofen and without ibuprofen (blank) could not be confirmed, ($P < 0.01$) which points to significant differences in surface pH.

Alterations to the surface pH of the films with ibuprofen during 8 hours in the conditions simulating a wound environment are shown in Figure 5. This evaluation is very important because it reflects the impact of the wound dressing on the wound environment. It is known that pH plays a significant role in wound healing. The pH value within the wound has been shown to affect matrix metalloproteinases (MMPs) activity, tissue inhibitors of MMPs activity, fibroblast activity, keratinocyte proliferation, microbial proliferation, and also immunological responses in a wound [44]. In general, lowering pH has shown to result in an improvement of wound healing. Dressings that directly or indirectly reduce the pH of wound fluid decrease the elevated levels of MMPs which can delay the healing process and may help to prevent infection and improve the antimicrobial activity of some antimicrobials; likewise, oxyhemoglobin releases its oxygen more readily in an acidic environment [44].

Figure 5 demonstrates that all films with ibuprofen retained acidic pH values. Films with the higher concentration of ibuprofen (1.0-Ibu) maintained the lower pH values compared with those containing a reduced amount. In the case of the lower concentration, film 0.5-Ibu-2 was more resistant to PBS than 0.5-Ibu-1. Thus, prepared films, in addition to having an analgesic and anti-inflammatory effect, can also positively influence wound healing rate.

3.2.3. Swelling Property of Films. The swelling behavior of the films is an important property for their practical application. Liquid uptake of the film creates conditions for moist wound healing. It may be affected by several factors such as pH or the presence and character of ions. A physiological buffer solution of pH 7.2 is similar to wound fluid with regard to ion content as well as pH value, and thus determined swelling values of prepared films could adequately reflect those in a real wound.

Films exhibited a mild degree of swelling, indicating moderate holding capacity for the exudate while still maintaining their structural integrity for a reasonable time period. It has been reported that exudate levels in wounds of various etiology differ significantly, as they do in leg ulcers at a range of 0 to 1.2 g/cm^2/day [43]. In the current study, it was observed that 1 cm^2 of film with ibuprofen absorbed on average of 0.09 g PBS after 8 hours which indicated that these dressings could be optimal for wounds with low exudate levels.

Degree of swelling (Sw) was time-dependent and it was in the ascending order 0.5-Ibu-2 < 1.0-Ibu-2 < 0.5-Ibu-1 < 1.0-Ibu-1 < 1-blank < 2-blank < 3-blank < 4-blank (Figure 6). Not surprisingly, the highest degree of swelling was obtained in the case of films without ibuprofen and Sanatyl. Films without ibuprofen and with Sanatyl showed lower swelling values than previous ones due to the minimal swelling capacity of Sanatyl. In the case of all films without ibuprofen, films exposed to acetone during preparation (1-blank, 3-blank) versus others (2-blank, 4-blank) showed a little bit less swelling. Swelling values of all films increased gradually up to 5 hours. The liquid uptake (degree of swelling) of the films without ibuprofen and 0.5-Ibu-1 decreased at the end of the 8-hour observation, possibly due to the partial polymer erosion and dissolving of NaCMC. Film 0.5-Ibu-2 demonstrated the lowest initial degree of swelling, though it continued to swell up until the end of the testing period. 1.0-Ibu-2 demonstrated similar behavior only with a little bit higher liquid uptake. This is most likely due to small particles of suspended ibuprofen in NaCMC dispersion enabling an ion-exchange reaction during preparation with the formation of an insoluble acidic form of CMC. Then, a gradual formation of soluble sodium or potassium salts of the CMC came about after its contact with PBS, which contained monovalent ions, and gradual swelling subsequently ensued.

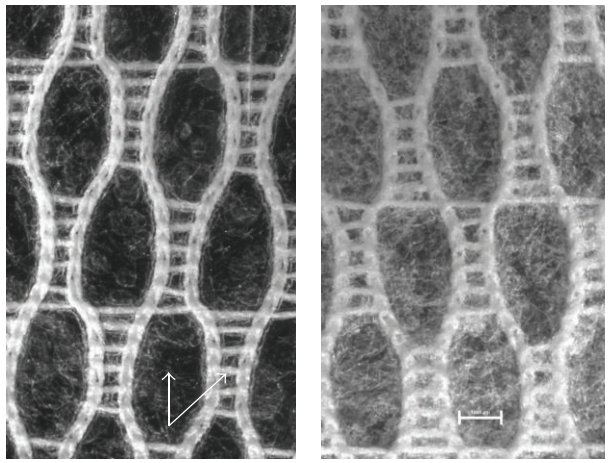

(a) (b)

Figure 4: Microscopic appearance of the films with Sanatyl and the same concentration of ibuprofen (magnified 7.5x, bar 1000 μm): (a) film with suspended drug (0.5-Ibu-2), (b) film with drug incorporated as acetone solution (0.5-Ibu-1); arrows mark points where the thickness of films was measured.

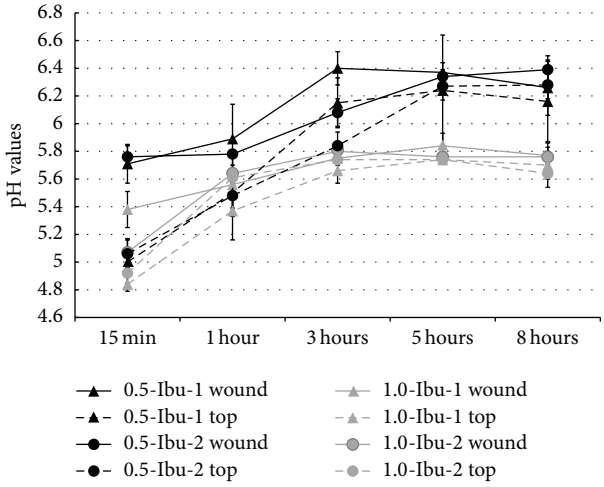

Figure 5: Surface pH of the films with ibuprofen in the conditions simulating a wound environment.

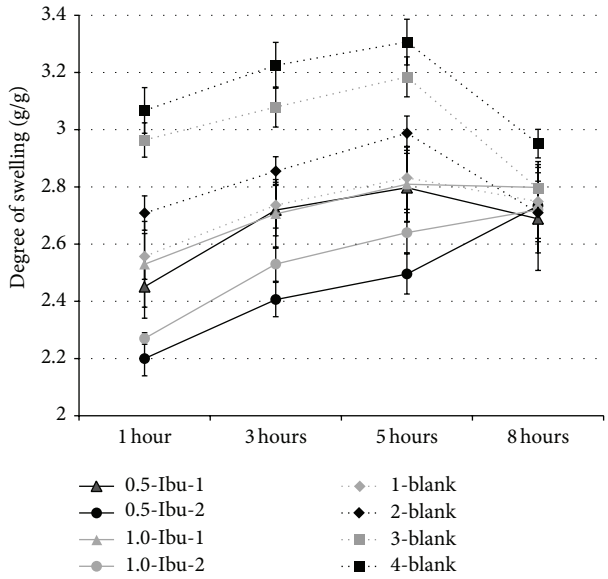

Figure 6: Swelling behavior of prepared films.

3.2.4. Mechanical Properties. The mechanical properties of the prepared films are shown in Table 3. Texturometric analysis was used to measure tensile strength (brittleness and hardness of films), deformation/elongation (elasticity and flexibility), and work done during measurement (resilience).

Mechanical properties of the films without ibuprofen were evaluated by Scheffe's test of pair comparisons which confirm a significant effect ($P < 0.05$) of Sanatyl on the work necessary to tear the film and deformation/elongation at the moment of tearing. Films without Sanatyl needed less work and coincidentally elongated more at the moment of tearing (Figure 7).

The influence of process-formulation variables on the mechanical properties of films with ibuprofen was evaluated with MLR regression using ANOVA. The obtained regression models had the following goodness of fit characteristics: R-square > 0.7, predicted R-square > 0.5, CV < 18%, and the models $P < 0.01$. The impact of ibuprofen concentration and incorporation method was significant (interaction effect $P < 0.01$) in the case of film 0.5-Ibu-2, which needed approximately twice as much tensile strength to tear, and the elongation of film 0.5-Ibu-2 was approximately doubled in comparison with the others (Table 3). This effect may be explained by the formation of an acidic form of CMC during preparation and even dispersion of ibuprofen in the film matrix. The same effect was not observed in the case of 1.0-Ibu-2 probably due to the disturbing influence of the higher content of suspended solid particles on the film matrix. The effect of the method used to incorporate the ibuprofen

Table 3: Mechanical properties of films.

Formulation	Tensile strength [N]	Deformation/ elongation [mm]	Work [mJ]
0.5-Ibu-1	13.35 ± 1.62	3.79 ± 0.71	119.36 ± 20.65
0.5-Ibu-2	22.24 ± 1.62	7.34 ± 1.33	151.47 ± 20.5
1.0-Ibu-1	11.0 ± 0.97	3.72 ± 0.57	110.95 ± 20.04
1.0-Ibu-2	12.89 ± 1.87	4.08 ± 0.61	140.97 ± 21.69
1-blank	17.19 ± 2.36	5.36 ± 0.68	119.11 ± 31.97
2-blank	15.4 ± 1.24	5.32 ± 0.51	112.11 ± 8.02
3-blank	15.87 ± 0.78	6.28 ± 0.48	68.15 ± 5.27
4-blank	17.61 ± 1.39	6.76 ± 0.45	83.8 ± 12.8

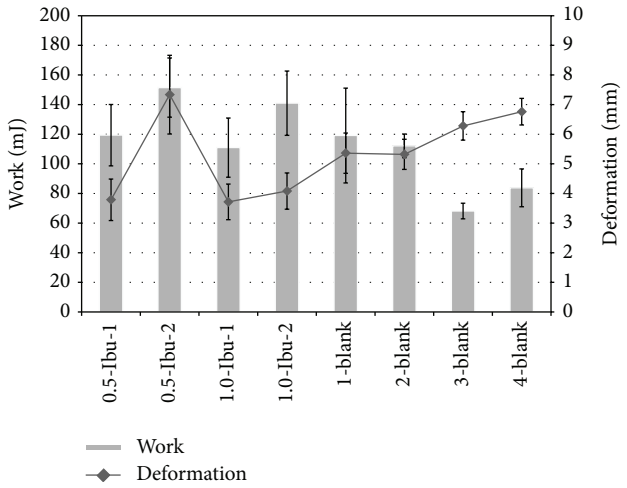

Figure 7: Mechanical properties of films: work done during the process of measurement and deformation/elongation of film at the moment of tearing.

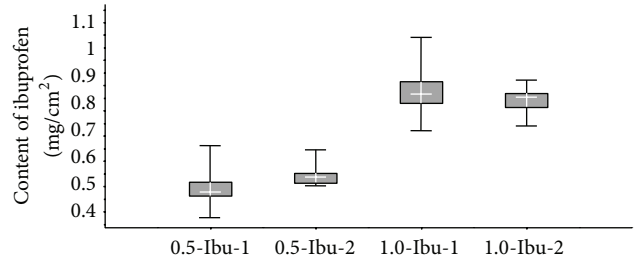

Figure 8: Box diagrams for the drug content uniformity: box encloses 50% of the data and the median as the center of the cross; the whiskers indicate the maximum or minimum value.

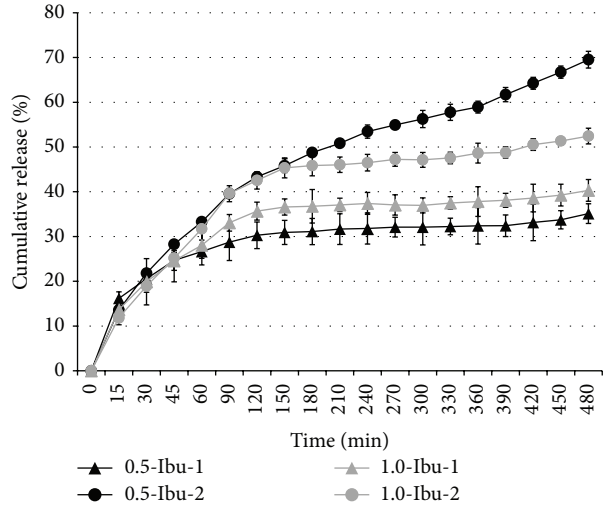

Figure 9: Release of ibuprofen from prepared films.

(Ibu-1 versus Ibu-2) was made most evident in the case of work done ($P < 0.01$), where films with suspended ibuprofen (Ibu-2) yielded values approximately 30 mJ higher than those of Ibu-1 (Table 3, Figure 7).

3.2.5. Drug Content Uniformity. The drug content uniformity ($n = 10$) of the layered films is shown in Table 4. Films with suspended ibuprofen (Ibu-2) showed an accurate drug dosage. Ibu-1 films showed wide variation which suggests that the drug was not uniformly distributed. Differences in drug content uniformity are even more noticeable in Figure 8, where the considerable variance is observed in films prepared with an acetone solution (Ibu-1), and, by contrast, the least variance is visible in the case of 0.5-Ibu-2. Crystals of ibuprofen were clustered together during the evaporation of acetone (Ibu-1) (Figure 3), and this was probably the reason why the drug was not evenly dispersed in the film matrix. The negative effect of the clustered ibuprofen crystals on the drug content uniformity in alginate bilayer films was also observed by Thu and Ng [45]. The low variation of values in the case of Ibu-2 indicated that this method of drug incorporation provided reproducible results and could be used to produce a homogeneous drug/polymer matrix system.

3.2.6. In Vitro Drug Release. Generally, ibuprofen release was dependent on the method of its incorporation. When the drug was suspended in an NaCMC dispersion (Ibu-2), about 70% and 50% of ibuprofen were released in the case of 0.5-Ibu-2 and 1.0-Ibu-2, respectively. Incorporation of ibuprofen as an acetone solution retarded drug release, as only about 35% and 40% in the case of 0.5-Ibu-1 and 1.0-Ibu-1 of the drug had been released from the films by the end of 8-hour testing period (Figure 9).

The reason why a larger amount of the released drug in Ibu-2 films was achieved could be that the films with ibuprofen suspended in an NaCMC dispersion (Ibu-2) had smaller particles in comparison with Ibu-1 films, and ibuprofen was released from them more easily. Tang et al. [46] observed a similar impact of ibuprofen crystal size on the drug release profile from chitosan buccal films. Another explanation may be that more soluble and more easily releasable sodium salt of ibuprofen created a parallel with the formation of an acidic form of CMC by ion exchange during film preparation. This

Table 4: Drug content uniformity in films with ibuprofen.

Formulation	Ibuprofen content (mg/cm^2)	Number of samples within interval ±10%	Number of samples out of interval ±15%	Number of samples out of interval ±25%
0.5-Ibu-1	0.498 ± 0.091	6	2	2
0.5-Ibu-2	0.542 ± 0.042	9	1	—
1.0-Ibu-1	0.872 ± 0.102	8	2	—
1.0-Ibu-2	0.839 ± 0.056	10	—	—

$n = 10$.

Table 5: Kinetic models for the time interval 0–150 min.

Model	Zero order	First order	Higuchi	Hixson-Crowell	Korsmeyer-Peppas		Baker-Lonsdale
Sample	R^2	R^2	R^2	R^2	R^2	n	R^2
0.5-Ibu-1	0.828	0.764	0.924	0.828	0.962	0.285	0.883
0.5-Ibu-2	0.905	0.792	0.972	0.905	0.975	0.530	0.968
1.0-Ibu-1	0.887	0.799	0.962	0.887	0.978	0.437	0.944
1.0-Ibu-2	0.913	0.809	0.974	0.913	0.980	0.600	0.966

Table 6: Kinetic models for the time interval 150–480 min.

Model	Zero order	First order	Higuchi	Hixson-Crowell	Korsmeyer-Peppas		Baker-Lonsdale
Sample	R^2	R^2	R^2	R^2	R^2	n	R^2
0.5-Ibu-1	0.846	0.858	0.812	0.846	0.787	0.083	0.832
0.5-Ibu-2	0.989	0.989	0.979	0.989	0.978	0.335	0.981
1.0-Ibu-1	0.821	0.829	0.770	0.821	0.722	0.066	0.813
1.0-Ibu-2	0.931	0.940	0.893	0.931	0.858	0.116	0.922

explanation is supported also by kinetic models referred to hereinafter.

All prepared films were found intact after the 8-hour dissolution study and exhibited biphasic drug release (Figure 9). This biphasic behavior suggested different mechanisms acting during drug release at each phase. This theory was confirmed by the subsequent analysis in which none of the used kinetic models was able to well describe the obtained dissolution profiles. For this reason, dissolution data were fitted to different kinetic models and the R^2 values for the six models were calculated for time intervals 0–150 min and 150–480 min (Tables 5 and 6).

Korsmeyer-Peppas, Higuchi, and Baker-Lonsdale models properly described the release of ibuprofen from all films during the first 150 min. In this period, all the films predominantly acted as an insoluble matrix, and the drug was released in two ways, mainly based on Fickian diffusion—by extraction from the matrix into the medium and by leaching through the media which entered into the matrix through the pores. In this stage, the films contained sodium salt of ibuprofen and an acidic form of CMC.

The first order model best described the drug release from all the films in the interval 150–480 min, and Fickian diffusion remained the main mechanism of drug release. Because the drug release was also well described by Hixson-Crowell and zero order models, CMC in the films was probably gradually dissolved due to the gradual formation of soluble sodium or potassium salts of CMC which arose from the acidic form of CMC after contact with PBS containing monovalent ions.

The diffusion process was the main drug release mechanism during both stages of the dissolution study. This finding is supported by Perioli et al.'s statistical evaluation of *in vitro* release of ibuprofen from mucoadhesive patches based on NaCMC for buccal administration [47]. In the earlier stages, the rate of diffusion of the drug from the film polymer was higher than the later stages, which is most likely due to higher concentration gradient. The release of the drug from the polymer matrix occurred slowly after maintaining a certain concentration, and this is a very important observation for designing the controlled drug delivery systems [48]. It was observed that the slow release of drugs from polymeric medicated dressings offers some potential advantages which generally include prolonging the action of the active drug over longer periods of time and allowing continual release from such dosage form and thus improving patient compliance by avoiding the problems brought on by frequent dressing changes [25].

4. Conclusions

New film wound dressings with ibuprofen were successfully prepared using an innovative solvent casting method with a sequential coating technique. The films had adequate mechanical and swelling properties and advantageous acidic surface pH for wound application. An *in vitro* drug release study implied that layered films retained the drug for a longer period of time and thus could minimize the frequency of

dressing changes. Films with suspended ibuprofen demonstrated better *in vitro* drug release characteristics as well as drug content uniformity. The concentration of suspended ibuprofen which provided the optimal characteristics for a medicated film wound dressing was 0.5 mg/cm^2 of film.

Conflict of Interests

The authors declare that there is no conflict of interests regarding the publication of this paper.

Acknowledgments

This work was supported by finances from the Technology Agency of the Czech Republic ALFA Program (Research Project no. TA04010065) and IGA VFU Brno, Czech Republic (Research Project no. 53/2014/FaF).

References

[1] C. J. Moffatt, P. J. Franks, and H. Hollinworth, "Understanding wound pain and trauma: an international perspective," in *Pain at Wound Dressing Changes*, pp. 2–7, European Wound Management Association (EWMA), MEP Ltd, London, UK, 2002.

[2] K. Solowiej, V. Mason, and D. Upton, "Psychological stress and pain in wound care, part 2: a review of pain and stress assessment tools," *Journal of Wound Care*, vol. 19, no. 3, pp. 110–115, 2010.

[3] K. Woo, G. Sibbald, K. Fogh et al., "Assessment and management of persistent (chronic) and total wound pain," *International Wound Journal*, vol. 5, no. 2, pp. 205–215, 2008.

[4] M. Briggs, I. Torra, and J. E. Bou, "Pain at wound dressing changes: a guide to management," in *EWMA Position Document. Pain at Wound Dressing Changes*, pp. 12–17, MEP, London, UK, 2002.

[5] P. Vowden, J. Apelqvist, and C. Moffatt, "Wound complexity and healing," in *European Wound Management Association (EWMA). Position Document. Hard-to-Heal Wounds: A Holistic Approach*, pp. 2–9, MEP Ltd, London, UK, 2008.

[6] J. L. Wallace and L. Vong, "NSAID-induced gastrointestinal damage and the design of GI-sparing NSAIDs," *Current Opinion in Investigational Drugs*, vol. 9, no. 11, pp. 1151–1156, 2008.

[7] I. L. Meek, M. A. F. J. van de Laar, and H. E. Vonkeman, "Nonsteroidal anti-inflammatory drugs: an overview of cardiovascular risks," *Pharmaceuticals*, vol. 3, no. 7, pp. 2146–2162, 2010.

[8] C. S. Crystal, T. J. McArthur, and B. Harrison, "Anestetic and procedural sedation techniques for wound management," *Emergency Medicine Clinics of North America*, vol. 25, no. 1, pp. 41–71, 2007.

[9] W. Blanke and B. V. Hallern, "Sharp wound debridement in local anaesthesia using EMLA cream: 6 years' experience in 1084 patients," *European Journal of Emergency Medicine*, vol. 10, no. 3, pp. 229–231, 2003.

[10] R. G. Sibbald, A. Katchky, and D. Queen, "Medical management of chronic wound pain," *Wounds UK*, vol. 2, no. 4, pp. 74–89, 2006.

[11] K. Y. Woo, L. K. Abbott, and L. Librach, "Evidence-based approach to manage persistent wound-related pain," *Current Opinion in Supportive and Palliative Care*, vol. 7, no. 1, pp. 86–94, 2013.

[12] T. Massey, S. Derry, R. A. Moore, and H. J. McQuay, "Topical NSAIDs for acute pain in adults," *Cochrane Database of Systematic Reviews*, vol. 6, Article ID CD007402, 2010.

[13] R. G. Sibbald, P. Coutts, M. Fierheller, and K. Woo, "A pilot (real-life) randomised clinical evaluation of a pain-relieving foam dressing: (Ibuprofen-foam versus local best practice)," *International Wound Journal*, vol. 4, no. 1, pp. 16–23, 2007.

[14] M. Romanelli, V. Dini, R. Polignano, P. Bonadeo, and G. Maggio, "Ibuprofen slow-release foam dressing reduces wound pain in painful exuding wounds: preliminary findings from an international real-life study," *Journal of Dermatological Treatment*, vol. 20, no. 1, pp. 19–26, 2009.

[15] E. Cigna, M. Tarallo, G. Bistoni et al., "Evaluation of polyurethane dressing with ibuprofen in the management of split-thickness skin graft donor sites," *In Vivo*, vol. 23, no. 6, pp. 983–986, 2009.

[16] V. Arapoglou, K. Katsenis, K. N. Syrigos et al., "Analgesic efficacy of an ibuprofen-releasing foam dressing compared with local best practice for painful exuding wounds," *Journal of Wound Care*, vol. 20, no. 7, pp. 319–325, 2011.

[17] K. Fogh, M. B. Andersen, M. Bischoff-Mikkelsen et al., "Clinically relevant pain relief with an ibuprofen-releasing foam dressing: results from a randomized, controlled, double-blind clinical trial in exuding, painful venous leg ulcers," *Wound Repair and Regeneration*, vol. 20, no. 6, pp. 815–821, 2012.

[18] B. Petersen, H. S. Knoth, and O. K. Nielsen, "Ibuprofen foam dressings for wound pain potential as substitute for oral NSAIDs to reduce systemic side effects," http://ewma.org/fileadmin/user_upload/EWMA/pdf/conference_abstracts/2010/Poster/EWMA2010_P%2030.pdf.

[19] M. Briggs, T. Taverner, and B. S. Hodge, "Pharmacological methods of pain control," in *Trauma and Pain in Wound Care*, R. White and K. Harding, Eds., vol. 2, pp. 155–175, Wounds UK, Aberdeen, Scotland, 2009.

[20] G. Sussman, "Technology update: understanding film dressings," *Wounds International*, vol. 1, no. 4, 2010, http://www.woundsinternational.com/product-reviews/technology-update-understanding-film-dressings.

[21] G. Gultekin, C. Atalay-Oral, S. Erkal et al., "Fatty acid-based polyurethane films for wound dressing applications," *Journal of Materials Science: Materials in Medicine*, vol. 20, no. 1, pp. 421–431, 2009.

[22] H. Xu, L. Ma, H. Shi, C. Gao, and C. Han, "Chitosan-hyaluronic acid hybrid film as a novel wound dressing: in vitro and in vivo studies," *Polymers for Advanced Technologies*, vol. 18, no. 11, pp. 869–875, 2007.

[23] R. F. Pereira, A. Mendes, and P. J. Bártolo, "Novel alginate/aloe vera hydrogel blends as wound dressings for the treatment of several types of wounds," *Chemical Engineering Transactions*, vol. 32, pp. 1009–1014, 2013.

[24] N. A. Ramli and T. W. Wong, "Sodium carboxymethylcellulose scaffolds and their physicochemical effects on partial thickness wound healing," *International Journal of Pharmaceutics*, vol. 403, no. 1-2, pp. 73–82, 2011.

[25] H.-E. Thu, M. H. Zulfakar, and S.-F. Ng, "Alginate based bilayer hydrocolloid films as potential slow-release modern wound dressing," *International Journal of Pharmaceutics*, vol. 434, no. 1-2, pp. 375–383, 2012.

[26] S. Paunonen, "Strength and barrier enhancements of cellophane and cellulose derivative films: a review," *BioResources*, vol. 8, no. 2, pp. 3098–3121, 2013.

[27] R. C. Rowe, P. J. Sheskey, S. C. Owen, and American Pharmacists Association, *Handbook of Pharmaceutical Excipients*, Pharmaceutical Press, London, UK, 5th edition, 2006.

[28] Q. Garrett, P. A. Simmons, S. Xu et al., "Carboxymethylcellulose binds to human corneal epithelial cells and is a modulator of corneal epithelial wound healing," *Investigative Ophthalmology & Visual Science*, vol. 48, no. 4, pp. 1559–1567, 2007.

[29] M. Y. Karami, O. R. Zekavat, and A. Amant, "Excisional wound healing activity of carboxymethyle cellulose in diabetic rat," *Journal of Jahrom University of Medical Sciences*, vol. 9, no. 4, pp. 48–57, 2012.

[30] I. R. Sweeney, M. Miraftab, and G. Collyer, "A critical review of modern and emerging absorbent dressings used to treat exuding wounds," *International Wound Journal*, vol. 9, no. 6, pp. 601–612, 2012.

[31] D. Vetchý, H. Landová, J. Gajdziok, P. Doležel, Z. Daněk, and J. Štembírek, "Determination of dependencies among in vitro and in vivo properties of prepared mucoadhesive buccal films using multivariate data analysis," *European Journal of Pharmaceutics and Biopharmaceutics*, vol. 86, no. 3, pp. 498–506, 2014.

[32] S. Saha, C. Tomaro-Duchesneau, J. T. Daoud, M. Tabrizian, and S. Prakash, "Novel probiotic dissolvable carboxymethyl cellulose films as oral health biotherapeutics: *in vitro* preparation and characterization," *Expert Opinion on Drug Delivery*, vol. 10, no. 11, pp. 1471–1482, 2013.

[33] N. Khatoon, N. G. R. Rao, and B. M. Reddy, "Overview on fast dissolving oral films," *International Journal of Chemistry and Pharmaceutical Sciences*, vol. 1, no. 1, pp. 63–75, 2013.

[34] S. Raju, P. Sandeep Reddy, V. Anirudh Kumar, A. Deepthi, K. Reddy Sreeramulu, and P. V. Madhava Reddy, "Flash release oral films of metoclopramide hydrochloride for pediatric use: formulation and in-vitro evaluation," *Journal of Chemical and Pharmaceutical Research*, vol. 3, no. 4, pp. 636–646, 2011.

[35] R. P. Dixit and S. P. Puthli, "Oral strip technology: overview and future potential," *Journal of Controlled Release*, vol. 139, no. 2, pp. 94–107, 2009.

[36] S. K. Ramineni, L. L. Cunningham, T. D. Dziubla, and D. A. Puleo, "Development of imiquimod-loaded mucoadhesive films for oral dysplasia," *Journal of Pharmaceutical Sciences*, vol. 102, no. 2, pp. 593–603, 2013.

[37] J. Boateng, J. Mani, and F. Kianfar, "Improving drug loading of mucosal solvent cast films using a combination of hydrophilic polymers with amoxicillin and paracetamol as model drugs," *BioMed Research International*, vol. 2013, Article ID 198137, 8 pages, 2013.

[38] J. Gajdziok and M. Rabišková, "Orodispersable dosage forms and technologies used in their production," *Česká a Slovenská Farmacie*, vol. 59, no. 6, pp. 251–255, 2010.

[39] P. Rachtanapun, S. Luangkamin, K. Tanprasert, and R. Suriyatem, "Carboxymethyl cellulose film from durian rind," *LWT: Food Science and Technology*, vol. 48, no. 1, pp. 52–58, 2012.

[40] Y. Quin, "Smart wound-care materials," in *Smart Textiles for Medicine and Healthcare*, pp. 27–49, Woodhead Publishing Limited, Cambridge, UK, 2007.

[41] S. S. Shidhaye, N. S. Saindane, S. Sutar, and V. Kadam, "Mucoadhesive bilayered patches for administration of sumatriptan succinate," *AAPS PharmSciTech*, vol. 9, no. 3, pp. 909–916, 2008.

[42] H. V. Pawar, J. Tetteh, and J. S. Boateng, "Preparation, optimisation and characterisation of novel wound healing film dressings loaded with streptomycin and diclofenac," *Colloids and Surfaces B: Biointerfaces*, vol. 102, pp. 102–110, 2013.

[43] B. Steffansen and S. P. K. Herping, "Novel wound models for characterizing ibuprofen release from foam dressings," *International Journal of Pharmaceutics*, vol. 364, no. 1, pp. 150–155, 2008.

[44] S. L. Percival, S. Mccarty, J. A. Hunt, and E. J. Woods, "The effects of pH on wound healing, biofilms, and antimicrobial efficacy," *Wound Repair and Regeneration*, vol. 22, no. 2, pp. 174–186, 2014.

[45] H.-E. Thu and S.-F. Ng, "Gelatine enhances drug dispersion in alginate bilayer film via the formation of crystalline microaggregates," *International Journal of Pharmaceutics*, vol. 454, no. 1, pp. 99–106, 2013.

[46] C. Tang, Y.-X. Guan, S.-J. Yao, and Z.-Q. Zhu, "Preparation of ibuprofen-loaded chitosan films for oral mucosal drug delivery using supercritical solution impregnation," *International Journal of Pharmaceutics*, vol. 473, no. 1-2, pp. 434–441, 2014.

[47] L. Perioli, V. Ambrogi, F. Angelici et al., "Development of mucoadhesive patches for buccal administration of ibuprofen," *Journal of Controlled Release*, vol. 99, no. 1, pp. 73–82, 2004.

[48] B. Singh and L. Pal, "Sterculia crosslinked PVA and PVA-poly(AAm) hydrogel wound dressings for slow drug delivery: Mechanical, mucoadhesive, biocompatible and permeability properties," *Journal of the Mechanical Behavior of Biomedical Materials*, vol. 9, pp. 9–21, 2012.

Hindawi Publishing Corporation
BioMed Research International
Volume 2015, Article ID 109563, 11 pages
http://dx.doi.org/10.1155/2015/109563

Research Article

Preparation and Characterization of Solid Dispersions of Artemether by Freeze-Dried Method

Muhammad Tayyab Ansari,[1] Altaf Hussain,[1] Sumaira Nadeem,[1] Humaira Majeed,[1] Syed Saeed-Ul-Hassan,[2] Imran Tariq,[2] Qaisar Mahmood,[3] Abida Kalsoom Khan,[4] and Ghulam Murtaza[5]

[1]*Faculty of Pharmacy, Bahauddin Zakariya University, Multan 6000, Pakistan*
[2]*College of Pharmacy, University of the Punjab, Lahore 54000, Pakistan*
[3]*Department of Environmental Sciences, COMSATS Institute of Information Technology, Abbottabad 22060, Pakistan*
[4]*Department of Chemistry, COMSATS Institute of Information Technology, Abbottabad 22060, Pakistan*
[5]*Department of Pharmacy, COMSATS Institute of Information Technology, Abbottabad 22060, Pakistan*

Correspondence should be addressed to Ghulam Murtaza; gmdogar356@gmail.com

Received 23 May 2014; Revised 15 July 2014; Accepted 10 August 2014

Academic Editor: Josef Jampilek

Solid dispersions of artemether and polyethylene glycol 6000 (PEG6000) were prepared in ratio 12 : 88 (group-1). Self-emulsified solid dispersions of artemether were prepared by using polyethylene glycol 6000, Cremophor-A25, olive oil, Transcutol, and hydroxypropyl methylcellulose (HPMC) in ratio 12 : 75 : 5 : 4 : 2 : 2, respectively (group-2). In third group, only Cremophor-A25 was replaced with Poloxamer 188 compared to group-2. The solid dispersions and self-emulsified solid dispersions were prepared by physical and freeze dried methods, respectively. All samples were characterized by X-ray diffraction, attenuated total reflectance Fourier transform infrared spectroscopy, differential scanning calorimeter, scanning electron microscopy, and solubility, dissolution, and stability studies. X-ray diffraction pattern revealed artemether complete crystalline, whereas physical mixture and freeze-dried mixture of all three groups showed reduced peak intensities. In attenuated total reflectance Fourier transform infrared spectroscopy spectra, C–H stretching vibrations of artemether were masked in all prepared samples, while C–H stretching vibrations were representative of polyethylene glycol 6000, Cremophor-A25, and Poloxamer 188. Differential scanning calorimetry showed decreased melting endotherm and increased enthalpy change (ΔH) in both physical mixture and freeze-dried mixtures of all groups. Scanning electron microscopy of freeze-dried mixtures of all samples showed glassy appearance, size reduction, and embedment, while their physical mixture showed size reduction and embedment of artemether by excipients. In group-1, solubility was improved up to 15 times, whereas group-2 showed up to 121 times increase but, in group-3, when Poloxamer 188 was used instead of Cremophor-A25, solubility of freeze-dried mixtures was increased up to 135 times. In fasted state simulated gastric fluid at pH 1.6, the dissolution of physical mixture was increased up to 12 times and freeze-dried mixtures up to 15 times. The stability of artemether was substantially enhanced in freeze-dried mixtures by using polyethylene glycol 6000, Cremophor-A25, and Poloxamer 188 of self-emulsified solid dispersions of artemether in Hank's balanced salt solution at pH 7.4.

1. Introduction

Malaria is the infection caused by protozoan parasites transmitted with female Anopheles mosquitoes belonging to the genus, *Plasmodium* [1]. The five different species of *Plasmodium* which are the basis of malarial disease in many human beings are *P. vivax, P. falciparum, P. malariae, P. ovale,* and *P. knowlesi*. The symptoms of malaria at first may be nonspecific such as joint pain, abdominal pain, asthenia, high fever, anorexia, and vomiting as well as shivering. *P. falciparum* may cause the most severe form of malaria particularly in children as well as in nonimmune travellers who are from nonendemic countries and also in pregnant women [2].

According to a wide survey of malaria, ninety-nine countries out of 106 malaria endemic countries had ongoing

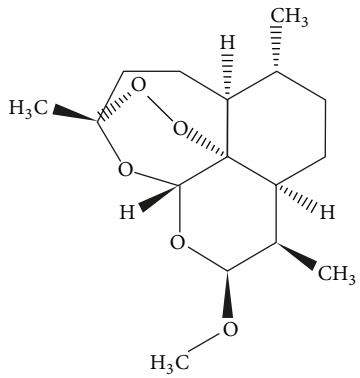

Figure 1: Structure of the ARTM [10].

malaria transmission. About 3.3 billion people in the world were endangered of malaria according to estimation. Malaria is the infectious disease as well as most prevalent disease in the world which in each year affects 515–600 million humans. About 40% of world population was vulnerable to malarial infection. In 2010, an estimated 655,000 persons died because of malaria; out of them, 86% were only the children with age of less than five years [3].

In order to advance the cure rates and clinical responses as well as to slow the development of resistance of malaria parasite, WHO has suggested that artemisinin derivatives should be present in antimalarial regimens. Artemether (ARTM) which is artemisinin derivative reduces malaria transmission and may also reduce the gametocyte carriage [4, 5]. ARTM belongs to artemisinin family and is the active component of the Chinese herbs, that is, the *qinghao*, known as *Artemisia annua*. ARTM has quick start of the schizontocidal actions and then it is metabolized in the liver into its demethylated derivatives, known as dihydroartemisinin (DHA). ARTM has been proved to be efficient against acute *P. falciparum* as well as uncomplicated malaria. Its structural unit consists of 1,2,4-trioxane ring constituting the active pharmacophore of the ARTM which was responsible for its antimalarial activity [6]. Solubility of ARTM in water is poor, so it has been synthesized in tablets as well as intramuscular injections, but short half-life of about 3 to 5 hours is the significant drawback of ARTM [7]. ARTM results in incomplete absorption after oral administration due to poor aqueous solubility. By using more water soluble formulation, the solubility and dissolution can be increased [8].

In the literature, various technological strategies are reported such as solid dispersions, self-emulsifying drug delivery systems (SEDDSs), micronizations, and complex formation with cyclodextrins [9]. The chemical structure of ARTM is shown in Figure 1.

The aim of this study was to prepare self-emulsified solid dispersions (SESDs) of ARTM by using PEG6000, Poloxamer 188, Cremophor-A25, Transcutol, olive oil, and HPMC in order to improve solubility and dissolution behavior of ARTM.

2. Materials and Methods

2.1. Materials. Artemether (ARTM) (Alchem, China), acetonitrile HPLC grade (Merck, Germany), analytical grade methanol (Merck, Germany), Cremophor-A25 (chemically known as polyethylene glycol 1100 mono(hexadecyl/octadecyl) ether, YunGou Chemicals, China), polyethylene glycol 6000 (PEG 6000, Fluka, USA), Poloxamer 188 (chemically known as poly(ethylene glycol)-*block*-poly(propylene glycol)-*block*-poly(ethylene glycol), YunGou Chemicals, China), olive oil (Mezoa Chemicals, Spain), hydroxypropyl methylcellulose-K15M (HPMC-K15M, Fluka, USA), Transcutol (chemically known as 2-(2-ethoxyethoxy)ethanol, YunGou Chemicals, China), starch (Fluka limited company), lactose (as monohydrate, DMV International, Pakistan), Primogel (chemically known as sodium Starch glycolate, Yung Zip Chemicals, China), magnesium stearates (Mg Stearate, Royal Tiger, Pakistan), potassium bromides (KBr, Merck, Germany), hydrochloric acid (HCl, Merck, Germany), sodium chloride (NaCl, Sigma-Aldrich, Germany), sodium taurocholate (Sigma-Aldrich, Germany), and silica gel were purchased through commercial sources and used without further treatment.

2.2. Physical Mixture (PM) Method. Physical mixtures (PMs) were prepared using weighed amount of ARTM and PEG6000 in ratio 12 : 88 named group-1 and ARTM, PEG6000, Cremophor-A25, olive oil, Transcutol, and HPMC with ratio 12 : 75 : 5 : 4 : 2 : 2, respectively, named group-2. Similarly, ARTM, PEG6000, Poloxamer 188, olive oil, Transcutol, and HPMC with ratio 12 : 75 : 5 : 4 : 2 : 2, respectively, was named group-3. These physical mixtures were dried in oven at 37°C and then, after complete drying, homogenous mixture was made by using pestle and mortar with soft grinding. These mixtures were passed through a sieve of 180 μm mesh size, placed in dried, labeled brown glass bottles and then kept in desiccators at room temperature for further analysis.

2.3. Freeze-Dried (FD) Method. Via freeze drying method, soluble mixtures of weighed amount of ARTM and PEG6000 in ratio 12 : 88 (Group-1) and ARTM, PEG6000, Cremophor-A25, olive oil, Transcutol, and HPMC with ratio 12 : 75 : 5 : 4 : 2 : 2, respectively (group-2) were prepared. Similarly ARTM, PEG6000, Poloxamer 188, olive oil, Transcutol and HPMC with ratio 12 : 75 : 5 : 4 : 2 : 2, respectively (group-3) were mixed to prepare soluble mixture. According to these corresponding groups, solutions were transferred to round bottom flasks and shaked on orbit shaker (BioTechnics, India) for mixing. After proper mixing, solvents were evaporated by using rotary evaporator (Prolific Instruments, India). Then, small amount of deionize water was added, shaken well, and frozen at temperature of −70°C to −80°C in the electronic deep-freezer (Dawlance, Pakistan). The frozen form is then freeze-dried using lyophilizer (Labconco, England) at temperature of −42°C using vacuum of 0.100 mBar for complete removal of solvents. After complete drying, the freeze-dried (FD) mixtures were transferred to pestle and mortar, softly grinded, and passed through a sieve (180 μm).

These preparations were then stored in dried, labeled brown glass bottles and stored in desiccators for further process.

2.4. X-Ray Diffraction Studies. The X-ray powder diffraction (XRD) study of all samples was done by using apparatus named Siemens D-500. The measurements and conditions of XRD consisted of the targeting of CuKα, by using voltage of 40 KV and the current of 30 mA. A modified system of diverging and receiving as well as receiving and antiscattering slits of 1°, 1°, 1°, and 0.15°, respectively, was utilized. For data processing, Jade 6.0 (Materials Delta Inc.) was used. By utilizing a step width of about 0.04° 2θ between 5° and 50°, the XRD patterns were obtained.

2.5. Attenuated Total Reflectance Fourier Transform Infrared (ATR-FTIR) Spectrophotometric Analysis. By using potassium bromide (KBr) disc method (i.e., 0.5–1% of the sample in 200 mg KBr disc), ATR-FTIR spectra of SESDs of ARTM were obtained through Perkin Elmer spectrum 1. The scanning was at 400–4000 cm^{-1} and a resolution was then 1 cm^{-1}. Instrument calibration was occasionally repeated during these operations.

2.6. Differential Scanning Calorimetric Analysis. Differential scanning calorimetric (DSC) analysis of physical and freeze-dried mixtures of ARTM and excipients was performed by using Q2000 DSC (TA instrument, USA). The samples were heated at a rate of 5°C/min from 25 to 250°C under a dry nitrogen gas purge. Tzero aluminum was used to calibrate the cell constant. All measurements were conducted in sealed nonhermetic aluminum pans. The typical sample weight was 5–10 mg.

2.7. Scanning Electron Microscopy. In order to identify and confirm the nature as well as surface topography of all formulated samples of ARTM, scanning electron microscopy (SEM, Perkin Elmer, USA) was used. SEM analysis was also performed to study the morphologies of pure drug as well as different self-emulsifying agents. For scanning electron photographs, an accelerating voltage of 5 kV was utilized and the resultant micrographs were then examined at magnifications of ×1000, ×1500, and ×2500.

2.8. Equilibrium Solubility Studies. For solubility in equilibrium studies, 0.4 g of each group was weighed properly and then transferred into test tubes containing 10 mL of the deionized water and mixed by using vortex mixture for period of about 1 to 2 min at 1400 revolutions per minutes (RPM). The prepared samples were fixed on orbit shaker for mixing and shaken for a period of 7 days at about 150 RPM at a temperature of 37°C. After a period of 7 days, each sample was then centrifuged at about 6000 RPM for 20 min. Then, upper layer of about 5 mL was decanted carefully by using micropipette and was then further diluted with 20 mL of deionized water. They were then analyzed on HPLC at 215 nm ultraviolet (UV) wavelength.

2.9. Preparation and Characterization of Tablets. Tablets were prepared employing direct compression method using single punch tablet machine. To make tablets, the homogenous mixture of preformulated grains and lactose (quantity sufficient for 500 mg tablet weight) was prepared followed by passing through a sieve of 180 μm mesh size. Magnesium stearate (0.5%), Primogel (5%), and talcum powder (0.5%) were also mixed with these grains and mixing was carried out for about 10–20 min. The weight of each tablet was 500 mg, out of which 333 mg consisted of granules containing 40 mg of pure ARTM and another portion was 167 mg consisting of inactive material. The prepared tablets of different formulations were then stored and labeled properly. For assessment of quality, these tablets were characterized for various compendial requirements including weight variation, friability, and drug contents.

2.10. Dissolution Studies. The dissolution studies of all formulations of ARTM were done by utilizing USP dissolution apparatus II (Digitek, Lahore, Pakistan) with stirring speed of 100 RPM at 37°C. Fasted state simulated gastric fluid (FaSSGF) with pH of 1.6 with composition of sodium taurocholate 80 μM, sodium chloride (NaCl) 34.2 mM, hydrochloric acid (HCl) q.s. to adjust pH to 1.6, and deionized water q.s. to make 1 L with pH 1.6 was used as biorelevant dissolution medium. The tablets containing SESDs of ARTM as well as other excipients in various ratios were put in dissolution medium of about 1000 mL. In the dissolution experiment, each tablet contained a specific quantity of powder in which 40 mg ARTM was present. On specific time intervals such as 5, 15, 30, 60, 90, 120, 180, and 240 min, aliquots of about 10 mL were taken out which were replaced through the addition of 10 mL of fresh FaSSGF. These obtained samples were then analyzed using HPLC at 215 nm. The obtained dissolution data was analyzed using various kinetic models including zero order, first order, Higuchi, and Korsemeyer-Peppas model. Indifferent to other models, Korsmeyer-Peppas model involves the fitting of initial 60% drug release data to find out the mode of drug release, n [8].

2.11. Stability Studies. For pure ARTM, SDs, and SESDs of ARTM, the stability tests in Hank's balanced salt solutions were carried out at 37°C that indicated the dissolution test temperature. The Hank's balanced salt solution was formulated with 0.40 gL^{-1} KCl, 8.00 gL^{-1} NaCl, 0.06 gL^{-1} KH_2PO_4, 0.35 gL^{-1} $NaHCO_3$, 0.19 gL^{-1} $CaCl_2 \cdot 2H_2O$, 0.05 gL^{-1} Na_2HPO_4, 0.09 gL^{-1} $MgSO_4$, and 1.00 gL^{-1} glucose and the pH was adjusted to 7.4 (with $NaHCO_3$, 3.8 mM, pH 11.2, solution). For stability tests in Hank's balanced salt solutions (pH 7.4), ARTM and its SESDs solution with concentration of 100 $\mu g\,mL^{-1}$ were firstly put into 10 mL test tubes with plugs. Then, aliquots of about 0.5 mL were taken out at intervals of 1 hour at 37°C in 6 hour. The concentration of pure ARTM and prepared samples was measured by HPLC at 215 nm and each test was performed in triplicate. Since the degradation of ARTM followed first-order kinetics, apparent degradation rate constants (k) were used to calculate the stability of ARTM and its SESDs from the slope of the degradation diagrams according to the following equation:

$$\ln [C] = \ln [C_o] - kt, \quad (C \neq C_o), \tag{1}$$

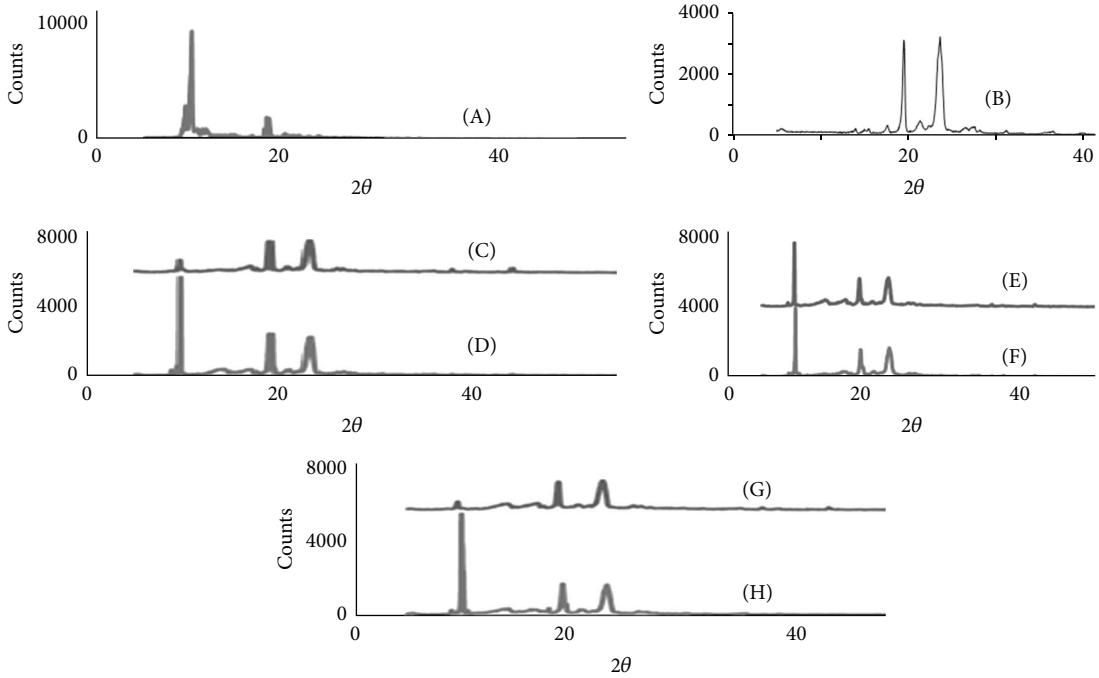

Figure 2: X-ray diffraction patterns of ARTM (A), PEG6000 (B), physical mixture of group-1 (C), freeze-dried mixture of group-1 (D), physical mixture of group-2 (E), freeze-dried mixture of group-2 (F), physical mixture of group-3 (G), and freeze-dried mixture of group-3 (H).

where $[C_o]$ was the initial concentration of ARTM, $[C]$ was the concentration of ARTM at time t, and k was the slope of the fitted linear regression for the first order reaction.

2.12. High Performance Liquid Chromatography (HPLC) Analysis. The supernatant solutions of each group of SESDs of ARTM were withdrawn and then filtered through the cellulose acetates filters of 0.22 μm in pore size. The amount of drug dissolved was then analyzed by using HPLC (Perkin Elmer, USA) at 215 nm after suitable dilution. This assay was determined by using reverse phase C18 column (4.6 mm × 250 mm, 5 μ), while UV detector was set at a wavelength of about 215 nm. Mobile phase consisted of a mixture of acetonitrile and water (75 : 25, v/v) operated at a flow rate of 1 mL/min. The injection volume was 20 μL.

The validation data shows that the used HPLC method follows linearity in the range of 0.078 to 2.5 mg, as evident from the value of $R^2 = 0.999$ with $Y = 462.5X - 21.32$. It relates to the closeness of the test results to true values, that is, measure of exactness of analytical method. It is expressed as percentage recovery by the assay of known amount of analyte in the linearity range. For the determination of accuracy, the ARTM percentage recovery was 99.98, 100.34, 101.64, 101.75, 101.83, and 101.94% for dilutions 0.078, 0.1562, 0.3125, 0.625, 1.25, and 2.5 mg/mL, respectively. The accuracy and precision of method were 99.31 ± 2.94 and 98.72 ± 2.02, respectively [11].

2.13. Statistics. In all cases, analysis of the data was carried out by applying one-way ANOVA with a probability of $P < 0.05$ set as statistically significant.

3. Results and Discussion

3.1. X-Ray Diffraction Studies. The XRD patterns of artemether (ARTM) showed very strong characteristic diffraction peaks at 2θ of 9.88°, 17.64°, 18.04°, and 19.68°. It signifies that artemether is purely a crystalline compound (Figure 2(A)). The XRD pattern of PEG6000 showed characteristic diffraction peaks at 2θ of 19.6° and 23.76° (Figure 2(B)).

Poloxamer 188 is crystalline in nature and gives three characteristic peaks, that is, at 19°, 22°, and 23° [11]. X-ray diffraction analysis of physical mixture of group-1 showed characteristic diffraction peaks at 2θ of 9.80°, 19.20°, and 23.40°, similarly freeze-dried mixture of group-1 showed diffraction peaks at 2θ of 9.72°, 19.12°, and 23.32°. These peaks represent ARTM and PEG6000. It was noted that intensity of ARTM diffraction peaks in physical mixture of group-1 was lower than the intensity of pure ARTM, while in freeze-dried mixtures crystalline peaks of ARTM were very less intense than pure ARTM (Figures 2(C) and 2(D)).

The X-ray diffraction analysis of physical mixture of group-2 showed characteristic diffraction peaks at 2θ of 9.88°, 19.28°, and 23.44°, while its freeze-dried form showed peaks at 2θ of 9.72°, 19.12°, and 23.36°, respectively. These peaks represent ARTM and PEG6000 also. The principal ARTM peak of ARTM and PEG6000 in physical and freeze-dried mixtures of group-2 were present but having lower intensity compared to pure ARTM and this decrease of intensity were more pronounced in freeze-dried mixture than in physical mixture (Figures 2(E) and 2(F)), as also seen for rofecoxib [12].

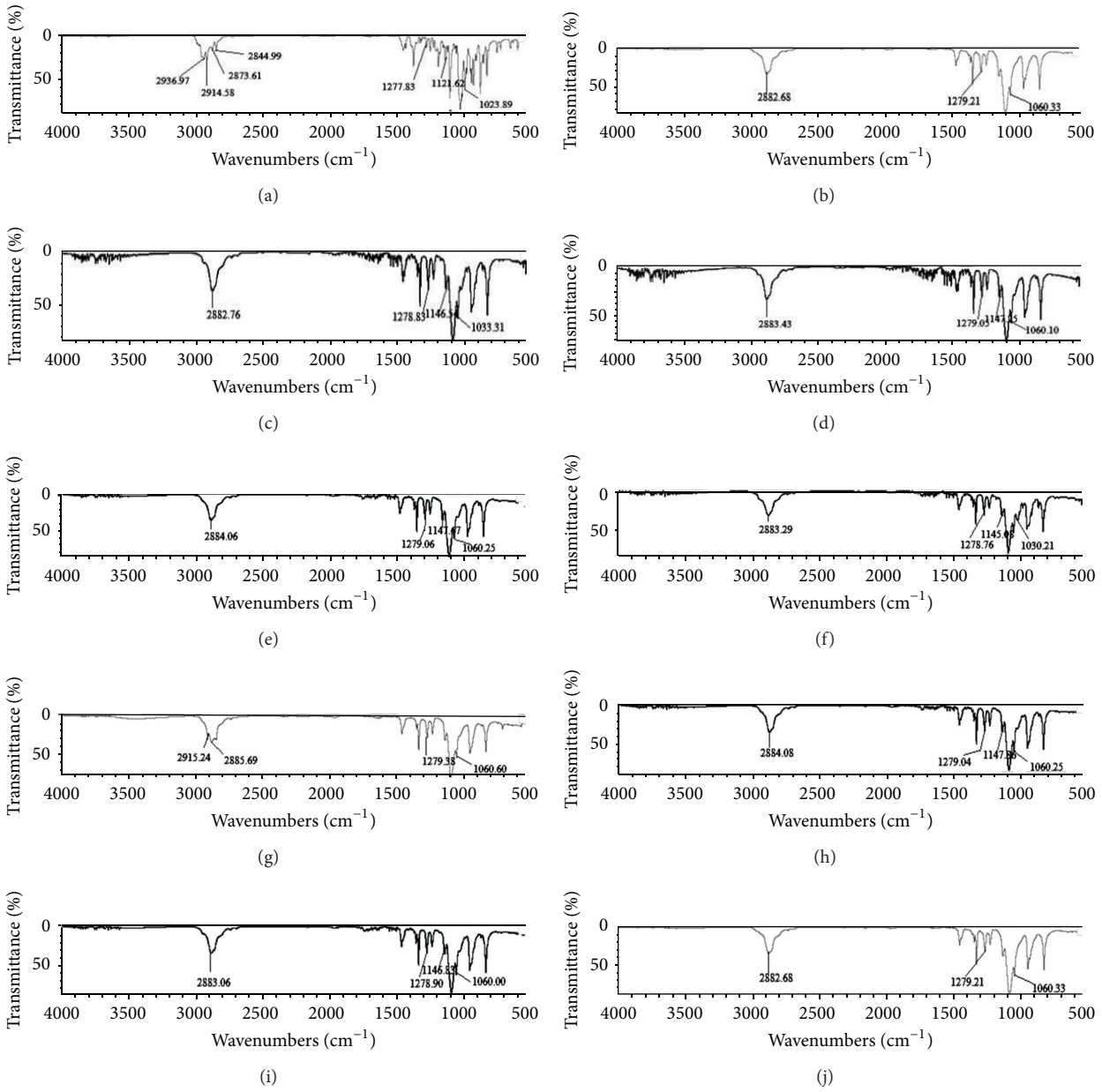

Figure 3: ATR-FTIR spectra of pure ARTM (a), PEG6000 (b), physical mixture of group-1 (c), freeze-dried mixture of group-1 (d), Cremophor-A25 (e), physical mixture of group-2 (f), freeze-dried mixture of group-2 (g), Poloxamer 188 (h), physical mixture of group-3 (i), and freeze-dried mixture of group-3 (j).

When Poloxamer 188 was incorporated in place of Cremophor-A25 in SESDs compared to XRD of physical mixture of group-3, SESDs showed diffraction peaks at 2θ of 10.12°, 19.48°, and 23.76° and its freeze-dried mixture showed peaks at 2θ of 9.64°, 19.04°, and 23.20°, respectively, which were representative of ARTM and PEG6000. The peak intensity of two peaks of PEG6000 in both physical and freeze-dried mixture of group-3 was substantially decreased, while principal ARTM peak in its freeze-dried mixture was 12 times less than intense compared to pure ARTM (Figures 2(G) and 2(H)), as also seen for rofecoxib [12, 13].

3.2. Attenuated Total Reflectance Fourier Transform Infrared Spectroscopy (ATR-FTIR) Studies. ATR-FTIR spectra of artemether (ARTM) indicated the presence of four characteristic peaks of C–H stretching vibrations at 2844.99 cm^{-1}, 2873.61 cm^{-1}, 2914.58 cm^{-1}, and 2936.97 cm^{-1}, C–O–O–C bending vibrations at 1121.62 cm^{-1}, C–O–C stretching vibrations at 1023.89 cm^{-1} and 1277.83 cm^{-1}, and C–H bending vibrations at 1451.05 cm^{-1} (Figure 3(a)).

The ATR-FTIR spectra of PEG6000 showed characteristic bands of C–H stretching vibrations at 2882 cm^{-1}, O–H bending vibrations at 1341.02 cm^{-1} and 359.52 cm^{-1}, C–O

stretching vibrations at 1059.97 cm^{-1} and 1278.91 cm^{-1}, and C–H bending vibrations at 1466.38 cm^{-1} (Figure 3(b)).

Physical and freeze-dried mixtures of group-1 showed characteristic bands of C–H stretching vibrations in functional group region at 2882.76 cm^{-1} and 2883.43 cm^{-1} which was single broader peak instead of four peaks of ARTM alone; in the fingerprint region, C–O–O–C bending vibrations of both physical and freeze-dried mixtures of group-1 were unaltered. C–O–C stretching vibrations of physical mixtures of group-1 were red shifted at 1033.31 cm^{-1} and 1278.83 cm^{-1}, while its freeze-dried mixtures were also red shifted at 1060.12 cm^{-1} and 1279.05 cm^{-1}, respectively. C–H bending vibrations of physical mixtures of group-1 were red shifted at 1456.79 cm^{-1} and 1465.91 cm^{-1}, while its freeze-dried mixtures were red shifted at 1456.91 cm^{-1} and 1465.74 cm^{-1}, respectively. ATR-FTIR spectra tell about presence and absence of bonding interaction among ARTM and excipients due to mixing, grinding, and freeze drying (Figures 3(c) and 3(d)).

ATR-FTIR spectra of Cremophor-A25 showed characteristic bands of C–H stretching vibrations at 2885.69 cm^{-1} and 2915.24 cm^{-1}, O–H bending vibrations at 1341.58 cm^{-1} and 1359.54 cm^{-1}, and C–O–C stretching vibrations at 1060.60 cm^{-1} and 1279.38 cm^{-1}. In group-2 of SESDs of ARTM, physical and freeze-dried mixture showed characteristic bands of C–H stretching vibrations in the functional group region at 2883.29 cm^{-1} and 2884.06 cm^{-1}, respectively, which indicated that C–H stretching vibrations of ARTM were masked as compared to pure ARTM and the C–H stretching vibrations of both physical and freeze-dried mixtures showed characteristics bands of Cremophor-A25. Similarly, in the fingerprint region, the C–O–O–C bending vibrations were unaltered which showed that there was no change in trioxane ring that indicated that our SESDs retained their antimalarial activity. The C–O–C stretching vibrations of physical mixtures of group-2 were red shifted at 1030.21 cm^{-1} and 1278.76 cm^{-1}, while its freeze-dried mixtures were red shifted at 1060.25 cm^{-1} and 1279.06 cm^{-1}; C–H bending vibrations of physical mixture of group-2 were red shifted at 1465.92 cm^{-1} and its freeze-dried mixture was red shifted at 1466.15 cm^{-1} (Figures 3(e)–3(g)).

ATR-FTIR spectra of Poloxamer 188 showed characteristic bands of C–H stretching vibrations at 2882.68 cm^{-1}, O–H bending vibrations at 1341.58 cm^{-1} and 1359.38 cm^{-1}, and C–O–C stretching vibrations at 1060.33 cm^{-1} and 1279.21 cm^{-1}. When Poloxamer 188 was substituted with Cremophor-A25 in group-3 of SESDs of ARTM, the peak intensities and frequency of transmittance were not changed significantly. Physical and freeze-dried mixtures of group-3 showed characteristic bands of C–H stretching vibrations at 2883.06 cm^{-1} and 2884.08 cm^{-1} which indicated that C–H stretching vibrations of ARTM were masked and the C–H stretching vibrations of both physical and freeze-dried mixtures showed characteristics of Poloxamer 188. There was no change in C–O–O–C bending vibrations in physical and freeze-dried mixtures of group-3. C–O–C stretching vibrations of physical mixtures of group-3 were also red shifted at 1060 cm^{-1} and 1278.90 cm^{-1}, whereas its freeze-dried mixture was red shifted at 1060.25 cm^{-1} and 1279.04 cm^{-1}, respectively. C–H bending vibrations of physical and freeze-dried mixtures of group-3 were red shifted at 1466.13 cm^{-1} and 1466.11 cm^{-1}, respectively (Figures 3(h)–3(j)).

The disruption in crystalline structure was similar to that of DHA [14]. The shifting and broadening agreed with previous ketoconazole results [15]. The shifting in the carbonyl stretching confirms a chemical interaction between ARTM and PEG, as occurs for norfloxacin [16]. Most bands were broad compared to pure ARTM, confirming an interaction between ARTM and PEG [17].

3.3. Differential Scanning Calorimetry. The DSC thermogram of ARTM showed typical characteristics of a crystalline substance having one endothermic peak at 86.64°C while melting onset temperature at 84.86°C. An enthalpy change (ΔH) of ARTM was 56.68 J/g. The DSC thermogram of ARTM is shown in Figure 4(A).

Physical mixture of group-1 showed melting onset at 65.90°C, peak temperature at 66.55°C, and enthalpy change of 186.5 J/g, while its freeze-dried mixture showed decreased melting onset at 56.84°C, peak temperature at 61.90°C, and ΔH at 162.8 J/g. Both physical and freeze-dried mixtures of group-1 showed decreased melting peak temperature and increased enthalpy change. It was noted that decrease in melting endotherm [18] was more pronounced in case of freeze-dried mixture and increase in ΔH was more in case of physical mixture. All these changes were due to less crystalline nature of ARTM in SESDs of group-1 (Figures 4(B) and 4(C)).

Physical mixture of group-2 showed melting onset temperature at 61.84°C, peak temperature at 66.31°C, and ΔH at 109.4 J/g, while freeze-dried mixture of group-2 showed melting onset at 53.36°C, peak temperature at 60.93°C, and ΔH at 150.1 J/g. Both physical and freeze-dried mixtures showed lower endothermic peak temperature [18] and increased enthalpy change as compared to ARTM alone. The increase in enthalpy lowered melting endotherm effect which was more pronounced in case of freeze-dried mixture of group-2 than its physical mixture. Group-2 SESDs of ARTM were more stable than group-1 SESDs (Figures 4(D) and 4(E)).

3.4. Scanning Electron Microscopy (SEM) Studies. Scanning electron microscopic photographs of artemether (ARTM) alone showed typical crystalline blocks of ARTM, while in group-1 SDs of ARTM, SEM showed that these crystalline structures of ARTM were decreased in size enormously having no sharp edges in both physical and freeze-dried mixtures of group-1. Scanning electron micrographs of physical mixture of group-2 showed formation of flakes representing amorphous agglomerates with smooth surfaces, whereas its freeze-dried mixture showed glassy appearance in addition to size reduction and embedment. SEM of physical mixture of group-3 in which Cremophor-A25 was substituted with Poloxamer 188, showed flakes having no smooth surface, while its freeze-dried mixture showed modified irregular shaped glassy appearance (Figure 5), comparable to the result of ARTM as obtained earlier [19].

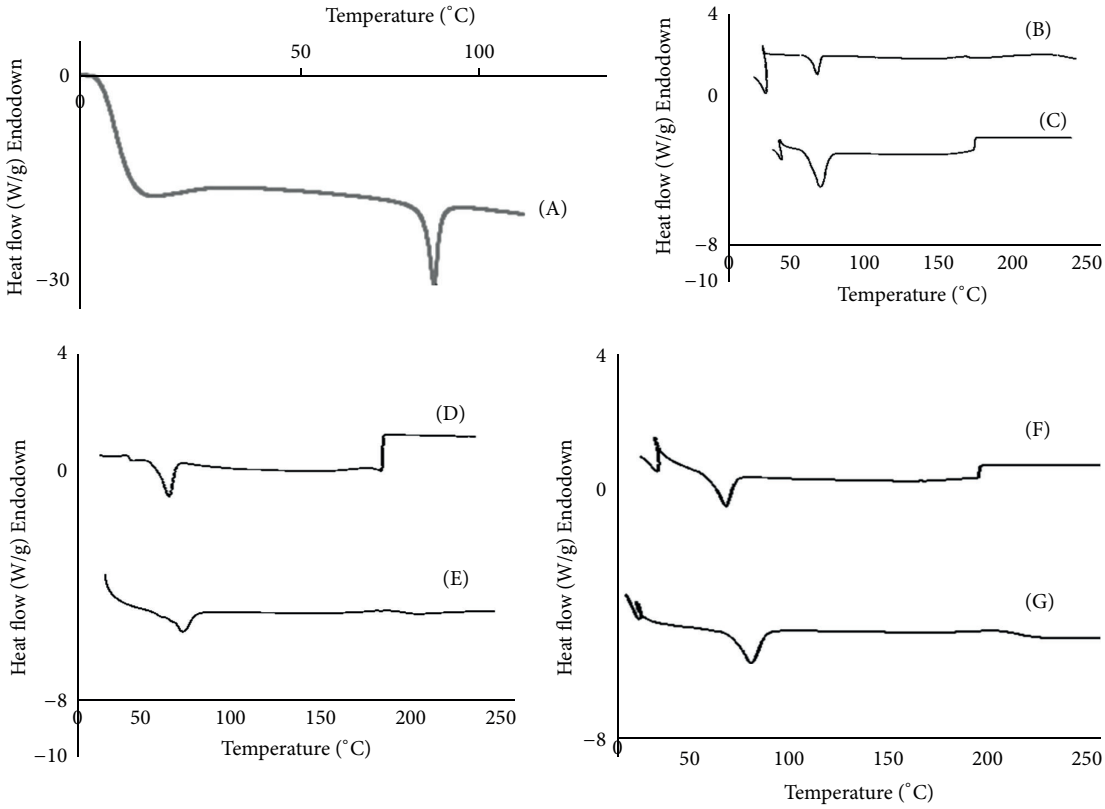

Figure 4: DSC thermogram of ARTM (A), physical mixture of group-1 (B), freeze-dried mixture of group-1 (C), physical mixture of group-2 (D), freeze-dried mixture of group-2 (E), physical mixture of group-3 (F), and freeze-dried mixture of group-3 (G).

3.5. Equilibrium Solubility Studies. In group-1 of the prepared samples of artemether (ARTM), the solubility of physical mixture (PM) was increased up to 9 times (2.74 mg/mL) and solubility of its freeze-dried (FD) mixture was improved up to 15 times (4.74 mg/mL) as compared to ARTM alone (0.30 mg/mL). While in group-2 of SESDs, the solubility of physical mixture was increased up to 94 times (28.38 mg/mL) and its freeze-dried mixture was improved up to 121 times (36.33 mg/mL). In group-3 of SESDs when Cremophor-A25 was replaced with Poloxamer 188, the solubility of physical mixture was up to 65 times (19.49 mg/mL), while solubility of its freeze-dried mixture was increased further up to 135 times (40.56 mg/mL). In all cases, the solubility was in the decreasing order of FD > PM > ARTM (Figure 6).

All the physical and freeze-dried mixtures of all samples showed a substantial increase in equilibrium solubility. The increase in solubility was due to amorphous nature of prepared samples or inhibition of crystallization by polymers as obtained earlier [20–22]. Moreover, this increase in solubility can be a result of the formation of more soluble dispersion between the drug and the polymer [23]. The effect of temperature on solubility was similar to artemisinin [24], aspirin, and paracetamol [25]. Generally, solubility profile of SESDs of ARTM was agreed with data of XRD, FTIR, DSC, and SEM, which indicated that both procedures such as physical mixture method and freeze-dried method improved the solubility profile of ARTM.

3.6. Preparation and Characterization of Tablets. The quality control parameters of all prepared tablets were in accordance with official requirements [22]. Weight variation and friability were ±4.92% and <0.5%, respectively. The ARTM contents (%) in all the tablets ranged between 99.91 ± 0.73% and 102.01 ± 0.32%.

3.7. Dissolution Studies. From dissolution data (Table 1), it is found that rate of drug dissolution (K) is faster in all formulations as compared to pure ARTM as evident from zero order, first order, and Higuchian model analysis. Moreover, that rate of drug dissolution is faster in all products formulated by freeze drying compared to that of physical mixing. In addition, drug release data was best fit to the Higuchian model which illustrates that drug release from the products occurs through the diffusion process. This mode of drug release is further supported by n-value, that is, in range of 0.437–0.483. If n is equal to or less than 0.5, dissolution data follows the Fickian diffusion. The diffusion is Fickian when liquid diffusion takes place at slower rate than the rate of relaxation of polymeric chains. The n-value is assessed from the slope of Korsmeyer-Peppas curve [8]. Figure 6 shows dissolution profiles of ARTM alone and its formulations.

The rate of dissolution was increased by using Cremophor-A25 as well as Poloxamer 188 in addition to PEG6000, olive oil, Transcutol, and HPMC. By comparing physical and freeze-dried mixtures of SESDs of ARTM,

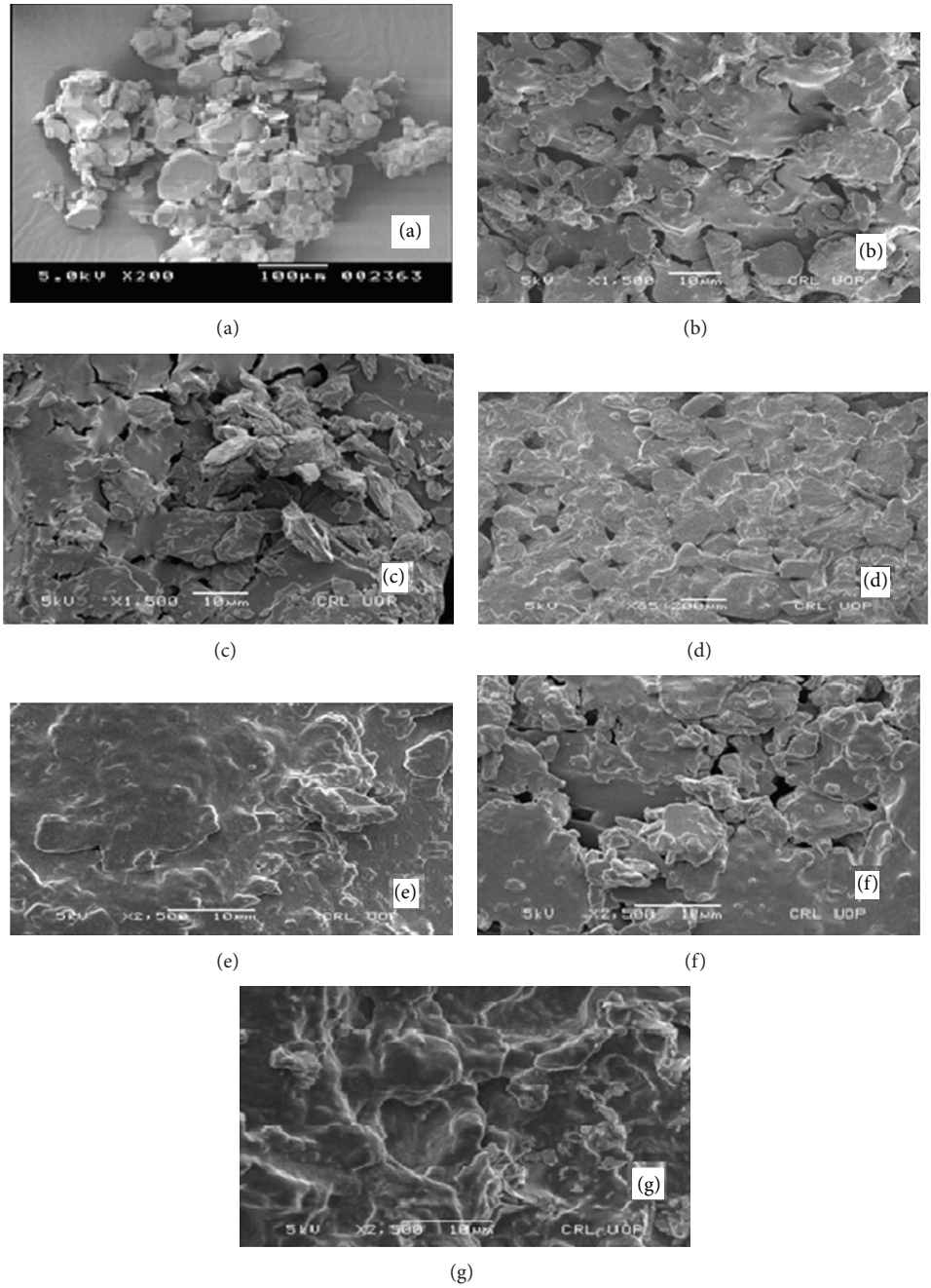

Figure 5: SEM of ARTM (a), physical mixture of group-1 (b), freeze-dried mixture of group-1 (c), physical mixture of group-2 (d), freeze-dried mixture of group-2 (e), physical mixture of group-3 (f), and freeze-dried mixture of group-3 (g).

Table 1: Kinetic analysis of dissolution data.

Formulations	Zero order model		First order model		Higuchi model		Korsmeyer-Peppas model
	K	R^2	K	R^2	K	R^2	n
Pure ARTM	0.013	0.7857	0.000	0.7913	0.171	0.9569	0.549
Physical mixture of group-1	0.036	0.5417	0.000	0.5622	0.478	0.8383	0.459
Freeze-dried mixture of group-1	0.044	0.5961	0.000	0.6199	0.589	0.8535	0.483
Physical mixture of group-2	0.181	0.5622	0.002	0.6719	2.403	0.8322	0.473
Freeze-dried mixture of group-2	0.194	0.5651	0.003	0.6839	2.573	0.8336	0.475
Physical mixture of group-3	0.115	0.5002	0.001	0.5739	1.546	0.8346	0.437
Freeze-dried mixture of group-3	0.227	0.5121	0.003	0.6677	3.035	0.8215	0.450

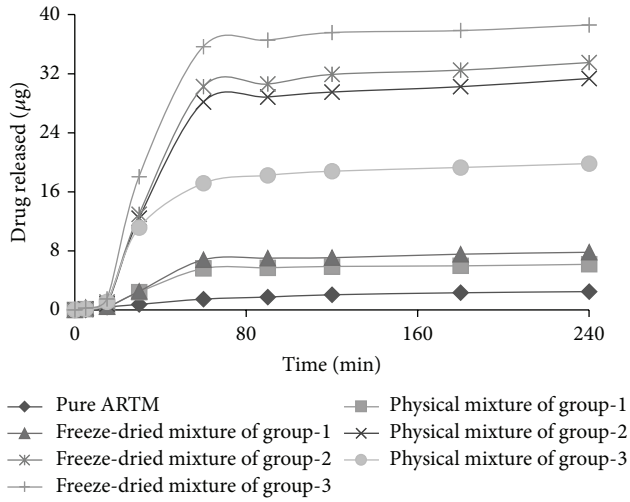

Figure 6: Dissolution profiles of ARTM alone and its formulations.

the freeze-dried mixtures showed enhanced dissolution as compared to physical mixtures and ARTM alone. This enhanced dissolution of SESDs of ARTM was due to less crystalline structure and their conversion into amorphous form [18]. The order of decrease in dissolution was FD > PM > ARTM alone. The dissolution profile of SESDs of ARTM agreed with data of XRD, FTIR, DSC, and SEM, which indicated that both procedures such as physical mixture method and freeze-dried method improved the dissolution profile of ARTM. This increase in dissolution was comparable to that observed earlier for ARTM [26].

3.8. Stability Studies. The stability of artemether (ARTM) in Hank's balanced salt solution of pH 7.4 was very poor and only 8% of ARTM was left at the end of 6 hours. Therefore, Hank's balanced salt solution pH 7.4 was chosen as medium for the stability analysis of ARTM in the SDs and SESDs at 37°C, as used previously for dihydroartemisinin [27]. The degradation of ARTM in Hank's balanced salt solutions (pH 7.4) followed first order reaction described by the following equation with $R^2 > 0.984$. The degradation rate constant values were calculated by linear regression of $\ln[C]$ and t. The changes of concentration of ARTM as well as SESDs of ARTM as a function of time were shown in Figures 7, 8, and 9.

The degradation rate constant (k) of ARTM alone was $0.52\,h^{-1}$. Physical mixture (PM) as well as freeze-dried (FD) mixture of group-1 showed values of k $0.46\,h^{-1}$ and $0.42\,h^{-1}$, respectively. Physical and freeze-dried mixtures of group-2 of ARTM showed decreased k values $0.22\,h^{-1}$ and $0.18\,h^{-1}$, respectively. Similarly, physical and freeze-dried mixture of group-3 showed lowest values of k $0.25\,h^{-1}$ and $0.11\,h^{-1}$, respectively.

The rank order of the k values was ARTM alone > FD mixture > PM. The stability of ARTM in Hank's balanced salt solution at pH 7.4 was substantially improved by using PEG6000, Cremophor-A25, and Poloxamer 188, comparable to DHA [27, 28].

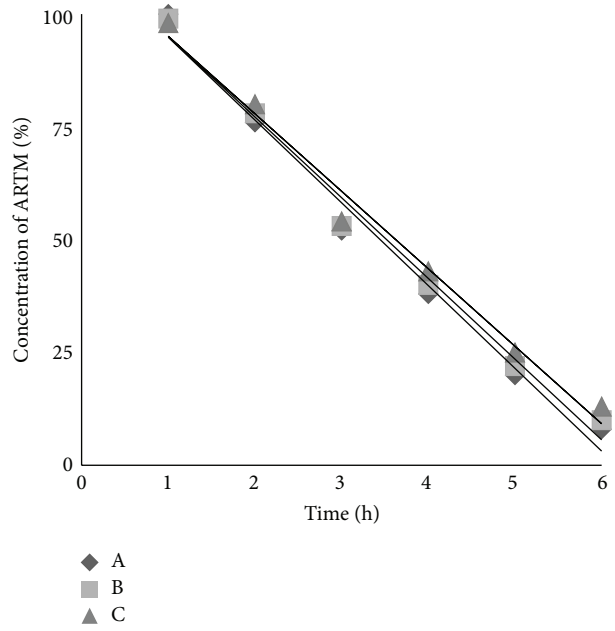

Figure 7: The changes of ARTM concentration percentage as a function of time in Hank's balanced salt solution (pH 7.4) at 37°C for ARTM alone (A), physical mixture of group-1 (B), and freeze-dried mixture of group-1 (C).

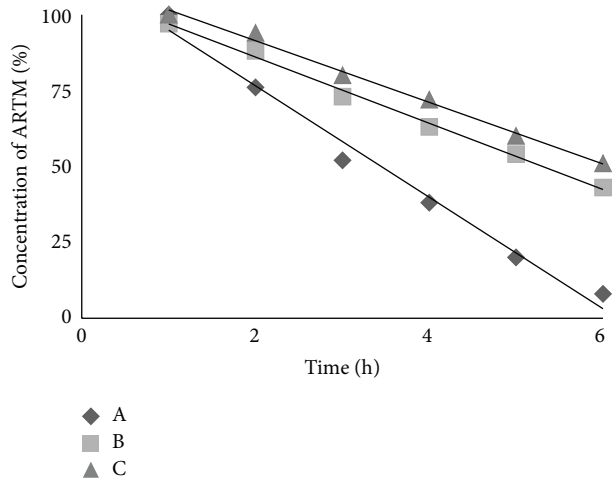

Figure 8: The changes of ARTM concentration percentage as a function of time in Hank's balanced salt solution (pH 7.4) at 37°C for ARTM alone (A), physical mixture of group-2 (B), and freeze-dried mixture of group-2 (C).

4. Conclusions

It can be concluded from our results that solubility and dissolution profile of artemether (ARTM) can be increased by preparing their self-emulsified solid dispersions (SESDs) with PEG6000, Poloxamer188, Cremophor-A25, olive oil, HPMC, and Transcutol by using freeze-dried method. The increase in solubility and dissolution profile of SESDs of ARTM agreed with data of XRD, FTIR, DSC, and SEM, which indicated

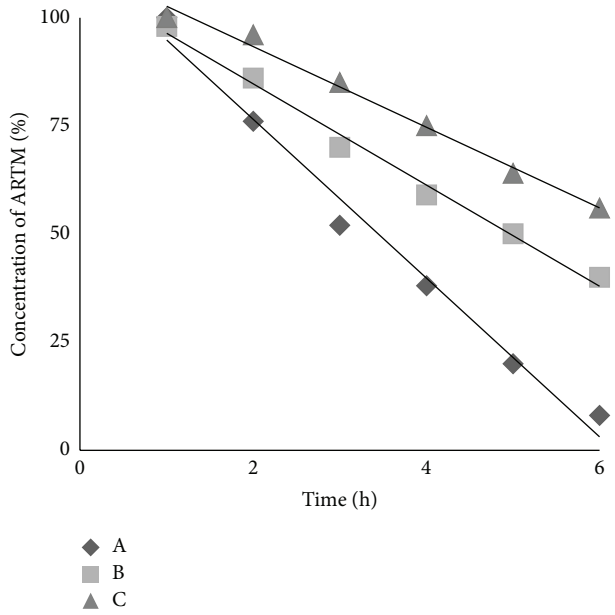

Figure 9: The changes of ARTM concentration percentage as a function of time in Hank's balanced salt solution (pH 7.4) at 37°C for ARTM alone (A), physical mixture of group-3 (B), and freeze-dried mixture of group-3 (C).

that self-emulsified solid dispersions by freeze-dried method improved the physicochemical properties of ARTM.

Conflict of Interests

The authors declare that there is no conflict of interests regarding the publication of this paper.

Acknowledgments

The authors are thankful to Higher Education Commission (HEC) of Pakistan for providing funding for research project due to which this work was possible and Hamaz Pharmaceutical Company, Multan, Pakistan, for providing facility of some instruments.

References

[1] F. E. Cox, "History of the discovery of the malaria parasites and their vectors," *Parasites and Vectors*, vol. 3, no. 1, article 5, 2010.

[2] F. Castelli, S. Odolini, B. Autino, E. Foca, and R. Russo, "Malaria prophylaxis: a comprehensive review," *Pharmaceuticals*, vol. 3, no. 10, pp. 3212–3239, 2010.

[3] World Health Organization, *World Malaria Report*, World Health Organization, 2011.

[4] N. J. White, F. Nosten, S. Looareesuwan et al., "Averting a malaria disaster," *The Lancet*, vol. 353, no. 9168, pp. 1965–1967, 1999.

[5] World Health Organization, *World Malaria Report*, World Health Organization, Geneva, Switzerland, 2010.

[6] M. H. El-Dakdoky, "Evaluation of the developmental toxicity of artemether during different phases of rat pregnancy," *Food and Chemical Toxicology*, vol. 47, no. 7, pp. 1437–1441, 2009.

[7] G. Lefèvre, M. Bindschedler, F. Ezzet, N. Schaeffer, I. Meyer, and M. S. Thomsen, "Pharmacokinetic interaction trial between co-artemether and mefloquine," *European Journal of Pharmaceutical Sciences*, vol. 10, no. 2, pp. 141–151, 2000.

[8] A. Baseer, F. Hassan, S. M. F. Hassan et al., "Physico-chemical comparison of famotidine tablets prepared via dry granulation and direct compression techniques," *Pakistan Journal of Pharmaceutical Sciences*, vol. 26, no. 3, pp. 439–443, 2013.

[9] F. Rasool, M. Ahmad, G. Murtaza, H. M. S. Khan, and S. A. Khan, "Metoprolol tartrate-ethylcellulose tabletted microparticles: formulation and in vitro evaluation," *Latin American Journal of Pharmacy*, vol. 29, no. 6, pp. 984–990, 2010.

[10] C. Souppart, N. Gauducheau, N. Sandrenan, and F. Richard, "Development and validation of a high-performance liquid chromatography-mass spectrometry assay for the determination of artemether and its metabolite dihydroartemisinin in human plasma," *Journal of Chromatography B*, vol. 774, no. 2, pp. 195–203, 2002.

[11] B. Nasir, S. N. H. Shah, and G. Murtaza, "New HPLC method for the determination of artemether in injections," *Scientific Research and Essays*, vol. 7, no. 10, pp. 1165–1168, 2012.

[12] N. Ahuja, O. P. Katare, and B. Singh, "Studies on dissolution enhancement and mathematical modeling of drug release of a poorly water-soluble drug using water-soluble carriers," *European Journal of Pharmaceutics and Biopharmaceutics*, vol. 65, no. 1, pp. 26–38, 2007.

[13] G. V. Betageri and K. R. Makarla, "Enhancement of dissolution of glyburide by solid dispersion and lyophilization techniques," *International Journal of Pharmaceutics*, vol. 126, no. 1-2, pp. 155–160, 1995.

[14] B. Sethabouppha, S. Puttipipatkhachorn, Y. Tozuka, and K. Yamamoto, "Amorphization of dihydroartemisinin by co-grinding with additives," in *Proceedings of the 1st Asian Particle Technology Symposium (APT '00)*, pp. 13–15, Bangkok, Thailand, 2000.

[15] G. van den Mooter, M. Wuyts, N. Blaton et al., "Physical stabilisation of amorphous ketoconazole in solid dispersions with polyvinylpyrrolidone K25," *European Journal of Pharmaceutical Sciences*, vol. 12, no. 3, pp. 261–269, 2000.

[16] M. Guyot, F. Fawaz, J. Bildet, F. Bonini, and A.-M. Lagueny, "Physicochemical characterization and dissolution of norfloxacin/cyclodextrin inclusion compounds and PEG solid dispersions," *International Journal of Pharmaceutics*, vol. 123, no. 1, pp. 53–63, 1995.

[17] R. M. Silverstein, G. C. Bassler, and T. C. Morril, *Spectrometric Identification of Organic Compounds*, John Wiley & Sons, New York, NY, USA, 1991.

[18] M. T. Ansari, S. Karim, N. M. Ranjha, N. H. Shah, and S. Muhammad, "Physicochemical characterization of artemether solid dispersions with hydrophilic carriers by freeze dried and melt methods," *Archives of Pharmacal Research*, vol. 33, no. 6, pp. 901–910, 2010.

[19] P. D. Amin, "Artemether-soluplus hot-melt extrudate solid dispersion systems for solubility and dissolution rate enhancement with amorphous state characteristics," *Journal of Pharmaceutics*, vol. 2013, Article ID 151432, 15 pages, 2013.

[20] D. Bikiaris, G. Z. Papageorgiou, A. Stergiou et al., "Physicochemical studies on solid dispersions of poorly water-soluble

drugs: evaluation of capabilities and limitations of thermal analysis techniques," *Thermochimica Acta*, vol. 439, no. 1-2, pp. 58–67, 2005.

[21] A. A. Ambike, K. R. Mahadik, and A. Paradkar, "Stability study of amorphous valdecoxib," *International Journal of Pharmaceutics*, vol. 282, no. 1-2, pp. 151–162, 2004.

[22] USP, *Drug Information for the Health Care Professional*, vol. 1, United States Pharmacopoeial Convention, Rockville, Md, USA, 18th edition, 1998.

[23] M. C. Tros de Ilarduya, C. Martín, M. M. Goñi, and M. C. Martínez-Ohárriz, "Solubilization and interaction of sulindac with polyvinylpyrrolidone K30 in the solid state and in aqueous solution," *Drug Development and Industrial Pharmacy*, vol. 24, no. 3, pp. 295–300, 1998.

[24] L.-H. Wang, Y.-T. Song, Y. Chen, and Y.-Y. Cheng, "Solubility of artemisinin in ethanol + water from (278.2 to 343.2) K," *Journal of Chemical & Engineering Data*, vol. 52, no. 3, pp. 757–758, 2007.

[25] C. M. McLoughlin, W. A. M. McMinn, and T. R. A. Magee, "Physical and dielectric properties of pharmaceutical powders," *Powder Technology*, vol. 134, no. 1-2, pp. 40–51, 2003.

[26] P. P. Shah and R. C. Mashru, "Development and evaluation of artemether taste masked rapid disintegrating tablets with improved dissolution using solid dispersion technique," *The American Association of Pharmaceutical Sciences PharmSciTech*, vol. 9, no. 2, pp. 494–500, 2008.

[27] D. Wang, H. Li, J. Gu et al., "Ternary system of dihydroartemisinin with hydroxypropyl-β-cyclodextrin and lecithin: simultaneous enhancement of drug solubility and stability in aqueous solutions," *Journal of Pharmaceutical and Biomedical Analysis*, vol. 83, pp. 141–148, 2013.

[28] G. Murtaza, M. Ahmad, and G. Shahnaz, "Microencapsulation of diclofenac sodium by non-solvent addition technique," *Tropical Journal of Pharmaceutical Research*, vol. 9, no. 2, pp. 187–195, 2010.

Hindawi Publishing Corporation
BioMed Research International
Volume 2015, Article ID 608435, 12 pages
http://dx.doi.org/10.1155/2015/608435

Research Article

Modern Evaluation of Liquisolid Systems with Varying Amounts of Liquid Phase Prepared Using Two Different Methods

Barbora Vraníková, Jan Gajdziok, and David Vetchý

Department of Pharmaceutics, Faculty of Pharmacy, University of Veterinary and Pharmaceutical Sciences, Palackého 1/3, 612 42 Brno, Czech Republic

Correspondence should be addressed to Jan Gajdziok; gajdziokj@vfu.cz

Received 2 September 2014; Accepted 7 October 2014

Academic Editor: Josef Jampilek

Liquisolid systems are an innovative dosage form used for enhancing dissolution rate and improving *in vivo* bioavailability of poorly soluble drugs. These formulations require specific evaluation methods for their quality assurance (e.g., evaluation of angle of slide, contact angle, or water absorption ratio). The presented study is focused on the preparation, modern *in vitro* testing, and evaluation of differences of liquisolid systems containing varying amounts of a drug in liquid state (polyethylene glycol 400 solution of rosuvastatin) in relation to an aluminometasilicate carrier (Neusilin US2). Liquisolid powders used for the formulation of final tablets were prepared using two different methods: simple blending and spraying of drug solution onto a carrier in fluid bed equipment. The obtained results imply that the amount of liquid phase in relation to carrier material had an effect on the hardness, friability, and disintegration of tablets, as well as their height. The use of spraying technique enhanced flow properties of the prepared mixtures, increased hardness values, decreased friability, and improved homogeneity of the final dosage form.

1. Introduction

Bioavailability of drugs after oral administration depends on several factors such as aqueous solubility, drug permeability, dissolution rate, first-pass and presystemic metabolism, and susceptibility to efflux mechanisms. Poor solubility and low permeability represent the most frequent causes of limited bioavailability for a number of drugs. Solubility is the most important parameter for orally administered drugs which enable them to achieve the required concentration in systemic circulation necessary for the desired pharmacological response. The improvement of drug solubility remains one of the most challenging aspects of the drug development process especially for solid dosage forms designated for systemic absorption of the drug after oral administration [1]. Therefore, one of the most important and promising areas of the modern pharmaceutical technology is focused on modern approaches to the formulation and evaluation of solid dosage forms with enhanced bioavailability of poorly soluble drugs. These drugs represent up to 40% of commonly used active substances and almost 70% of newly synthesized molecules. Scientific literature describes a number of different techniques for improving the solubility and bioavailability of mentioned drugs (such as reducing particle size via micronization [2], using surfactants [3], lyophilization [4], and the preparation of self-emulsifying drug delivery systems [5]). Of all these, the formulation of liquisolid systems (LSS) represents one of the most promising and innovative techniques for promoting dissolution rate and *in vivo* bioavailability of poorly soluble drugs.

Liquisolid systems essentially refer to formulations prepared by converting a liquid drug or a drug in liquid state (solutions, suspensions, or emulsions) into dry, nonadherent, free-flowing, and readily compressible powder mixtures by blending or spraying a liquid dispersion onto specific powder carriers and coating materials [6]. The prepared dry blends can be subsequently transformed into conventional solid dosage forms (filled into capsules and compressed into tablets) which represents one important advantage of these systems [7]. Various grades of cellulose, a granulated form of magnesium aluminometasilicates (Neusilin), and a specifically prepared form of anhydrous dibasic calcium

phosphate (Fujicalin) may be used as the carriers while very fine powders, such as colloidal silica or a powdered form of magnesium aluminometasilicates, could be used as coating materials.

Due to the their advantages, a number of poorly soluble drugs (such as atorvastatin [8], carbamazepine [9], furosemide [10], and indomethacin [11]) have been formulated as liquisolid systems to ensure enhanced drug release and improved bioavailability of active ingredients. Several mechanisms of enhanced drug release from liquisolid systems have been described in scientific literature. Increased surface area of the available drug and the drug in dissolved state represents the most important one of these. The drug within the liquisolid system is usually already dissolved in a nonvolatile solvent (propylene glycol, polyethylene glycol, glycerol, etc.) which keeps the drug from having to dissolve in the gastrointestinal tract, which is the most limiting step during drug absorption. Moreover, the solubilized drug in its molecularly dispersed state is still fixed on the large surface of the carrier material available for GI fluids [7, 12, 13].

The improved wetting properties of the liquisolid tablets by the dissolution media represent another one of the proposed mechanisms of the enhanced dissolution rate in liquisolid systems. The nonvolatile solvents used for liquisolid system formulations facilitate the wetting of the final solid dosage form by decreasing interfacial tension between dissolution medium and tablet/powder surface [14]. Improved wettability of these systems is usually demonstrated by measuring contact angles and water rising times (wetting times) [12, 14]. The improved wettability was proved, for example, by V. B. Yadav and A. V. Yadav [15]. In their study, they claimed that liquisolid granules containing indomethacin showed a significantly shorter rising time of water in comparison to raw indomethacin and also granules prepared using the compression (dry granulation) technique. This finding can be explained by the fact that water poorly soluble drug is, in the hydrophilic dissolved form (polyethylene glycol 400 solution), absorbed in the powder particles of the carrier of the liquisolid formulation [15].

In addition to the first two mentioned mechanisms of drug release enhancement, it could be expected that the solubility of the drug might be increased through the use of a suspension when formulated as a liquisolid system. In fact, the relatively small amount of liquid vehicle in a liquisolid compact is not sufficient to increase the overall solubility of the drug in an aqueous dissolution medium. However, it could also be expected that, in the microenvironment of the solid/liquid interface between an individual liquisolid primary particle and the release medium, the amount of the liquid vehicle diffusing out of a single liquisolid particle together with the drug molecules is sufficient to increase the aqueous solubility of the active ingredient by acting as a cosolvent [7, 12, 16].

In addition to conventional evaluation methods, specific tests for assessing liquisolid systems' quality parameters can be used (e.g., angle of slide and water absorption ratio or contact angle). Angle of slide (θ) is a specific parameter used to evaluate the flow properties of powder excipients. During such tests, an angle of 33° is regarded as optimal flow behavior for an LSS powder mixture [17]. To evaluate the improved wettability of the final liquisolid formulation, contact angle or water absorption ratio tests are performed. The contact angle is calculated by measuring the height and diameter of drop of dissolution medium placed on the tablet surface [6]. Water absorption ratio is related to the wetting time (time necessary for complete wetting of the tablet) and refers to the amount of water (in %) absorbed by the tablet during wetting [18].

Drugs from the group of hypolipidemic agents represent one of the best selling drugs. Mixed dyslipidemia, a common lipid abnormality characterized by altered levels of lipids and lipoproteins in blood plasma, is associated with increased risk of coronary heart disease which has been identified as the leading cause of death in developed countries [19, 20]. Statins, selective inhibitors of 3-hydroxy-3-methylglutaryl coenzyme A (HMG-CoA) reductase, are first-line drugs in the treatment of hypercholesterolemia due to their lowering effect on LDL-cholesterol [21]. Compared with other statins (lovastatin, simvastatin, fluvastatin, cerivastatin, and atorvastatin), rosuvastatin has the greatest amount of bonding interaction with HMG-CoA reductase and exhibits the minimal metabolization via cytochrome P450 3A4, the isoenzyme implicated in a wide variety of drug-drug interactions [22, 23]. However, rosuvastatin is poorly soluble in water which leads to low estimated absorption (~50%) and inadequate absolute bioavailability (~20%) [24].

The presented study is focused on the preparation, *in vitro* testing, and evaluation of differences of liquisolid systems containing varying amounts of liquid state drug (polyethylene glycol 400 solution of rosuvastatin) in relation to aluminometasilicate carrier Neusilin US2. Liquisolid powders used for the formulation of final tablets were prepared using two different methods: simple blending and spraying of drug dispersion onto carrier material in fluid bed equipment. The effect of the amount of the drug in liquid state and the method used for preparing liquisolid systems on their quality parameters were studied and evaluated with the aim of finding a formulation most suitable for *in vivo* testing.

2. Materials and Methods

2.1. Materials. Modern hypolipidemic agent, rosuvastatin calcium (Jai Radhe Sales, India), was used as the model drug. Polyethylene glycol 400 (Dr. Kulich Pharma, Czech Republic), Neusilin US2 (Fuji Chemical Industry Co., Ltd., Japan), Aerosil 200 (Eurošarm spol. s.r.o., Czech Republic), Lactose DCL 11 (DMV International GmbH, the Netherlands), and magnesium stearate (Zentiva a.s., Czech Republic) were used as the nonvolatile solvent, carrier, coating material, filler, and lubricant, respectively. Superdisintegrant Kollidon CL-F was received as a gift from BASF SE (Germany).

2.2. Methods

2.2.1. Preparation of Liquisolid Powders and Formulation of Tablets. Liquisolid powder blends were prepared by simple blending using mortar and pestle and/or by spraying in fluid bed equipment (Glatt AG, Switzerland). Rosuvastatin was

Table 1: Composition of liquisolid tablets.

Sample	Rosuvastatin		PEG 400		Neusilin US2		Aerosil 200		Kollidon CL-F		Mg stearate		Lactose		L_f*
	[mg]	[%]	[mg]	[%]	[mg]	[%]	[mg]	[%]	[mg]	[%]	[mg]	[%]	[mg]	[%]	
40%w	10	1.5	123	18.9	332.5	51.2	6.5	1.0	32.5	5.0	6.5	1.0	139.0	21.4	0.4
50%w	10	1.5	123	18.9	266.0	40.9	5.3	0.8	32.5	5.0	6.5	1.0	206.7	31.8	0.5
60%w	10	1.5	123	18.9	221.7	34.1	4.4	0.7	32.5	5.0	6.5	1.0	251.9	38.8	0.6
70%w	10	1.5	123	18.9	190.0	29.2	3.8	0.6	32.5	5.0	6.5	1.0	284.2	43.7	0.7
80%w	10	1.5	123	18.9	166.4	25.6	3.3	0.5	32.5	5.0	6.5	1.0	308.3	47.4	0.8
90%w	10	1.5	123	18.9	147.8	22.7	3.0	0.5	32.5	5.0	6.5	1.0	327.2	50.3	0.9
100%w	10	1.5	123	18.9	133.0	20.5	2.7	0.4	32.5	5.0	6.5	1.0	342.3	52.7	1.0
110%w	10	1.5	123	18.9	121.0	18.6	2.4	0.4	32.5	5.0	6.5	1.0	354.6	54.6	1.1
120%w	10	1.5	123	18.9	110.8	17.1	2.2	0.3	32.5	5.0	6.5	1.0	365.0	56.2	1.2

*L_f means liquid load factor.

dissolved in polyethylene glycol 400 (PEG 400) to obtain a 7.5% (w/w) solution (experimentally measured saturated concentration at 20°C). The resulting solution was applied to a precisely calculated amount of Neusilin US2 (carrier) and coated with Aerosil 200 (coating material) to obtain a dry powder with sufficient flow properties for further processing.

Powder materials used for the formulation of LSS can retain only a limited amount of liquid while maintaining acceptable flow and compression properties. Therefore, Spireas and Bolton [25, 26] established a mathematical approach for calculating the required amounts of carriers and coating materials. According to the previous study [27], the maximum liquid load factor (L_f) (the ratio of the weight of the drug in liquid state to the carrier material weight) was determined to be 1.2 and the excipient ratio (R) (the weight ratio of the carrier material to the coating material) was determined to be 50. The appropriate quantities of carrier (Q) and coating material (q) required to transform a given amount of drug in liquid state (m) into an acceptably flowing and compressible liquisolid system were calculated from the following equation:

$$L_f = \frac{m}{Q}, \qquad R = \frac{Q}{q}. \tag{1}$$

In the case of simple blending, the liquid form of the drug was mixed with a calculated amount of carrier and coating material. The blend was passed through a sieve (mesh size 1 mm) and subsequently mixed in a three-axial homogenizer (T2C, TURBULA System Schatr, Switzerland) for 10 minutes. Lactose and Kollidon CL-F were added; the mixture was sieved (mesh size 1 mm) and homogenized in the homogenizer for another 10 minutes. At the end, magnesium stearate (a lubricant) was added and the whole blend was sieved (mesh size 1 mm) and mixed for 2 more minutes.

For the fluid-bed spraying method, the drug solution was sprayed onto Neusilin US2, and the mixture was then passed through a sieve (mesh size 1 mm) and mixed in a homogenizer for 10 minutes. After this, Aerosil 200 was added and the whole mixture was sieved (mesh size 1 mm) and mixed for 5 minutes. Lactose and Kollidon CL-F were then added, and powder blend was sieved (mesh size 1 mm) and mixed for another 10 minutes. For the final part of the preparation procedure, magnesium stearate was added, and the mixture was sieved (mesh size 1 mm) and mixed for 2 more minutes.

Oblong tablets (18 × 8 mm) with constant weight of 650 mg were directly compressed from the prepared dry blends using an excentric tablet press (EK 0, KORSCH, Germany). The prepared tablets were kept in polyethylene bag for 48 hours before testing.

Samples were marked according to the representation (percentage w/w) of the drug in liquid state in relation to the carrier (Table 1). For example, sample 60%w contained 60% liquid phase in relation to the weight of Neusilin US2.

2.2.2. Powder Flow of the Liquisolid Tableting Mixtures. The flow properties of prepared liquisolid tableting mixtures were established by determining the flowability (flow through the orifice), angle of repose, compressibility index, and Hausner ratio. A defined stainless steel funnel with an orifice of 2.5 cm in diameter and a fixed glass funnel were used to measure the flowability and angle of repose as implies Ph. Eur. 8.0. Bulk and tapped densities were determined also according to Ph. Eur. 8.0 for the calculation of Hausner ratio (HR) and compressibility index (CI) [28].

2.2.3. Angle of Slide. Angle of slide is a specific parameter for evaluating the flow behaviour of liquisolid mixtures [29]. Angle of slide was used to evaluate the flow properties of liquisolid tableting mixtures. The tested powder sample (10 g) was placed on one end of a metal plate with a polished surface (Figure 1). This end was gradually raised until the plate with the horizontal surface formed an angle at which the sample was about to slide. The measurement was repeated 3 times; average and standard deviations were calculated. Angle of slide corresponding to 33° is regarded as optimal flow behaviour [16].

2.2.4. Pycnometric Density. The density of tableting mixtures was evaluated using the gas displacement technique with

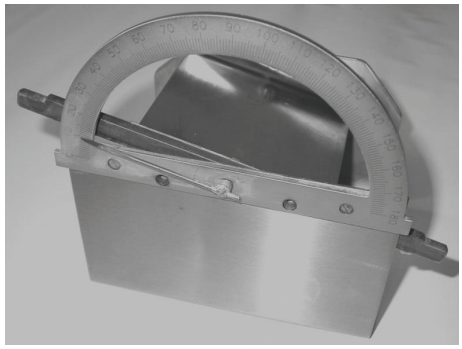

Figure 1: Equipment for evaluation of angle of slide.

a helium pycnometer (PYCNOMATIC ATC, POROTEC, Germany). An accurately weighed and completely dry test cell was filled with the powder sample and weighed again. The test cell containing the sample was sealed in the pycnometer and analysis commenced. Each sample was measured three times and average and standard deviations were calculated.

2.2.5. Tablet Hardness. Hardness of liquisolid tablets (the force in Newton required to crush the tested tablet) was evaluated using a hardness tester (C 50 Tablet Hardness & Compression tester, ENGINEERING SYSTEMS (Nottm) Ltd., UK). Ten randomly selected oblong tablets of each formulation were tested in both directions (transversely and lengthwise); mean values and standard deviations were calculated.

2.2.6. Friability. Approximately 6.5 g of dedusted tablets was weighed precisely using an analytical balance (KERN 870-13, Gottl. KERN & Sohn, Germany) and placed into the plastic drum of an abrasion tester (TAR 10, ERWEKA GmbH, Germany) and rotated for 4 minutes at 25 rpm, corresponding to Ph. Eur. 8.0. Afterwards, the dust was removed and tablets were reweighed. The loss of mass in each tablets' sample was determined. Percentages were calculated using the following equation [28]:

$$\%\ \text{Friability} = \frac{\text{loss of mass}}{\text{initial mass}} * 100. \quad (2)$$

2.2.7. Disintegration. The disintegration test was performed at 37.0 ± 2.0°C in distilled water on six tablets from each formulation using a disintegration test apparatus (ZT4, ERWEKA GmbH, Germany). The tablets were considered completely disintegrated when no residue remained in the basket. The presented values are the means and SDs of six determinations.

2.2.8. Uniformity of Mass. From each formulation, 10 randomly selected tablets were weighed individually on an analytical balance (KERN 870-13, Gottl. KERN & Sohn, Germany). The average weight of all tablets and percentage deviation from the mean value for each tablet were determined.

2.2.9. Drug Content. For this process, 10 randomly selected representative tablets from each batch were evaluated for their drug content. 500 mL of distilled water was added to each tablet to dissolve the drug. The dispersion was kept at laboratory temperature (20°C) for at least 3 hours. Samples were filtered and then analysed spectrophotometrically (LAMBDA 25, PERKIN ELMER INSTRUMENTS, USA) at 242 nm. The percentages of individual drug content were calculated and compared to the theoretical drug content (10 mg).

2.2.10. Tablet Height. The heights of 3 tablets were measured using a digital slide caliper (DS 150, QUANTUM MASCHINEN, Germany). Measurement was carried out 5 times for each batch of tablets. The average weight of one tablet and the standard deviation of measurement were calculated.

2.2.11. Determination of Wetting Time and Water Absorption Ratio. Wetting time and water absorption ratio of liquisolid tablets were determined in a Petri dish using a sponge (5 × 5 cm), impregnated by ten grams of water containing a water-soluble green colour (brilliant green) for identification of complete tablet surface wetting. Tested liquisolid tablet was carefully placed on the surface of the impregnated sponge in the Petri dish at laboratory temperature (20°C). The time required to reach the upper surface of the tablet by the colour solution was noted as the wetting time (time necessary for complete wetting of the tablet). The weight of the tablet in the dry state (before being placed on the sponge) was noted as m_0. The wetted tablet was removed and reweighed (m_1). The water absorption ratio (WA) was calculated using the equation:

$$WA = 100 * \frac{(m_1 - m_0)}{m_0}. \quad (3)$$

The measurement was carried out 5 times for each batch of tablets; results are presented as mean values and standard deviations.

2.2.12. In Vitro Dissolution Studies. *In vitro* release of rosuvastatin was determined using a standard paddle dissolution apparatus (Sotax AT 7 Smart, Sotax, Switzerland) with a paddle speed of 50 rpm in 500 mL of artificial gastric fluid (pH 1.2) at 37.0 ± 0.5°C. Throughout the experiment, the withdrawn samples were analysed spectrophotometrically online at 242 nm at time intervals 5, 10, 15, 20, 25, and 30 min. Six randomly selected tablets of each formulation were tested; results are presented as mean values and standard deviations.

3. Results and Discussion

3.1. Powder Flow of the Liquisolid Tableting Mixtures. Currently, a number of various methods are used for characterizing the flow properties of pharmaceutical powder materials. Therefore, several parameters, such as flowability, angle of repose, angle of slide, compressibility index, and the Hausner ratio, were used to determine the flow properties of prepared

liquisolid powder mixtures. Angle of slide is a specific parameter used to evaluate flow properties of prepared liquisolid powdered blends. Spireas et al. [30] claimed that angle of slide is the preferred method to determine the flowability of powders with particles smaller than 150 μm.

The evaluation of flowability (Table 2) of powdered mixtures prepared by simple blending implied that increasing the amount of liquid phase in relation to aluminometasilicate carrier Neusilin US2 improved the flowability of the prepared powder blend. The flowability improvement is a result of the increased weight of the Neusilin US2 granules with sorbed rosuvastatin solution, hence decreasing the pycnometric density of the liquisolid tableting mixtures (Table 3). The decreased pycnometric density with the increasing amount of liquid phase in relation to the carrier material could be explained, as Neusilin pores became filled with liquid. Gumaste et al. in their study [31] proved that the majority of the liquid is adsorbed into mesopores and deep into the channels of the Neusilin US2's macropores. Hentzschel et al. [32] showed that the addition of liquid phase (tocopherol acetate) to Neusilin US2 decreased flowability. In general, the flow properties of the liquisolid blends were enhanced in comparison to Neusilin US2 alone [27, 32]. Moreover, samples with more liquid contained higher amounts of spray-dried lactose (DCL 11) as filler, with excellent flow properties [33], supporting their improved flowability. The flowability values of the powder blends prepared by spraying in fluid bed equipment did not indicate any dependence of the amount of the drug in the liquid state added to carrier. The highest flowability value (57.90 ± 0.90 s/100 g) was exhibited by sample 80%w and the lowest value (5.19 ± 0.01 s/100 g) by sample 90%w. Excluding samples 100%w, 110%w, and 120%w, flowability of the samples prepared by spraying was lower in comparison to mixtures prepared by simple blending. This improvement of the flow properties could be explained by the improved homogeneity of blends obtained by spraying in fluid bed equipment [34].

Determination of angle of repose (Table 2) did not reveal any dependence on the amount of the used drug in liquid state or the used method. This finding supports the argument that measurement of angle of slide is more suitable for determining flow properties of liquisolid systems. The measured values of angle of repose for samples prepared by simple blending ranged between 26.43 ± 0.48° and 31.51 ± 0.87° and corresponded with excellent to good flow characteristics [28]. Blends obtained by spraying in fluid bed equipment showed values of angle of repose in range between 21.19 ± 0.53° and 30.70 ± 0.88° which responded to excellent flow properties in compliance with European Pharmacopoeia [28].

Results obtained from measuring angle of slide implied that sample 110%w prepared by simple blending and 120%w prepared by spraying exhibited the recommended angle of slide (about 33°) [16] (Table 2). Values lower than 33° were observed in only three samples prepared by spraying (40%w, 60%w, and 110%w). Other blends provided angle of slide values higher than the recommended angle of 33°, which indicated inferior flow properties of the blends. In general, mixtures prepared by spraying showed lower values of angle of slide than blends achieved by simple blending. This observation could be explained by the improved homogeneity of blends created by spraying in fluid bed equipment [34].

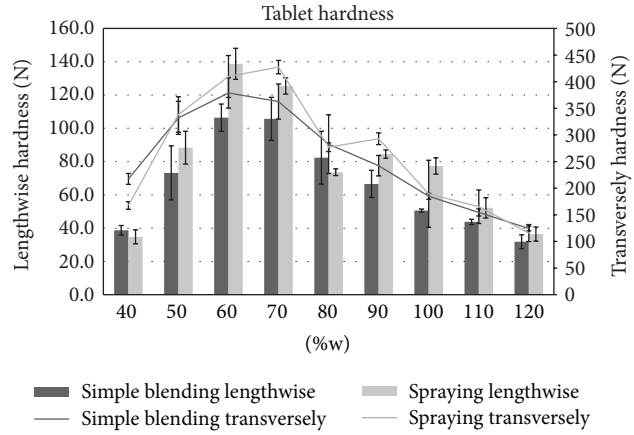

Figure 2: Tablet hardness.

Evaluation of compressibility index and Hausner ratio (Table 2) implied that blends prepared by simple mixing exhibited fair flow characteristics in compliance with European Pharmacopoeia [28]. Tableting mixtures prepared by spraying provided lower CI and HR values in comparison to blends obtained by simple blending. Their values corresponded to good and fair flow properties. The results confirmed previous studies dealing with liquisolid blends where HR values ranging between passable and excellent flow properties were observed after adding a liquid phase. The sorption of 0.9% solution of griseofulvin in PEG 300 [35] and olmesartan medoxomil in Acrysol EL 135 [36] onto carrier Neusilin US2 are two examples of this.

3.2. Tablet Hardness. Tablet hardness is one of the basic tests of final dosage form quality and mechanical durability. This parameter depends on a number of factors such as tablet shape, size, composition, and used compression force and equipment [37]. Therefore, prepared liquisolid tablets were evaluated in two directions (transversely and lengthwise) due to their oblong shape. All tablets were compressed to the experimentally adjusted maximum hardness. In general, it was observed that the hardness of the tablets placed between the hardness testers' jaws lengthwise was lower than those measured transversely (Figure 2). The obtained results implied that hardness increased initially with the increasing amount of liquid phase up to 60% in relation to carrier Neusilin US2 (Figure 2). However, from the 70% representation of drug in liquid phase, values decreased again in both measured directions (Figure 2). A similar tendency was observed by Hentzschel et al. [32] in their study, where Neusilin US2 was able to absorb up to 50% of tocopherol acetate while maintaining acceptable mechanical properties of the prepared tablets. The decreasing values of hardness could be explained by the squeezing of the liquid from the tablets structure during compression (liquid-squeezing out phenomena) and by the negative effect of liquid on the bonds

Table 2: Flow properties of the tableting mixtures.

Sample	Simple blending					Spraying				
	Flowability [s/100 g]	Angle of repose [°]	Angle of slide [°]	CI [%]	HR	Flowability [s/100 g]	Angle of repose [°]	Angle of slide [°]	CI [%]	HR
40%w	102.19 ± 0.36	28.06 ± 1.09	36.00 ± 2.00	16.67	1.20	8.88 ± 0.12	29.38 ± 2.36	28.67 ± 1.15	13.08	1.15
50%w	83.16 ± 0.64	27.29 ± 0.46	38.00 ± 2.00	17.53	1.21	7.54 ± 0.61	28.33 ± 1.22	35.67 ± 0.58	14.89	1.18
60%w	63.63 ± 0.49	30.32 ± 0.35	37.67 ± 2.08	17.58	1.21	6.25 ± 0.23	31.21 ± 1.16	29.33 ± 1.53	13.58	1.16
70%w	65.43 ± 0.41	28.97 ± 1.43	36.67 ± 0.58	17.33	1.21	56.37 ± 0.62	26.70 ± 1.28	35.33 ± 0.58	15.38	1.18
80%w	64.80 ± 4.32	26.43 ± 0.48	36.33 ± 0.58	17.02	1.21	57.90 ± 0.90	28.07 ± 0.46	34.33 ± 0.58	15.28	1.18
90%w	60.90 ± 2.70	27.25 ± 0.47	35.67 ± 0.58	16.85	1.20	5.19 ± 0.01	28.57 ± 0.85	38.33 ± 1.53	16.22	1.19
100%w	4.85 ± 0.42	29.40 ± 0.79	35.67 ± 1.15	16.22	1.19	27.72 ± 0.48	30.70 ± 0.88	34.33 ± 1.53	14.29	1.17
110%w	4.60 ± 0.12	31.51 ± 0.87	33.00 ± 1.00	16.90	1.20	32.81 ± 0.98	21.19 ± 0.53	32.33 ± 0.58	15.15	1.18
120%w	4.14 ± 0.34	27.77 ± 0.52	34.33 ± 2.08	18.75	1.23	30.49 ± 1.59	23.83 ± 2.68	33.00 ± 1.00	13.11	1.15

Table 3: Pycnometric densities (g/cm^3) of tableting blends.

Sample	Simple blending		Spraying	
	Density	SD	Density	SD
40%w	1.7765	0.0018	1.7377	0.0039
50%w	1.7639	0.0051	1.6271	0.0020
60%w	1.6088	0.0011	1.6093	0.0023
70%w	1.5854	0.0028	1.5781	0.0024
80%w	1.5530	0.0010	1.5177	0.0013
90%w	1.5318	0.0006	1.5201	0.0028
100%w	1.5441	0.0032	1.5368	0.0025
110%w	1.5269	0.0030	1.5120	0.0055
120%w	1.5340	0.0019	1.5138	0.0006

between solid carrier particles necessary for adequate tablet quality [38]. Figure 2 illustrates that tablets compressed from the blends prepared by simple blending had a generally lower hardness in comparison to tablets from mixtures prepared by spraying, which could be related to better flowability and compressibility of these blends as shown in the results of the compressibility index (Table 2).

3.3. Friability. All the tested tablet samples showed friability values (Table 4) lower than the Ph. Eur. 8.2 limit, which for uncoated tablets is 1% [28]. The only exception to this was observed in sample 120%w prepared by simple blending (1.45%). This finding correlates with this sample's lower hardness values (31.9 ± 4.4 N and 124.35 ± 4.34 N). In general, it can be stated that the rest of the tablets, which fulfilled the requirements for friability, are expected to withstand the stress and attrition of common handling, packaging, and transporting processes.

3.4. Disintegration. Rapid tablet disintegration is necessary to ensure tablets' quick collapse into smaller fragments to obtain the largest possible surface area accessible for dissolution media [39]. The determined disintegration times of liquisolid tablets are shown in Table 4. The disintegration test revealed that all liquisolid system formulations disintegrated within a maximum of 159 ± 3 s, which complies with the specifications given for the uncoated tablets in the Ph. Eur. [28]. All the prepared liquisolid formulations could also be marked as fast disintegrating tablets which disintegrate rapidly (within 3 min) and could be beneficial for patients with difficulty in swallowing [28, 40]. The observed fast tablet disintegration could be explained by the presence of superdisintegrant Kollidon CL-F in combination with hydrophilic solvent PEG 400 which improves wetting properties of the liquisolid tablet and shortens its disintegration time [14]. Preparing fast disintegrating tablets could improve the bioavailability of rosuvastatin thanks to the fast and easy transition of the dissolved drug in a hydrophilic liquid (PEG 400) to GI fluids, from which the active ingredient could be absorbed into systemic circulation.

3.5. Uniformity of Mass. All the prepared liquisolid tablets met the requirements for the uniformity of mass test. None of the tablets deviated from the average value by more than 5% (Table 4), which is the limit given by European Pharmacopoeia [28]. The results proved that both methods of preparations led to the formulation of blends with good flow properties and processability and to tablets with homogeneous weight, as indicated by low values of standard deviations.

3.6. Drug Content. Fahmy and Kassem [13] claimed that the process of adsorption of liquid phase onto carriers provides uniform drug distribution in the final dosage form, thereby ensuring good content uniformity. However, evaluation of the drug content (Table 4) implied that samples 90%w (66.10 ± 3.83%), 100%w (116.76 ± 5.03%), 110%w (118.19 ± 13.15%), and 120%w (85.68 ± 23.70%) obtained by simple blending did not meet content uniformity criteria in compliance with Eur. Ph. [28]. This problem could be a result of inhomogeneous distribution of the drug solution in the tableting blends, as high values of standard deviation implied. This issue might be resolved by spraying the drug in liquid phase onto the carrier in fluid bed equipment or mixing the blends in high-shear mixers. The results of drug content evaluations of tablets prepared by spraying have proved this assumption, as shown in Table 4. Moreover, standard deviations of the tablets prepared by spraying (maximum value 5%) were lower in comparison to tablets obtained by simple blending (maximum value 23.70%).

3.7. Tablet Height. The amount of the drug in the liquid state presented in the formulation showed an impact also on tablet height. Initially, the height of the prepared liquisolid tablets decreased with increasing amount of liquid in relation to the carrier Neusilin US2 (from sample 40%w with 8.20 ± 0.07 mm to sample 70%w with 4.90 ± 0.04 mm). Subsequently, the height of tablets containing 70% and more liquid phase was very similar due to the saturation of carrier pores by liquid and the presence of higher amounts of lactose with limited compaction properties (Table 4). In addition, it was observed that the tablets' height was influenced by the formulation method. Tablets prepared from mixtures obtained by spraying had generally lower height values (6.22 ± 0.13 to 4.30 ± 0.00 mm) in comparison to tablets prepared by simple blending (8.20 ± 0.07 to 4.73 ± 0.08 mm). These results are related to the better compressibility of the liquisolid blends, which contain higher amounts of liquid in relation to carrier material and better flow properties of mixtures prepared by spraying in fluid bed equipment.

3.8. Wetting Time and Water Absorption Ratio. One mechanism that might explain the enhanced dissolution rate from the liquisolid systems is the improved wettability of the final liquisolid dosage form by the dissolution media (natural or artificial GI fluids). This is caused by hydrophilization of the solid particles' surface through the incorporation of hydrophilic liquid media (drug solution, emulsion, and suspension) [14]. As a result, water absorption ratio and time

Table 4: Properties of liquisolid tablets prepared by simple blending and spraying.

Sample	Simple blending					Spraying				
	Friability [%]	Disintegration [s]	Uniformity of mass [mg]	Drug content [%]	Height [mm]	Friability [%]	Disintegration [s]	Uniformity of mass [mg]	Drug content [%]	Height [mm]
40%w	0.52	3.0 ± 0.0	650.23 ± 5.28	103.01 ± 5.08	8.20 ± 0.07	0.95	18.0 ± 0.0	650.12 ± 3.37	95.58 ± 5.00	6.06 ± 0.05
50%w	0.10	38.0 ± 3.0	649.76 ± 4.25	98.82 ± 7.95	6.48 ± 0.15	0.18	24.0 ± 5.0	657.07 ± 6.70	96.55 ± 1.70	6.22 ± 0.13
60%w	0.06	50.0 ± 3.0	654.43 ± 5.98	99.86 ± 6.66	5.59 ± 0.09	0.04	60.0 ± 13.0	650.50 ± 1.97	106.07 ± 0.77	4.96 ± 0.11
70%w	0.23	159.0 ± 3.0	651.31 ± 4.13	92.29 ± 3.11	4.90 ± 0.04	0.04	98.0 ± 17.0	656.66 ± 6.33	97.35 ± 0.80	4.66 ± 0.06
80%w	0.43	107.0 ± 5.0	655.13 ± 7.71	109.42 ± 4.67	4.73 ± 0.08	0.05	35.0 ± 0.0	656.82 ± 4.30	103.43 ± 4.29	5.05 ± 0.02
90%w	0.56	51.0 ± 0.0	664.31 ± 5.46	66.10 ± 3.83	4.88 ± 0.03	0.03	73.0 ± 0.0	654.74 ± 5.60	95.92 ± 1.89	4.81 ± 0.02
100%w	0.79	39.0 ± 0.0	649.44 ± 3.68	116.76 ± 5.03	4.87 ± 0.03	0.08	30.0 ± 0.0	655.75 ± 0.82	90.55 ± 1.95	4.47 ± 0.17
110%w	0.85	40.0 ± 4.0	659.11 ± 3.29	118.19 ± 13.15	4.94 ± 0.05	0.25	25.0 ± 0.0	652.93 ± 1.70	109.20 ± 1.14	4.61 ± 0.05
120%w	1.45	21.0 ± 0.0	653.12 ± 1.78	85.68 ± 23.70	4.82 ± 0.05	0.16	18.0 ± 0.0	658.05 ± 1.05	112.38 ± 0.92	4.30 ± 0.00

Table 5: Water absorption ratio and wetting time.

Sample	Simple blending		Spraying	
	Water absorption ratio [%]	Wetting time [min]	Water absorption ratio [%]	Wetting time [min]
40%w	173.17 ± 12.60	3.18 ± 0.03	170.60 ± 15.06	6.32 ± 2.53
50%w	119.93 ± 12.59	4.48 ± 3.02	118.48 ± 6.32	3.38 ± 1.75
60%w	104.22 ± 10.14	7.00 ± 1.12	74.60 ± 3.35	8.70 ± 2.42
70%w	75.26 ± 11.03	12.82 ± 4.92	64.36 ± 9.57	7.25 ± 2.77
80%w	78.10 ± 13.07	26.30 ± 24.52	69.73 ± 15.28	9.37 ± 4.63
90%w	79.98 ± 5.45	25.01 ± 2.28	73.64 ± 8.59	8.07 ± 2.82
100%w	84.19 ± 11.42	31.01 ± 3.37	75.66 ± 5.63	9.93 ± 2.78
110%w	93.58 ± 7.56	52.65 ± 13.27	76.08 ± 7.56	1.67 ± 1.05
120%w	92.94 ± 10.76	55.87 ± 4.77	78.06 ± 3.22	2.87 ± 1.92

required for complete wetting of the tablet by aqueous media (wetting time) were evaluated (Table 5). The water absorption ratio of tablets prepared by simple blending ranged between 75.26 ± 11.03% (70%w) and 173.17 ± 12.60% (40%w). The absorption ratio initially decreased as the amount of drug in liquid state increased up to 90% in relation to Neusilin US2. After 90%, the ratio began to increase. An explanation for this could be the saturation of pores of the carrier particles in formulations with lower representation of the drug in liquid state (40%w–70%w). The subsequent slight increase of water uptake could be caused by the improved hydrophilicity of Neusilin particles surface which contains a higher amount of drug in hydrophilic liquid state, as well as a higher amount of lactose as hydrophilic filler in the formulation. Water absorption ratio of tablets obtained by spraying was generally lower compared to tablets prepared by simple blending.

The lower absorption ratios are related to the faster wetting time of these samples (1.67 ± 1.05–9.93 ± 2.78 min). In terms of tablets prepared by spraying, this parameter did not imply any evident dependence on the amount of drug in liquid phase in relation to the carrier material and testing of faster wetting time could be affected by measurement errors resulting in higher values of standard deviation (Table 5). The wetting time of tablets compressed from mixtures prepared by simple blending increased as the amount of Neusilin US2 in the formulation decreased. This prolongation of the wetting time could be caused by saturation of Neusilin particles pores by the drug solution, thus reducing its ability to absorb another liquid. The slowest wetting time was exhibited by sample 120%w (55.87 ± 4.77) prepared by simple blending and the fastest sample was 110%w (1.67 ± 1.05 min) prepared by spraying. The obtained values of wetting time were higher in comparison to wetting times measured by Kapure et al. [41]. In their study, rosuvastatin tablets containing microcrystalline cellulose as a carrier were completely wetted after 20 s. Wetting time is closely related to the inner structure of the tablets and to the hydrophilicity of the excipients used. Therefore, liquisolid systems containing microcrystalline cellulose with a fast water wicking rate [42] are wetted faster than those containing insoluble and less hydrophilic Neusilin US2 [35].

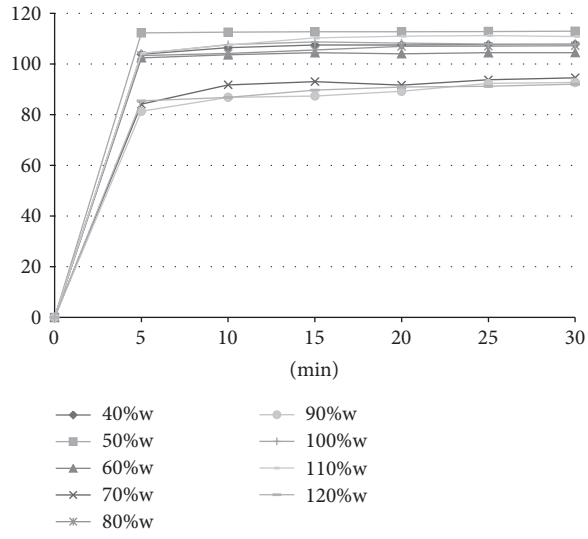

Figure 3: Dissolution profiles of tablets compressed from powders prepared by simple blending.

3.9. In Vitro Dissolution Studies. The dissolution profiles of rosuvastatin liquisolid tablets are presented in Figures 3 and 4, respectively. The percentage of rosuvastatin released from tablets prepared by simple blending during the first 5 minutes ranged between 81.34 ± 24.27% (90%w) and 112.27 ± 3.42% (50%w). Higher values of standard deviations of these measurements (Table 6) are related to poorer homogeneity of the tablets, as was previously mentioned. The similar dissolution profiles were obtained also for tablets prepared by spraying. The amount of rosuvastatin released from these compacts during the first 5 minutes ranged between 74.27 ± 2.30% (100%w) and 110.25 ± 1.39% (80%w). The release of rosuvastatin from all liquisolid tablets was faster in comparison to the results of the directly compressed tablets introduced by Kapure et al. [42]. In this study, the amount of drug released after 15 minutes from conventional rosuvastatin tablets was about 15% (as 450 mL of a pH 1.2 solution was used as a dissolution medium). This value is

Table 6: Standard deviation of dissolution studies (%).

Minutes	Simple blending									Spraying								
	40%w	50%w	60%w	70%w	80%w	90%w	100%w	110%w	120%w	40%w	50%w	60%w	70%w	80%w	90%w	100%w	110%w	120%w
5	0.66	3.42	0.71	15.80	3.72	24.27	3.81	10.26	12.79	2.92	3.09	3.37	4.47	1.39	0.64	2.30	3.71	5.15
10	1.60	3.63	2.07	17.00	0.94	23.79	2.32	7.91	13.70	3.32	1.69	2.77	2.06	0.06	1.36	1.46	2.28	2.31
15	1.84	4.20	1.27	17.77	0.90	27.53	3.18	8.33	14.50	3.85	3.72	4.04	1.37	0.25	2.28	1.60	1.44	1.65
20	1.52	4.15	1.66	21.01	1.45	27.39	3.75	8.19	14.97	4.19	0.63	5.90	0.62	0.08	1.64	2.02	0.99	1.03
25	1.58	3.98	1.44	17.89	0.57	25.66	3.83	8.16	15.75	4.61	1.28	6.04	0.55	0.35	0.73	2.26	0.84	0.88
30	1.92	4.68	1.34	17.64	0.60	26.59	3.97	7.48	16.14	5.00	3.48	6.09	0.54	0.24	0.95	2.38	1.14	0.92

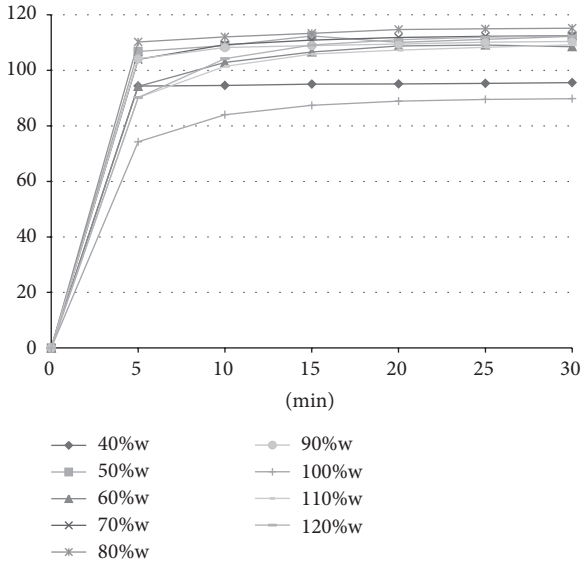

Figure 4: Dissolution profiles of tablets compressed from powders prepared by spraying in fluid bed equipment.

considerably lower in comparison to liquisolid tablets, which showed an 80% release of drug during the first five minutes of testing. The same enhanced release profile has already been proved in several studies dealing with liquisolid systems, such as those of liquisolid compacts containing clonazepam [43], candesartan cilexetil [44], and griseofulvin [35]. The enhanced release could be caused by the presence of a nonvolatile liquid vehicle which improved the wettability of the compacts and hence their disintegration time and by the presence of the drug in its dissolved form without the need to dissolve it in the dissolution medium [14].

4. Conclusion

Preparation of liquisolid systems is one of the most promising and innovative techniques for enhancing *in vitro* dissolution rate and improving *in vivo* bioavailability of poorly soluble drugs. A liquisolid system can be prepared by incorporating a drug in liquid state (liquid drug; drug solution, suspension, or emulsion) onto a specific carrier and coating material while forming a dry, free-flowing, and readily compressible powdered blend. Liquisolid systems are unique medical forms which require specific evaluation for their quality assurance. The presented work was aimed at the modern evaluation of liquisolid systems and the evaluation of differences among liquisolid tablets containing varying amounts of rosuvastatin solution in relation to a magnesium aluminometasilicate carrier (Neusilin US2). Liquisolid powder blends were prepared using two different methods: simple blending and spraying in fluid bed equipment. From the obtained results, it could be stated that all liquisolid tablets had very fast disintegration times connected to enhanced dissolution profiles. It was also observed that the amount of liquid phase in relation to carrier material had an effect on hardness, friability, disintegration of tablet, and tablet height. The use of spraying technique enhanced flow properties of the prepared mixtures, increased hardness, decreased friability, and improved the homogeneity of the final dosage form. Therefore, spraying of a drug in liquid phase onto a carrier in fluid bed equipment seems to be a better preparation method for liquisolid systems as a perspective candidate for clinical usage as dosage forms with improved bioavailability.

Conflict of Interests

The authors declare that there is no conflict of interests regarding the publication of this paper.

References

[1] K. T. Savjani, A. K. Gajjar, and J. K. Savjani, "Drug solubility: importance and enhancement techniques," *ISRN Pharmaceutics*, vol. 2012, Article ID 195727, 10 pages, 2012.

[2] S. Hiendrawan, B. Veriansyah, and R. R. Tjandrawinata, "Micronization of fenofibrate by rapid expansion of supercritical solution," *Journal of Industrial and Engineering Chemistry*, vol. 20, no. 1, pp. 54–60, 2014.

[3] A. B. Nighute and S. B. Bhise, "Enhancement of dissolution rate of rifabutin by preparation of microcrystals using solvent change method," *International Journal of PharmTech Research*, vol. 1, no. 2, pp. 142–148, 2009.

[4] M. Burra, R. Jukanti, K. Y. Janga et al., "Enhanced intestinal absorption and bioavailability of raloxifene hydrochloride via lyophilized solid lipid nanoparticles," *Advanced Powder Technology*, vol. 24, no. 1, pp. 393–402, 2013.

[5] X. Qi, J. Qin, N. Ma, X. Chou, and Z. Wu, "Solid self-microemulsifying dispersible tablets of celastrol: formulation development, charaterization and bioavailability evaluation," *International Journal of Pharmaceutics*, vol. 472, no. 1-2, pp. 40–47, 2014.

[6] K. Kavitha, K. N. S. Lova Raju, N. S. Ganesh, and B. Ramesh, "Effect of dissolution rate by liquisolid compact approach: an overview," *Der Pharmacia Lettre*, vol. 3, no. 1, pp. 71–83, 2011.

[7] V. K. Nagabandi, T. Ramarao, and K. N. Jayaveera, "Liquisolid compacts: a novel approach to enhance bioavailability of poorly soluble drugs," *International Journal of Pharma and Bio Sciences*, vol. 1, pp. 89–102, 2011.

[8] S. R. Gubbi and R. Jarag, "Formulation and characterization of atorvastatin calcium liquisolid compacts," *Asian Journal of Pharmaceutical Sciences*, vol. 5, no. 2, pp. 50–60, 2010.

[9] Y. Javadzadeh, B. Jafari-Navimipour, and A. Nokhodchi, "Liquisolid technique for dissolution rate enhancement of a high dose water-insoluble drug (carbamazepine)," *International Journal of Pharmaceutics*, vol. 341, no. 1-2, pp. 26–34, 2007.

[10] B. Akinlade, A. A. Elkordy, E. A. Essa, and S. Elhagar, "Liquisolid systems to improve the dissolution of Furosemide," *Scientia Pharmaceutica*, vol. 78, no. 2, pp. 325–344, 2010.

[11] M. Saeedi, J. Akbari, K. Morteza-Semnani, R. Enayati-Fard, S. Sar-Reshteh-dar, and A. Soleymani, "Enhancement of dissolution rate of indomethacin using liquisolid compacts," *Iranian Journal of Pharmaceutical Research*, vol. 10, no. 1, pp. 25–34, 2011.

[12] A. Nokhodchi, C. M. Hentzschel, and C. S. Leopold, "Drug release from liquisolid systems: speed it up, slow it down," *Expert Opinion on Drug Delivery*, vol. 8, no. 2, pp. 191–205, 2011.

[13] R. H. Fahmy and M. A. Kassem, "Enhancement of famotidine dissolution rate through liquisolid tablets formulation: *in vitro*

and *in vivo* evaluation," *European Journal of Pharmaceutics and Biopharmaceutics*, vol. 69, no. 3, pp. 993–1003, 2008.

[14] S. M. Gavali, S. S. Pacharane, S. V. Sankpal, K. R. Jadhav, and V. J. Kadam, "Liquisolid compact: a new technique for enhancement of drug dissolution," *International Journal of Research in Pharmacy and Chemistry*, vol. 1, pp. 2231–2781, 2011.

[15] V. B. Yadav and A. V. Yadav, "Improvement of solubility and dissolution of indomethacin by liquisolid and compaction granulation technique," *Journal of Pharmaceutical Sciences and Research*, vol. 1, no. 3, pp. 44–51, 2009.

[16] A. B. Karmarkar, I. D. Gonjari, and A. H. Hosmani, "Liquisolid technology for dissolution rate enhancement or sustained release," *Expert Opinion on Drug Delivery*, vol. 7, no. 10, pp. 1227–1234, 2010.

[17] N. Tiong and A. A. Elkordy, "Effects of liquisolid formulations on dissolution of naproxen," *European Journal of Pharmaceutics and Biopharmaceutics*, vol. 73, no. 3, pp. 373–384, 2009.

[18] M. Kaur, R. Bala, and S. Arora, "Formulation and evaluation of liquisolid compacts of amlodipine besylate," *International Research Journal of Pharma*, vol. 4, pp. 156–160, 2013.

[19] P. H. Jones, M. H. Davidson, A. C. Goldberg et al., "Efficacy and safety of fenofibric acid in combination with a statin in patients with mixed dyslipidemia: pooled analysis of three phase 3, 12-week randomized, controlled studies," *Journal of Clinical Lipidology*, vol. 3, no. 2, pp. 125–137, 2009.

[20] P. P. Toth, V. Zarotsky, J. M. Sullivan, and D. Laitinen, "Lipid therapy utilization rates in a managed-care mixed dyslipidemia population," *Journal of Clinical Lipidology*, vol. 2, no. 5, pp. 365–374, 2008.

[21] G. Anfossi, P. Massucco, K. Bonomo, and M. Trovati, "Prescription of statins to dyslipidemic patients affected by liver diseases: a subtle balance between risks and benefits," *Nutrition, Metabolism and Cardiovascular Diseases*, vol. 14, no. 4, pp. 215–224, 2004.

[22] F. McTaggart, "Comparative pharmacology of rosuvastatin," *Atherosclerosis Supplements*, vol. 4, no. 1, pp. 9–14, 2003.

[23] M. J. Chapman and F. McTaggart, "Optimizing the pharmacology of statins: characteristics of rosuvastatin," *Atherosclerosis Supplements*, vol. 2, no. 4, pp. 33–37, 2002.

[24] P. D. Martin, M. J. Warwick, A. L. Dane et al., "Metabolism, excretion, and pharmacokinetics of rosuvastatin in healthy adult male volunteers," *Clinical Therapeutics*, vol. 25, no. 11, pp. 2822–2835, 2003.

[25] S. Spireas and S. M. Bolton, "Liquisolid systems and methods of preparing same," US6423339; 2002.

[26] S. Spireas and S. M. Bolton, "Liquisolid systems and methods of preparing same," Tech. Rep. US8096337, 2000.

[27] B. Vraníková, J. Gajdziok, and D. Vetchý, "Determination of flowable liquid retention potential of aluminometasilicate carrier for liquisolid systems preparation," *Pharmaceutical Development and Technology*, 2014.

[28] "The European Directorate for the Quality of Medicines & HealthCare: European Pharmacopoeia 8.2," 2014, http://online6.edqm.eu/ep802.

[29] A. B. Karmarkar, I. D. Gonjari, A. H. Hosmani, P. N. Dhabale, and S. B. Bhise, "Liquisolid tablets: a novel approach for drug delivery," *International Journal of Health Research*, vol. 2, no. 1, pp. 45–50, 2009.

[30] S. S. Spireas, C. I. Jarowski, and B. D. Rohera, "Powdered solution technology: principles and mechanism," *Pharmaceutical Research*, vol. 9, no. 10, pp. 1351–1358, 1992.

[31] S. G. Gumaste, S. A. Pawlak, D. M. Dalrymple, C. J. Nider, L. D. Trombetta, and A. T. M. Serajuddin, "Development of solid SEDDS, IV: effect of adsorbed lipid and surfactant on tableting properties and surface structures of different silicates," *Pharmaceutical Research*, vol. 30, no. 12, pp. 3170–3185, 2013.

[32] C. M. Hentzschel, A. Sakmann, and C. S. Leopold, "Suitability of various excipients as carrier and coating materials for liquisolid compacts," *Drug Development and Industrial Pharmacy*, vol. 37, no. 10, pp. 1200–1207, 2011.

[33] "DMV Excipient Guide. [Internet]," 2014, http://www.phexcom.cn/UploadFiles/20130217102234_5017.pdf.

[34] S. Poutiainen, S. Matero, T. Hämäläinen, J. Leskinen, J. Ketolainen, and K. Järvinen, "Predicting granule size distribution of a fluidized bed spray granulation process by regime based PLS modeling of acoustic emission data," *Powder Technology*, vol. 228, pp. 149–157, 2012.

[35] C. M. Hentzschel, M. Alnaief, I. Smirnova, A. Sakmann, and C. S. Leopold, "Enhancement of griseofulvin release from liquisolid compacts," *European Journal of Pharmaceutics and Biopharmaceutics*, vol. 80, no. 1, pp. 130–135, 2012.

[36] S. T. Prajapati, H. H. Bulchandani, D. M. Patel, S. K. Dumaniya, and C. N. Patel, "Formulation and evaluation of liquisolid compacts for olmesartan medoxomil," *Journal of Drug Delivery*, vol. 2013, Article ID 870579, 9 pages, 2013.

[37] P. Komárek and M. Rabišková, *Technologie léků Třetí, přepracované a doplněné vydání*, Galén, Praha, Czech Republic, 2006.

[38] S. G. Gumaste, D. M. Dalrymple, and A. T. M. Serajuddin, "Development of solid SEDDS, V: compaction and drug release properties of tablets prepared by adsorbing lipid-based formulations onto neusilin US2," *Pharmaceutical Research*, vol. 30, no. 12, pp. 3186–3199, 2013.

[39] A. A. Elkordy, X. N. Tan, and E. A. Essa, "Spironolactone release from liquisolid formulations prepared with Capryol 90, Solutol HS-15 and Kollicoat SR 30 D as non-volatile liquid vehicles," *European Journal of Pharmaceutics and Biopharmaceutics*, vol. 83, no. 2, pp. 203–223, 2013.

[40] S. Gubbi and R. Jarag, "Liquisolid technique for enhancement of dissolution properties of bromhexine hydrochloride," *Research Journal of Pharmacy and Technology*, vol. 2, no. 2, pp. 382–386, 2009.

[41] V. J. Kapure, V. V. Pande, and P. K. Deshmukh, "Dissolution enhancement of rosuvastatin calcium by liquisolid compact technique," *Journal of Pharmaceutics*, vol. 2013, Article ID 315902, 9 pages, 2013.

[42] N. Saigal, S. Baboota, A. Ahuja, and J. Ali, "Microcrystalline cellulose as a versatile excipient in drug research," *Journal of Young Pharmacists*, vol. 1, pp. 6–12, 2009.

[43] K. Sanka, S. Poienti, A. B. Mohd, and P. V. Diwan, "Improved oral delivery of clonazepam through liquisolid powder compact formulations: in-vitro and ex-vivo characterization," *Powder Technology*, vol. 256, pp. 336–344, 2014.

[44] F. J. Sayyad, S. L. Tulsankar, and U. B. Kolap, "Design and development of liquisolid compact of candesartan cilexetil to enhance dissolution," *Journal of Pharmacy Research*, vol. 7, no. 5, pp. 381–388, 2013.

Hindawi Publishing Corporation
BioMed Research International
Volume 2015, Article ID 812673, 9 pages
http://dx.doi.org/10.1155/2015/812673

Research Article

Preparation of Silica Nanoparticles Loaded with Nootropics and Their *In Vivo* Permeation through Blood-Brain Barrier

Josef Jampilek,[1] Kamil Zaruba,[2] Michal Oravec,[3] Martin Kunes,[1] Petr Babula,[1] Pavel Ulbrich,[4] Ingrid Brezaniova,[2] Radka Opatrilova,[1] Jan Triska,[3] and Pavel Suchy[1]

[1]*Faculty of Pharmacy, University of Veterinary and Pharmaceutical Sciences Brno, Palackeho 1/3, 612 42 Brno, Czech Republic*
[2]*Faculty of Chemical Engineering, University of Chemistry and Technology Prague, Technicka 5, 166 28 Prague 6, Czech Republic*
[3]*Global Change Research Centre AS CR, Belidla 986/4a, 603 00 Brno, Czech Republic*
[4]*Faculty of Food and Biochemical Technology, University of Chemistry and Technology Prague, Technicka 5, 166 28 Prague 6, Czech Republic*

Correspondence should be addressed to Josef Jampilek; josef.jampilek@gmail.com

Received 4 September 2014; Revised 15 January 2015; Accepted 15 February 2015

Academic Editor: Narasimha Murthy

The blood-brain barrier prevents the passage of many drugs that target the central nervous system. This paper presents the preparation and characterization of silica-based nanocarriers loaded with piracetam, pentoxifylline, and pyridoxine (drugs from the class of nootropics), which are designed to enhance the permeation of the drugs from the circulatory system through the blood-brain barrier. Their permeation was compared with non-nanoparticle drug substances (bulk materials) by means of an *in vivo* model of rat brain perfusion. The size and morphology of the nanoparticles were characterized by transmission electron microscopy. The content of the drug substances in silica-based nanocarriers was analysed by elemental analysis and UV spectrometry. Microscopic analysis of visualized silica nanocarriers in the perfused brain tissue was performed. The concentration of the drug substances in the tissue was determined by means of UHPLC-DAD/HRMS LTQ Orbitrap XL. It was found that the drug substances in silica-based nanocarriers permeated through the blood brain barrier to the brain tissue, whereas bulk materials were not detected in the brain.

1. Introduction

Nootropics are a wide and structurally heterogeneous class of drugs (also supplements, nutraceuticals, and functional foods) that improve one or more aspects of mental function, such as working memory, motivation, and attention. They can be also referred to as smart drugs, memory enhancers, neuroenhancers, cognitive enhancers, and intelligence enhancers. Their therapeutic effect is based on positive affection of metabolic pathways in brain tissue (improved utilization of nutrients and mediators) and their impact manifests after some time of administration. They are used especially at insult of brain by a trauma, ischemia, intoxication, and hypoxia as well as at neurodegenerative disorders such as Alzheimer's disease, Parkinson's disease, Huntington's disease, and attention deficit hyperactivity disorder (ADHD). A number of nootropics are synthetic analogues of physiological compounds (such as acetylcholine, pyridoxine, GABA, or coenzyme Q_{10}); others are natural compounds (e.g., vinpocetine); and the rest are other cerebral-active compounds (e.g., nimodipine, pentoxifylline, etc.) [1, 2].

The site of action of all these drugs is brain; that is, they must overcome all barriers to achieve the brain tissue, and the blood-brain barrier (BBB) is the last, critical, and serious obstacle for the permeation of drugs that require CNS action. The BBB represents a structure with complex cellular organisation that separates the brain parenchyma from the systemic circulation. It consists of brain capillaries that support endothelial cells and are surrounded by astrocytic end-foot processes. The BBB also acts as a metabolic barrier due to the presence of numerous enzymes. These enzymes can either metabolise potentially harmful drugs to CNS-inactive compounds or convert inactive drugs to their active CNS metabolites or degrade them into metabolites or substrates of

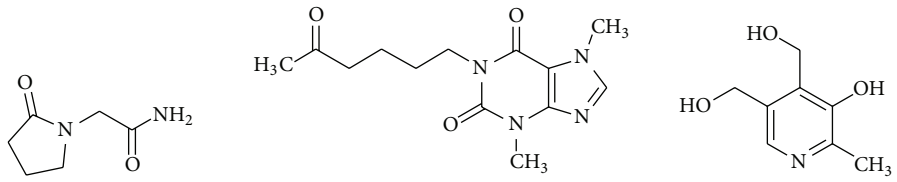

Figure 1: Structures of investigated drugs.

specific efflux transporters, such as P-glycoprotein/multidrug resistance proteins [3–5].

All the above mentioned properties of the barrier result in strong selection of permeating drugs depending on their physicochemical properties, such as molecular weight, molecular volume, lipophilicity, ionisation state, and/or their affinity to specific transporters (uptake/efflux transporters) [3, 5]. The cellular organisation of the BBB and the presence of transmembrane proteins enable a selective regulation of the passage of molecules from the blood to the brain. Molecules present in the blood stream can reach the CNS by two different pathways, the paracellular pathway (through tight junctions) and the transcellular pathway (through endothelial cells). Molecules that reach the CNS via the transcellular pathway can diffuse passively, be actively transported by specific transporters, or undergo endocytosis [5, 6]. To circumvent the BBB and allow an active CNS compound to reach its target, many strategies exist. They can be sorted with respect to the BBB as either invasive (direct injection into the cerebrospinal fluid or therapeutic opening of the BBB) or noninvasive such as use of alternative routes of administration (e.g., nose-to-brain route and olfactory and trigeminal pathways to brain), inhibition of efflux transporters, chemical modification of drugs (prodrugs and bioprecursors), and encapsulation of drugs into nanocarriers (e.g., liposomes, polymeric nanoparticles, and solid lipid nanoparticles) [5, 7]. Nanoparticles as drug carriers have also been extensively studied recently. Their uptake into the brain is hypothesised to occur via adsorptive transcytosis and receptor-mediated endocytosis [8, 9]. Particle size, surface affinity, and stability in circulation are important factors influencing the brain distribution of colloidal particles [10, 11].

Silica-based nanoparticles are widely used in nanotechnology in the biomedical sector, because they are easy to prepare and inexpensive to produce. Their specific surface characteristics, porosity, and capacity for functionalization make them good tools for biomolecule detection and separation, providing solid media for drug delivery systems and for contrast agent protectors. In addition, they are used as safe and biocompatible pharmaceutical additives [12–17]. Incorporation of a drug into nanocarriers may change the drug bioavailability, physicochemistry, and pharmacokinetics, which can be advantageous in many applications [18, 19].

As mentioned above, silica-based nanoparticles are well-known to be biocompatible easy-to-prepare nontoxic carriers that are able to transport loaded drugs in living organisms [12–17]. What is not so well-known (only a few papers have been published so far), they are also able to penetrate through BBB which is used for transport of silica nanoparticles [20] and silica-coated nanoparticles [21]. The aim of this study was the preparation of these silica-based nanocarriers loaded with piracetam, pentoxifylline, and pyridoxine (see Figure 1) and investigation of their permeation through the BBB in comparison with bulk drug substances to enhance absorption and concentration of these cerebral-active drugs in brain.

2. Experimental and Methods

2.1. General. All reagents were purchased from Sigma-Aldrich, Life Technologies, or Fisher Chemical and were of analytical grade. Acetonitrile hypergrade for LC-MS LiChrosolvR was supplied by Merck KGaA (Darmstadt, Germany). Methanol hypergrade for LC-MS LiChrosolvR was supplied by Merck KGaA (Darmstadt, Germany). Acetic acid was obtained from Sigma-Aldrich Chemie GmbH (Steinheim, Germany). The Purelab Classic (ELGA LabWater, High Wycombe, Bucks, UK) was used to generate high purity water for preparation of aqueous mobile phase.

2.2. Preparation of Nanoparticles. The silica nanoparticles were made via a modified Stober method [22–25]. The typical reaction solution consisted of methanol (99.9%, 94 mL), ammonium hydroxide (25% wt of ammonia, 30 mL), and drug solution (20 mg/mL for piracetam, 5–20 mg/mL for others, 2 mL). On mixing the solution by vigorous magnetic stirring, tetraethylorthosilicate (TEOS) (99.9%, 0.8 mL) was added dropwise to initiate the hydrolysis reaction. The resulting solution was stirred at room temperature for 2 h. The particle suspension was repeatedly (4 times) collected by centrifugation (10 min, 9,000 G) and washed with methanol to ensure the removal of all unreacted reactants. Finally, the nanoparticles were dried to yield a final product of drug-loaded silica nanocarriers.

2.3. Elemental Analysis and UV Spectrometry. The content of API (1.5 mg/50 mg nanoparticles) in silica nanoparticles was determined by elemental analysis and UV absorption. Elemental analysis was performed using a Vario EL III Universal CHNOS Elemental Analyzer (Elementar Analysensysteme, Germany) and loading was calculated from the corresponding increase of nitrogen content when drug-loaded nanoparticles were analysed in comparison with non-loaded nanoparticles. Calculated loadings for pentoxifylline and pyridoxine were in accordance with those estimated by UV absorption by determination of unbound drug removed by nanoparticle washing. The corresponding verification

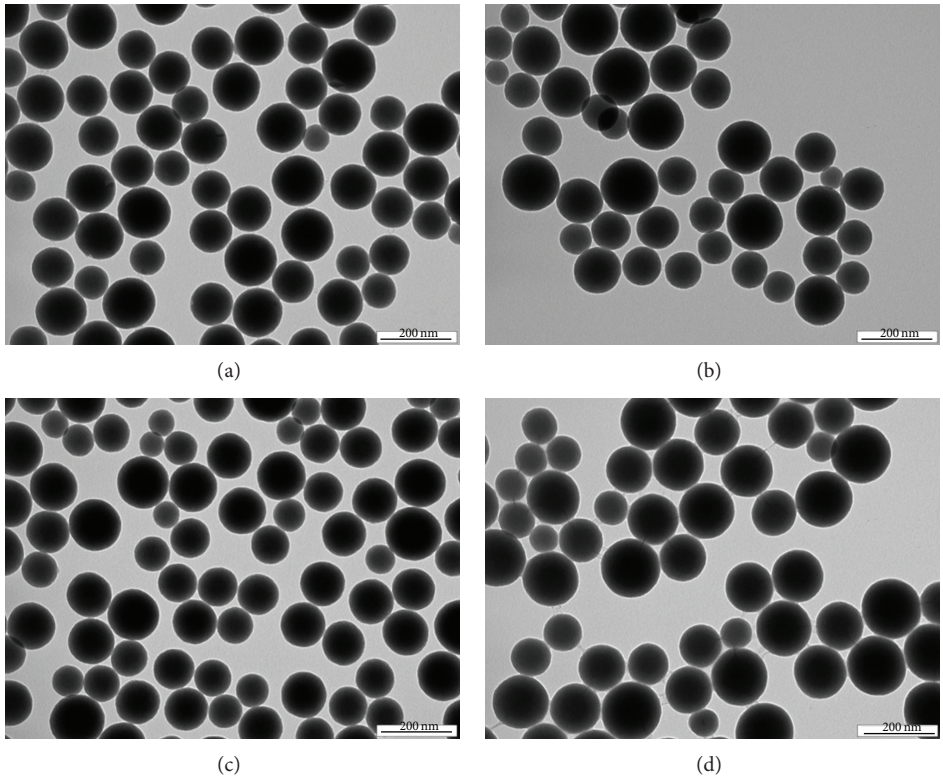

Figure 2: TEM microphotographs of pure silica nanoparticle (a), silica-based nanocarriers loaded with piracetam (b), pentoxifylline (c), and pyridoxine (d).

of piracetam loading estimated by elemental analysis was not possible due to piracetam absorption below 210 nm. Absorption measurements were performed using a Cintra 404 spectrometer (GBC Scientific Equipment, USA).

2.4. Transmission Electron Microscopy. The particle size and the morphology of the samples were examined by transmission electron microscopy (TEM). Samples for TEM were prepared by putting a drop of the colloidal dispersion in methanol (10 μL) on a copper grid covered with thin amorphous carbon film. Samples were dried before inserting them in the specimen holder of a transmission electron microscope JEOL JEM-1010 and observed at 80 kV. Pictures were taken by a digital camera SIS Megaview III (Soft Imaging Systems) and analysed by AnalySIS 2.0 software. The average particle size was calculated from at least 50 particles. The results are illustrated in Figures 2 and 3.

2.5. Rat Brain Perfusion. Male Wistar rats (310–380 g) purchased from the breeding facility Anlab (Prague, Czech Republic) were used in the study. Animals were maintained under standard conditions of temperature and lighting and given food and water *ad libitum*. For surgical preparation, rats were anesthetized intramuscularly with ketamine and xylazine. The in situ rat brain perfusion technique was used with modifications according to the previously described methods [26–28]. External jugular veins were prepared and cannulated for freely blood flowing out of the veins. At the same time, carotid arteries (on the left and right sides) were

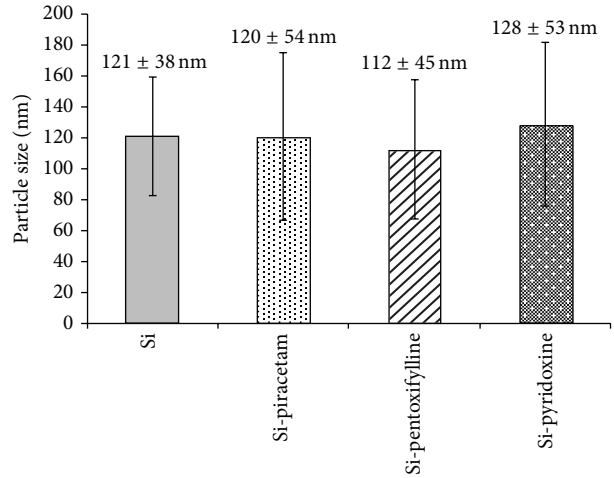

Figure 3: Particle size [nm] of individual nanoparticles: pure silica nanoparticles, Si-piracetam, Si-pentoxifylline, and Si-pyridoxine. Particle size is expressed as mean diameter ± 2∗SD ($n > 50$ particles).

prepared and cannulated using intravascular catheter filled with heparinized saline (60 U/mL) for perfusion. Ligation was accomplished caudally to the catheter implantation site. The catheter in the carotid artery was connected to a syringe filled with buffered Krebs-Henseleit saline solution containing NaCl (7.48 g/L), $NaHCO_3$ (2.02 g/L), KCl (0.31 g/L), $NaH_2PO_4{\cdot}2H_2O$ (0.37 g/L), $CaCl_2$ (0.166 g/L), $MgCl_2{\cdot}6H_2O$

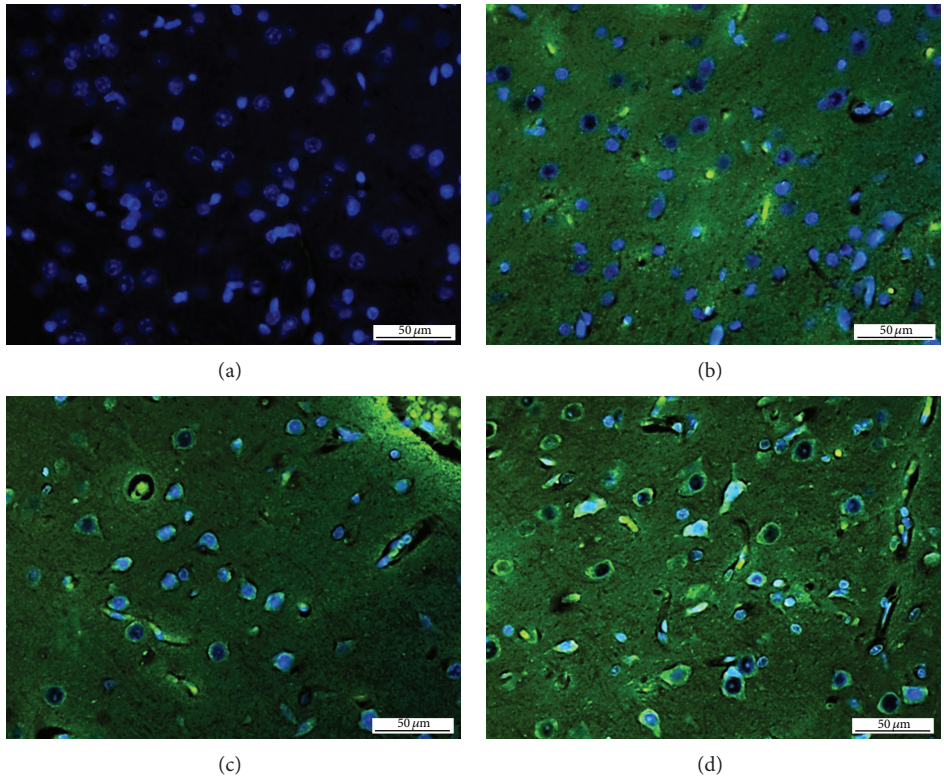

(a) (b)

(c) (d)

Figure 4: Microscopic photographs of histological preparations of control rat brain tissue (a) and rat brain tissues treated with Si-piracetam (b), Si-pentoxifylline (c), and Si-pyridoxine (d) as stained with PDMPO (green fluorescence) in combination with Hoechst 33258 (nuclei, blue fluorescence).

(0.18 g/L), and D-glucose 1.803 g/L, as also used in previous perfusion studies [29, 30]. Polyvinylpyrrolidone (35 g/L) was added into the perfusate to maintain physiological oncotic pressure in the perfusion medium. The perfusion fluid was filtered, warmed to 37°C, and gassed with 95% O_2 and 5% CO_2. Immediately prior to the perfusion the pH and osmolarity of this solution were 7.35 and 290 mOsm, respectively. The perfusion fluid was infused into the carotid artery with an infusion pump for 240 s at flow rate 10.4 mL/min. This perfusion rate was selected to maintain the carotid artery pressure of 120 mmHg [26]. The rectal temperature of the animal was maintained at 37 ± 0.5°C throughout the surgery by a heat pad connected to a feedback device. At the end of perfusion, rats were decapitated and the whole brain was removed from the skull. Cerebral hemispheres were dissected and stored to next analysis after removal of the arachnoid membrane and meningeal vessels (deeply frozen at −80°C for HPLC analysis and tissues for histological examination were fixed in 10% formaldehyde).

2.6. Microscopic Analysis of Brain Tissue: Visualization of Silicates. The deposition of silicates in brain tissue was visualized using *N*-[2-(dimethylamino)ethyl]-2-{4-[2-(pyridin-4-yl)-1,3-oxazol-5-yl]phenoxy}acetamide (PDMPO). The modified procedure described by Shimizu et al. was used [31]. Briefly, sections were deparaffinised and rehydrated (xylene, mixture xylene/ethanol 1 : 1, ethanol, 95% ethanol, 70% ethanol, 50% ethanol, Na-phosphate buffer (0.1 M, pH 7.0)). Then the sections were incubated in 1 μM solution of PDMPO in 0.1 M Na-phosphate buffer (pH 7.0) for 3 hours at 22°C (laboratory temperature). After incubation, the sections were costained with a Hoechst 33258 fluorescent probe (Sigma-Aldrich, USA) to visualize nuclei washed three times with PBS buffer and observed with a microscope using an appropriate excitation filter (Axioscop 40, Zeiss, Germany). Typical photographs are shown in Figure 4.

2.7. Analysis of Brain Tissue. Samples of brain tissue after perfusion with bulk materials (non-nanoparticle drug substances) and drug-loaded silica nanocarriers were frozen and homogenized before extraction. Solid-liquid extraction in methanol was used as an efficient method. Extracts were subsequently purified, concentrated, and analysed. The samples of brain tissue (without purification) perfused with piracetam were also analysed by direct injection (overdosing loop) on UHPLC-HRMS. Direct injection was used for the samples where the concentration of the drug was close to or lower than the limit of detection or quantification. Direct injection was not useful for more samples because it can contaminate UHPLC-HRMS.

Isolated drugs from brain tissue and from silica nanoparticles were analysed by a UHPLC-HRMS separation system (Dionex UltiMate 3000 Liquid Chromatography Systems) equipped with diode array detection (DAD) and a hybrid high resolution mass spectrometer LTQ Orbitrap XL (ThermoFisher Scientific, USA/Dionex RSLC, Dionex, USA).

A chromatographic column Hypersil Gold (Thermo Scientific, USA), C18 3 μm, 2.1 × 50 mm, was used. The mixture of MeCN-HPLC grade (20.0%) and H_2O-HPLC grade with 0.1% AcOH (80.0%) was used as a mobile phase. The total flow of the column was 0.3 mL/min, column temperature was 30°C, and the time of analysis was 15 min.

The records were evaluated from the DAD and HRMS-Orbitrap. The wavelengths of 254 nm, 272 nm, 274 nm, 331 nm, and 190–800 nm were monitored. MS and MS^n were performed using the HRMS LTQ Orbitrap XL (ThermoFisher Scientific, USA) equipped with a HESI II (heated electrospray ionization) source. Orbitrap was operated in full scan with resolution 60,000. Full scan spectra were acquired over mass range m/z 50–1000 in the positive mode. Orbitrap was also operated in SIM (select ion monitoring): 143.0810 (as a qualifier ion) and 126.0548 (as a qualifier ion without NH_2 group) under 1 Δppm for piracetam; 279.1461 under 1 Δppm for pentoxifylline; and 170.0810 (as a qualifier ion) and 152.0700 (as qualifier ion without OH group) under 1 Δppm for pyridoxine. The resolution and sensitivity of Orbitrap were controlled by injection of the standard (piracetam, pentoxifylline, and pyridoxine) after analysing of every 5 samples, and the resolution was also checked by the help of lock masses (phthalates). Blanks were also analysed within the sequence after analysis of each sample. The compounds were checked in the mass library that was created from measurement of standards of piracetam and pentoxifylline and pyridoxine in the MS and MS^n modes of Orbitrap.

3. Results and Discussion

The content of drug substances in silica-based nanocarriers was analysed by elemental analysis and confirmed by UV absorption analysis of supernatants (except of piracetam). Loading efficiency was tested by the addition of an increasing concentration (5, 10, and 20 mg/mL) of drug solution to the reaction mixture for nanoparticle preparation. For both compounds (pentoxifylline and pyridoxine) the loading efficiency was about 10% for concentration of drug stock solution 10 and 20 mg/mL. When 5 mg/mL drug stock solution was added, the amount of the drug loaded was below the detection limit of the used method. Approximately the same loading efficiency (i.e., 10%) was confirmed for all three drugs by elemental analysis. Only nanoparticles with the highest loading (i.e., those prepared using a drug stock solution of 20 mg/mL) were subjected to the animal study. It was found that 1.5 mg of drug substance is in 50 mg of nanoparticles with batch to batch variance less than 10%. The particle size and the shape of prepared silica nanocarriers with loaded piracetam, pentoxifylline, and pyridoxine (Si-piracetam, Si-pentoxifylline, and Si-pyridoxine) were measured by TEM (see Figure 2). A control sample of pure silica nanoparticles was prepared and characterised. It was found that the average particle size of all prepared nanoparticles was approximately 120 nm (TEM microphotographs of pure silica nanoparticles and nanocarriers with loaded drugs in Figure 2 are shown with 10^5x magnification). It is evident that the general shape of all particles can be considered as spherical. Based on 95% confidence interval computed from the mean diameter plus or minus *twice* the standard deviations (see Figure 3), it can be stated that no statistical significance was found for the samples.

Microscopic photographs of histological preparations (samples of brain tissue after perfusion with bulk drug solution and Si-drugs) are shown in Figure 4. In comparison with control rat brain tissue (Figure 4(a)), significant changes in fluorescence in silica-based nanocarriers were recorded for piracetam (Figure 4(b)), pentoxifylline (Figure 4(c)), and pyridoxine (Figure 4(d)). In these photographs, both nuclei and cytoplasmic structures have been identified as PDMPO-positive (green fluorescence). No PDMPO fluoresce has been identified in control, untreated samples. In addition, also tissue treated with bulk material alone was investigated. In this case, no changes in fluorescence (not shown) were observed. PDMPO (Lysosensor DND-160 Yellow/Blue) was originally developed to visualize acidic compartments in the cells [32]. On the other hand, it has been established that it has unique properties allowing to evaluate the deposition of silica in cells and tissues. PDMPO-Si complex possesses unique fluorescent properties in the presence of silicic acid, producing bright green fluorescence after UV excitation. PDMPO has successfully been established to visualize silica in diatoms and other organisms. For example, Znachor et al. used PDMPO to study the deposition of silica in *Fragilaria crotonensis* Kitton [33]. This compound was also studied for the distribution and deposition of silicates in horsetail, *Equisetum arvense* L. Shimizu et al. showed on the silica gel that PDMPO is able to label silicates directly [31]. In the light of this fact, it was decided to use it as a probe to visualize deposition of silica-based nanoparticles in tissues.

The samples of brain tissue after perfusion with bulk materials (drugs solutions) and drug-loaded silica nanocarriers were analysed by direct injection (over dosing loop) on UHPLC-HRMS. Also extracted drug substances from the samples of the perfused tissues were analysed. While the bulk drug substances were extracted from perfused brain tissues easily practically by any of the applied methods, the extraction of the nanonized drug substances from the tissues or from silica nanocarriers was problematic. Different extraction techniques for isolation of the drugs from the tissue and the nanocarriers were tested, such as classical liquid extraction (LE), sequent extraction by various solvents (methanol, water, acetonitrile, etc.), solid-liquid extraction, accelerated solvent extraction (ASE), and ultrasound extraction (USE). The individual extraction methods were compared. The used methods showed similar effectivity; nevertheless the solid-liquid extraction in methanol with minimum losses of the studied compounds was selected.

For example, the brain tissue samples with piracetam and Si-piracetam were compared. Concentrations of piracetam in brain tissues measured by the UHPLC-HRMS using individual extraction methods were comparable (4–10 ng/mL, 10–40 ng/g brain tissue). For Si-piracetam concentrations measured by individual extraction methods were also comparable (50 pg/mL–1 ng/mL, 100 pg/g brain tissue–2.5 ng/g brain tissues) but with lower extraction efficiency. The extraction efficiency was especially influenced by sorption of the drug substances in silica-based nanocarriers. The determined

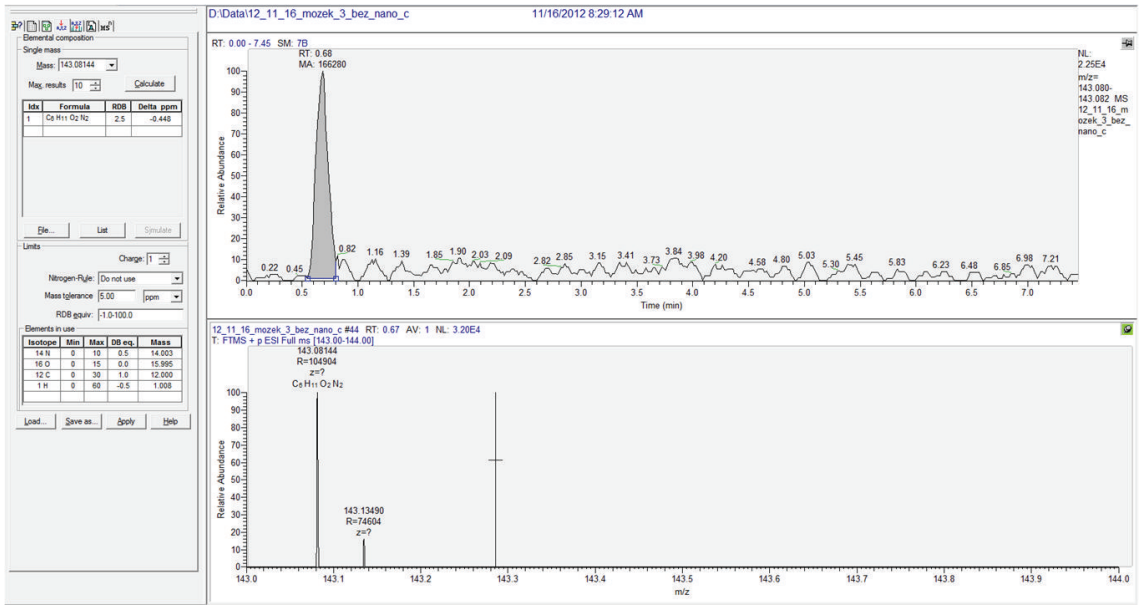

(a)

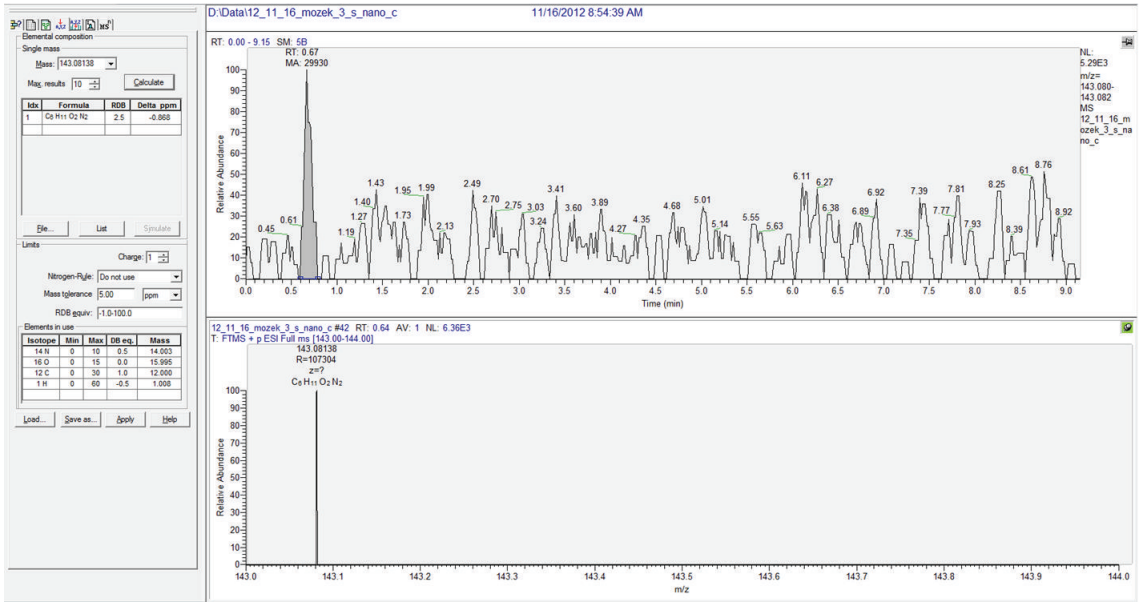

(b)

Figure 5: Comparison of concentration of bulk piracetam (a) and Si-piracetam (b) in brain tissue samples: this chromatogram presents very low concentration of drug, close to limit of quantification (S/N close 20/1). Found ratio of piracetam/Si-piracetam is approximately 20 : 1.

concentrations in the samples of bulk piracetam were higher than in the brain tissue samples with nanoparticles; see Figure 5. The fact of the strong sorption of piracetam in silica nanocarriers was confirmed using direct injection of the brain tissue with the nanoparticles into the dosing loop and subsequent multiple rinsing by solvent (methanol) and analysis by LC-MS (as mentioned below). Processing of extracts (filtration and centrifugation) caused high losses; nevertheless the highest losses were observed at purification of the extracts (30–40%), because nanocarriers were adsorbed in the filters and on the vial wall. Therefore, silica-based nanoparticles were destroyed by borate buffer (pH = 10.5), but at following LC-MS analysis various borate adducts and dimers were determined; that is, the method does not seem to be suitable.

As a solution of the above mentioned problems (sorption, dimers, etc.), the samples were analysed by direct injection to a sampling loop with subsequent multiple elution by MeOH. The concentration of Si-piracetam determined by direct injection was by several orders of magnitude higher compared with the concentrations determined in the extracts. By repeated injection of pure methanol the nanocarriers were gradually disintegrated and Si-piracetam was released, as illustrated in chromatograms in Figure 6. Concentrations

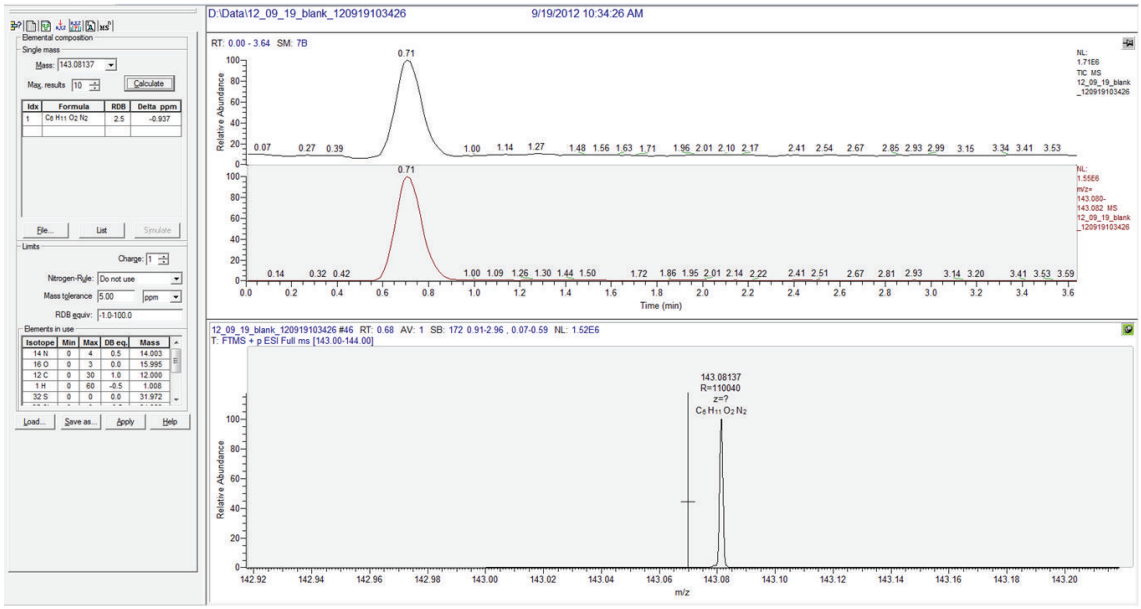

(a)

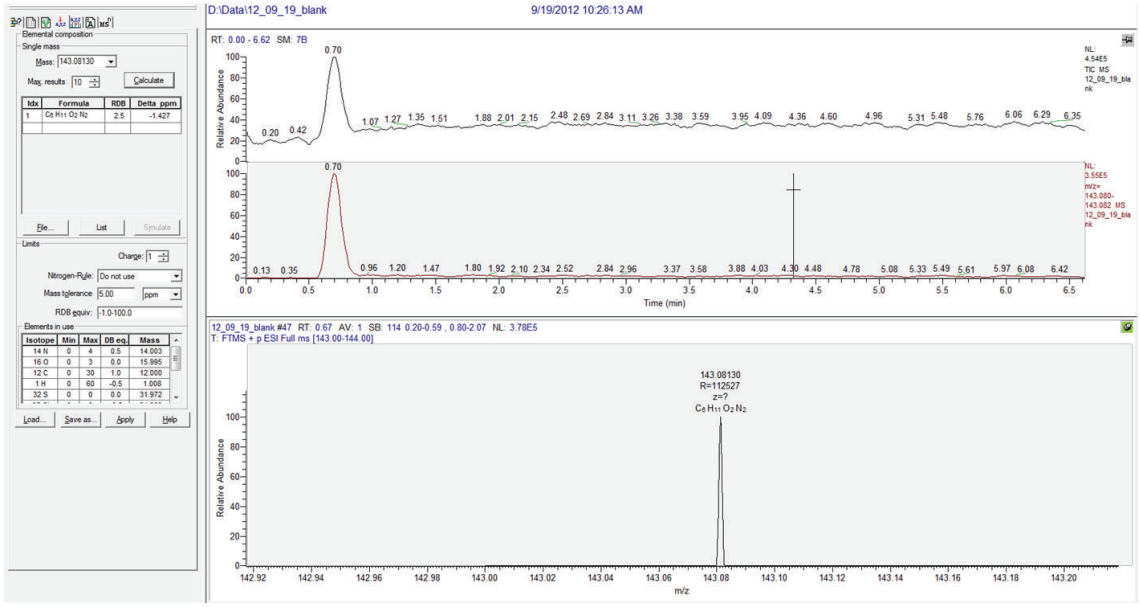

(b)

Figure 6: Chromatograms after first (a) and second (b) injections of pure methanol to sample of brain tissue with piracetam-loaded silica nanocarriers (labelled samples as blank-pure solvent injected into sample of brain with nanoparticles.).

determined at the first injection of pure solvent was 1500–1000 ng/mL (375–250 ng/mL in 100 mg brain tissue), at the second injection 250–100 ng/mL (65–25 ng/mL in 100 mg brain tissue), which was by 2-3 orders of magnitude higher than those measured during the extraction of brain tissue with nanoparticles.

Based on this semiquantitative method of direct injection, the concentrations of Si-piracetam that permeated through the BBB to the brain can be determined in comparison with drugs in bulk material; see Table 1. The concentration of the permeated bulk piracetam in the brain tissue was 2.8–1.0 ng/mL in 100 mg brain tissue, while that of Si-piracetam was 440–275 ng/mL in 100 mg brain tissue; that is, the application of nanoparticles led to an increase of piracetam approximately 200-fold. Similar strong sorption in silica nanocarriers can be found for pentoxifylline and pyridoxine; nevertheless, as mentioned in Section 2.7, the direct injection of the pentoxifylline samples was not performed due to the contamination of UHPLC-HRMS system. However, based on the results obtained for piracetam, it can be supposed that the concentration of Si-pentoxifylline in the brain tissue would be much higher, approximately 44000–20600 ng/mL in 100 mg of brain tissue. Although the silica nanocarriers loaded with pyridoxine were detected by microscopic analysis

Table 1: Concentrations of drug-loaded silica nanocarriers permeated through the BBB to brain in comparison with drugs in bulk (n.d. = not detected).

Drug substance	Concentration [ng/mL] in 100 mg of brain tissue		
	Bulk	Extraction of nanocarriers	Direct injection of tissue with nanoparticles
Piracetam	2.8–1.0	0.25–0.01	440–275
Pentoxifylline	6000–2000	2.5–0.75	44000–20600*
Pyridoxine	n.d	n.d	—

*Predicted based on the ratio bulk/direct injection of piracetam.

of brain tissue, no pyridoxine was found by UHPLC-HRMS; see Table 1.

It can be stated that loading of drugs to silica nanocarriers and extraction of drugs from nanocarriers is governed by general principles of normal-phase adsorption chromatography; it means that the retention of a molecule (the strength of interactions between the molecule and silica surface/silanol groups) is determined by its polar functional groups/double bonds and steric factors. Silica gel has acidic properties, and, therefore, basic compounds interact with the surface of this gel strongly [34]. Thus the observed strong binding of the discussed drug substances in silica nanocarriers may be caused by the presence of free electron pairs in the compounds (basicity). The basicity of pyridoxine expressed as the strongest pK_a(base) was 5.0±0.1 (predicted by ACD/Percepta ver. 2012), while for pentoxifylline the strongest pK_a(base) was 0.5 ± 0.7 (ACD/Percepta ver. 2012) and for piracetam the strongest pK_a(base) was −0.6 ± 0.2 (ACD/Percepta ver. 2012). Based on these data, pyridoxine shows the strongest potential bonding power, which may be a reason why it was not extracted in a detectable amount.

4. Conclusions

The silica-based nanocarriers loaded with piracetam, pentoxifylline, and pyridoxine were prepared. The content of the drug substances in silica-based nanocarriers was determined by elemental analysis and spectrophotometry as 1.5 mg of drug in 50 mg of nanoparticles. By transmission electron microscopy it was found that the average particle size of all prepared nanoparticles was approximately 120 nm, and they had spherical shape. The permeation of the prepared nanoparticles was compared with bulk materials by means of the *in vivo* model of rat brain perfusion. Samples of rat brain tissues were analysed by microscope, and it was found that all silica-based nanoparticles permeated to the brain tissue. The concentration of the drug substances in the tissue was determined by LC-HRMS. It was found that all the drugs exhibited very strong sorption in silica nanocarriers. The direct injection of samples of brain tissue (without purification) treated with Si-piracetam to a sampling loop with subsequent multiple elution by MeOH confirmed approximately 200-fold higher concentration of piracetam loaded in silica-based nanocarriers in the brain tissue in comparison with bulk piracetam.

The field of nanomedicine proposes many opportunities of finding novel solutions to improve health care. This study confirmed that silica nanoparticles can permeate through the blood-brain barrier and effectively transport drugs to the brain and so help in the treatment of different difficult to treat cerebral diseases. However, further investigation and, primarily, selection of suitable drug candidates (bulky and nonbasic) for immobilization into silica nanoparticle drug formulations are needed.

Conflict of Interests

The authors declare that there is no conflict of interests regarding the publication of this paper.

Acknowledgments

This study was supported by the Czech Science Foundation, GACR P304/11/2246, by the EfCOP, IPo Project ENVIMET (CZ.1.07/2.3.00/20.0246) and by the National Infrastructure CzeCos/ICOS (LM2010007). Ingrid Brezaniova received fund no. A1_FCHI_2014_003.

References

[1] H. J. Roth and H. Fenner, *Arzneistoffe*, Deutscher Apotheker, Stuttgart, Germany, 3rd edition, 2000.

[2] D. J. Abraham and D. P. Rotella, *Burger's Medicinal Chemistry, Drug Discovery and Development*, Wiley, New York, NY, USA, 7th edition, 2010.

[3] M. S. Alavijeh, M. Chishty, M. Z. Qaiser, and A. M. Palmer, "Drug metabolism and pharmacokinetics, the blood-brain barrier, and central nervous system drug discovery," *NeuroRx*, vol. 2, no. 4, pp. 554–571, 2005.

[4] N. J. Abbott, A. A. K. Patabendige, D. E. M. Dolman, S. R. Yusof, and D. J. Begley, "Structure and function of the blood-brain barrier," *Neurobiology of Disease*, vol. 37, no. 1, pp. 13–25, 2010.

[5] C. Passeleu-Le Bourdonnec, P.-A. Carrupt, J. M. Scherrmann, and S. Martel, "Methodologies to assess drug permeation through the blood-brain barrier for pharmaceutical research," *Pharmaceutical Research*, vol. 30, no. 11, pp. 2729–2756, 2013.

[6] N. J. Abbott, L. Rönnbäck, and E. Hansson, "Astrocyte-endothelial interactions at the blood-brain barrier," *Nature Reviews Neuroscience*, vol. 7, no. 1, pp. 41–53, 2006.

[7] C.-T. Lu, Y.-Z. Zhao, H. L. Wong, J. Cai, L. Peng, and X.-Q. Tian, "Current approaches to enhance CNS delivery of drugs across the brain barriers," *International Journal of Nanomedicine*, vol. 9, no. 1, pp. 2241–2257, 2014.

[8] Z. Yang, Z. W. Liu, R. P. Allaker et al., "A review of nanoparticle functionality and toxicity on the central nervous system," *The Journal of the Royal Society Interface*, vol. 7, supplement 4, pp. S411–S422, 2010.

[9] H. L. Wong, X. Y. Wu, and R. Bendayan, "Nanotechnological advances for the delivery of CNS therapeutics," *Advanced Drug Delivery Reviews*, vol. 64, no. 7, pp. 686–700, 2012.

[10] S. Bhaskar, F. Tian, T. Stoeger et al., "Multifunctional Nanocarriers for diagnostics, drug delivery and targeted treatment across blood-brain barrier: Perspectives on tracking and neuroimaging," *Particle and Fibre Toxicology*, vol. 7, article 3, 25 pages, 2010.

[11] M. Simko and M.-O. Mattsson, "Interactions between nanosized materials and the brain," *Current Medicinal Chemistry*, vol. 21, no. 37, pp. 4200–4214, 2014.

[12] A. Bitar, N. M. Ahmad, H. Fessi, and A. Elaissari, "Silica-based nanoparticles for biomedical applications," *Drug Discovery Today*, vol. 17, no. 19-20, pp. 1147–1154, 2012.

[13] H. Nehoff, N. N. Parayath, L. Domanovitch, S. Taurin, and K. Greish, "Nanomedicine for drug targeting: strategies beyond the enhanced permeability and retention effect," *International Journal of Nanomedicine*, vol. 9, no. 1, pp. 2539–2555, 2014.

[14] Y. T. Liao, C. H. Liu, J. Yu, and K. C. W. Wu, "Liver cancer cells: targeting and prolonged-release drug carriers consisting of mesoporous silica nanoparticles and alginate microspheres," *International Journal of Nanomedicine*, vol. 9, pp. 2767–2778, 2014.

[15] V. Marzaioli, J. A. Aguilar-Pimentel, I. Weichenmeier et al., "Surface modifications of silica nanoparticles are crucial for their inert versus proinflammatory and immunomodulatory properties," *International Journal of Nanomedicine*, vol. 9, pp. 2815–2832, 2014.

[16] L. Tang and J. Cheng, "Nonporous silica nanoparticles for nanomedicine application," *Nano Today*, vol. 8, no. 3, pp. 290–312, 2013.

[17] E. Vaculikova, D. Placha, and J. Jampílek, "Toxicology of drug nanocarriers," *Chemické Listy*, vol. 109, no. 5, 2015.

[18] L. Costantino, G. Tosi, B. Ruozi, L. Bondioli, M. A. Vandelli, and F. Forni, "Colloidal systems for CNS drug delivery," in *Progress in Brain Research Nanoneuroscience and Nanoneuropharmacology*, S. S. Hari, Ed., pp. 35–69, Elsevier, 2009.

[19] Y. Wang, Q. Zhao, N. Han et al., "Mesoporous silica nanoparticles in drug delivery and biomedical applications," *Nanomedicine: Nanotechnology, Biology and Medicine*, vol. 11, no. 2, pp. 313–327, 2015.

[20] D. Liu, B. Lin, W. Shao, Z. Zhu, T. Ji, and C. Yang, "In vitro and in vivo studies on the transport of PEGylated silica nanoparticles across the blood-brain barrier," *ACS Applied Materials and Interfaces*, vol. 6, no. 3, pp. 2131–2136, 2014.

[21] S. Ku, F. Yan, Y. Wang, Y. Sun, N. Yang, and L. Ye, "The blood-brain barrier penetration and distribution of PEGylated fluorescein-doped magnetic silica nanoparticles in rat brain," *Biochemical and Biophysical Research Communications*, vol. 394, no. 4, pp. 871–876, 2010.

[22] H. Xu, F. Yan, E. E. Monson, and R. Kopelman, "Room-temperature preparation and characterization of poly(ethylene glycol)-coated silica nanoparticles for biomedical applications," *Journal of Biomedical Materials Research: Part A*, vol. 66, no. 4, pp. 870–879, 2003.

[23] W. Stöber, A. Fink, and E. Bohn, "Controlled growth of monodisperse silica spheres in the micron size range," *Journal of Colloid And Interface Science*, vol. 26, no. 1, pp. 62–69, 1968.

[24] H. Xu, J. W. Aylott, R. Kopelman, T. J. Miller, and M. A. Philbert, "A real-time ratiometric method for the determination of molecular oxygen inside living cells using sol-gel-based spherical optical nanosensors with applications to rat C6 glioma," *Analytical Chemistry*, vol. 73, no. 17, pp. 4124–4133, 2001.

[25] W. Tang, H. Xu, R. Kopelman, and M. A. Philbert, "Photodynamic characterization and *in vitro* application of methylene blue-containing nanoparticle platforms," *Photochemistry and Photobiology*, vol. 81, no. 2, pp. 242–249, 2005.

[26] Y. Takasato, S. I. Rapoport, and Q. R. Smith, "An in situ brain perfusion technique to study cerebrovascular transport in the rat," *The American Journal of Physiology*, vol. 247, no. 3, pp. H484–H493, 1984.

[27] D. D. Allen, J. Oki, and Q. R. Smith, "An update on the in situ brain perfusion technique: simple, faster, better," *Pharmacological Research*, vol. 14, p. s337, 1997.

[28] R. Q. Smith and D. D. Allen, "In situ brain perfusion technique," in *Methods in Molecular Medicine—The Blood-Brain Barrier: Biology and Research Protocols*, S. Nag, Ed., vol. 89, pp. 209–218, Humana Press, Totowa, NJ, USA, 2003.

[29] M. Kuneš, J. Květina, P. Kubant, J. Maláková, V. Herout, and Z. Svoboda, "Influence of methotrexate and L-carnitine on transintestinal transport of model substances (the rat small intestine in situ perfusion)," *Chemicke Listy*, vol. 101, no. 14, pp. s209–s211, 2007.

[30] M. Kuneš, J. Květina, Z. Svoboda, and V. Herout, "Study of the mechanisms of intestinal absorption of xenobiotics using in situ perfusion of rat intestine," *Biologia*, vol. 60, no. 17, pp. s89–s92, 2005.

[31] K. Shimizu, Y. del Amo, M. A. Brzezinski, G. D. Stucky, and D. E. Morse, "A novel fluorescent silica tracer for biological silicification studies," *Chemistry and Biology*, vol. 8, no. 11, pp. 1051–1060, 2001.

[32] S. J. Swanson, P. C. Bethke, and R. L. Jones, "Barley aleurone cells contain two types of vacuoles: characterization of lytic organelles by use of fluorescent probes," *Plant Cell*, vol. 10, no. 5, pp. 685–698, 1998.

[33] P. Znachor, J. Nedoma, and P. Rychtecký, "Kinetics of glucose stimulatory effect on silica deposition and growth of natural populations of Fragilaria crotonensis," *Phycological Research*, vol. 59, no. 2, pp. 123–128, 2011.

[34] V. R. Meyer, "Adsorption chromatography: normal-phase," in *Chromatography Practical High-Performance Liquid Chromatography*, pp. 159–172, John Wiley & Sons, Chichester, UK, 5th edition, 2010.

Hindawi Publishing Corporation
BioMed Research International
Volume 2015, Article ID 670420, 7 pages
http://dx.doi.org/10.1155/2015/670420

Review Article

Assurance of Medical Device Quality with Quality Management System: An Analysis of Good Manufacturing Practice Implementation in Taiwan

Tzu-Wei Li,[1] Pei-Weng Tu,[2] Li-Ling Liu,[3] and Shiow-Ing Wu[4]

[1]*Office of Medical Device Evaluation, Center for Measurement Standards, Industrial Technology Research Institute, 321 Sec. 2, Kuang Fu Road, Hsinchu 30011, Taiwan*
[2]*Division of Medical Devices and Cosmetics, Food and Drug Administration, 161-2 Kunyang Street, Nangang District, Taipei City 11561, Taiwan*
[3]*Division of Medicinal Products, Food and Drug Administration, 161-2 Kunyang Street, Nangang District, Taipei City 11561, Taiwan*
[4]*Food and Drug Administration, 161-2 Kunyang Street, Nangang District, Taipei City 11561, Taiwan*

Correspondence should be addressed to Tzu-Wei Li; alberttwli@itri.org.tw

Received 11 September 2014; Revised 4 December 2014; Accepted 4 December 2014

Academic Editor: Josef Jampilek

The implementation of an effective quality management system has always been considered a principal method for a manufacturer to maintain and improve its product and service quality. Globally many regulatory authorities incorporate quality management system as one of the mandatory requirements for the regulatory control of high-risk medical devices. The present study aims to analyze the GMP enforcement experience in Taiwan between 1998 and 2013. It describes the regulatory implementation of medical device GMP requirement and initiatives taken to assist small and medium-sized enterprises in compliance with the regulatory requirement. Based on statistical data collected by the competent authority and industry research institutes, the present paper reports the growth of Taiwan local medical device industry after the enforcement of GMP regulation. Transition in the production, technologies, and number of employees of Taiwan medical device industry between 1998 and 2013 provides the competent authorities around the world with an empirical foundation for further policy development.

1. Introduction

An effective quality management system has always been considered to be a good strategy for a manufacturer to maintain and improve its product and service quality. The Food and Drug Administration of the United States of America (the US FDA) was the first competent authority for medical device to mandate medical device quality system requirement to ensure the safety and effectiveness of medical devices. The US FDA issued a final rule in the Federal Register of July 21, 1978 (43 FR 31 508), prescribing CGMP (current good manufacturing practice) requirements for medical devices. This quality system requirement provided the government and industry with a foundation for ensuring that medical devices manufactured comply with the established specifications and with continuous improvement strategy. The quality system regulation also requires establishment of documentation and records for investigating quality problems and patient injuries of the medical devices concerned.

The US FDA CGMP had been the only regulatory quality system requirements specifically for medical device until the publication of ISO 13485:1996. The European norm version of ISO 13485:1996 (i.e., EN 46001) was adopted as part of the conformity assessment prescribed in European Community' (European Economic Community was renamed as European Community in 1993), Active Implantable Medical Device Directive (90/385/EEC), Medical Device Directive (93/42/EC), and later In Vitro Diagnostic Medical Device Directive (98/79/EC) for higher-risk medical devices. US FDA replaced 1987 CGMP with Quality System Regulation (QSR) to harmonize with ISO 13485:1996 in 1997.

Following the approaches taken by the United States and the European Union, many competent authorities have

decided to incorporate quality management system implementation as one of mandatory requirements for high-risk medical devices. This is analogous to the International Conference on Harmonisation (ICH) approaches. The ICH developed a harmonized guideline on pharmaceutical quality system for the lifecycle of the product and emphasized an integrated approach to quality risk management. ICH published Q9 Quality Risk Management in November 2005 and Q10 Pharmaceutical Quality System in June 2008.

The international standard, ISO 13485:2003, medical devices—quality management systems—requirements for regulatory purposes, as the title suggested specifies quality management requirements for the medical device sector for regulatory purposes. By the end of 2012, at least 22,237 ISO 13485:2003 certificates had been issued in 97 countries and economies. The 2012 total represents an increase of 2,388 (+12%) over 2011. The top three countries for the total of certificates were Germany, the USA, and Italy and the top three in growth since the 2011 survey were Italy, Germany, and the USA [1].

2. Medical Device GMP Regulation and Corresponding Measures

2.1. Medical Device GMP Regulation. Taiwan is one of the pioneers in Asia in its medical device regulation, which dates back to the 1970s. The Department of Health of Taiwan (DOH, later reorganized as the Ministry of Health and Welfare in 2010) revised medical device regulations in 1998 for the establishment of a risk-based regulatory system. The system classified medical devices into three classes according to their risk, promulgating mandatory medical device good manufacturing practice (GMP) regulation for medical devices, and introduction of the premarket review and postmarket controls. The revision of the regulations completed in 2005 aims to provide the government and industry with an international harmonized regulatory ecosystem to improve the safety, effectiveness, and quality of medical device marketed in Taiwan.

The DOH established the Medical Device GMP Promotion Task Force and convened the first meeting on 19 November 1996 to draft GMP regulation and supporting measures. After a series of stakeholder meetings and public workshops held in the following 18 months, DOH released medical device GMP regulation on 10 February 1999. To harmonize with the international standards at that time, DOH GMP regulation was based on ISO 13485:1996 with additional regulatory requirements on issues, such as outsourcing, adverse event reporting, and product recall. Following the establishment of medical device GMP, DOH published the regulation on "Classification and Management of Medical Devices" on 21 June 2000. More than 1,600 types of medical devices were classified into three classes according to risk level of the products. Class I medical device includes 700 lowest risk products such as tong tongue depressors, elastic bandages, and manual wheelchairs. GMP regulation is not mandatory for Class I medical device manufacturers unless their products are labeled as sterile or with measuring function. Over half of the medical devices on the Taiwan market were classified as Class II. Examples of Class II medical devices include blood pressure monitors, diagnostic X-ray system, and glucose monitoring systems. Class III medical devices are the highest risk level and subject to the most stringent controls. Typical Class III medical devices include HIV diagnostic reagents, pacemakers, and coronary stents. Manufacturers of Class II and Class III medical devices need to establish quality systems in accordance with GMP regulation before their product licenses are issued by DOH. Table 1 illustrates the number of medical devices under each classification and GMP requirement for different classes of the products.

Medical device manufacturers were required to complete the GMP registration process by the end of a 5-year transition period (2001–2005).

The current GMP regulation was revised in 2013 by TFDA to harmonize with ISO 13485:2003.

2.2. Supporting Measures to Support SMEs. To assist medical device manufacturers, in particular small and medium-sized enterprises (SMEs), in understanding GMP regulation and establishing quality system within the company, DOH supported many organizations such as industry/trade associations and not-for-profit research organizations to hold training workshops and to provide consultancy services during 2000–2005.

Besides DOH, Industry Development Bureau of Ministry of Economic Affairs and Science Industrial Park Administration also provided financial and technical support to firms to establish quality system and recruit qualified employees. It was estimated that more than a dozen public training workshops supported by government departments were held and more than 500 employees were trained each year. These supporting measures were aimed at reducing the burden and resources needed for SME to comply with GMP regulation.

The majority of medical device manufacturers in Taiwan produced Class I and some Class II medical devices at the time when GMP was first enforced. It was estimated that 75% of SMEs seek outside consultation services for the establishment of quality systems. It was reported that a typical consultation for medical device GMP took 8.8 months and cost 10~15 thousand USD in average [5].

The supporting measures provided by the government, industry associations, and nonprofit organizations are still available for SMEs that would like to enter into the medical device sector.

3. Impact on Local SMEs Medical Device Manufacturers Brought by GMP Regulation Requirement

Small and medium-sized enterprises (SMEs) are defined by OECD as "non-subsidiary, independent firms which employ fewer than a given number of employees." However, the number of employees of SMEs is defined differently across economies. For example, a firm employing fewer than 250 workers is designated as an SME in the European Union, while the United States considers SMEs as firms with fewer than 500 employees, and companies with fewer than 50

Table 1: Taiwan GMP requirement for medical devices.

Classification	Class I		Class II	Class III
Number of medical device classification names (2014)	737		936	153
GMP	Not required	Required for sterile devices or devices with measuring function	Required for all Class II medical devices	Required for all Class III medical devices

employees are small firms, and companies with employees below 10 are microfirms [8].

Globally, medical device industry is innovative and a technology-based sector consists of predominately SMEs. More than 80% of medical device companies have fewer than 50 employees, and many (notably innovative startup companies) have little or no sales revenue [9]. In Europe, 95% of medical device firms are SMEs [10] with the majority of the medical device companies being small and microsized, employing less than 50 people [11].

In Taiwan, SME is defined as enterprise with fewer than 200 employees. A firm which employs fewer than 5 workers is defined as small enterprise [12]. According to a government statistics in 2001, essentially all medical device manufacturers were SMEs [13].

The tightening of medical device regulation generally discourages the creation of new medical device companies and startup firms [14]. Although medical device regulation may provide quality system exemptions, they are, however, generally based upon the risk level of medical device and not on the size of company. Potential adverse impact of new regulations hence can be harmful to SMEs in particular [15]. SMEs tend to have less human and financial resources than large firms to implement the regulation and deal with additional bureaucratic processes [16]. Therefore, as would be expected, new medical device regulation tends to be more burdensome to SMEs than large firms [17]. A 2001 study in the USA showed that small business bears a disproportionately large share of federal regulatory burden [18].

The two main components of the compliance costs to the companies are as follows:

(1) the time cost of internal staff on collecting, maintaining and understanding regulatory requirements, establishing procedures, completing forms and preparing the necessary information, and dealing with the relevant government authority;

(2) the financial costs of external professional [19].

During the scheduling of medical device GMP regulation, oppositions and concerns were raised by industries. By analogy with the experience of pharmaceutical GMP implementation which reduced the number of local SME drug manufacturers, some policy analysts argued that quality management system regulation might raise the burden of SME medical device manufacturers and jeopardize the survival of such companies. This reduction in number of local manufacturers could lower the accessibility of lower-price medical devices, raise healthcare cost, and weaken sector's competiveness in general [20–23].

The dissentient voices might not be unfound. According to a 1961 government statistics of Taiwan, before the enforcement of the pharmaceutical factory standard in 1959, there were 468 pharmaceutical factories (not including 359 Chinese herbal medicine factories) in Taiwan. Some pharmaceutical factories failed to comply with the regulatory requirement and were not allowed to operate as a result. It was estimated that 250 pharmaceutical factories were closed down between 1961 and 1968. The number of pharmaceutical factories increased again in 1970s. It was estimated that there were 900 pharmaceutical factories in Taiwan in 1981. DOH mandated pharmaceutical GMP in 1982 and the number of factories decreased again. There were only 231 GMP registered pharmaceutical factories in 1995 [24]. Nearly two-thirds of Taiwan pharmaceutical companies discontinued operation after the enforcement of pharmaceutical GMP. Although the quality and competiveness of Taiwan pharmaceutical industry improved, the number of companies did not reach the 1980s level again [25].

3.1. The Development of Taiwan Medical Device SMEs after GMP Implementation. Before DOH revised medical device regulations in 2000, the differentiation between medical devices and other medical products was not clear. This might lead to underestimation of the actual scale of production and number of products in medical device industry before 2000.

There were about 200 medical device manufacturers in Taiwan in 2000, with most of them located in northern part of the island such as Taipei, Taoyuan and Hsinchu (see Table 2). Taiwan medical device industry started from making wound care products such as gauze and bandage provided by textile factories after the Second World War. Medical masks, surgical gowns, patient bed sheets, and examination gloves were the leading manufacturing products in 1960s. Metallic surgical instruments, electrocardiography (ECG), mercury sphygmomanometers, intravenous infusion sets, syringes, sutures, blood sampling devices, and scalp needles caught on in 1970s. Blood pressure monitors, hearing aids, wheelchairs, clinical thermometers, surgical operation tables, bone implants, electrical surgical knives, and transcutaneous electrical nerve stimulation (TENS) became dominated products in 2000 [26].

According to DOH (and TFDA), there were 208 medical device manufacturers across the island in 1999. The number of registered medical device manufacturers firms increased constantly to the level of 1,229 in 2013 [2] (see Figure 1) .

Table 2: Number of medical device manufacturers in 2005 and 2013.

City/county	2005	2013
Taipei City	37	56
Taipei County	197	361
Yilan County	10	17
Taoyuan County	52	145
Hsinchu City	11	26
Hsinchu County	25	58
Miaoli County	9	22
Taichung City	22	175*
Taichung County	45	
Changhua County	34	99
Chiayi City	2	5
Nantou County	6	13
Yunlin County	6	9
Chiayi County	10	25
Tainan City	13	109*
Tainan County	29	
Kaohsiung City	8	88*
Kaohsiung County	14	
Pingtung County	6	10
Hualien County	2	1
Keelung	2	10
Total	**540**	**1,229**

Source [2].
*Taichung City/County, Tainan City/County, and Kaohsiung City/County were combined in 2010.

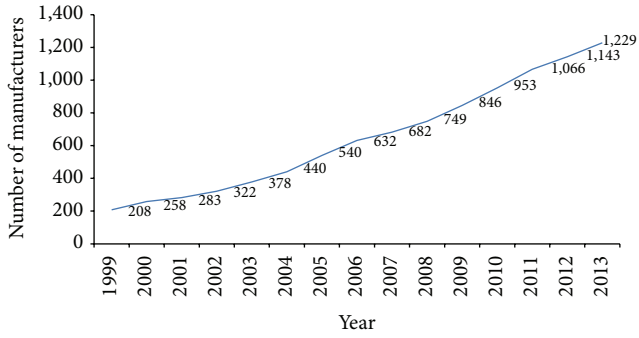

Figure 1: Taiwan medical device manufacturers during 1999~2013. Source [2].

The production and export of Taiwan medical device increased significantly in the past ten years (see Figures 2 and 3).

3.2. The Development of Medical Device Manufacturer Association. With the improvement in product quality, Taiwan's medical device is more competitive globally as the growth rate of export showed, which also explained the overall growth of production of Taiwan medical device industry.

By analyzing the transition of the medical device manufacturer association in Taiwan after the implementation of GMP regulation, it helps us to understand how quality of

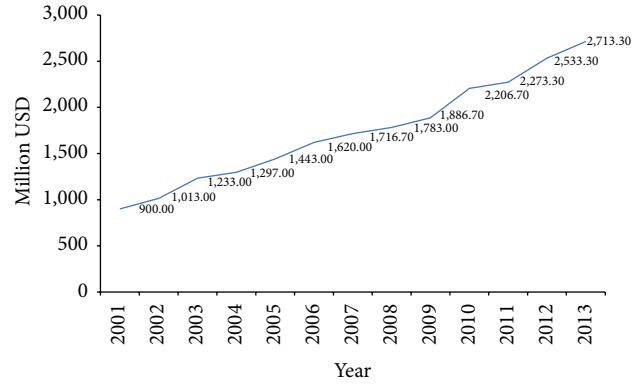

Figure 2: Taiwan medical device production during 2001~2013. Source [4, 6].

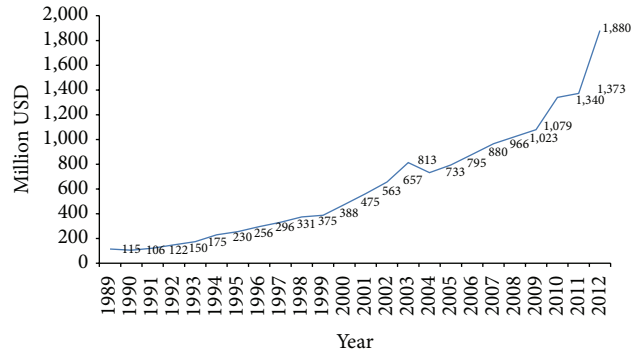

Figure 3: Taiwan medical device export during 1989~2012. Source [4, 6, 7].

medical device manufactured in Taiwan was enhanced as a result of the implementation of the GMP regulation.

The impact of GMP regulation on local manufacturers may also be observed from analyzing the evolution of the medical device association in Taiwan.

The current medical device manufacturer association in Taiwan was originally the "Taiwan Absorbent Cotton Industry Association" established in 1953. It was reorganized to become "Taiwan Medical Device Industry Association" (TMDIA) in 1995 and later renamed as "Taiwan Medical and Biotech Industry Association" (TMBIA) in 2013 to reflect the composition of its members [3].

In the 1970s, most of medical device manufacturers in Taiwan were family-owned company. In addition to gauze and bandages, various products such as hospital beds, wheelchairs, surgical tables, surgical lamps, dental chairs, sterilization devices, and laboratory instruments were later added into the product list of medical devices made by association members. Now, Taiwan is a major supplier of blood glucose monitoring system, powered wheelchairs/scooters, and blood pressure monitors in the world (see Table 3).

The rapid growth of Taiwan medical device industry began in 1990s. TMDIA played an important role in promoting medical device GMP. TMDIA was entrusted by DOH to assist firms in complying with regulation by providing

Table 3: Taiwan top export medical devices during 1997~2012 (in amount of sales).

Year	Top export medical devices
1997	Examination gloves, physical therapy devices, manual wheelchairs, powered wheelchairs/scooters, hearing aids, and sphygmomanometers
2000	Powered wheelchairs/scooters, manual wheelchairs, glucose meters, artificial limbs, physical therapy devices, blood pressure monitors, medical instruments, prosthesis devices, and syringes
2002	Powered wheelchair/scooter, examination gloves, physical therapy devices, surgical devices, prosthesis devices, blood pressure monitors, manual wheelchairs, glucose meters, and contact lenses
2003	Powered wheelchairs/scooters, physical therapy devices, examination gloves, surgical devices, blood pressure monitors, prosthesis devices, manual wheelchairs, and glucose meters
2004	Powered wheelchairs/scooters, physical therapy devices, examination gloves, surgical devices, prosthesis devices, manual wheelchairs, laboratory devices, contact lenses, and blood pressure monitors
2005	Powered wheelchairs/scooters, physical therapy devices, examination gloves, surgical devices, prosthesis devices, contact lenses, glucose meters, laboratory devices
2006	Powered wheelchairs/scooters, surgical devices, physical therapy devices, contact lenses, laboratory devices, examination gloves, surgical devices, and glucose meters
2009	Powered wheelchairs/scooters, laboratory devices, glucose test strips, surgical devices, contact lenses, glucose meters, and physical therapy devices
2010	Powered wheelchairs/scooters, glucose test strips, laboratory devices, surgical devices, contact lenses, glucose meters, and physical therapy devices
2011	Glucose test strips, laboratory devices, powered wheelchairs/scooters, contact lenses, surgical devices, glucose meters, and IVDs
2012	Glucose test strips, contact lenses, laboratory devices, surgical devices, powered wheelchairs/scooters, glucose meters, and IVDs

Source [3, 4].

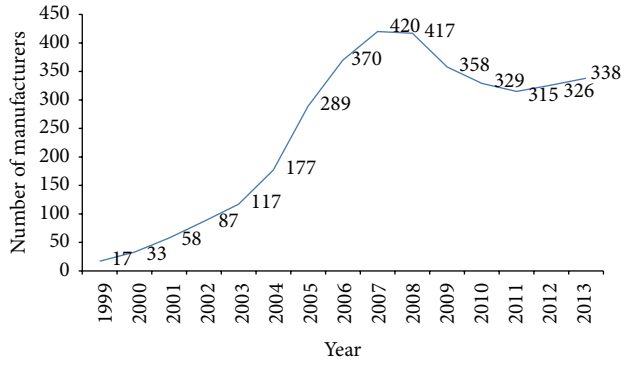

Figure 4: Number of medical device GMP manufacturers during 1999~2013. Source: the authors [2].

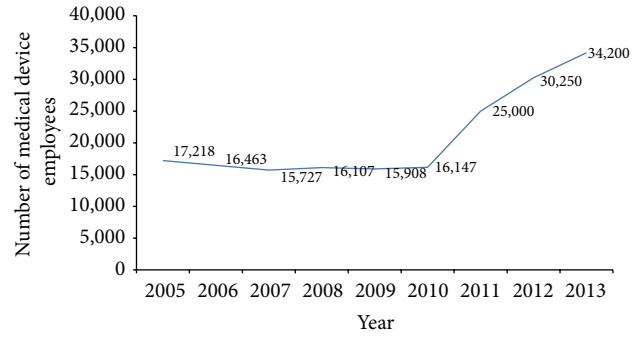

Figure 5: Taiwan medical device industry employees. Source [4].

qualified trainers and consultants to firms. Before the end of the transition period of GMP in 2005, more companies producing medical devices joined TMDIA. The membership grew by as many as 50% to 260 members in 2005. Many information and communication technologies companies developing medical devices also become members of the TMBIA in recent years. Investment in in vitro diagnostic medical devices, medical imaging system, artificial joints, dental implants, medical apps, and mobile health devices has increased significantly since 2010. Currently, there are 350 companies registered under TMBIA [3].

3.3. Medical Device GMP Registered Manufacturers. Medical device GMP requirement is mandatory for the manufacturers of Class I sterile or with measuring function, Class II, and Class III devices. In addition, Class I medical devices manufacturers may also apply for GMP registration voluntarily. The number of medical device GMP registered manufacturers was only 17 in the first year (1999) and increased to 289 at the end of the transition period in 2005, and, by 2013, the number increases to as many as 338 [2] (see Figure 4).

3.4. The Taiwan Medical Device Manufacturing Workforce. In addition to the growth in number of medical device manufacturers after the enforcement of GMP regulation, the size of firms was also enlarged. The number of the workforce employed by the medical device manufacturers increased constantly from 2005 to 2013 (see Figure 5). Statistical data regarding the number of employees of medical device firms

audited by Center for Measurement Standards/Industrial Technology Research Institute (one of four TFDA medical device GMP designated auditing organizations) in 2006 showed that 26% of the firms employed fewer than 10 workers, 67% of the firms hired less than 50 employees, and only 4 firms had more than 100 employees. In 2009, 25% of the firms hired less than 10 employees, 86% of the firms employed no more than 50 workers, and 3 firms had more than 100 employees. A similar data was also collected for 2013, showing that 17% of the firms hired fewer than 10 employees, 61% of the firms did not hire more than 50 employees, and 13 firms had more than 100 employees.

Some manufacturers enjoy a constant growth in business after GMP regulation enforcement. According to Taiwan Stock Exchange Corporation, examples of local large medical device manufacturers which employ more than 500 persons include ApexBio (592 employees), Kang Na Hsiung (KNH, 569 employees), Bionime (826 employees), Pacific Hospital Supply (515 employees), Microlife (3,400 employees), Taidoc (850 employees), St. Shine (2,000 employees), Rossmax (1,554 employees), and Avita (520 employees) [4].

4. Conclusion

The success of Taiwan medical device industry in the last decade is contributed by different factors such as global market growth, technology innovation, increased financial investment, educated human resources, and governmental initiatives.

Based on statistical data collected by the government and market survey organizations, the present paper reports the growth of Taiwan medical device industry after the enforcement of GMP regulation. As shown by the growth rates of the production and export, the international competiveness of Taiwan medical device industry is enhanced. Quality of Taiwan medical devices is recognized by global healthcare providers and consumers. Transition in the production, technologies, and number of employees of Taiwan medical device industry between 1998 and 2013 provides the competent authorities around the world with an empirical foundation for further policy development.

Policy makers around the world need to understand and evaluate the impact of regulatory requirements on the local small-to-medium-sized manufacturers and implement a harmonized regulatory system with care to mitigate the impact, thereby ensuring the success of the implementation of their policy.

The present study suggested that the implementation of GMP regulation facilitates the transformation of local medical device industry. The standard set forth by GMP regulation did not jeopardize the development of local industry as some analyst believed. Supporting measures assisting SMEs in quality system establishment and human resource improvement is essential for the success. SMEs which comply with GMP regulation can strengthen their competiveness in both domestic and global markets.

Further studies should be conducted in order to understand the key factors of GMP regulation implementation. Nonetheless, this study agrees that improving the information availability to SMEs, a friendly environment for SMEs to conduct new product development, and broad channels for SMEs to access regulatory information will ensure the success of new regulation as well as industry development [16, 27, 28].

Abbreviations

CGMP:	Current good manufacturing practice. "CGMP requirements for devices in part 820 (21 CFR part 820) were first authorized by Section 520(f) of the Federal Food, Drug, and Cosmetic Act (the act). Under Section 520(f) of the act, FDA issued a final rule in the Federal Register of July 21, 1978 (43 FR 31 508), prescribing CGMP requirements for medical devices. This regulation became effective on December 18, 1978, and was codified under part 820." See http://www.fda.gov/medicaldevices/deviceregulationandguidance/postmarketrequirements/qualitysystemsregulations/
DOH:	Department of Health of Taiwan
GMP:	Good manufacturing practice
ICH:	International Conference on Harmonisation
QSR:	Quality System Regulation. In 1996, FDA revised the CGMP regulation to add the design controls authorized by the Safe Medical Devices Act. The part 820 revision was published on October 7, 1996 (61 FR 52602), and went into effect June 1, 1997. See http://www.fda.gov/medicaldevices/deviceregulationandguidance/postmarketrequirements/qualitysystemsregulations/
SME:	Small and medium-sized enterprise
TFDA/MOHW:	Food and Drug Administration/Ministry of Health and Welfare of Taiwan
TMBIA:	Taiwan Medical and Biotech Industry Association
TMDIA:	Taiwan Medical Device Industry Association
US FDA:	The United States Food and Drug Administration
21 CFR 820:	Part 820, CFR, Code of Federal Regulations Title 21.

Conflict of Interests

The authors declare that there is no conflict of interests regarding the publication of this paper.

References

[1] ISO, *The ISO Survey of Management Standard Certifications*, ISO, 2012.

[2] Food and Drug Administration and Ministry of Health and Welfare, *Statistics of Pharmaceutical Affairs*, Food and Drug Administration, Ministry of Health and Welfare, 2013, (Chinese).

[3] Taiwan Medical Device and Biotech Industry Association Website, http://www.tmbia.org.tw/eng/.

[4] Industrial Technology Research Institute, *Medical Device Industry Year Book*, Industrial Technology Research Institute, 2003–2013, (Chinese).

[5] S. Huang, *The Benefits and Difficulties of Implementing GMP for Medical Device Manufacturers in Taiwan*, Graduate Institute of Business and Administration, Chang Gung University, 2007 (Chinese).

[6] Taiwan Institute of Economic Research Database, Taiwan Medical Device Industry Production Statistics, (Chinese), http://tie.tier.org.tw/.

[7] Invest in Taiwan, Ministry of Economic Affairs, Medical Device Industry Analysis and Investment Opportunity, 2008.

[8] OECD Website, *Glossary of Statistical Terms*, OECD Publishing, 2008.

[9] SelectUSA.

[10] EUCOMED, *Financial Impact of the Revision of the EU Medical Devices Directives on European SMEs and Industry*, EUCOMED, 2013.

[11] Eucomed.

[12] Ministry of Economic Affairs Taiwan, Definition of SME, 2009.

[13] Department of Statistics and Ministry of Economic Affairs, *List of Factories in Taiwan*, Department of Statistics, Ministry of Economic Affairs, 2001, (Chinese).

[14] EUCOMED, "Factsheet: financial impact of the revision of the EU medical device directives on european SMEs and industry, 2013," in *Proceedings of the ECD, SMEs, Employment, Innovation and Growth—The Washington Workshop*, Paris, France, 1996.

[15] Small Business Policy Branch, *Small Business and Regulatory Burden*, Industry Canada, 2003.

[16] OECD, "SMEs: employment, innovation and growth," in *Proceedings of the Washington Workshop*, Paris, France, 1996.

[17] Organisation for Economic Co-operation and Development, *Small Business, Job Creation and Growth: Facts, Obstacles and Best Practices*, section 3, Organisation for Economic Co-operation and Development, 1997.

[18] W. M. Crains and T. D. Hopkins, "The impact of regulatory costs on small firms," Tech. Rep., Office of Advocacy, U.S. Small Business Administration, 2001.

[19] I. Bickerdyke and R. Lattimore, "Reducing the regulatory burden: does firm size matter," Industry Commission Staff Research Paper, AGPS, Canberra, Australia, 1997.

[20] P. B. Jayakumar, *Small-Scale Pharma Firms Struggling for Survival*, Business Standard, 2008.

[21] B. Paul, *Pharma Industry Demands Immediate Govt. Intervention for Survival*, SupportBiz, 2013.

[22] Y. Lin, *Milestone of Taiwan Herb Medicine—Chinese Medicine GMP*, Shungtien Medicine, 2005, (Chinese).

[23] C. Kuangjen, Economic Daily News, New GMP in Mainland China, 2011, (Chinese).

[24] S. Lin, *Pharmaceutical Standards and Development of Pharmaceutical Trading*, NCCU, 2008, (Chinese).

[25] L. Tseng, Y. Chang, C. Chiang, K. Chen, W. Chiu, and C. Kuo, "Taiwan pharmaceutical industry status quo and strategy," *Journal of Far East University*, vol. 20, no. 1, 2002 (Chinese).

[26] Industrial Technology Research Institute, *Medical Device Industry Analysis*, chapter 4, December 2001 (Chinese).

[27] *United Nations Conference on Trade and Development, Integrating Developing Countries'SMEs into Global Value Chains*, 2010.

[28] O. Gorlova, M. Grzybowska-Brzezińska, and I. Żuchowski, "ISO standards and quality costs as instruments of companies' competitive advantage," *Socio-Economic Research Bulletin*, vol. 46, no. 3, p. 1, 2012.

Hindawi Publishing Corporation
BioMed Research International
Volume 2014, Article ID 929248, 9 pages
http://dx.doi.org/10.1155/2014/929248

Research Article

Determination of Critical Parameters of Drug Substance Influencing Dissolution: A Case Study

Erika Bojnanska,[1] Michal Kalina,[2] Ladislav Parizek,[2] Eva Bartonickova,[2] Tomas Opravil,[2] Michal Vesely,[2] Miloslav Pekar,[2] and Josef Jampilek[1]

[1] *Faculty of Pharmacy, University of Veterinary and Pharmaceutical Sciences Brno, Palackeho 1/3, 612 42 Brno, Czech Republic*
[2] *Faculty of Chemistry, Brno University of Technology, Purkynova 464/118, 612 00 Brno, Czech Republic*

Correspondence should be addressed to Josef Jampilek; josef.jampilek@gmail.com

Received 2 August 2014; Revised 25 August 2014; Accepted 27 August 2014; Published 15 September 2014

Academic Editor: Kin Tam

The purpose of this study was to specify critical parameters (physicochemical characteristics) of drug substance that can affect dissolution profile/dissolution rate of the final drug product manufactured by validated procedure from various batches of the same drug substance received from different suppliers. The target was to design a sufficiently robust drug substance specification allowing to obtain a satisfactory drug product. For this reason, five batches of the drug substance and five samples of the final peroral drug products were analysed with the use of solid state analysis methods on the bulk level. Besides polymorphism, particle size distribution, surface area, zeta potential, and water content were identified as important parameters, and the zeta potential and the particle size distribution of the drug substance seem to be critical quality attributes affecting the dissolution rate of the drug substance released from the final peroral drug formulation.

1. Introduction

In the past, drug development was primarily empirical and data based [1]. Nowadays pharmaceutical development should be systematic; that is, the process should be understood; a mere change of some parameters of active pharmaceutical ingredients (APIs) of drug formulations so that they comply with some requirements is not sufficient. Process analytical technology (PAT) was defined by the United States Food and Drug Administration (FDA) as a mechanism to design, analyse, and control pharmaceutical manufacturing processes through the measurement of critical process parameters (CPP) which affect critical quality attributes (CQA) and thus by identification of these critical parameters the production process is improved, for example, by in-line or on-line monitoring to minimize production defects [2]. Quality by design (QbD) [1, 3] is connected with PAT. This innovative paradigm is inspired by ICH Q8-Q11 [4–7] and should lead to understanding the effect of incoming material parameters, formulation, and process variables on CQA [8, 9]. Older approved and registered APIs and pharmaceuticals are analysed/controlled by methods used at the time of their registration; that is, their specification cannot include modern analytical methods, such as solid-state analysis. Thus really critical parameters affecting the quality need not be defined in a specification prepared in this manner. This can become a great problem, when API source, site of manufacturing, or manufacturing equipment is changed.

This case study discusses prompt determination of critical parameters of the API purchased from a new supplier to afford the drug formulation to conform to the valid specification. Although the newly supplied API corresponded to the requirements of the current specification, after the change of the API supplier it was found that the drug formulations hardly met the required specification. Therefore the aim of this investigation was to find critical parameters/physicochemical properties of the drug substance that affect the quality of the peroral dosage form. Subsequently these new critical quality attributes were recommended as

new parameters for modification of the current API specification. As a result, the composition of the tablet should not be changed, and any change management process should not be initiated. The investigated API contains a tertiary amino group ($pK_a \approx 9$) and a carboxyl moiety ($pK_a \approx 4$); its lipophilicity expressed as $\log P$ is ca. 6, and the API can be used as hydrochloride. Due to confidentiality reasons it is not possible to characterise the API more specifically.

2. Experimental and Methods

2.1. Samples. All the samples of APIs (AS-1–AS-5), that is, five different batches, were received from external suppliers; samples AS-1, AS-2, AS-4, and AS-5 were from a new supplier and sample AS-3 was from a previous supplier. The final drug products, tablet samples TS-1–TS-5, were produced by the same validated manufacturing procedure (preforms with hardness 70–160 N were prepared on a tablet press from the homogenized mixture of the API, diluent, glidant, disintegrant, and calcium stearate; the prepared preforms were milled and then homogenized with calcium stearate, and from the prepared tableting mixture the final tablets were compressed using a tableting machine). It was found that the drug products TS-1 (from AS-1) and TS-2 (from AS-2) provided noncomplying and boundary results of dissolution testing, respectively, while TS-3 (from AS-3), TS-4 (from AS-4), and TS-5 (from AS-5) provided complying results according to the registered drug product specification.

2.2. Dissolution Testing. Dissolution tests were performed by a validated method using a USP apparatus 2 (paddle method) Varian Vankel VK 7000 Dissolution System (Agilent Technologies, Santa Clara, CA, USA). Powder samples (180 mg) or one tablet was introduced into 900 mL of dissolution medium (phosphate buffer pH = 7.2) maintained at 37 ± 0.5°C with the rotation speed of 100 rpm. Aliquots of the dissolution samples were withdrawn at predetermined times and filtered through a 0.45 μm PTFE filter. The loss in the volume of the liquid was compensated by addition of fresh dissolution medium maintained at the same temperature. The weight of each drug was used to calculate the dissolved percentage of the drug (Q [%]). The absorbance (drug concentration) of the sample solutions and the reference solution was measured in 1 cm quartz measuring cells at the maximum absorbance wavelength of the drug against the dissolution medium using a Varian Cary 50 UV-VIS Spectrophotometer (Agilent Technologies, Santa Clara, CA, USA). The measurements were repeated six times. All the presented results are reported as the mean value of these six independent measurements (mean ± SD, $n = 6$). All the results are summarized in Table 1.

2.3. Water Content. The determination was performed by a titrator 701 KF Titrino (Methrom, Herisau, Switzerland) according to the Ph.Eur 7.7, Chapter 2.5.32 (Water: Micro determination) using 200 mg of the API dissolved in 1 mL of dry methanol. The measurements were repeated three times. All the presented results are reported as the mean value of these three independent measurements (mean ± SD, $n = 3$). All the results are summarized in Table 2.

2.4. Wettability—Water Contact Angle. The tablets were made from each powder sample in a standard press for infrared spectroscopy tablets by the power of 80 kN for 20 seconds. Droplets (5 μL) of phosphate buffer (pH = 7.2) were used as the medium. The water contact angles were measured at 25°C by OCA20 (DataPhysics, Applied Photophysics, UK) using the sessile drop method. Sixteen values of the contact angle were measured and statistically evaluated. All the results are summarized in Table 2.

2.5. Zeta Potential. The zeta potential of the samples was obtained using Zetasizer Nano ZS (Malvern Instruments, UK) by means of electrophoretic light scattering. The zeta potential of the samples was measured in glass cuvettes with an inserted dip cell. The instrument detects the Doppler shift between the laser beam (5 mW, 633 nm) passing through the cuvette with the sample and the reference beam passing outside the cuvette. The data are evaluated using phase analysis light scattering. The samples were prepared by dissolving solid powder in phosphate buffer (pH = 7.2) to reach their final concentration 0.2 mg/mL. The measuring was carried out at laboratory temperature (25.0 ± 0.1°C). The measurements were repeated four times. All the presented results of the zeta potential of the samples are reported as the mean value of these four independent measurements (mean ± SD, $n = 4$). All the results are summarized in Table 2.

2.6. Particle Size Measurement. The particle/agglomerate size of samples was measured by means of a laser diffraction analyser HELOS/KR (SympaTec, Clausthal-Zellerfeld, Germany) using the combination of MIEE and Fraunhofer theory for calculation. The measured data were statistically calculated from the measurements by 3 types of objectives (range from 100 nm to 30 mm). The measurements were repeated five times. All the presented results of the particle size samples are reported as the mean value of these five independent measurements (mean ± SD, $n = 5$). All the results are summarized in Table 2.

2.7. Specific Surface Area. The values of specific surface area (SSA) were determined using a Quantachrome NOVA 2200 analyser (Quantachrome Instruments, Boynton Beach, FL, USA). The samples were degassed using vacuum under the temperature of 90°C for 3 h. The degassed samples were placed into the measuring chamber and evacuated under pressure around 1.33×10^{-6} MPa. The evacuated chamber was filled with pure nitrogen with partial pressure p/p_o varied from 0.03 to 0.5. The obtained data (from full absorption and desorption) were fitted by using Brunauer-Emmet-Teller isotherm [10] to determine specific surface values. The measurements were repeated three times. All the presented results of the SSA of the samples are reported as the mean value of these three independent measurements (mean ± SD, $n = 3$). All the results are summarized in Table 2.

Table 1: Dissolved amounts Q_n [%] of pure API and API from tablets. Q_n values are expressed as mean ± SD ($n = 6$ units). The means followed by different letters are significantly different at $P = 0.05$.

Sample	Dissolved amounts Q_n [%]					
	5 min	10 min	20 min	30 min	45 min	60 min
AS-1	28.5 ± 3.2^{a}	31.6 ± 4.0^{a}	37.8 ± 4.0^{a}	43.0 ± 4.3^{a}	48.2 ± 3.9^{a}	51.4 ± 4.0^{a}
AS-2	24.3 ± 3.9^{a}	28.2 ± 4.0^{a}	34.5 ± 4.8^{a}	40.1 ± 5.0^{a}	45.2 ± 6.1^{a}	48.4 ± 5.7^{a}
AS-3	41.7 ± 0.3^{c}	48.5 ± 0.4^{b}	55.8 ± 0.5^{b}	60.7 ± 0.5^{b}	65.7 ± 0.3^{c}	70.1 ± 0.4^{c}
AS-4	54.8 ± 0.4^{e}	57.9 ± 2.5^{c}	66.5 ± 2.7^{cd}	69.8 ± 1.5^{c}	75.2 ± 0.9^{d}	79.3 ± 1.3^{d}
AS-5	37.3 ± 0.3^{b}	49.3 ± 0.5^{b}	54.6 ± 2.3^{b}	58.5 ± 1.6^{b}	62.4 ± 1.1^{b}	66.6 ± 1.1^{b}
TS-1	49.3 ± 3.2^{d}	54.3 ± 2.1^{c}	63.4 ± 2.2^{c}	70.4 ± 2.3^{c}	73.7 ± 2.7^{d}	76.9 ± 2.0^{d}
TS-2	57.5 ± 1.2^{f}	62.9 ± 1.1^{d}	70.4 ± 1.2^{cd}	76.2 ± 1.4^{d}	83.0 ± 1.5^{e}	87.8 ± 1.9^{e}
TS-3	84.6 ± 1.9^{h}	96.4 ± 2.1^{e}	98.8 ± 2.2^{g}	99.7 ± 2.1^{f}	100.7 ± 2.4^{g}	101.4 ± 2.1^{g}
TS-4	86.2 ± 1.2^{h}	91.8 ± 0.9^{f}	95.4 ± 0.8^{f}	97.2 ± 0.8^{f}	98.8 ± 0.9^{g}	100.0 ± 0.8^{g}
TS-5	78.4 ± 1.7^{g}	87.4 ± 2.4^{e}	90.7 ± 2.1^{e}	93.1 ± 1.8^{e}	95.1 ± 1.8^{f}	96.3 ± 1.6^{f}

Table 2: Other determined characteristics of investigated samples of APIs AS-1–AS-5: water content [%], wettability (water contact angle θ [°]), zeta potential (ζ [mV]), particle size (x_{10}, x_{50}, x_{90} [μm]), and specific surface area (SSA [m^2/g]). Values are expressed as mean ± SD (see Section 2 for number of experiments for individual methodology). The means followed by different letters are significantly different at $P = 0.05$.

Sample	Water [%]	θ [°]	ζ [mV]	Particle size [μm]			SSA [m^2/g]
				x_{10}	x_{50}	x_{99}	
AS-1	0.18 ± 0.01^{c}	35.6 ± 1.7^{b}	-18.13 ± 1.94^{a}	0.51 ± 0.01^{a}	2.12 ± 0.01^{a}	8.57 ± 0.37^{a}	42.11 ± 0.03^{d}
AS-2	0.16 ± 0.01^{c}	34.9 ± 3.1^{b}	-17.98 ± 0.34^{a}	0.49 ± 0.01^{a}	2.18 ± 0.12^{b}	9.06 ± 0.39^{b}	59.65 ± 0.04^{e}
AS-3	0.13 ± 0.01^{b}	11.0 ± 6.6^{a}	-10.36 ± 0.40^{b}	0.74 ± 0.01^{b}	3.15 ± 0.08^{d}	13.36 ± 0.19^{d}	31.91 ± 0.04^{c}
AS-4	0.12 ± 0.01^{b}	35.2 ± 0.7^{b}	-2.64 ± 0.17^{c}	0.73 ± 0.06^{b}	2.36 ± 0.04^{c}	10.33 ± 0.14^{c}	23.21 ± 0.05^{b}
AS-5	0.08 ± 0.01^{a}	33.4 ± 2.7^{b}	-10.90 ± 0.37^{b}	1.02 ± 0.03^{c}	5.05 ± 0.05^{e}	15.97 ± 0.24^{e}	19.69 ± 0.06^{a}

2.8. Scanning Electron Microscopy. The morphologies of the samples were examined using a scanning electron microscope (SEM). The Au sputtering was applied to avoid unfavourable sample conductivity. The samples were analysed using the scanning electron microscope equipped with an EDX analyzer (Zeiss EVO LS10, Zeiss, Germany) and using accelerating voltage 10.0 kV, working distance 8.0 mm, and probe current 100 pA.

2.9. Statistical Analysis. All experiments were repeated and the data were expressed as means ± SD. The differences were evaluated by one-way analysis of the variance (ANOVA) completed with the Bonferroni's multicomparison test (ORIGIN PRO7). The differences (marked by different small letters) were considered significant at $P = 0.05$.

3. Results and Discussion

A new supplier provided two batches of API (AS-1 and AS-2) that gave noncomplying results of dissolution testing of the drug product, tablet sample, TS-1, and boundary results of dissolution testing of tablet sample TS-2. The results of these analyses were verified by comparison with the results of dissolution of tablet sample TS-3 that was manufactured under the same validated procedure as samples TS-1 and TS-2 from API sample AS-3 purchased from the previous supplier. Tablet sample TS-3 met all the criteria of the valid drug product specification. Based on these observation patterns, API batches AS-1, AS-2, and AS-3 were also tested for their dissolution profiles/dissolution rate and great differences were found; see Figure 1. The subsequent investigation of samples AS-1–AS-3 was started by determination of polymorphism by powder X-ray diffraction (PXRD). It can be stated that all evaluated API samples contained the same polymorph (diffractograms are not presented due to confidentiality reasons). Although both new samples AS-1 and AS-2 met the criteria of the API specification for the first time, the change of the quality of new API samples was found in the production of the drug formulation; the new samples showed considerable adhesiveness and electrostatic charge in comparison with the API from the previous supplier. In the light of the below discussed results it can be supposed that these properties are connected with particle size distribution. Additionally other parameters such as zeta potential, particle size, surface area, water content, and water contact angle of all three batches of the API (AS-1, AS-2, and AS-3) were tested. Based on the obtained preliminary results some recommendations were made for modification of API parameters. Subsequently two new batches of the API from the new supplier manufactured according to these criteria and the tablets produced from these APIs (AS-4/TS-4 and AS-5/TS-5) were subjected to all the above mentioned tests, and critical parameters were suggested. Although the total number of

samples was limited, some noteworthy relationships between the properties/parameters of APIs and their dissolution were found.

The comparison of dissolution profiles (dissolution amounts Q_n [%]) of individual samples is shown in Table 1 and illustrated in Figure 1. The dissolution testing of the API batches (AS-1–AS-5) and the tablets (TS-1–TS-5) was performed according to the valid specification in phosphate buffer (pH = 7.2). The same medium and concentration were used for determination of zeta potential and wetting (contact) angle; see below. It is evident that Q_n values of the pure API are significantly lower (see Figure 1(a)) than Q_n values of APIs from the tablets (see Figure 1(b)). This fact can be caused by the excipient (calcium stearate) that facilitates solubilisation of the API. Different behaviour of AS-1 and AS-2 in comparison with AS-3, AS-4, and AS-5 was observed. Both AS-1 and AS-2 stayed on the surface nonwetted, while the others sank and dissolved. From the data presented in Figures 1(a) and 1(b) it can be assumed that if the amount of the dissolved API achieved in the 10th minute (Q_{10}) approximately equals to 50%, the dissolution testing of the tablets will comply with the valid specification (Q = 75% of the stated amount after 45 min).

All the experimental results were compared by means of statistical analysis. The results of one-way analysis of the variance (ANOVA) completed with the results of the Bonferroni's multicomparison test are presented in Table 1, where differences were considered significant at $P = 0.05$. Significant differences between the Q_n values determined for samples AS-1/TS-1 and AS-2/TS-2 and complying samples AS-3/TS-3–AS-5/TS-5 were estimated.

From the slope of the curves of the graphs in Figures 1(a) and 1(b), that is, from the dissolution rate, it seems that the pure or formulated API is most rapidly dissolved by the 5th minute. Within subsequent 5 minutes the rate of dissolution decreased; nevertheless, it can be stated that in comparison with the following time interval (from the 10th to the 60th minute) the amount of the API dissolved within the first 10 minutes is the most important, especially for the formulation and for satisfactory results of dissolution testing. For this reason all the graphs presented below (Figures 2–4 and 6) illustrate the amount of the dissolved API in the 10th minute (Q_{10}). It is important to note that the dependence shown and discussed below is obviously valid also for dissolved amount Q_n in other measured time-intervals.

As mentioned above, API samples AS-1–AS-5 were evaluated for their water content, wettability, zeta potential, particle size, and specific surface area. Also the shapes of individual API samples were investigated by scanning electron microscope analysis. All these results are presented in Table 2 and illustrated in Figures 2–6.

The results of one-way analysis of the variance (ANOVA) completed with the results of the Bonferroni's multicomparison test are presented in Table 2, where differences were considered significant at $P = 0.05$. Significant differences between water content, zeta potential, particle sizes, and surface area for samples AS-1/TS-1 and AS-2/TS-2 and complying samples AS-3/TS-3–AS-5/TS-5 were determined. No statistical significance was found for samples AS-1, AS-2, AS-4, and AS-5 with regard to water contact angle.

The bilinear dependence of the Q_{10} values on water content in APIs is shown in Figure 2. It is evident that the Q_{10} values of APIs AS-1 and AS-2 that afforded noncomplying formulations TS-1 and TS-2 are low and represent remote points. The decreasing dependence in Figure 2(a) has correlation coefficient = −0.9140 ($n = 4$); the increasing dependence in Figure 2(b) has correlation coefficient $r = 0.9406$ ($n = 3$), and the decreasing dependence in Figure 2(b) has $r = -0.9772$ ($n = 3$). The optimum seems to be 0.12-0.13% of water. It can be stated that the samples with water content higher than 0.13% can stop complying in relation to dissolution testing. Unambiguously it can be found that the API with water content higher than 0.16% does not comply.

Wettability expressed as water contact angle (θ [°]) unfortunately did not provide the required information. From the results presented in Table 2 it is apparent that all the samples of APIs are wetted ($\theta < 90^\circ$ involves compounds with good wettability) [11]. All angles were up to 35°; AS-3 is a drug substance with excellent wettability that caused the API to absorb water too fast.

Generally, zeta potential is used for determination of stability of colloidal systems. A high zeta potential ($\zeta > \pm 30$ mV) is an indicative of the system stability (resistance to aggregation). When the potential is small (interval from 0 to ±30 mV), attractive forces may exceed this repulsion and the system tends to coagulate [12]. Nevertheless, as phosphate buffer with pH = 7.2 and the concentration of the API were chosen for the measurement of zeta potential to reflect real conditions at dissolution testing, and as the investigated compounds can be considered as zwitterions (tertiary amino and carboxyl moieties), it can be supposed that the value of pH = 7.2 is close to the point of zero charge. At this point, when the compounds have zero zeta potential, minimum stability, maximum solubility of the solid phase, and other peculiarities are demonstrated [13, 14]. The zeta potential values of boundary samples AS-1 and AS-2 ($\zeta \approx -18$ mV) are significantly different from those of complying samples AS-3, AS-4, and AS-5 ($\zeta \approx -3$ mV, $\zeta \approx -11$ mV); see Table 2, and it can be stated that the samples with zeta potential close to zero expressed significantly higher solubility. The dependence of the Q_{10} values of the samples on zeta potential is illustrated in Figure 3. The dependence of the dissolution of the pure API on the zeta potential seems to be linear-increasing (correlation coefficient $r = 0.9654$, $n = 5$) with the zeta potential close to 0 mV (see Figure 3(a)), while for the dissolution of the API from the tablets, a biphasic course was found (Figure 3(b)). Up to an optimum $\zeta \approx -11$ mV a linear increase of Q_{10} was observed ($r = 0.9774$, $n = 4$), and further increase in zeta potential did not affect significantly the dissolved amount. The different course of the dependence illustrated in Figures 3(a) and 3(b) can be explained by the influence of excipients on the API. Based on the data it can be concluded that the more different the values of zeta potential are from zero, the less soluble the substances are. Despite the limited number of the samples, the values of zeta potential ranged from 0 to −11 mV can be considered as advisable for good solubility.

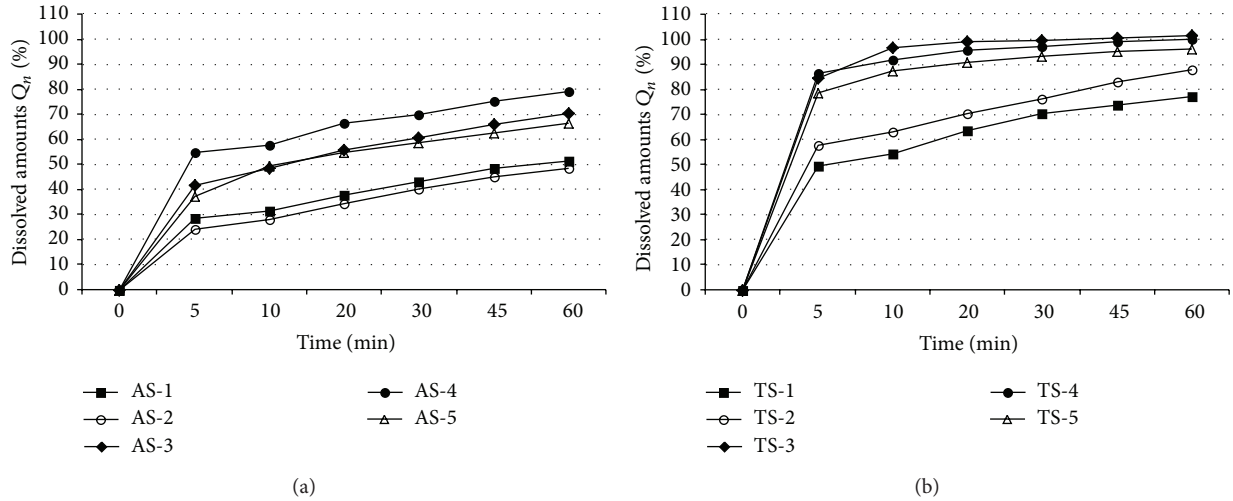

Figure 1: Dissolution profiles (dissolved amounts Q_n [%]) of individual API samples AS-1–AS-5 (a) and individual tablets TS-1–TS-5 (b). Q_n values are expressed as mean ± SD (n = 6 units). SDs are not illustrated to improve visualisation.

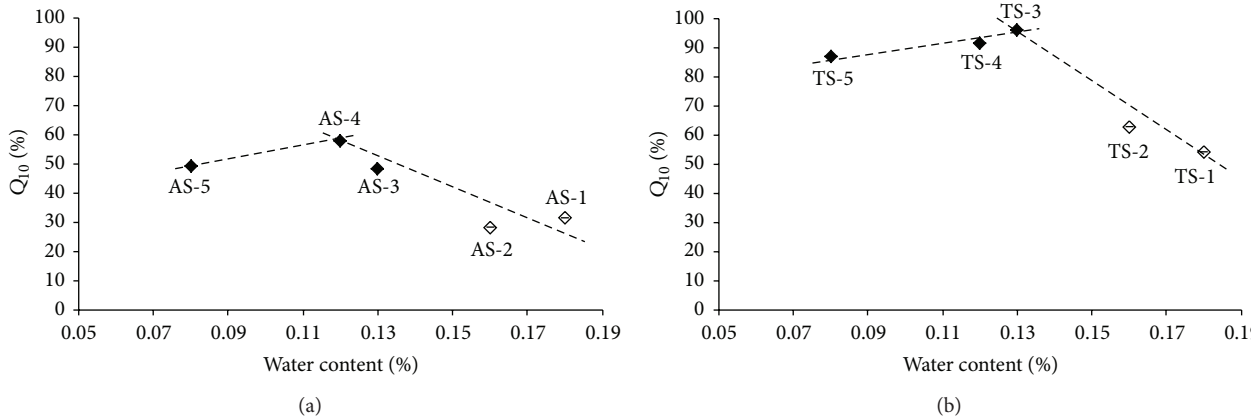

Figure 2: Dependence of dissolved amounts Q_{10} [%] of individual API samples AS-1–AS-5 (a) and individual tablets TS-1–TS-5 (b) in the 10th minute on water content [%]. Samples with boundary values AS-1, AS-2, TS-1, and TS-2 are marked by empty symbols. The data represent the mean ± SD of three samples.

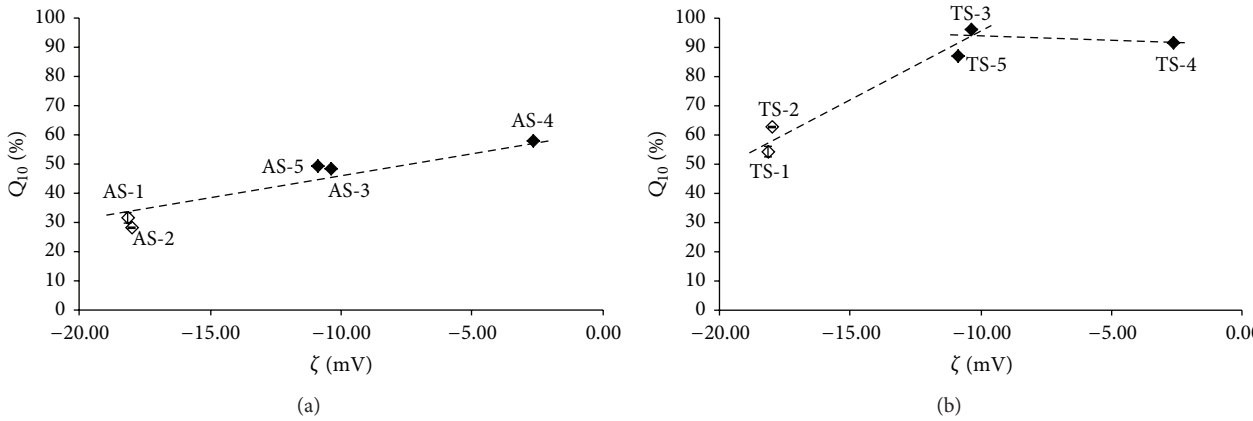

Figure 3: Dependence of dissolved amounts Q_{10} [%] of individual API samples AS-1–AS-5 (a) and individual tablets TS-1–TS-5 (b) in the 10th minute on zeta potential values (ζ [mV]). Samples with boundary values AS-1, AS-2, TS-1, and TS-2 are marked by empty symbols. The data represent the mean ± SD of four samples.

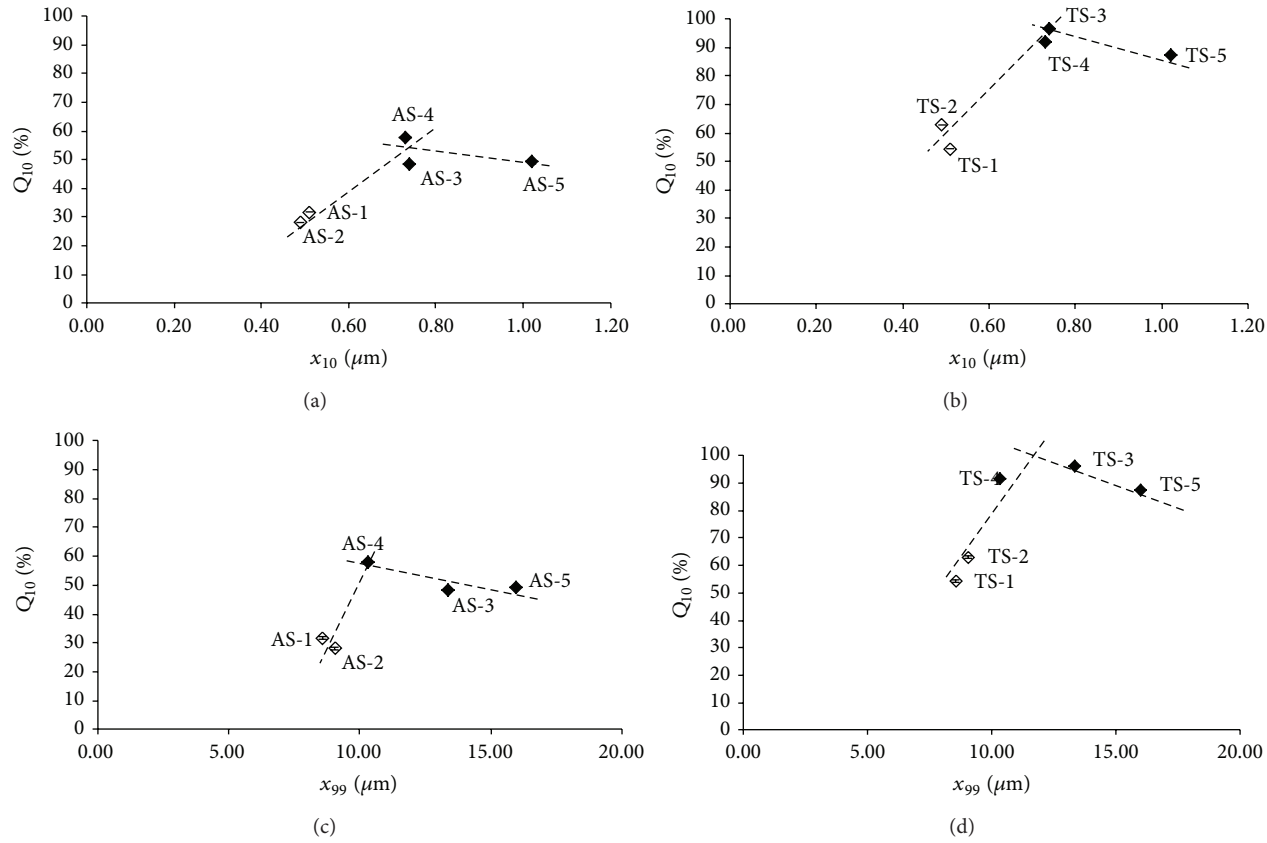

Figure 4: Dependence of dissolved amounts Q_{10} [%] of individual API samples AS-1–AS-5 ((a), (c)) and individual tablets TS-1–TS-5 ((b), (d)) in the 10th minute on particle size (x_{10} and x_{99} [μm]). Samples with boundary values AS-1, AS-2, TS-1, and TS-2 are marked by empty symbols. The data represent the mean ± SD of five samples.

Figure 4 shows the dependence of the Q_{10} values of the individual API samples (Figures 4(a) and 4(c)) or the dissolved API released from individual tablets (Figures 4(b) and 4(d)) on particle size. The terminal particle sizes x_{10} and x_{99} were chosen for highlighting this dependence. Bilinear curves can be observed for the dependence of dissolution on particle size with an optimum of particle size $x_{10} \approx 0.74\ \mu$m and $x_{99} \approx 10$–$13\ \mu$m. It is possible to see that the total increase of particle size distribution profile of the substance causes less significant effect on the amount of the dissolved compound than a particle size reduction, especially in Figures 4(b) and 4(d) illustrating the dissolution of the API from the tablets (compare samples 1, 2, and 5). Although reduced particle size aids the formulation of poorly water soluble APIs [15], in this case, a large share of small particles results in a significant decrease of dissolution and probably also causes processability difficulties as mentioned above. The significant decrease of the dissolved API with a large share of small particles can be also related to particle surface area; see below. Based on the results listed in Table 2 and illustrated in Figure 4, it can be stated that particle size limits should be 0.8–1.0 μm for x_{10}, 2.4–5.1 μm for x_{50}, and 11–16 μm for x_{99}.

The investigation of particle size distribution is closely connected with shape analysis of the particles. The SEM analysis of all the API samples supported the results of particle size distribution analysis. The microphotographs of samples AS-1, AS-3, and AS-5 with 500x magnification are presented in Figure 5. The general shape of all particles can be considered as tabular or laths. The laths of AS-1 and AS-2 are very fine, those of AS-4 are medium, and those of AS-3 and AS-5 are coarse.

The specific surface area (SSA) is often correlated with the rates of dissolution. The SSA is increased with decreasing particle size and with increasing porosity of the particles. The generation of porosity, especially in the case of small pores, can produce SSA far in excess of that produced by particle size reduction. The SSA influences processing and behaviour of powders and porous solids, since the surface area corresponds to the roughness of the particle exterior and its porous interior [16, 17]. One of the possibilities to measure SSA is using the BET approach [10]. The dependence of the Q_{10} values of the individual samples of the API or the API released from the tablets on the SSA (porosity) expressed as SSA values [m^2/g] is illustrated in Figure 6. Both boundary APIs 1 and 2 (samples AS-1/TS-1 and AS-2/TS-2) represent the remote points in Figures 6(a) and 6(b), where bilinear courses can be found again; the correlation coefficient of the decreasing part of the course in Figure 6(a) is $r = -0.9299$

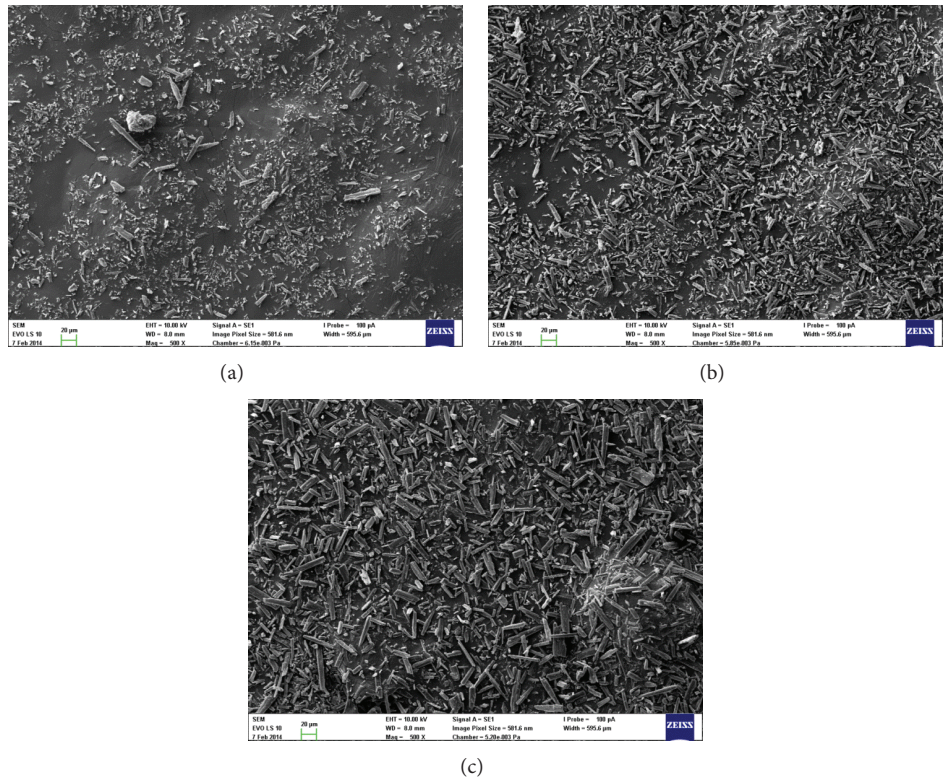

(a) (b)

(c)

Figure 5: SEM microphotographs of noncomplying sample AS-1 (a) and complying samples AS-3 (b) and AS-5 (c).

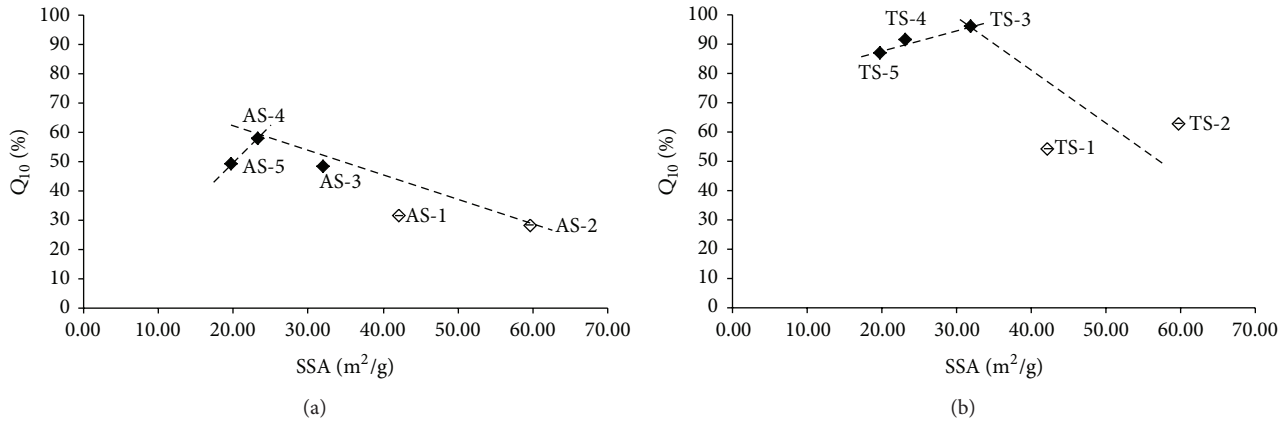

(a) (b)

Figure 6: Dependence of dissolved amounts Q_{10} [%] of individual API samples AS-1–AS-5 (a) and individual tablets TS-1–TS-5 (b) in the 10th minute on SSA [m^2/g]. Samples with boundary values AS-1, AS-2, TS-1, and TS-2 are marked by empty symbols. The data represent the mean ± SD of three samples.

($n = 4$) and the increasing part of the course in Figure 6(b) is = 0.9742($n = 3$). According to the results SSA ≈ 23 m^2/g (AS-4) is preferable for the dissolution of pure API, while SSA ≈ 32 m^2/g (AS-3) is favoured for the dissolution of the drug formulation. As mentioned above, a slight change of the dissolution rate/amount of the pure API in comparison with the formulated API is caused by an excipient. Apparently for both cases it can be summarized that for satisfactory dissolution testing the specific surface area should be in the range 20–32 m^2/g. An increase of the surface area (porosity) leads to a rapid decrease of dissolution.

Similar results can be found for some drugs, particularly for those that are lipophilic in nature, where particle size reduction can result in aggregation of the material. This causes a consequent reduction in the effective surface area of the drugs exposed to liquids and hence a reduction in their

dissolution rate. For example, acetylsalicylic acid, phenacetin, or phenobarbital is prone to aggregation in particle size reduction. Thus, although a particle size reduction and an increase of the surface area are recommended to increase the dissolution rate of drugs in general, for some APIs, the improvement of solubility by particle size reduction/increase of the surface area ceases when the particle size reaches a particular value. Hence, the particle size is critical and beyond a particular value the solubility of solid substances decreases. It can be stated that such changes can arise because of the presence of an electrical charge on the particle, which is predominant in small particles [17–20]. Based on the above-mentioned facts zeta potential and particle size were evaluated as critical for satisfactory dissolution.

4. Conclusions

A change of the supplier of the API for an older medicament led to noncomplying results of the dissolution test (samples TS-1 and TS-2). Firstly a sample of the API from the original supplier (AP-3) and two different samples of the API from the new supplier (AS-1 and AS-2) were analysed in detail. The sample of the API from the original supplier and its final peroral dosage form were used as standards (AP-3 and TS-3), and based on the parameters of this API (sample AS-3) some criteria were advised. The results of analytical evaluation of other two samples/batches of the APIs (AS-4 and AS-5) and the tablets manufactured therefrom (samples TS-4 and TS-5) confirmed the presumptions and led to the following recommendations. Based on the performed analytical testing, finding and interpretation of relationships between the amount of soluble pure API/API released from the tablets and the determined physicochemical parameters, particle size, surface area, zeta potential and, perhaps, water content can be considered as critical parameters affecting the dissolution rate of the final product. It can be summarized that for satisfactory dissolution test of the final product the specification of the API should be modified and completed as follows. Zeta potential should be in the range from 0 to −11 mV, particle size limits should be $x_{10} > 0.80\,\mu$m and $x_{99} < 13\,\mu$m, specific surface area (BET) should be in the range 19–32 m^2/g, and the water content in the API should not be higher than 0.13%, provided that similar instrumentation and the same experimental conditions of measurement are chosen.

Conflict of Interests

The authors declare that there is no conflict of interests regarding the publication of this paper.

Acknowledgments

This study was supported by the Czech Science Foundation-GACR P304/11/2246 and the Materials Research Centre, at FCH BUT-Sustainability and Development, REG LO1211, with financial support from National Program for Sustainability I (Ministry of Education, Youth, and Sports). The authors also gratefully acknowledge the funding from the Project "Excellent teams no. CZ.1.07/2.3.00/30.0005."

References

[1] *Pharmaceutical Quality for the 21st Century—A Risk based Approach*, Food and Drug Administration, 2007.

[2] "Guidance for industry: PAT—A framework for innovative pharmaceutical development, manufacturing and quality assurance," Food and Drug Administration, 2004.

[3] L. X. Yu, "Pharmaceutical quality by design: product and process development, understanding, and control," *Pharmaceutical Research*, vol. 25, no. 4, pp. 781–791, 2008.

[4] "ICH Guideline Q8(R2)—Pharmaceutical development," in *Proceedings of the International Conference on Harmonisation of Technical Requirements for Registration of Pharmaceuticals for Human Use*, 2009.

[5] "ICH Guideline Q9—Quality risk management," in *Proceedings of the International Conference on Harmonisation of Technical Requirements for Registration of Pharmaceuticals for Human Use*, 2005.

[6] "ICH guideline Q10—Pharmaceutical quality system," in *Proceedings of the International Conference on Harmonisation of Technical Requirements for Registration of Pharmaceuticals for Human Use*, 2008.

[7] "ICH Guideline Q11—Development and manufacture of drug substances (chemical entities and biotechnological/biological entities)," in *Proceedings of the International Conference on Harmonisation of Technical Requirements for Registration of Pharmaceuticals for Human Use*, 2012.

[8] R. K. Varu and A. Khanna, "Opportunities and challenges to implementing Quality by Design approach in generic drug development," *Journal of Generic Medicines*, vol. 7, no. 1, pp. 60–73, 2010.

[9] P. J. Purohit and K. V. Shah, "Quality by design (QbD): new parameter for quality improvement & pharmaceutical drug development," *Pharma Science Monitor*, vol. 4, pp. 1–19, 2013.

[10] S. Brunauer, P. H. Emmett, and E. Teller, "Adsorption of gases in multimolecular layers," *Journal of the American Chemical Society*, vol. 60, no. 2, pp. 309–319, 1938.

[11] Y. Yuan and T. R. Lee, "Contact angle and wetting properties," in *Surface Science Techniques*, G. Bracco and B. Holst, Eds., vol. 51 of *Springer Series in Surface Sciences*, pp. 3–34, Springer, Berlin, Germany, 2013.

[12] W. B. Russel, D. A. Saville, and W. R. Schowalter, *Colloidal Dispersions*, Cambridge University Press, Cambridge, UK, 1989.

[13] J. Lyklema, *Fundamentals of Interface and Colloid Science*, vol. 2 of *Solid-Liquid Interface*, Academic Press, London, UK, 1995.

[14] A. Salis, M. Boström, L. Medda et al., "Measurements and theoretical interpretation of points of zero charge/potential of BSA protein," *Langmuir*, vol. 27, no. 18, pp. 11597–11604, 2011.

[15] K. R. Chu, E. Lee, S. H. Jeong, and E.-S. Park, "Effect of particle size on the dissolution behaviors of poorly water-soluble drugs," *Archives of Pharmacal Research*, vol. 35, no. 7, pp. 1187–1195, 2012.

[16] D. S. Phadke and J. L. Eichorst, "Evaluation of particle size distribution and specific surface area of magnesium stearate," *Drug Development and Industrial Pharmacy*, vol. 17, no. 6, pp. 901–906, 1991.

[17] M. E. Aulton and K. Taylor, *Aulton's Pharmaceutics: The Design and Manufacture of Medicines*, Churchill Livingstone/Elsevier, London, UK, 4th edition, 2013.

[18] P. Finholt, "Influence of formulation on dissolution rate," in *Dissolution Technology*, L. J. Leeson and T. J. Catensen, Eds., p. 108, APHA, Washington, DC, USA, 1974.

[19] A. L. Behera, S. K. Sahoo, and S. V. Patil, "Enhancement of solubility: a pharmaceutical overview," *Der Pharmacia Lettre*, vol. 2, pp. 310–318, 2010.

[20] L. V. Allen and H. C. Ansel, *Ansel's Pharmaceutical Dosage Forms and Drug Delivery Systems*, Kluwer Academic Publishers, Baltimor, Md, USA, 10th edition, 2013.

Hindawi Publishing Corporation
BioMed Research International
Volume 2014, Article ID 179568, 9 pages
http://dx.doi.org/10.1155/2014/179568

Research Article

Evaluation of the Influence of Formulation and Process Variables on Mechanical Properties of Oral Mucoadhesive Films Using Multivariate Data Analysis

Hana Landová,[1] David Vetchý,[1] Jan Gajdziok,[1] Petr Doležel,[1] Jan Muselík,[1] Kateřina Dvořáčková,[1] Vladimír Jekl,[2] Karel Hauptman,[2] and Zdeněk Knotek[2]

[1] *Department of Pharmaceutics, Faculty of Pharmacy, University of Veterinary and Pharmaceutical Sciences Brno, Palackého třída 1/3, 612 42 Brno, Czech Republic*
[2] *Avian and Exotic Animal Clinic, Faculty of Veterinary Medicine, University of Veterinary and Pharmaceutical Sciences Brno, Palackého třída 1/3, 612 42 Brno, Czech Republic*

Correspondence should be addressed to David Vetchý; vetchy@email.cz

Received 18 June 2014; Accepted 6 July 2014; Published 23 July 2014

Academic Editor: Josef Jampilek

Oral mucosa is an attractive region for the local and systemic application of many drugs. Oral mucoadhesive films are preferred for their prolonged time of residence, the improved bioavailability of the drug they contain, their painless application, their protection against lesions, and their nonirritating properties. This work was focused on preparation of nonmedicated carmellose-based films using both solvent casting and impregnation methods, respectively. Moreover, a modern approach to evaluation of mucoadhesive films applying analysis of texture and subsequent multivariate data analysis was used. In this experiment, puncture strength strongly correlated with tensile strength and could be used to obtain necessary information about the mechanical film characteristics in films prepared using both methods. Puncture work and tensile work were not correlated in films prepared using the solvent casting method, as increasing the amount of glycerol led to an increase in the puncture work in thinner films. All measured texture parameters in films prepared by impregnation were significantly smaller compared to films prepared by solvent casting. Moreover, a relationship between the amount of glycerol and film thickness was observed, and a greater recalculated tensile/puncture strength was needed for an increased thickness in films prepared by impregnation.

1. Introduction

The oral cavity and its mucosa represent an attractive region for local and systemic applications of many active pharmaceutical ingredients. Direct absorption of drugs through the oral mucosa into systemic circulation circumvents undesirable hepatic metabolism (first-pass effect) and leads to higher bioavailability and faster onset of the action [1]. The lower enzymatic activity in the oral cavity compared to further parts of gastrointestinal tract limits the possibility of drug degradation, thus presenting yet another advantage [2].

The wide range of innovative dosage forms based on mucoadhesive polymers [3] for application to oral mucosa could be an attractive alternative to conventional dosage forms (oral rinses, gels, and pastes) for a number of reasons, such as extended residence time at the application site leading to prolonged therapeutic effect, easy manipulation, painless application, and possibility of preparation removal in the case of adverse drug effect [4]. Mucoadhesive oral films (MOFs) are preferred over mucoadhesive tablets because they are thin and flexible, which reduces uncomfortable feelings during normal activities such as eating, drinking, and speaking. Moreover, they can play the role of lesion dressings, which could minimize further irritation and reduce pain at the site of application [5].

MOFs as an innovative rapidly developed dosage form, recently also listed in *European Pharmacopoeia*, can be formulated for the application of a wide range of drugs

for local or systemic therapy. Investigated mucoadhesive delivery systems for local action include, for example, antiseptics (chlorhexidine, cetylpyridinium chloride), antibiotics (ciprofloxacin, ofloxacin, and tetracycline), antifungal drugs (miconazole, nystatin, and clotrimazole), local anaesthetics (lidocaine, tetracaine), and other drugs for treatment of oral diseases such as recurrent aphthous stomatitis and others [6, 7]. Numerous drugs were investigated as possible active ingredients for oral mucoadhesive films with systemic action. These include peptidic hormones degradable in lower parts of the gastrointestinal tract (insulin, calcitonin, and oxytocin), antihypertensive drugs (metoprolol, carvedilol, nifedipine, and losartan), analgetics (particularly opioid drugs as buprenorphine or fentanyl—registered buccal films Onsolis and Breakyl), or drugs used for the treatment of asthma (salbutamol, terbutaline), diabetes (glipizide, glibenclamide), and other diseases [7].

The most widely used technology for the formulation of oral mucoadhesive films is the *solvent casting method* using homogenous dispersions of active ingredients and excipients. These liquid mixtures are poured into the casting moulds and the solvent is evaporated. Problems that may occur when employing this technology include inadequate rheological properties of the solution or suspension (high viscosity may affect dosing accuracy), entrapped air bubbles, insufficient content uniformity, and residual solvents presented in the final dosage form [2].

The second technology used for preparing MOFs is *hot-melt extrusion*, widely used in plastics and metal processing and the food industry. This method of MOF preparation was optimized by Repka et al. [8]. The principle of this method is controlled extrusion of the molten raw material through an orifice (the die) onto rolls which form the final homogenous sheets of film [9]. The described technology has many advantages in comparison with the solvent casting method, such as greater time effectiveness due to shorter processing time, no need of solvents (and therefore no solvent residues in the final dosage form), high stability of prepared films, and improved solubility and bioavailability of poorly soluble drugs. The relevant disadvantage is the requirement of thermal stability in all materials, moisture free components, limited and expensive excipients, and the requirement of specialized equipment [10]. Alternative methods for manufacturing MOFs consist of compressing or freeze-drying polymer powders and mixtures or printing active pharmaceutical ingredients onto a base film layer [11, 12].

A frequently discussed topic connected to MOFs is their evaluation, as authorized methods for testing this innovative medical form have still not been defined. *European Pharmacopoeia* describes only a dissolution test [13]. Authorised and justified methods for solid dosage forms (tablets, capsules, etc.) are usually unsuitable, cannot be used, or provide results which are irrelevant in the context of MOFs. Methods used to evaluate therapeutic transdermal systems seem to be suitable, but they must be significantly modified and special equipment is needed, for example, a modified physical balance for measuring mucoadhesive strength [14].

One suitable solution could be found in the innovative and sophisticated use of a texture analyzer, a special device widely used in the food and cosmetic industry, which has recently been also introduced into the pharmaceutical industry for evaluation of several dosage forms (tablets, semisolid preparations) and packaging (extrusion of ointment from the tube, etc.) [15, 16].

The texture (relations in the internal structure) of MOFs significantly affects their physicomechanical (strength, elasticity, durability, etc.) as well as mucoadhesive properties (residence time, water uptake, mucoadhesive strength, etc.), which together form the basis of dosage form with nonproblematic application, prolonged residence time, nonirritating properties, and easy handling and packaging, resulting in better patient compliance and higher therapy effectiveness.

For this reason, one of the modern trends in the evaluation of MOFs' properties could become the seeking of mutual relations between their texture and other *in vitro* or *in vivo* properties using multivariate data analysis.

There are two basic tests suitable for evaluation of films' durability against tension and compression using texture analyzer. The tensile strength represents the stress needed to stretch the film until it tears. For this assessment, a texture analyzer equipped with a special probe with two clamps is used. The influence of the cross-sectional area of the sample and the speed of upper clamp movement are recorded. The amount of the sample's deformation, in this case, namely, elongation, depends on the type and content of mucoadhesive polymer, the drug, and the amount of plasticizer [17]. Tear resistance and porosity, which also affect the mechanical resistance, depend upon the nature, type, and content of the polymer. It was observed that tear resistance increases with polymer concentration [18]. Using a texture analyzer with cylindrical probes, the puncture test can measure the resistance of the film against puncture. The area under the curve and the maximum stress or strength required to rupture the film determine its toughness [14].

The aim of the presented research was to analyze the texture of MOFs and then evaluate the influence of formulation and process variables on mechanical properties of prepared mucoadhesive films using multivariate data analysis. Until now, the number of known general dependencies related to tensile strength is limited. The presented research evaluates also the mechanical resistance of the films against puncture which is not usually published in scientific literature [19]. Moreover, the new modification of solvent casting method, the method of impregnation first described by Vetchý et al. [12], was used, evaluated, and compared to unmodified solvent casting method. The presented research illustrates the advantages of this innovative approach for evaluating oral mucoadhesive films' properties.

2. Material and Methods

2.1. Materials. Carmellose sodium (NaCMC), type Blanose 7LF Pharm, donated by Ashland Specialty Ingredients (Wilmington, USA) was used (in the form of water dispersion) as the basic mucoadhesive and film-forming polymer.

Table 1: Formulations of mucoadhesive films.

Sample	NaCMC	Glycerol	Textile	Water	Casted amount
A1	2%	1%	No	97%	18 mL
A2	2%	1.5%	No	96.5%	18 mL
A3	2%	2%	No	96%	18 mL
A4	2%	2.5%	No	95.5%	18 mL
A5	2%	3%	No	95%	18 mL
B1	2%	1%	No	97%	27 mL
B2	2%	1.5%	No	96.5%	27 mL
B3	2%	2%	No	96%	27 mL
B4	2%	2.5%	No	95.5%	27 mL
B5	2%	3%	No	95%	27 mL
C1	2%	1%	Yes	97%	up to 18 mL*
C2	2%	1.5%	Yes	96.5%	up to 18 mL*
C3	2%	2%	Yes	96%	up to 18 mL*
C4	2%	2.5%	Yes	95.5%	up to 18 mL*
C5	2%	3%	Yes	95%	up to 18 mL*
D1	2%	1%	Yes	97%	up to 27 mL*
D2	2%	1.5%	Yes	96.5%	up to 27 mL*
D3	2%	2%	Yes	96%	up to 27 mL*
D4	2%	2.5%	Yes	95.5%	up to 27 mL*
D5	2%	3%	Yes	95%	up to 27 mL*

*The textile was impregnated with an amount of prepared dispersion to ensure the weight of resulting films corresponded to films prepared using the solvent casting method.

Moreover for the method of impregnation, an acid form of carmellose in the form of nonwoven textile (Hcel HT) donated by Holzbecher Medical (Pardubice, CZ) was incorporated into the structure of the MOFs. Glycerol purchased from Dr. Kulich Pharma (Hradec Králové, CZ) was used as a plasticizer. All the other chemicals used in this experiment were of analytical grade.

2.2. Methods of Film Preparation. 20 samples of mucoadhesive oral films with different concentrations of plasticizer (1–3%) were prepared using two different methods (Table 1). One-half of the samples were prepared by the standard solvent casting method and the second half using the innovative impregnation method. After drying, two different shapes of samples (25 × 25 mm and 10 × 40 mm) were punched from the prepared films for the testing of physicomechanical properties.

2.2.1. Solvent Casting Method (Sample Series A and B). Using an automatic pipette 18 mL (series A) or 27 mL (series B) in length, prepared uniform carmellose dispersions were cast into a round plastic mold (diameter 63 mm) and the solvent was left to evaporate at 30°C for 72 hours.

2.2.2. Impregnation Method. Nonwoven carmellose textile was cut into circles 63 mm in diameter and placed into the casting molds. The textile was impregnated with an amount of prepared dispersion to ensure the weight of resulting films corresponded to films prepared using the solvent casting method (i.e., up to 18 mL in series C and up to 27 mL in series D). The solvent was similarly left to evaporate at 30°C for 72 hours.

2.3. Testing Methods. A modified method according to Shidhaye was used to evaluate the mechanical properties of the prepared films [20]. A Texture Analyzer CT3 (Brookfield, USA) equipped with a 4.5 kg load cell and TexturePro CT software was used to determine the tensile strength (ten. strength) of the prepared films. Rectangular samples (10 × 40 mm) were held between two clamps of probe TA-DGA positioned at a distance of 2 cm. The lower clamp was held stationary and the strips of MOF were stretched by the upper clamp moving at a rate of 0.5 mm/sec until the strip tore. The tensile work done during this process (ten. work) and the tensile deformation/elongation of the film at the moment of tearing (ten. def.) were also measured. The measurement was repeated three times for each film sample.

The texture analyzer with probe TA39 (a cylindrical probe with a diameter of 2 mm; probe motion speed 0.5 mm/sec) was used for the puncture test. The force needed to puncture square samples (25 × 25 mm) fixed in jig TA-CJ (puncture strength or pun. strength), the work done during this process (puncture work or pun. work), and the deformation of the film at the moment of puncture (puncture deformation or pun. def.) were measured. The measurement was repeated three times for each film sample.

Since the films were prepared in different ways (solvent casting method or impregnation method) and had different thicknesses, values measured by the texture analyzer were recalculated for a film thickness of 100 μm for better comparison.

Table 2: Mechanical properties of mucoadhesive films.

Sample	Tensile testing			Puncture testing			Thickness (mm)
	Strength* (N)	Work* (mJ)	Deformation* (mm)	Strength* (N)	Work* (mJ)	Deformation* (mm)	
A1	26.55 ± 1.74	149.67 ± 31.31	9.18 ± 2.02	19.35 ± 0.86	22.55 ± 0.68	3.35 ± 0.07	83.76 ± 10.02
A2	18.54 ± 3.10	177.97 ± 29.62	14.27 ± 1.01	13.87 ± 1.08	20.20 ± 2.09	3.48 ± 0.11	101.69 ± 4.13
A3	14.07 ± 1.75	154.84 ± 24.40	19.77 ± 1.35	11.17 ± 2.31	23.29 ± 7.57	4.94 ± 0.71	109.90 ± 2.12
A4	7.43 ± 1.80	87.42 ± 11.11	35.56 ± 8.56	9.71 ± 2.89	34.64 ± 9.95	11.68 ± 0.36	83.84 ± 1.58
A5	4.06 ± 0.76	78.45 ± 22.73	35.78 ± 3.41	6.74 ± 0.95	24.53 ± 2.19	9.91 ± 0.34	112.05 ± 5.87
B1	20.77 ± 1.41	226.06 ± 11.19	6.50 ± 0.47	14.15 ± 1.79	18.33 ± 2.56	2.18 ± 0.20	145.70 ± 6.56
B2	15.86 ± 2.16	148.26 ± 42.46	12.04 ± 0.73	9.95 ± 1.38	21.39 ± 4.40	3.50 ± 0.22	156.18 ± 13.37
B3	5.94 ± 0.60	110.21 ± 11.47	21.02 ± 1.27	6.54 ± 1.36	21.57 ± 4.22	4.42 ± 0.07	205.13 ± 17.12
B4	5.83 ± 0.59	66.09 ± 1.83	24.71 ± 0.00	2.38 ± 0.30	12.05 ± 1.00	4.56 ± 0.17	250.85 ± 26.00
B5	0.82 ± 0.11	30.49 ± 4.56	20.89 ± 0.01	1.06 ± 0.11	6.97 ± 0.33	3.42 ± 0.14	296.64 ± 24.03
C1	10.45 ± 0.53	19.30 ± 5.16	0.96 ± 0.14	4.28 ± 0.45	3.35 ± 0.92	0.65 ± 0.08	268.17 ± 46.09
C2	7.69 ± 0.72	17.07 ± 3.32	1.22 ± 0.15	3.86 ± 0.52	4.28 ± 0.56	1.06 ± 0.03	221.46 ± 27.28
C3	5.29 ± 0.23	19.24 ± 3.85	1.18 ± 0.06	3.00 ± 0.12	3.75 ± 0.48	1.04 ± 0.04	246.93 ± 36.82
C4	4.59 ± 0.28	16.92 ± 4.28	1.41 ± 0.04	2.84 ± 0.41	3.93 ± 0.41	1.12 ± 0.07	217.33 ± 28.71
C5	3.39 ± 0.17	14.99 ± 1.69	1.10 ± 0.03	1.87 ± 0.25	3.09 ± 0.42	0.96 ± 0.04	257.23 ± 26.41
D1	17.96 ± 0.40	34.05 ± 2.33	1.22 ± 0.08	7.98 ± 0.59	5.74 ± 0.84	0.71 ± 0.05	220.00 ± 21.09
D2	12.07 ± 0.12	33.07 ± 2.86	1.31 ± 0.08	5.86 ± 0.57	5.68 ± 0.82	0.81 ± 0.06	266.97 ± 12.08
D3	7.65 ± 0.05	26.21 ± 6.85	1.30 ± 0.16	4.42 ± 0.56	4.82 ± 0.30	0.80 ± 0.07	302.97 ± 6.13
D4	4.36 ± 0.27	23.14 ± 4.04	1.25 ± 0.14	2.82 ± 0.55	4.20 ± 0.69	0.89 ± 0.09	315.90 ± 5.75
D5	3.71 ± 0.30	18.87 ± 4.92	1.13 ± 0.05	1.92 ± 0.12	2.97 ± 0.24	0.79 ± 0.11	322.70 ± 23.51

*Recalculated for 100 μm film thickness.

Film thickness was measured by microscopic analysis, using an optical microscope (STM-902 ZOOM, Opting, CZ) and NIS Elements software. A rectangular sample was vertically fixed in a holder, the microscope was focused on the edge of the film, and its thickness was measured at 5 places throughout the film. This was repeated 3 times for each film sample.

2.4. Methods of Data Analysis. The experiment was designed as a full factorial composed of 3 variables (glycerol; film thickness; nonwoven textile), where glycerol was used in 5 levels (1%; 1.5%; 2%; 2.5%; 3%), film thickness in 2 levels (18 mL, 27 mL), and nonwoven textile in 2 levels (presence—yes; absence—no). Data were initially checked using descriptive statistics. Subsequently, exploratory evaluation of data using PCA was carried out in order to study systematic variability in the data, relationships among variables and objects, and their correlations and to detect outliers. Prior to modeling, the variables were adjusted by autoscaling, that is, mean centering and scaling by standard deviation. MLR regression together with ANOVA was used to identify important variables and quantitative expression of their effect. Analysis was performed using the program Unscrambler X, v 1.3 (Camo software).

3. Results and Discussion

The results are summarized in Table 2.

The full data set of obtained results was analyzed using principal component analysis (PCA) models in order to describe the systematic variability. PCA is one of the oldest and most widely used methods to study dependencies in multivariate data set containing multiple variables and objects. Correlations of the original variables are evaluated on the basis of a smaller number of latent variables, the so-called principal component (PC), which represent a part of total variability. Their advantage is that they are independent (orthogonal), which greatly simplifies interpretation.

The PCA biplot (Figure 1) shows the variability of objects and variables in the area of the first two components. A presence/absence of nonwoven textile is shown by the formation of two groups along the components of PC-1. The effect of the amount of glycerol used is described along the components of PC-2. The first two components describe 92% of explained variance. With regard to the data structure, further PCA models were calculated separately for the data group with and without a nonwoven textile.

A PCA model was constructed for data of films without a nonwoven textile. A systematic distribution of objects along the PC-1 depending on the content of glycerol in the films is shown in the scores plot (Figure 2(a)). The data distribution of the films with higher concentrations of glycerol (2.5%, 3%) is divided into two branches along the PC-2 component, which can be assigned to the variable pun. work. The correlation loadings plot (Figure 2(b)) together with the scores

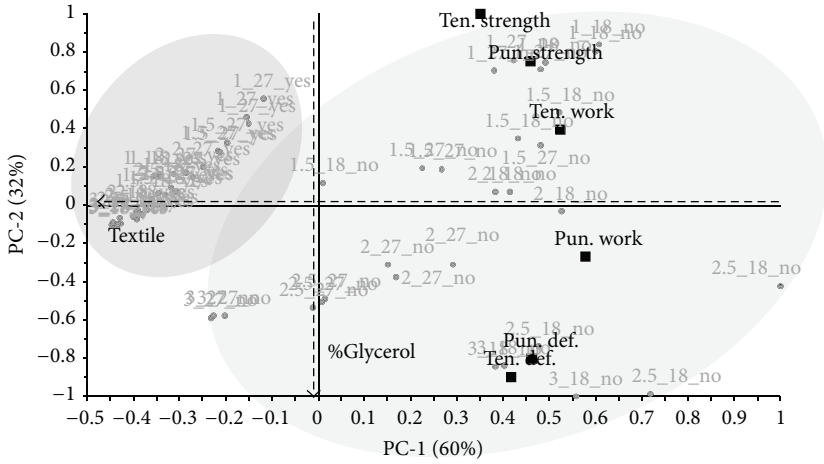

Figure 1: PCA biplot in Figure 1 shows the distribution of objects (circles) and variables (boxes) in the area of the first two components. Objects are labeled according to design parameters: %(glycerol)_ml(casted amount)_yes or no(non-woven textile). Groups with and without nonwoven textile are highlighted.

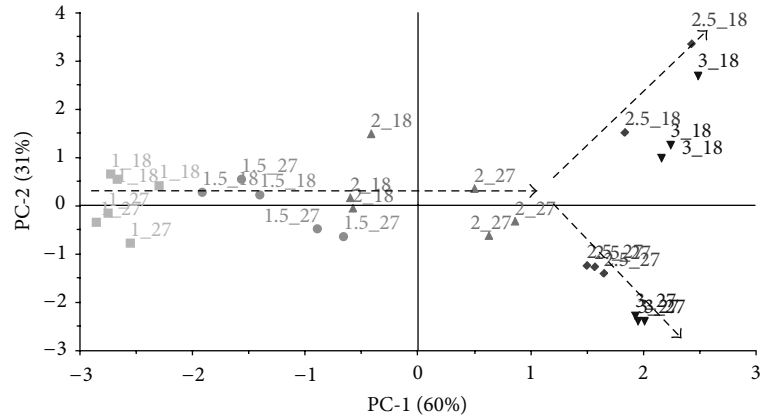

(a)

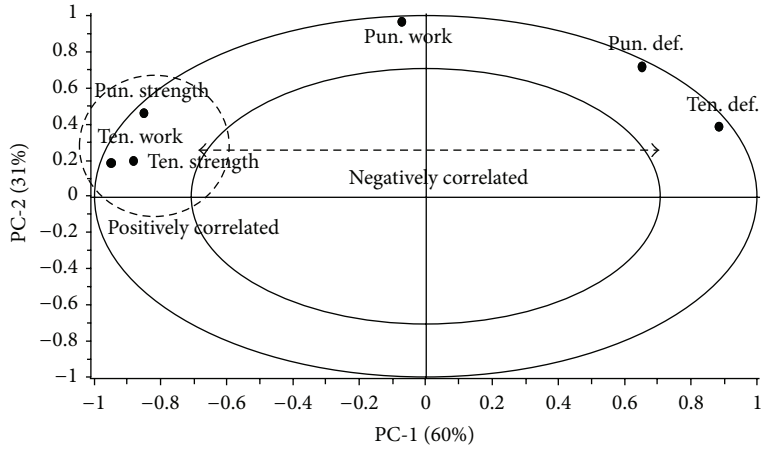

(b)

Figure 2: PCA; (a) scores plot; (b) correlation loadings plot, data of films without a nonwoven textile, positive correlation marked with a circle, and negative correlation indicated by an arrow. Objects are labeled according to design parameters: %(glycerol)_ml(casted amount).

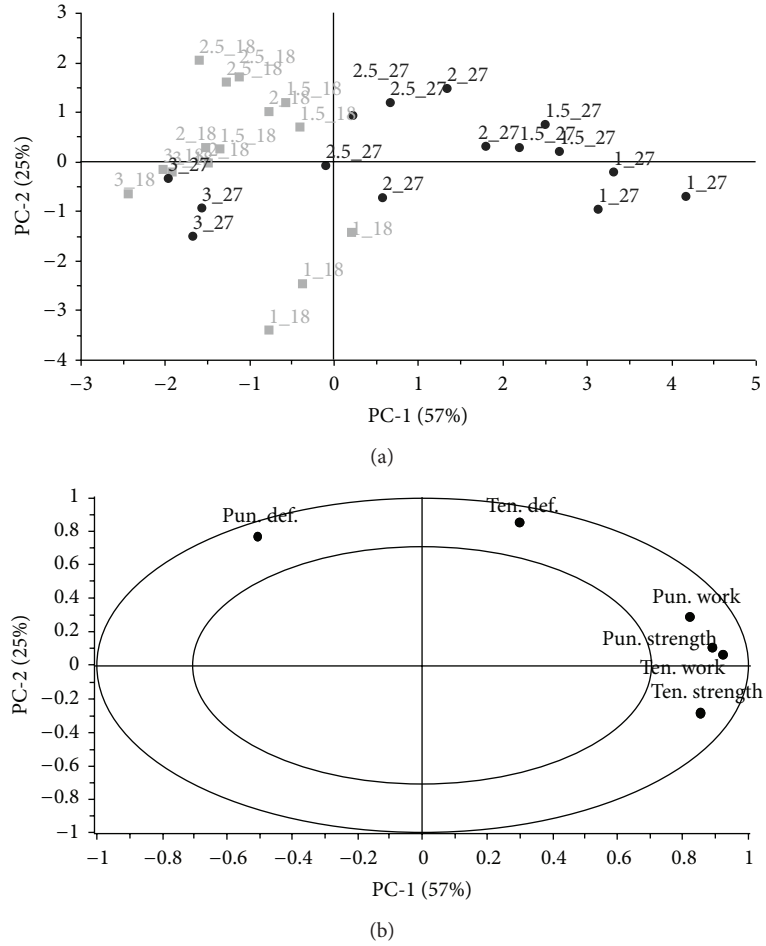

Figure 3: PCA; (a) scores plot; (b) correlation loadings plot, data of films with a nonwoven textile, positive correlation marked with a circle. Objects are labeled according to design parameters: %(glycerol)_ml(casted amount).

plot (Figure 2(a)) shows that puncture work was influenced by the thickness of the film differently compared to the rest of film characteristics, as the opposite effect in films containing 2.5–3% of glycerol was observed. The increased amount of glycerol in films C4 and C5 (18 mL) led to an increase in puncture work and conversely to a decrease in this work in films D4 and D5 (27 mL). The effect of the amount of glycerol used is well described by the parameters of the texture analysis located along PC-1 (Figure 2(b)). Moreover, some parameters are strongly correlated, both positively and negatively. Correlated parameters have the potential to explain a similar part of variability in the data. This may have the practical consequence of using only one of the parameters to obtain the necessary information about the film characteristics. Puncture strength, tensile strength, and tensile work positively correlated, and tensile deformation negatively correlated with these parameters.

A separate PCA model for the data of films with a nonwoven textile was further calculated. The correlation loadings plot (Figure 3(b)) describes the relationship between variables in the data. In particular, variability of strongly correlated variables of tensile strength and tensile work, puncture strength and, in the specific case of these nonwoven textile films, puncture work are explained to some extent by the distribution of films into two groups according to their thicknesses (Figure 3(a)). Thicker films (27 mL) have a greater variability depending on the amount of glycerol as compared to thinner films (18 mL) which reflects different variance of each group along PC-1 and PC-2, respectively.

MLR regression was performed to better explain the effect of formulation parameters on the parameters measured by texture analysis. Using ANOVA (analysis of variance), model significance was tested and was also used to evaluate individual effects and interaction effects. Goodness of fit coefficients was used to evaluate the models: R-square described explained variance of the model, R-square of prediction expressed predictive ability of the model, and C.V. (coefficient of variation) was expressed as a percentage of the mean. MLR models were calculated for two levels of each variable (min, max), which made interpretation easier. The output of the selected MLR models was interaction plots which represented an average value effect of one factor dependent upon the level of the second factor.

Table 3: Models for films without nonwoven textile.

		Pen. strength	Pen. work	Pen. def.	Ten. strength	Ten. work	Ten. def.
Significance (P value)	Model	0.000	0.000	0.000	0.000	0.000	0.000
	mL of glycerol	0.000	0.002	0.000	0.000	0.000	0.000
	Thickness	0.000	0.000	0.000	0.000	0.284	0.000
	mL of glycerol ∗ thickness	0.711	0.000	0.000	0.100	0.001	0.009
Goodness of fit	R-square	0.98	0.96	0.97	0.99	0.95	0.97
	R-square prediction	0.96	0.91	0.93	0.98	0.89	0.93
	C.V. in %	10.65	9.55	14.22	9.05	16.53	14.79

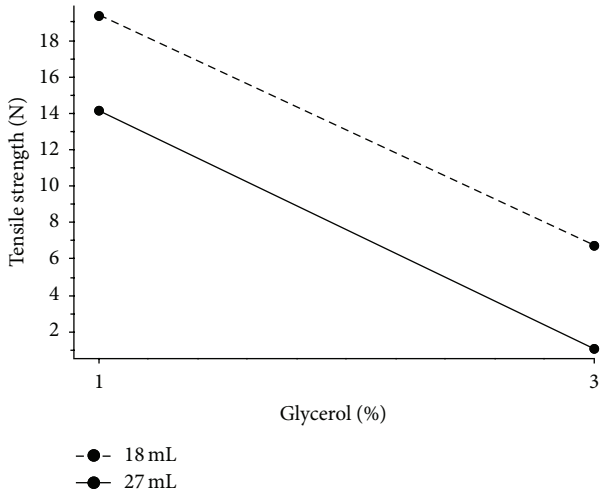

Figure 4: Interaction plot; effect of amount of glycerol on tensile strength at various thicknesses of films without nonwoven textile.

The characteristics of models for films without a nonwoven textile are summarized in Table 3. Until now, a general observation is known that the deformation/elongation of film increases with plasticizer content [14, 21]. In this experiment, it was found that puncture strength and tensile strength had similar regression characteristics. The effect of the interaction between the amount of glycerol and the film thickness did not occur as shown in Figure 4 where the lines are parallel; that is, increase in the amount of glycerol from 1% to 3% led to approximately the same decrease in the recalculated tensile strength for both film thicknesses. Greater recalculated tensile strength and puncture strength were needed for thinner films (dashed line). A greater recalculated tensile strength was also found for thinner films containing NaCMC and propylene glycol as plasticizer in Verma and Chattopadhyay's experiment [22]. Puncture work and tensile work were not correlated; therefore texture characteristics are manifested differently in graphs of interactions (Figures 5(a) and 5(b)).

Characteristics of models for films with a nonwoven textile are summarized in Table 4. In general, all measured texture parameters were significantly smaller compared to films without the nonwoven textile. Unlike films without a nonwoven textile, interaction between the amount of glycerol and film thickness was observed. The results show that the best texture parameter for describing dependence

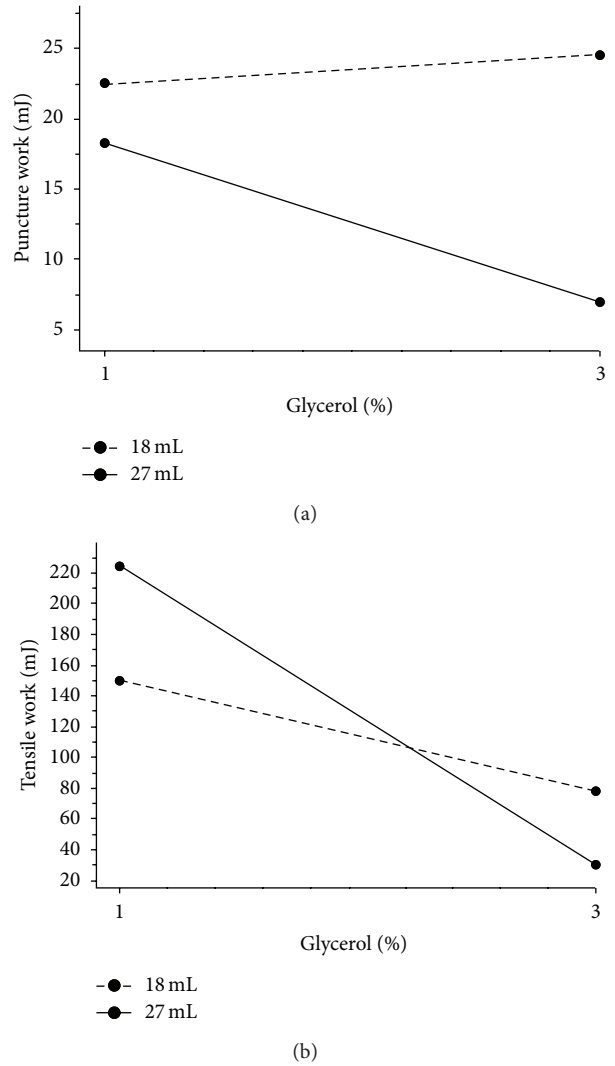

Figure 5: Interaction plot; (a) effect of the amount of glycerol on puncture work at various thicknesses of films without nonwoven textile; (b) effect of the amount of glycerol on tensile work at various thicknesses of films without nonwoven textile.

between the amount of glycerol and film thickness was tensile strength with excellent regression characteristics, followed by puncture strength. These parameters were again strongly correlated but increasing the amount of glycerol from 1% to 3% did not lead to a decrease similar to that in the films

Table 4: Models for films with nonwoven textile.

		Pen. strength	Pen. work	Pen. def.	Ten. strength	Ten. work	Ten. def.
Significance (P value)	Model	0.000	0.003	0.006	0.000	0.000	0.049
	mL of glycerol	0.000	0.004	0.002	0.000	0.000	0.803
	Thickness	0.000	0.018	0.284	0.000	0.002	0.029
	mL of glycerol ∗ thickness	0.000	0.012	0.033	0.000	0.007	0.052
Goodness of fit	R-square	0.98	0.81	0.77	1.00	0.90	0.61
	R-square prediction	0.96	0.58	0.49	0.99	0.77	0.11
	C.V. in %	9.83	17.64	9.97	4.67	14.46	8.15

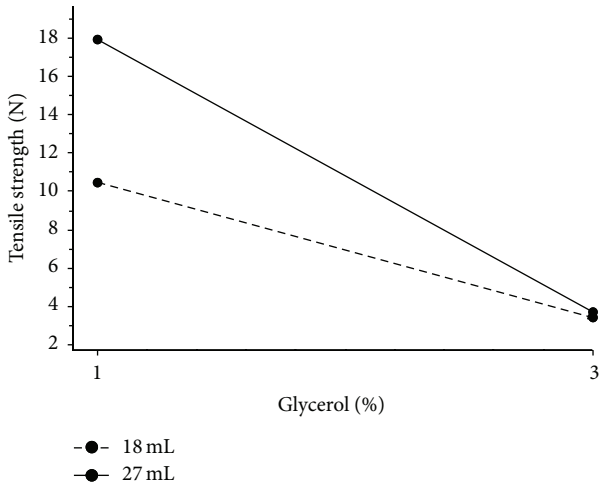

Figure 6: Interaction plot; effect of the amount of glycerol on tensile strength at various thicknesses of films with nonwoven textile.

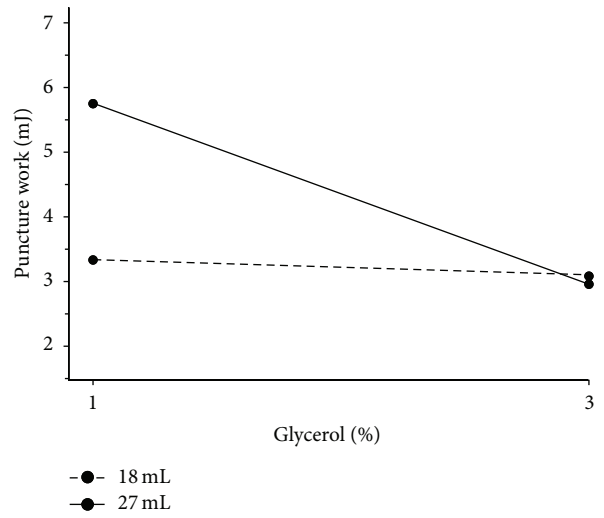

Figure 7: Interaction plot; effect of the amount of glycerol on the work done during film puncture at various thicknesses of films with nonwoven textile.

without a nonwoven textile (Table 2). Figure 6 shows that film thickness significantly affects tensile strength for 1% concentration of glycerol. Film thickness had practically no effect on films with 3% of glycerol. Greater recalculated tensile strength and puncture strength, respectively, were needed for thicker films (solid line), unlike films without nonwoven textile. The concentration of glycerol was a parameter which had a strong negative effect on tensile strength; that is, a high concentration of glycerol led to low tensile strength, regardless of the film thickness. Another suitable parameter to describe the dependence between the amount of glycerol and film thickness was tensile work. Again, film thickness affected tensile work and puncture work in films with a lower amount of glycerol and had almost no effect on films with higher amounts of glycerol (Figure 7).

4. Conclusion

New dependencies between formulation, process variables, and parameters describing mechanical properties of mucoadhesive films based on NaCMC were discovered. Puncture strength was strongly correlated with tensile strength and could be used to obtain necessary information about the mechanical characteristics of films. Puncture work and tensile work were not correlated in films prepared using the unmodified solvent casting method; increasing the amount of glycerol led to an increase in the puncture work in thinner films. All measured texture parameters in films prepared using the modified solvent casting method were significantly smaller compared to films without a nonwoven textile. Moreover, unlike films without a nonwoven textile, a relationship between the amount of glycerol and film thickness was observed, and greater recalculated tensile strength and puncture strength, respectively, were needed for thicker films with a nonwoven textile.

Conflict of Interests

The authors declare that there is no conflict of interests regarding the publication of this paper.

Acknowledgments

This work was supported by Ministry of Health of Czech Republic (Research Project no. NT14477) and IGA VFU Brno, Czech Republic (Research Project no. 96/2013/FaF).

References

[1] A. M. Avachat, K. N. Gujar, and K. V. Wagh, "Development and evaluation of tamarind seed xyloglucan-based mucoadhesive buccal films of rizatriptan benzoate," *Carbohydrate Polymers*, vol. 91, no. 2, pp. 537–542, 2013.

[2] J. O. Morales and J. T. McConville, "Manufacture and characterization of mucoadhesive buccal films," *European Journal of Pharmaceutics and Biopharmaceutics*, vol. 77, no. 2, pp. 187–199, 2011.

[3] J. Gajdziok and D. Vetchý, "Mucoadhesive polymers in medical forms," *Chemicke Listy*, vol. 106, no. 7, pp. 632–638, 2012.

[4] Y. Sudhakar, K. Kuotsu, and A. K. Bandyopadhyay, "Buccal bioadhesive drug delivery—a promising option for orally less efficient drugs," *Journal of Controlled Release*, vol. 114, no. 1, pp. 15–40, 2006.

[5] N. Salamat-Miller, M. Chittchang, and T. P. Johnston, "The use of mucoadhesive polymers in buccal drug delivery," *Advanced Drug Delivery Reviews*, vol. 57, no. 11, pp. 1666–1691, 2005.

[6] H. Landová, Z. Daněk, J. Gajdziok, D. Vetchý, and J. Štembírek, "Oral mucosa and therapy of recurrent aphthous stomatitis," *Ceská a Slovenská Farmacie*, vol. 62, no. 1, pp. 12–18, 2013.

[7] H. Landová, Z. Daněk, J. Gajdziok, D. Vetchý, and J. Štembírek, "Mucoadhesive films as perspective oral dosage form," *Česká a Slovenská Farmacie*, vol. 62, no. 1, pp. 4–11, 2013.

[8] M. A. Repka, S. L. Repka, and J. W. McGinity, "Bioadhesive hot-melt extruded film for topical and mucosal adhesion applications and drug delivery and process for preparation thereof," US Patent no. 6375963 B1, 2002.

[9] R. Chokshi and H. Zia, "Hot melt extrusion technique: a review," *Iranian Journal of Pharmaceutical Research*, vol. 3, pp. 3–16, 2004.

[10] M. A. Repka, J. W. McGinity, F. Zhang, and J. J. Koleng, "Hot-melt extrusion technology," in *Encyclopedia of Pharmaceutical Technology*, J. Swarbrick and J. Boylan, Eds., Marcel Dekker, New York, NY, USA, 2nd edition, 2002.

[11] M. Preis, C. Woertz, P. Kleinebudde, and J. Breitkreutz, "Oro-mucosal film preparations: classification and characterization methods," *Expert Opinion on Drug Delivery*, vol. 10, no. 9, pp. 1303–1317, 2013.

[12] D. Vetchý, H. Landová, J. Gajdziok, P. Doležel, Z. Daněk, and J. Štembírek, "Determination of dependences among *in vitro* and *in vivo* properties of prepared mucoadhesive buccal films using multivariate data analysis," *European Journal of Pharmaceutics and Biopharmaceutics*, vol. 86, pp. 498–506, 2014.

[13] *The European Pharmacopoeia*, supplement 7.8, European Directorate for the Quality of Medicines & Health Care, Strasbourg, France, 7th edition, 2013, http://online6.edqm.eu/ep801/.

[14] A. B. Nair, R. Kumria, S. Harsha, M. Attimarad, B. E. Al-Dhubiab, and I. A. Alhaider, "*In vitro* techniques to evaluate buccal films," *Journal of Controlled Release*, vol. 166, no. 1, pp. 10–21, 2013.

[15] B. N. Tukarama, I. V. Rajagopalana, and P. S. I. Shartchandraa, "The effects of lactose, microcrystalline cellulose and dicalcium phosphate on swelling and erosion of compressed HPMC matrix tablets: texture analyzer," *Iranian Journal of Pharmaceutical Research*, vol. 9, no. 4, pp. 349–358, 2010.

[16] B. Sołowiej, "Effect of whey preparations on adhesiveness of processed cheese analogues to different packaging materials," *Zywnosc: Nauka, Technologia, Jakosc*, vol. 20, no. 2, pp. 80–91, 2013.

[17] R. P. Dixit and S. P. Puthli, "Oral strip technology: overview and future potential," *Journal of Controlled Release*, vol. 139, no. 2, pp. 94–107, 2009.

[18] J. S. Boateng, A. D. Auffret, K. H. Matthews, M. J. Humphrey, H. N. E. Stevens, and G. M. Eccleston, "Characterisation of freeze-dried wafers and solvent evaporated films as potential drug delivery systems to mucosal surfaces," *International Journal of Pharmaceutics*, vol. 389, no. 1-2, pp. 24–31, 2010.

[19] M. Preis, K. Knop, and J. Breitkreutz, "Mechanical strength test for orodispersible and buccal films," *International Journal of Pharmaceutics*, vol. 461, pp. 22–29, 2014.

[20] S. S. Shidhaye, N. S. Saindane, S. Sutar, and V. Kadam, "Mucoadhesive bilayered patches for administration of sumatriptan succinate," *AAPS PharmSciTech*, vol. 9, no. 3, pp. 909–916, 2008.

[21] S. Singh, S. Jain, M. S. Muthu, S. Tiwari, and R. Tilak, "Preparation and evaluation of buccal bioadhesive films containing clotrimazole," *AAPS PharmSciTech*, vol. 9, no. 2, pp. 660–667, 2008.

[22] N. Verma and P. Chattopadhyay, "Preparation of mucoadhesive patches for buccal administration of metoprolol succinate: in vitro and in vivo drug release and bioadhesion," *Tropical Journal of Pharmaceutical Research*, vol. 11, no. 1, pp. 9–17, 2012.

Hindawi Publishing Corporation
BioMed Research International
Volume 2014, Article ID 832452, 6 pages
http://dx.doi.org/10.1155/2014/832452

Research Article

Hot-Stage Microscopy for Determination of API Particles in a Formulated Tablet

Michal Šimek,[1] Veronika Grünwaldová,[2] and Bohumil Kratochvíl[1]

[1] *Department of Solid State Chemistry, Institute of Chemical Technology Prague, Technická 5, 166 28 Prague, Czech Republic*
[2] *Zentiva k.s., U Kabelovny 130, 102 37 Prague, Czech Republic*

Correspondence should be addressed to Michal Šimek; michal.simek@vscht.cz

Received 21 May 2014; Revised 2 July 2014; Accepted 6 July 2014; Published 21 July 2014

Academic Editor: Josef Jampilek

Although methods exist to readily determine the particle size distribution (PSD) of an active pharmaceutical ingredient (API) before its formulation into a final product, the primary challenge is to develop a method to determine the PSD of APIs in a finished tablet. To address the limitations of existing PSD methods, we used hot-stage microscopy to observe tablet disintegration during temperature change and, thus, reveal the API particles in a tablet. Both mechanical and liquid disintegration were evaluated after we had identified optimum milling time for mechanical disintegration and optimum volume of water for liquid disintegration. In each case, hot-stage micrographs, taken before and after the API melting point, were compared with image analysis software to obtain the PSDs. Then, the PSDs of the APIs from the disintegrated tablets were compared with the PSDs of raw APIs. Good agreement was obtained, thereby confirming the robustness of our methodology. The availability of such a method equips pharmaceutical scientists with an in vitro assessment method that will more reliably determine the PSD of active substances in finished tablets.

1. Introduction

Particle size distribution is one of the most important physical parameters of the starting materials as well as the finished products of pharmaceutical solid dosage forms [1]. On the one hand, particle size distribution of a pharmaceutical solid governs its bulk properties such as flowability, which determines the processability of the starting and intermediate materials and finished products during the manufacturing process. On the other hand, particle size distribution (PSD) of either the excipients or the active pharmaceutical ingredients (APIs) has a profound effect on drug dissolution, bioavailability, stability, and content uniformity, thereby determining the safety, efficacy, and quality of the finished products. Therefore, the analysis and control of particle size distribution of both the excipients and APIs are often an essential part of pharmaceutical product development [2–4].

Tablet formulations typically contain, in addition to an API, sugars and a number of insoluble excipients, which may include microcrystalline cellulose, magnesium stearate, calcium phosphate anhydrous, pigments, and other ingredients. However, excipients often exhibit a broad PSD and a substantial number of excipients may occur in the same size range as the drug substance. This complicates determination of the drug substance. In addition, the majority of APIs and excipients are white powders with rarely predictable particle shape and size. Morphology is usually the only useful clue on how to distinguish API particles in almost all cases of white substances. This leads to inclusion of excipient particles into assessment of an API PSD [5]. In relation to limitations of existing PSD methods, we investigated a methodology for PSD determination based on hot-stage microscopy.

Hot-stage microscopy has been already used for the characterization of pharmaceutical substances. For example, Vitez et al. used hot-stage microscopy for observing polymorphic phase transformations of an API [6]. It is frequently used as a complementary technique to DSC during compatibility analyses [7]. Similar usage of this technique can be easily found in the literature. It is obvious that hot-stage microscopy is becoming a routine analytical tool for system observation over temperature [8].

Spectral techniques such as FTIR or Raman mapping are sometimes used for the approximation of particle size of drug substance in a tablet [9]. These techniques require

Table 1: List of used APIs, excipients, their melting points, and composition of mixture and tablets.

	Tadalafil	Meloxicam	Calcium carbonate	Methocel	Lactose monohydrate	Avicel PH102	Colloidal silicon dioxide	Crospovidone	Magnesium stearate	Povidone
Melting point [°C]	286–295	242–250	825	225–230	214–216	260–275	1600	150–180	117–150	150–180
Mixture 1	●			●						
TFL Tbl 1	●		●		●		●		●	
ME Tbl 1		●			●	●	●	●	●	
ME Tbl 2		●			●	●	●	●	●	●

a high quality cut of tablet. Methods of the cut preparation are described in our previous puplication [10]. A result map provides the spatial distributions of the various components within a sample by different colors. However, this does not preclude API particles agglomerate formation and the detection of agglomerates as single particles. It should be noted that images often cannot differentiate between a large particle and agglomerated particles [11]. Thus, a chemical distribution within the image is often described in terms of the "domain" size rather than the particle size [12, 13]. Comparison of the results of spectral mapping and hot-stage microscopy could be useful for discovering API agglomerates in a drug product.

2. Materials

2.1. Raw Materials. We used tadalafil and meloxicam as model APIs. Tadalafil is a phosphodiesterase-5 inhibitor used for a treatment of the erectile dysfunction [14–17]. Meloxicam is a nonsteroidal anti-inflammatory drug with an analgesic and fever reducer effect [18]. Common excipients were used with APIs to create an experimental mixture and model tablets. The list of compounds used and their melting points are shown in Table 1, as well as the composition of the mixture and tablets which are made of them.

2.2. Mixture 1. Mixture 1 consists of tadalafil (50%) and Methocel (50%). Mixture 1 was used for the demonstration of hot-stage microscopy as a useful technique in early stage of our work.

2.3. TFL Tbl 1. Tablets TFL Tbl 1 were prepared by direct compression of tadalafil (10%), calcium carbonate (39%), lactose monohydrate (46.2%), silicon dioxide (2.7%), and magnesium stearate (2.1%).

2.4. ME Tbl 1. Tablets ME Tbl 1 were prepared by direct compression of meloxicam (9.9%), lactose monohydrate (15.3%), Avicel PH102 (50.3%), silicon dioxide (1.6%), crospovidone (14.4%), and magnesium stearate (9.6%).

2.5. ME Tbl 2. Tablets ME Tbl 2 were prepared by compression of granules. Povidone was used as a granulation binder. Granules were made of meloxicam (9.6%), lactose monohydrate (14.9%), Avicel PH102 (48.8%), silicon dioxide (1.5%), crospovidone (13.9%), magnesium stearate (9.3%), and povidone (3%).

3. Methods

A tablet must first be disintegrated before analysis as hotstage microscopy was used for observation of solid powder mixture over change in temperature.

3.1. Mechanical Disintegration of Tablets. The mechanical method of powder preparation from a tablet is shortly described in the publication from Koradia et al. A small portion of a tablet core is pressed lightly between two glass slides. We consider this procedure suitable only for softer tablets [8]. Conversely, mechanical crushing of a tablet may cause breaking of a tablet as well as individual particles. Because of this, it was necessary to assess the dependency of particles size reduction on milling time.

3.2. Liquid Disintegration of Tablets. This method of disintegration is based on the dissolution of soluble components followed by the filtration and drying of insoluble components. Selected dissolution liquid must not dissolve the API. Elimination of soluble components causes increase of API content in the prepared powder. This is advantageous for API's identification by a microscope, especially in the case of tablets with a low amount of API [19]. The dependency of the API particle size change on a volume of used disintegration liquid was one of our experimental aims.

3.3. Analytical Methods

3.3.1. Size Analysis. The evaluations of the particle or domain size distribution of APIs were performed with image analysis (NIS Elements 4.11 software, LIM—Laboratory imaging spol. s.r.o., Za drahou 171/17, Prague, Czech Republic) of hot-stage micrographs as well as spectral images. Approximately 600 particles were evaluated in every analysis. Particle size distributions are often reported by parameters based upon the maximum particle size for a given percentage (10, 50, and 90%) of sample. For this reason, PSDs were compared by percentile d-values which are known as the lower decil—$d(0.1)$, median—$d(0.5)$, and upper decil—$d(0.9)$.

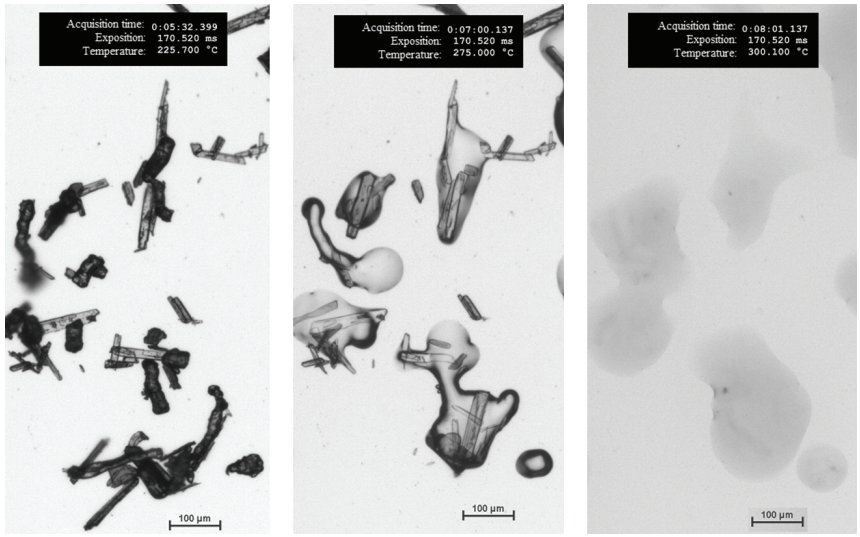

Figure 1: Mixture 1 at 225°C, 275°C, and 300°C temperatures. No change of the system was observed from 25 to 225°C. Methocel melted at 230°C and tadalafil melted at 295°C.

3.3.2. Hot-Stage Micrographs. Light microscope Nikon eclipse Ni with LTS420 temperature controlled stage (Nikon spol. s.r.o., K Radotínu 14, Prague, Czech Republic) was used for experiments with 4x and 10x lens. Heating rate was 10°C per minute.

3.3.3. Spectral Images. FTIR mapping was carried out using Nicolet iN10 MX Infrared Imaging Microscope (Thermo Fisher Scientific-Thermo Scientific Inc., Vienna, Austria) with OmnicSpecta software (Thermo Scientific Inc., Vienna, Austria). Full performance leads to resolution of 6.25 μm per pixel.

4. Results and Discussion

The aim of this paper was to show hot-stage microscopy as a suitable tool for the identification of API particles in a mixture and disintegrated tablet. Important part of this work was focused on finding the best parameters for tablet disintegration by the mechanical and liquid disintegration method. To find out the best parameters, the dependencies of the d-values of PSDs were observed. Each experiment, including selection of 600 API particles, was repeated five times and variation obtained.

4.1. Identification of API with Hot-Stage Microscopy. The principle of API identification is shown on the example of mixture 1 (Figure 1). As tadalafil has higher melting point than Methocel, needle-shaped particles of tadalafil melt later. API particles were identified by comparing pictures taken at 275°C and 300°C as the melting point of tadalafil is 295°C. The experiments were repeated until 600 particles of tadalafil were analyzed.

Tablet TFL Tbl 1 was disintegrated to powder by a few drops of water. Prepared powder was filtered and dried at room temperature and used for the analyses as described.

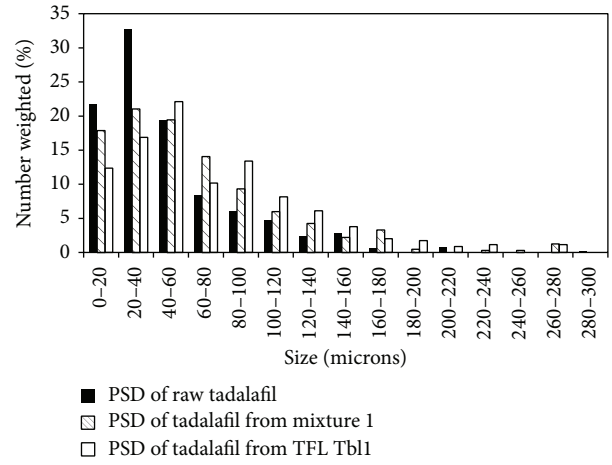

Figure 2: PSDs of raw tadalafil, tadalafil in mixture 1 and in TFL Tbl 1 tablets.

Three PSDs of tadalafil (raw, in mixture 1, and in TFL Tbl 1) are compared in Figure 2. The PSDs have similar range and occurrence of particle sizes.

4.2. Mechanical Disintegration of Tablets. Tablets ME Tbl 2 were prepared by the compression of granules and were used for experiments. An adverse phenomenon of the mechanical method is gradual destruction of particles over the milling time. Figure 3 shows the change of d-values of meloxicam particle size distributions over milling time. Reference values of raw meloxicam were measured before formulation into tablets. Minimal change (approximately 5 percent) of d-values was observed at 0.5 min milling time. The rapid decrease of particle size was observed if the milling time was longer than 0.5 min.

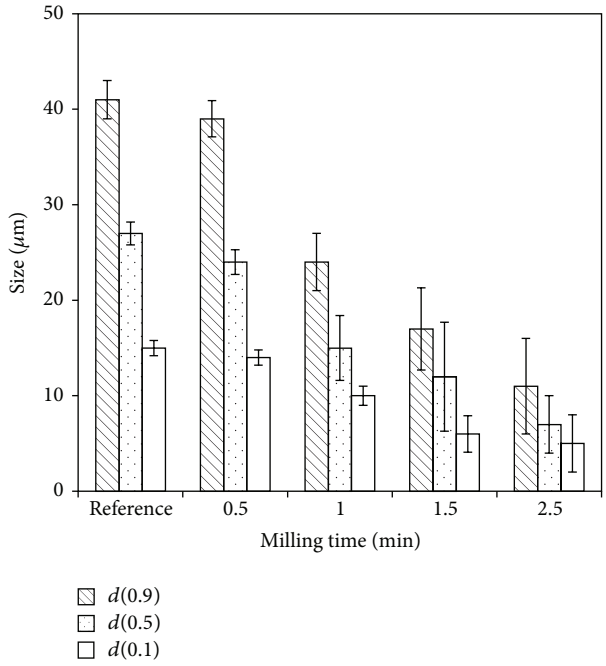

Figure 3: Change of $d(0.1)$, $d(0.5)$, and $d(0.9)$ of API particle size distributions over milling time. Reference values belong to raw meloxicam.

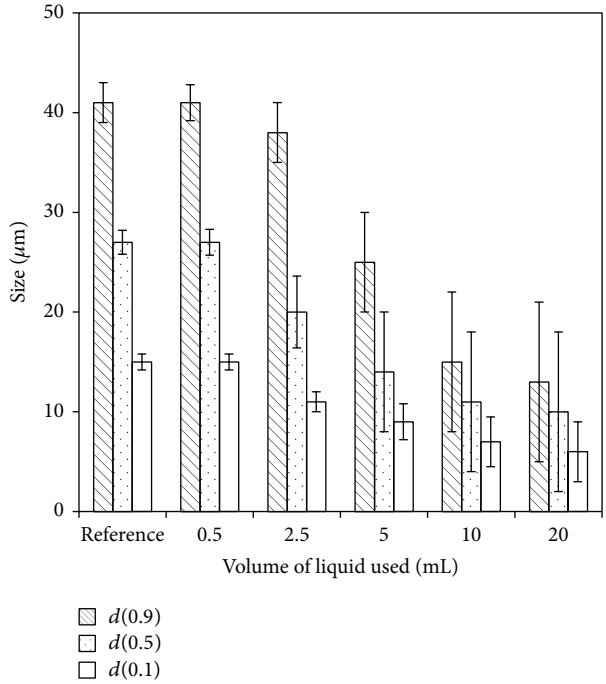

Figure 4: Change of $d(0.1)$, $d(0.5)$, and $d(0.9)$ of meloxicam PSDs over volume of water used. Reference values belong to raw meloxicam.

At first, a tablet is broken into small pieces. Then, small pieces are milled into granules. Till some granules are presented, smooth milling does not significantly destroy individual particles. This is the reason why some residual granules were presented in prepared samples and they were discarded during image analyses.

4.3. Liquid Disintegration of Tablets. Because it was found that granulation binders, used in the granulation process, caused hardening of prepared powder, directly compressed tablets ME Tbl 1 were used for these experiments. Figure 4 shows change of d-values of meloxicam PSDs over volume of water used for the disintegration. PSD analyses were carried out using the method described in mechanical disintegration. Almost no change of d-values was observed if 0.5 mL of water was used. This volume equals the volume being required to dissolve all sufficiently soluble components of ME Tbl 1 tablet [20]. It can be calculated as a saturated solution of all sufficiently soluble components in a tablet [21]. In our case, more than 0.5 mL of water caused partial dissolution of meloxicam particles.

4.4. Comparison of Hot-Stage Microscopy and FTIR Mapping. The preparation of tablet cut is described in our previous publication [10]. FTIR map of the microtome cut of ME Tbl 1 tablet is shown in Figure 5. FTIR mapping presents "domains" of all components (meloxicam—black, Avicel PH102—dark grey, lactose—light grey, and crospovidone—white). Image analysis results of meloxicam PSD, obtained from FTIR mapping and hot-stage microscopy, are compared in Figure 6. A lot of API "domains" from FTIR map are much bigger

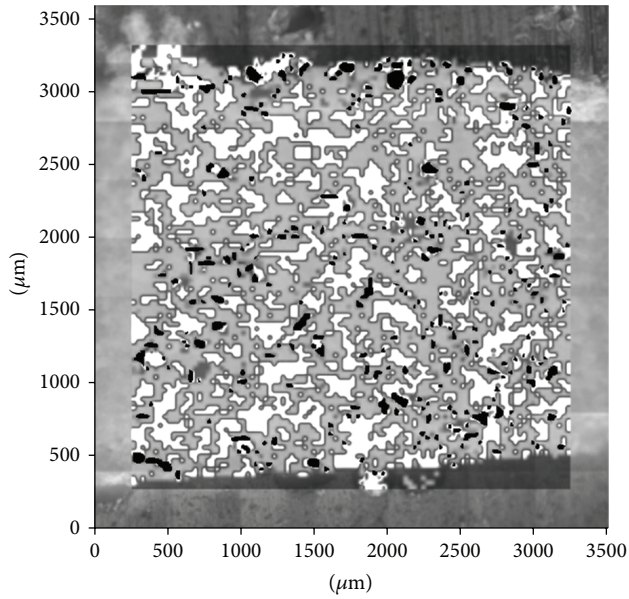

Figure 5: FTIR map of ME Tbl 1 cut. (meloxicam—black, Avicel PH102—dark grey, lactose—light grey, and crospovidone—white).

than particles analyzed with hot-stage microscopy which provides congruent results with reference PSD of meloxicam. FTIR mapping does not seem to be suitable for an API PSD assessment. On the other hand, comparison of FTIR map with hot-stage microscopy allows the determination of API agglomerates in a tablet.

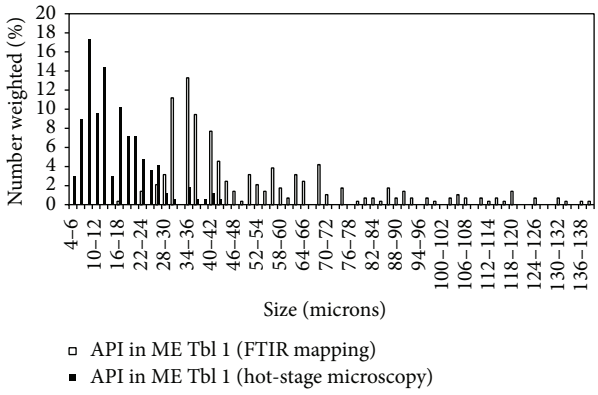

Figure 6: Results of meloxicam PSD in generic drug (ME Tbl 1) obtained by hot-stage microscopy and by FTIR mapping.

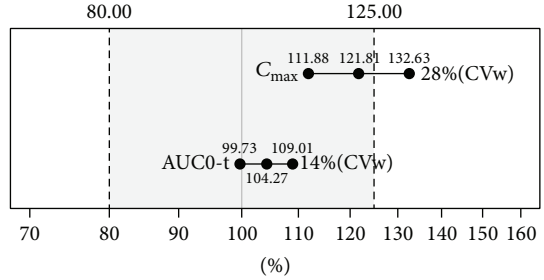

Figure 7: Results of failed bioequivalence study. The maximal concentration in blood (C_{max}) of generic product is out of the tolerance limit. Area under the curve of pharmacokinetic profile (AUC) complies.

4.5. Application of Hot-Stage Microscopy Analysis (Case Study). The aim of this part is to demonstrate the application of hot-stage microscopy analysis as a routine analytical method in the pharmaceutical industry. Bioequivalence studies are performed to demonstrate in vivo that two pharmaceutically equivalent products (in the US) or alternative pharmaceutical products (in the EU) are comparable in their rate and extent of absorption [22]. For reaching the bioequivalence, values of the maximal concentration in blood (C_{max}), the area under the curve of pharmacokinetic profile (AUC), and their deviations, must be situated inside the tolerance limit. Width of the limit (from 80 to 125%) is defined by the regulatory authorities and center point (100%) represents relative values of C_{max} and AUC of the reference listed drug (RLD). As shown in Figure 7, the bioequivalence study of generic and reference listed drug (RLD) was not reached. We used hot-stage microscopy to compare API PSD in the RLD and generic tablet and raw API used in the generic tablet (Figure 8). The results showed a difference in PSDs of API used in the RLD and generic tablet and helped to find out why the bioequivalent study had not matched in C_{max}. Higher C_{max} of the generic tablet was truly caused by the smaller size of API particles, as the smaller particles dissolved faster and led to higher C_{max}. API particles in the RLD are roughly double the size of the particles in the generic tablet. Almost

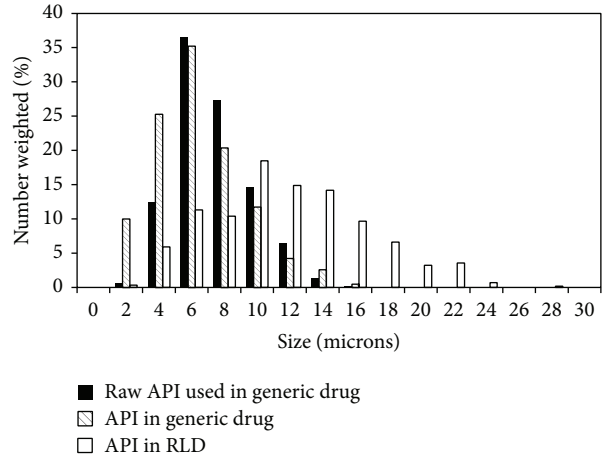

Figure 8: Comparison of PSD of raw API used in generic drug, API in generic tablet, and API in the RLD tablet.

identical PSDs of the raw API and API in the generic product confirm the robustness of the method.

5. Conclusion

The experiments demonstrated that hot-stage microscopy and image analysis allow identification of API particles in mixtures or in disintegrated tablets. The methodology is based on different melting points of individual substances. The disintegration of tablet into powder is essential for PSD analysis by hot-stage microscopy. The mechanical disintegration was suitable for both—tablets produced by direct compression and those compressed from granules. However, it is not recommended to completely grind a tablet into powder. If all bigger particles of a tablet were milled, individual API particles were partially broken. The liquid disintegration was suitable only for directly compressed tablets. In case of compressed granules, granulation binders caused hardening of the prepared powder. The API should be insoluble or, at least, minimally soluble in liquid. The qualitative and quantitative composition of a tablet are required for the right calculation of the liquid volume. The volume of the liquid is calculated like the volume of the saturated solution of all soluble excipients in a tablet. It was found that more API particles are partially dissolved when a volume greater than the calculated liquid volume is used. The elution of soluble excipients allows the API content in the prepared powder to be increased. The comparison of results produced by hot-stage microscopy and FTIR mapping is considered a useful way to identify API agglomerates in a tablet. Importantly, hot-stage microscopy can be used as a routine tool in pharmaceutical development for comparing particle size of the RLD and generic product.

Conflict of Interests

The authors declare that there is no conflict of interests regarding the publication of this paper.

Acknowledgment

The authors thank the Ministry of Education, Youth, and Sports of the Czech Republic (research programs no. 20/2014 and MSM6046137302) for financial support. They also thank T. Pekárek for FTIR mapping analysis.

References

[1] M. Šimek, V. Grünwaldová, and B. Kratochvíl, "Current methods of measurement of pharmaceutical particles size and their restrictions," *Chemické Listy*, vol. 108, no. 1, pp. 50–55, 2014.

[2] T. M. Crowder, A. J. Hickey, M. D. Louey, and N. Orr, *A Guide to Pharmaceutical Particulate Science*, Interpharm/CRC, New York, NY, USA, 2003.

[3] Council of Europe, *European Pharmacopoeia*, European Pharmacopoeia Secretariat, Strasbourg, France, 2008.

[4] R. A. Storey and I. Ymen, *Solid State Characterization of Pharmaceuticals*, Wiley-Blackwell, West Sussex, UK, 2011.

[5] R. C. Rowe, P. J. Sheskey, and M. E. Quinn, *Handbook of Pharmaceutical Excipients*, Pharmaceutical Press, London, UK, 6th edition, 2009.

[6] I. M. Vitez, A. W. Newman, M. Davidovich, and C. Kiesnowski, "The evolution of hot-stage microscopy to aid solid-state characterizations of pharmaceutical solids," *Thermochimica Acta*, vol. 324, no. 1-2, pp. 187–196, 1998.

[7] P. Mura, M. T. Faucci, A. Manderioli, G. Bramanti, and L. Ceccarelli, "Compatibility study between ibuproxam and pharmaceutical excipients using differential scanning calorimetry, hot-stage microscopy and scanning electron microscopy," *Journal of Pharmaceutical and Biomedical Analysis*, vol. 18, no. 1-2, pp. 151–163, 1998.

[8] V. S. Koradia, G. Chawla, and A. K. Bansal, "Comprehensive characterisation of the innovator product: targeting bioequivalent generics," *Journal of Generic Medicines*, vol. 2, no. 4, pp. 335–346, 2005.

[9] R. Salzer and H. W. Siesler, *Infrared and Raman Spectroscopic Imaging*, Wiley-VCH, Weinheim, Germany, 2009.

[10] M. Šimek, V. Grünwaldová, and B. Kratochvíl, "A new way of solid dosage form samples preparation for SEM and FTIR using microtome," *Pharmaceutical Development and Technology*, vol. 194, pp. 411–416, 2014.

[11] F. Franch-Lage, J. M. Amigo, E. Skibsted, S. Maspoch, and J. Coello, "Fast assessment of the surface distribution of API and excipients in tablets using NIR-hyperspectral imaging," *International Journal of Pharmaceutics*, vol. 411, no. 1-2, pp. 27–35, 2011.

[12] M. J. Henson and L. Zhang, "Drug characterization in low dosage pharmaceutical tablets using raman microscopic mapping," *Applied Spectroscopy*, vol. 60, no. 11, pp. 1247–1255, 2006.

[13] L. R. Hilden, C. J. Pommier, S. I. F. Badawy, and E. M. Friedman, "NIR chemical imaging to guide/support BMS-561389 tablet formulation development," *International Journal of Pharmaceutics*, vol. 353, no. 1-2, pp. 283–290, 2008.

[14] H. A. Feldman, I. Goldstein, D. G. Hatzichristou, R. J. Krane, and J. B. McKinlay, "Impotence and its medical and psychosocial correlates: results of the Massachusetts Male Aging Study," *Journal of Urology*, vol. 151, no. 1, pp. 54–61, 1994.

[15] T. F. Lue, "Erectile dysfunction," *The New England Journal of Medicine*, vol. 342, no. 24, pp. 1802–1813, 2000.

[16] C. Gazzaruso, S. Giordanetti, E. de Amici et al., "Relationship between erectile dysfunction and silent myocardial ischemia in apparently uncomplicated type 2 diabetic patients," *Circulation*, vol. 110, no. 1, pp. 22–26, 2004.

[17] M. Bocchio, G. Desideri, P. Scarpelli et al., "Endothelial cell activation in men with erectile dysfunction without cardiovascular risk factors and overt vascular damage," *Journal of Urology*, vol. 171, no. 4, pp. 1601–1604, 2004.

[18] "Meloxicam official FDA information," 2010, http://www.drugs.com/.

[19] D. J. Lamberto, B. Cohen, J. Marencic, C. Miranda, R. Petrova, and L. Sierra, "Laboratory methods for assessing API sensitivity to mechanical stress during agitated drying," *Chemical Engineering Science*, vol. 66, no. 17, pp. 3868–3875, 2011.

[20] "Open Notebook Science Solubility Challenge," 2013, http://lxsrv7.oru.edu/~alang/onsc/solubility/allsolvents.php?solute=meloxicam.

[21] DFE Pharma, Lactose—Some basic properties and characteristics, 2013, http://www.dfepharma.com/en/downloads.aspx?id=%7B2BB38A30-33EC-488D-9B1F-FEE0AD797636%7D.

[22] L. Tothfalusi, L. Endrenyi, and A. Garcia Arieta, "Evaluation of bioequivalence for highly variable drugs with scaled average bioequivalence," *Clinical Pharmacokinetics*, vol. 48, no. 11, pp. 725–743, 2009.